Investigating the role of human MSL2 and MSL1 within and beyond the MSL complex

Anna Meller

Epigenetics and Chromatin Biology Group,

Centre for Chromosome Biology,

School of Natural Sciences,

National University of Ireland, Galway

A thesis submitted to the National University of Ireland, Galway for the degree of Doctor of Philosophy

2017

Supervisor: Dr. Stephen Rea

Table of contents

List of figures

List of tables

Abbreviations

53BP1	p53-binding protein 1
AID	Auxin-inducible degradation
alt-NHEJ	Alternative-NHEJ
APC/C	Anaphase promoting complex/cyclosome
APOBEC3B	Apolipoprotein B mRNA editing enzyme catalytic subunit 3B
AT	Ataxia telangiectasia
ATCC	American tissue culture collection
ATM	Ataxia telangiectasia mutated
ATP	Adenosine triphosphate
ATR	Ataxia telangiectasia and Rad3 related
ATRIP	ATR-interacting protein
BARD1	BRCA1-associated RING domain 1
BER	Base excision repair
BEV	Baculoviral expression vector
BirA	Bifunctional ligase/repressor BirA
BLM	Bloom syndrome protein
BRCA1	Breast cancer type 1 susceptibility protein
BRD4	Bromodomain-containing protein 4
BRTC	BRCA1 carboxyl terminus
BSA	Bovine serum albumin
Cas	CRISPR-associated
cccDNA	closed circular DNA
CDC45	Cell division control protein 45 homologue
CDC45	Cycline dependent kinase 45
CDK1	Cycline dependent kinase 1
cDNA	Complementary DNA
CDT1	CDC6 and CDC10-dependent transcript 1
CHK1/2	Checkpoint kinase 1/2
CldU	5-chloro-2'-deoxyuridine
Co-IP	Co-immunoprecipitation
CoREST	Cofactor repressor element-1 silencing transcription factor
CPT	Camptothecin
CRISPR	Clustered regularly interspaced short palindromic repeats
CRL	Cullin Ring Ligase
$CRL3^{KEAP1}$	Cullin–RING E3 ligase 3
CtIP	CtBP-interacting protein
CXC	Cisteine-rich
DAPI	4',6-diamino-2-phenylindole
DCC	Dosage compensation complex
DDR	DNA damage response
DDT	DNA damage tolerance
DHJ	double holliday junction
DMEM	Dulbecco's modified Eagle's medium
DMSO	Dimethyl sulfoxide
DNA-PKcs	DNA-dependent protein kinase catalytic subunit
DUB	Deubiquitinase
E1	Ubiquitin-activating enzyme
E2	Ubiquitin-conjugating enzyme
E3	Ubiquitin-ligase enzyme
ELAVL1/HuR	Embryonic lethal abnormal vision/ Hu antigen R
ERAD	Endoplasmic reticulum-associated degradation
FHA	Forkhead-associated domain
Fobl	Fork blocking less
FOSL1	Fos-related antigen 1
FRT	Flp Recombination Target
GC	Gene conversion
GID	Glucose-induced degradation deficient
GINS	5-1-2-3 in Japanese (go-ichi-ni-san)
HAT	Histone acetyl transferase
HBV	hepatitis B virus
HDAC	Histone deacetylase
HERC2	HECT-type E3 ligase

HOXA9	Homeobox A9
HP1	Heterochromatin protein 1
HR	Homologous recombination
HRP	Horseradish peroxidase
IAA	Indole-3-acetic acid
IdU	5-Iodo-2′-deoxyuridine
IR	Ionizing radiation/ γ-irradiation
ISWI	Imitation SWI
lnRNA	Long noncoding RNA
LUBAC	Linear Ubiquitin Chain Assembly Complex
MCM	Mini-chromosome maintenance complex
MDC1	Mediator of DNA damage checkpoint protein 1
MEIS1	Meis Homeobox 1
MINDY	Motif interacting with Ub-containing novel DUB family
MJD	Machado-Joseph disease protease
MLE	Maleless
MMC	Mitomycin C
MMR	Mismatch repair
MMS	Methanesulfonate
MOF	Males absent on the first
mRNA	Messenger RNA
MSL	Male specific lethal
MSL1	Male specific lethal 1
MSL2	Male specific lethal 2
MSL3	Male specific lethal 3
Mtor	Megator
NAR	Nucleoporin associated region
NER	Nucleotide excision repair
NFR	Newly fired replication
NHEJ	Nonhomologous end joining
NODE	Nanog and Oct4-associated deacetylase
NSL	Nonspecific lethal
Nup153	Nucleoporin 153
NuRD	Nucleosome Remodeling and Deacetylase
NURF	Nucleosome-remodeling factor
NURF301	Nucleosome-remodeling factor 301
ORC	Origin recognition complex
ORI	Replication origin
OTU	Otubain protease
p53 (TP53)	Tumor protein 53
PALB2	Partner and localizer of BRCA2
PBS	Phosphate buffer saline
PCNA	Proliferating cell nuclear antigen
PEV	Position effect variegation
PIKK	PI3K-like kinase
Pol α	DNA polymerase α
Pol δ	DNA polymerase δ
Pol ε	DNA polymerase ε
PP2A	Protein phosphatase 2A
PP5	Serine-threonine phosphatase 5
PRC1	Polycomb Repressor Complex 1
pre-IC	Pre-initiation complex
pre-RC	Pre-replication complex
P-TEFb	Positive transcription elongation factor b
RCF	Replication factor C
RECQL4	ATP-dependent DNA helicase Q4
RHA	RNA helicase A
RING	Really Interesting New Gene
RNAi/siRNA	RNA interference/small interfering RNA
RNF20/40	Ring Finger Protein 20/40
ROS	Reactive oxygen species
roX1	RNA on the X 1
roX2	RNA on the X 2
RPA	Replication protein A
SCF	DNA supercoiling factor
SSA	Single-strand annealing
SUUR	Suppressor of underreplication
Su(var)3-7	Heterochromatin proteins suppressor of variegation 3-7
SXL	Sex lethal

Tip60	Tat – interacting protein
TIR1	F-box transport inhibitor response 1
TOPBP1	Topoisomerase II-binding protein 1
Treslin	TOPBP1-interacting, replication-stimulating protein
UCH	Ubiquitin C-terminal hydrolase
USP	Ubiquitin-specific protease
UV	Ultraviolet light
vWA	Von Willebrand A
WRN	Werner syndrome ATP-dependent helicase
XLF	XRCC4-like factor

Abstract

While the components of the MSL complex in *Drosophila* are well studied and known to play a critical role in dosage compensation, there is little known about the function of its evolutionary conserved human orthologues. So far the most well characterised member, MOF was found to take part in several cellular processes including transcriptional regulation, apoptosis and the DNA damage response. However, other subunits remained relatively uncharacterised and there is not much known about their functions. To follow up on previous findings and better understand how the MSL complex is involved in cellular processes this study focuses on two subunits, MSL2 and MSL1.

Human MSL2 and MSL1 knock-out cell lines were generated using CRISPR/Cas9 genome editing to address the loss of function effect of these two proteins. Cells lacking either MSL2 or MSL1 were found to have perturbed levels of several histone modifications. The loss of either protein also affected the acetylase function of MOF and its chromatin binding ability. Their role in the DNA damage response (DDR) was further studied using colony formation in response to different DNA damaging agents and foci formation of important DDR mediator proteins in response to ionising radiation (IR). Using *in vivo* HR and NHEJ assays also revealed a repair defect in MSL2 knock-out cells after DNA damage indicating that these pathways in particular are affected. Further studies revealed that the loss of MSL2 or MSL1 affects the foci formation of 53BP1 after damage but not the overall repair. In addition an increase in 53BP1 nuclear body formation was observed possibly indicating replication related damage repair defect. Recovery after stalled replication induced by hydroxyurea (HU) treatment revealed a slight increase in newly fired origins in both the MSL2 and MSL1 knock-out cell lines indicating a potential fork recovery defect. Using a modified BioID approach potential MSL2 interactors and substrates were identified and some interesting were selected as subjects of future experiments.

In summary, this work shows that the loss of either MSL1 or MSL1 negatively affects the DDR possibly via perturbance of the histone modification profile and the observed 53BP1 nuclear body phenotype might be due to replication related DNA damage.

"Sometimes the best way to learn something is by doing it wrong and looking at what you did."
Neil Gaiman

"It felt like a small forever."
Neil Gaiman, The Graveyard Book

Acknowledgement

Firstly, I would like to thank the support of the Hardiman Research Scholarship for funding my studies and my supervisor Dr. Stephen Rea for giving me the opportunity to join the lab. I would also like to thank the Beckman Fund and the Thomas Crawford Hayes Trust Fund for repeatedly supporting my research. Some of the performed assays would not have been possible without their financial aid.

Furthermore I will take the opportunity and thank all the principal investigators in the Centre for Chromosome Biology for the help and contribution to this work. In particular I am extremely grateful for the guidance, discussions and constructive criticism from Prof Ciaran Morrison who showed great support in struggles and helped in scientific advance. I would also like to highlight the help, support and enthusiasm of Dr. Andrew Flaus who awoke my interest in protein structures and of course made me like histones a little bit more than before. I also thank Prof Heinz-Peter Nasheuer for scientific support, Dr. Elaine Dunleavy as a young PI for being a role model for us, Prof Brian McStay and Prof Corrado Santocanale for making me judge my results with an outsiders eye and finally for Prof Robert Lahue for moral support and unexpected jokes. As part of the CCB I would also like to thank fellow researchers who helped this work with training, discussions, advice, reagents and moral support: Dr. Suzanna Prosser, Dr. Suraya Diaz, Dr. Muriel Voisin, Dr. Janna Lüβing, Dr. Sebastian Gornik and Dr. Michael Rainey. I would also like to thank all the people in the lab with whom I became friends with: Indu, Martin, Suzy, Janna, Sebastian, Kevin, Mairead, Tobias, Sebastian, Michael, Ebtissal, Yetty and Caitríona.

I would also like to thank Dr. Zheng Lai for accepting me in the lab and becoming a great support and a good friend in my first few months of PhD. As my partner in crime I would like to thank Karen Lane with whom we struggled, stumbled and hopefully learned together in these four years. I could not have imagined a better friend and colleague to work together with.

Finally I would also like to thank my family and friends (Annamari, Csilla, Zita, Petra és Brigi) at home for their unconditional, enduring support and friendship.

Declaration and contributions

I hereby declare that I have not obtained any previous qualification based on the work contained in this thesis. I performed all experiments and wrote the thesis under the supervision of Dr. Stephen Rea. Certain experiments performed by others were included in this work to complete the story are included below:

- Image capture of Figure 4.11 was performed by Dr. Muriel Voisin.
- Biotinylation time-course experiment and western blot analysis for the BioID analysis was performed by Karen Lane (Figure 5.2 A).
- The in house MSL2 antibody binding identification was performed by Alan O'Dwyer 4th year Biotechnology undergraduate student (**Appendix 1** - MSL2 and MSL1 antibody optimization).

1. Introduction

1.1. Chromatin structure and histone modifications

1.1.1. Chromatin structure

The eukaryotic genome is divided into chromosomes and each chromosome is packaged into a compact structure called chromatin. The basic unit of chromatin is the nucleosome. It contains two copies of four histone proteins (H2A, H2B, H3 and H4) called a histone octamer, with 146 bp of DNA wrapped 1.65 times around it (Luger et al., 1997, Kornberg and Lorch, 1999). The core nucleosome particles are connected to each other by variable length of linker DNA (~38 bp in humans) (Barski et al., 2007, Schones et al., 2008). With linker histone proteins (H1) the nucleosome arrays then fold into higher order chromatin structure. This structure can be modified by histone variants replacing canonical histones which leads to the alteration of the local fabric of the chromatin fibre (Volle and Dalal, 2014). The positioning of the nucleosome can also affect gene expression. The nucleosome spacing is established via chromatin remodelling or spacing complexes of imitation switch (ISWI) class enzymes (Gangaraju and Bartholomew, 2007, Zhou et al., 2016). Chromatin structure can also be altered through histone modifying enzymes which can facilitate DNA-templated process regulation and other chromatin related interactions by changing the chromatin accessibility (Kouzarides, 2007).

1.1.2. Histone modifications

Histones have a mainly globular structure with unstructured tails and can be subjected to a number of different modifications which can fundamentally alter the organization and function of chromatin (Figure 1.1). These modifications play an important role in the regulation of DNA related processes such as transcription, DNA repair and replication as well as the structure of the nucleosomes. In general they regulate transcription, repair, replication and mitosis, but acetylation, methylation, phosphorylation and ubiquitylation also plays role in DNA repair (Bannister and Kouzarides, 2011). Acetylation, methylation, phosphorylation and citrullination can also influence chromatin structure and dynamics, the binding of histones to chaperones and gene expression (Strahl and Allis, 2000, Jenuwein and Allis, 2001, Kouzarides, 2007, Tessarz and Kouzarides, 2014). In addition to providing binding

platforms for specific enzymatic complexes, histone modifications can also function as interaction-disrupting agents between a histone and a chromatin factor (Zegerman et al., 2002). So far over 15 different types of modifications have been identified: acetylation, methylation, phosphorylation, ubiquitylation, sumoylation, ADP ribosylation, citrullination, hydroxylation, butyrylation, 2-hydroxyisobutyrylation, crotonylation, propionylation, malonylation, formylation, succinylation and O-GlcNAcylation (Allfrey et al., 1964, Nishizuka et al., 1967, Rogers et al., 1977, Wilkinson, 1987, Matunis et al., 1996, Cohen, 2002, Chen et al., 2007, Jiang et al., 2007, Sakabe et al., 2010, Tan et al., 2011, Zhang et al., 2011b, Unoki et al., 2013, Christophorou et al., 2014, Dai et al., 2014).

These modifications can occur on different histones in a nucleosome and one histone can hold several modifications at a time, presenting a challenge for their identification and quantification (Garcia et al., 2007, DiMaggio et al., 2009). The process itself can also happen rapidly and the modified states predicted half-life can vary from being present for only a few minutes to longer and can also affect the half-life of the modified histone (Kouzarides, 2007, Barth and Imhof, 2010, Zee et al., 2010, Zheng et al., 2013, Zheng et al., 2016). Crosstalk between modifications is also possible and provides an extra level of complexity of the system (Lee et al., 2010a, Bannister and Kouzarides, 2011). Modifications either can be dependent upon another or can occupy the same site preventing the other from occurring (Lee et al., 2007, Kim et al., 2009).

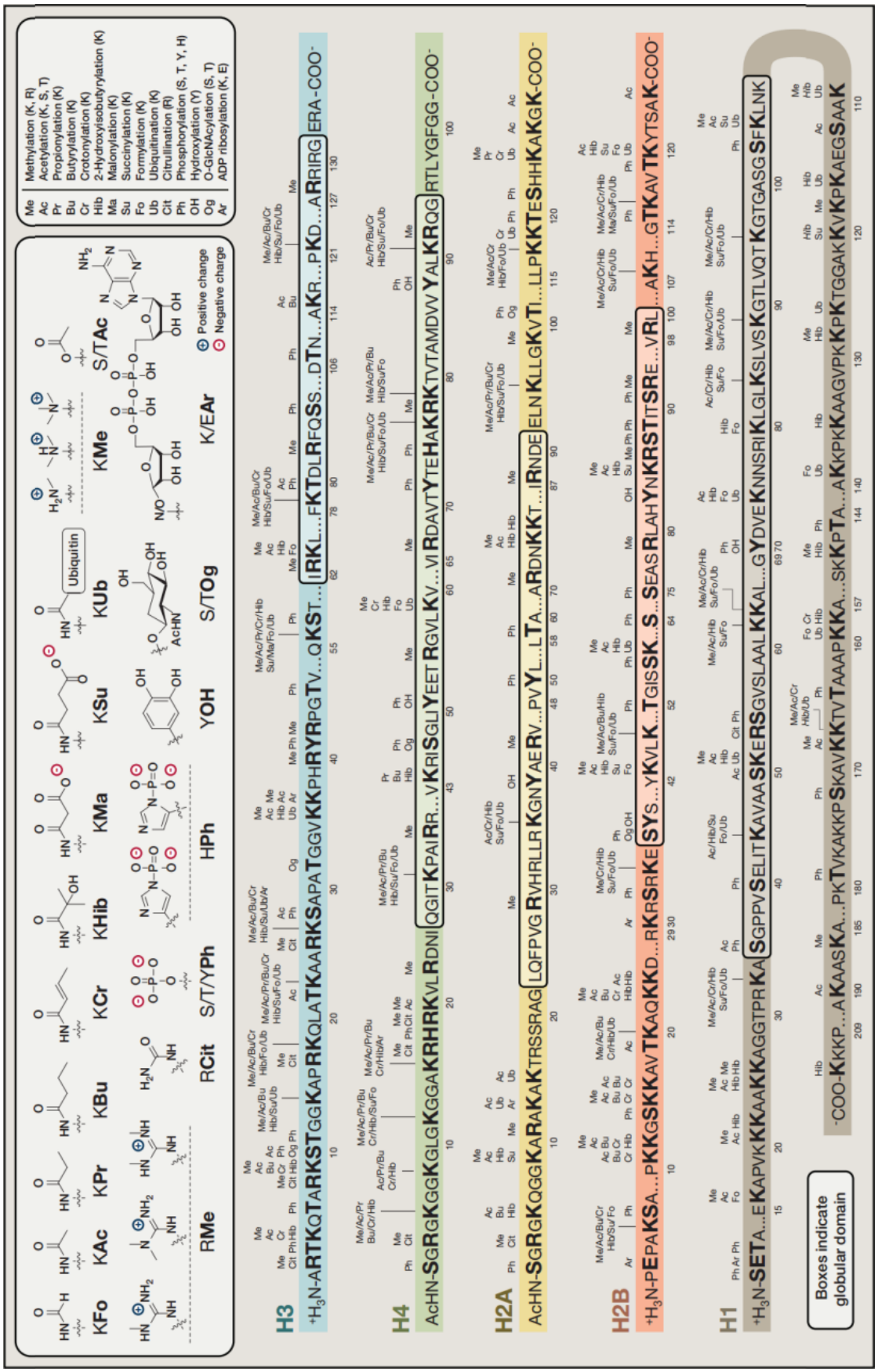

Figure 1.1: Posttranslational modifications of canonical histones. Schematic representation of the core histones and their known posttranslational modifications reported in human, mouse, and rat, including recently identified lysine acylation marks. Taken from (Huang et al., 2014).

Modifications relevant to this thesis are discussed in more details in the following sections.

1.1.2.1. Histone acetylation

Histone acetylation was the first discovered modification, originally related to active transcription (Allfrey et al., 1964). It is achieved by histone acetyl transferases enzymes (HATs) which transfer an acetyl group from acetyl-coenzyme A (acetyl-CoA) to the ε-amino group of a certain lysine residue. HATs are divided into three superfamilies based on their structural and acetylase domain similarities: GNAT, MYST, and CBP/p300. The GNAT (Gcn5-related N-acetyltransferase) family has highly conserved N- to C-terminal regions of C, D, A, and B motif. While region C is found in most GNATs but not in other HATs. Region A with a conserved Arg/Gln-X-X-Gly-X-Gly/Ala sequence is shared with the MYST family. This region was implicated in acetyl-CoA substrate recognition and binding (Dutnall et al., 1998, Wolf et al., 1998). The MYST (MOZ, Ybf2/Sas3, Sas2, and Tip60) family members contain the highly conserved MYST domain which is composed of an acetyl-CoA binding motif and a zinc finger. Members can also have additional common features such as chromodomains and plant homeodomain-linked (PHD) zinc fingers (Utley and Cote, 2003, Yang, 2004). Members of the MYST family are known to be involved in different cellular processes such as transcription, replication, DNA damage detection and repair. Hence problems with their activity are associated with numerous human diseases including cancer (Avvakumov and Cote, 2007). The CBP/p300 (CREB-binding protein and p300) complex is a unique class of acetyltransferase with distant relation to other HATs (Martinez-Balbas et al., 1998). CBP and p300 proteins are known transcriptional coactivators with close structural and functional homology but their HAT activity was a later discovery (Bannister and Kouzarides, 1996, Ogryzko et al., 1996). CBP/p300 is known to acetylate all histones both in the nucleosome and in their free form *in vitro*. Its HAT activity *in vivo* was shown to be required for activation mediated by different types of nuclear receptors (Korzus et al., 1998).

Histone acetylation is known to alter the nucleosomal fibre organisation and relaxing the DNA through neutralizing the positive charge of the lysine residues (Dion et al., 2005, Shogren-Knaak et al., 2006, Oppikofer et al., 2011). This permissive structural change provides access to DNA regions for different enzymes such as transcriptional

activators at promoter elements (Zentner and Henikoff, 2013). Most commonly the lysine acetylations are recognised by bromodomain (BRD) containing proteins, for example acetyltransferases such as bromodomain protein 4 (BRD4) which binds di- and tetra-acetylated H4 (Haynes et al., 1992, Dhalluin et al., 1999, Jung et al., 2014). Also, histone acetylation often correlates with additional, targeted acetylation of histones at promoter nucleosomes (Brown et al., 2000, Forsberg and Bresnick, 2001).

The acetylation of H4 at lysine 16 (H4K16ac) is particularly interesting for this study because the MSL (Male specific lethal) complex, the focus of this work, is the main acetyltransferase for this residue (originally identified in *Drososphila*) (Hilfiker et al., 1997). The histone acetylase MOF (Males absent on the first) a member of the MYST family of HATs, a catalytic subunit of the MSL complex is responsible for this modification. MOF is also part of the NSL (Nonspecific lethal) complex which was shown to perform H4K16ac as well and is suggested to regulate housekeeping gene expression (Lam et al., 2012). The two complexes also exist in humans and were found to possess the same H4K16 acetylation activity (Smith et al., 2005, Taipale et al., 2005). H4K16ac was found enriched in transcriptional start sites of active genes on autosomal chromosomes in mice and was shown to have a similar role to the *Drosophila* NSL complex (Taylor et al., 2013). Other findings show gene-body enrichment and a possible role in transcriptional elongation in mammals similar to the *Drosophila* MSL complex (Larschan et al., 2011). Transcriptional elongation of *FOSL1* gene was also found to be dependent on H3K9acS10ph/H4K16ac platform. At the *FOSL1* enhancer region pre-acetylated H3K9 is phosphorylated and bound by the 14-3-3 adaptor which then recruits MOF to the site for H4K16 acetylation. This event consequentially recruits BRD4 and he positive transcription elongation factor b (P-TEFb) to increase paused RNA polymerase II processivity (Zippo et al., 2009). H4K16ac level changes have been implicated in different types of cancer and alongside with H4K20 methylation was found to be a common hallmark of human cancer (Fraga et al., 2005). Breast tissue array analysis also showed that more invasive breast cancers seem to have low expression of MOF and H4K16 acetylation (Pfister et al., 2008). Besides, H4K16 acetylation plays a role in DNA repair, has been shown to help the recruitment of DNA repair proteins such as MDC1 (Li et al., 2010, Sharma et al., 2010) and cause impaired DNA repair upon reduction (Gupta et al., 2005, Taipale et al., 2005, Gupta et al., 2008). While the majority of acetylations

on H4K16 is performed by MOF, another member of the MYST acetyltransferase family, Tip60 is also able to acetylate the same residue (Miyamoto et al., 2008) and was shown to be a key factor in *C. elegans* male X chromosome decondensation (Lau et al., 2016).

Histone acetylation, like most posttranslational modifications, is a reversible process and histone deacetylases (HDACs) catalyse this process (Delcuve et al., 2012). These enzymes due to their role are involved in many repression phenomena (Khochbin et al., 2001). HDACs can be grouped into four different classes based on their sequence similarity to yeast deacetylases (de Ruijter et al., 2003). Class I HDAC family members are considered as classical HDACs and their deacetylation activity is Zn^{2+} dependent. This family contains HDAC1, HDAC2, HDAC3 and HDAC8 with the first three known to form multiprotein complexes such as NuRD, NODE or CoREST (Zhang et al., 1999, You et al., 2001, Liang et al., 2008). Class II HDACs are further subdivided into two categories Class IIa (HDAC4, HDAC5, HDAC7 and HDAC9) and Class IIb (HDAC6 and HDAC10). In relation to cancer and neurodegenerative diseases HDAC6 poses as a potential target since it is involved in the removal of misfolded proteins through aggresome formation or autophagy (Lee et al., 2010b, Ouyang et al., 2012). Class III HDACs similar to Class I require an additional molecule, the NAD^+ cofactor for their enzymatic activity. Class IV contains only HDAC11 which is also a zinc-dependent deacetylase but has low similarity to the other family members (Gao et al., 2002). Since its initial discovery it has emerged as a potential drug target in cancer since it plays a critical role in cancer cell survival (Delcuve et al., 2012, Deubzer et al., 2013, Thole et al., 2017).

1.1.2.2. Histone ubiquitylation

In contrast to other histone modifications, where small chemical groups are added to histone residues, ubiquitylation results in the transfer of an 8.5 kDa globular protein to a lysine residue (Kamadurai et al., 2009). Histone ubiquitylation has been shown to play important an role within the nucleus in transcription initiation and elongation, silencing, and DNA repair (Conaway et al., 2002, Schwertman et al., 2016).

The first ubiquitylation identified was at lysine 119 of histone H2A (H2AK119ub) which is also one of the most abundant histone modifications in mammalian cells (5–15% of total H2A) (Goldknopf et al., 1975, Osley et al., 2006, Vissers et al., 2008). It

has been shown that H2AK119ub represses transcription by blocking RNA polymerase II mediated elongation (Zhou et al., 2008). Its ubiquitylation is mediated by the Polycomb Repressor Complex 1 (PRC1) and it plays a critical role in the transcriptional silencing of the *HOX* genes and in X chromosome inactivation (Wang et al., 2004, Cao et al., 2005). However, more recent findings argue that a catalytically inactive PRC1 E3 ligase subunit ,RING1B, and subsequential loss of H2AK119ub does not affect gene upregulation or change in H3K27me3 status (Illingworth et al., 2015). H2AK119 ubiquitylation can also be induced by DNA damage, where it contributes to BRCA1 recruitment and DNA repair (Bergink et al., 2006, Wu et al., 2009, Ismail et al., 2010, Ginjala et al., 2011). Another important ubiquitylated histone is H2B which is the second most abundant ubiquitylated histone (1-2%) with an identified modification site at lysine 120 (H2BK120ub) (West and Bonner, 1980, Thorne et al., 1987). Both H2A119ub and H2B120ub have been found to be decreased in breast and prostate tumours, suggesting a role in cancer (Zhu et al., 2007, Prenzel et al., 2011). H2BK120ub modification is regulated by the Ring Finger Protein 20/40 (RNF20/40) and is associated with active gene expression. It is also involved in histone crosstalk and stimulation of H3K4 and H3K79 methylation via Dot1L and SET1 complex recruitment (Briggs et al., 2002, Zhu et al., 2005, McGinty et al., 2008, Kim et al., 2009). Another H2B ubiquitylation at lysine 34 (H2BK34ub) was shown to interact with PAF1 and promote RNA polymerase II processing after stalling. This modification is promoted by the human MSL2 (Male specific lethal 2), a subunit of the MSL (Male specific lethal) complex which is the main topic of this study (Wu et al., 2014a). This modification also affects H2BK120 ubiquitylation, H3K4 and H3K79 methylation and probably plays a role in the upstream activation of these modifications (Werner and Ruthenburg, 2011). H3 and H1 have also been reported to be ubiquitylated; H1 ubiquitylation at lysine 63 plays a key role in DNA double-strand break signalling where ubiquitylated H3 was found in elongating spermatids in rat testes (Chen et al., 1998, Pham and Sauer, 2000, Thorslund et al., 2015). H3 and H4 ubiquitylation have been observed in response to UV (ultraviolet) irradiation induced DNA damage, promoted by the CUL4-DDB-ROC1 complex (Wang et al., 2006). Histones are mainly monoubiquitylated, with one single ubiquitin molecule attachment to highly conserved lysine residues (Cao and Yan, 2012). However, H2A and H2B can also be modified by polyubiquitylation. K63-linked polyubiquitylation of H2A and H2A.X is

required for the DNA damage response, in particular for the assembly of DNA repair proteins (Huen et al., 2007, Kolas et al., 2007, Mailand et al., 2007).

1.2. Ubiquitylation

In recent years ubiquitylation has been recognised as an important modulator of numerous cellular processes, such as proteasomal degradation, DNA repair, endocytosis, autophagy, transcription, signalling, trafficking, immunity and inflammation (Conaway et al., 2002, Roos-Mattjus and Sistonen, 2004, Haglund and Dikic, 2005, Urbe, 2005, Bhoj and Chen, 2009, Kraft et al., 2010, Schwarz and Patrick, 2012, Corn and Vucic, 2014, Schwertman et al., 2016). The process of ubiquitylation is a cascade mechanism, where three distinctive group of enzymes transfer and covalently bind a ubiquitin molecule to a substrate protein (Figure 1.2).

Ubiquitin, first identified in 1975 (Goldknopf et al., 1975, Goldstein et al., 1975), is encoded by four different genes in humans: *Ubb*, *Ubc, Rps27a* and *Uba52*. *Ubb* and *Ubc* encode 3 and 9 tandem ubiquitin molecules which are cleaved by deubiquitylating enzymes (DUBs) to separate identical functional monomeric ubiquitin units (Kimura and Tanaka, 2010). *Rps27a* and *Uba52* encode fusions with ribosomal protein subunits of S27a and L40 respectively (Oh et al., 2013). Ubiquitin is an 8.5 kDa protein consisting of 76 amino acids (Hershko and Ciechanover, 1998). It forms a compact globular structure where its exposed C-terminal tail can be covalently linked to other proteins (Figure 1.3). In the first step of ubiquitylation, ubiquitin-activating (E1) enzymes activate ubiquitin by forming an E1-ubiquitin thioester bond in an ATP dependent manner. Then ubiquitin is transferred to ubiquitin-conjugating (E2) enzymes in the same manner to form an E2-ubiquitin thioester bond. At the last step, ubiquitin-ligating (E3) enzymes help the formation of an isopeptide bond between the lysine residue of the substrate and the C-terminal tail of the ubiquitin molecule (Komander, 2009). E3 enzymes can facilitate the ubiquitin-substrate binding in two different ways. They can either form a thioester bond with ubiquitin before transferring it to the substrate (HECT domain E3 group) or in the case of RING type E3 ligases the enzymes directly facilitate the ubiquitin transfer from the E2 enzyme to the substrate (Huibregtse et al., 1995, Scheffner et al., 1995). The role of E3 ligases is to determine the substrate specificity, while E2 enzymes mediate the change from ubiquitin chain initiation to chain elongation, regulate

ubiquitin chain processivity and define the type of ubiquitin linkage (Windheim et al., 2008, Ye and Rape, 2009). Since E2 and E3 enzymes have specific and distinct roles, it is expected that there are a larger number of these enzymes in the proteome. While there are only two reported E1 enzymes (Ciechanover et al., 1982, Pelzer et al., 2007), the number of E2 enzymes is over 30 (Wenzel et al., 2011b) and there are more than 500 E3 enzymes identified in mammals so far (Li et al., 2008b).

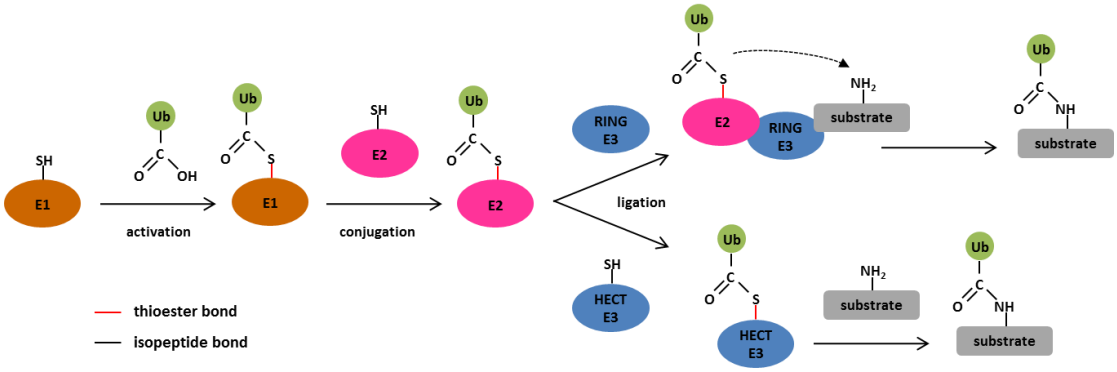

Figure 1.2: Schematic representation of the ubiquitin cascade system. Intermediate thioester bonds are formed between ubiquitin and E1, E2 (and E3 ligases) until ubiquitin is covalently bound to the substrate molecule. RING and HECT type E3 ligases differ in their way of promoting ubiquitin linkage to the substrate. Adapted from (Husnjak and Dikic, 2012).

Although ubiquitin-substrate linkage mainly occurs on lysine residues, ubiquitin can also be attached to cysteine, serine, and threonine residues (Cadwell and Coscoy, 2005, Ravid and Hochstrasser, 2007, Wang et al., 2007) and to the amino group at the N-terminus of the substrate (Ciechanover and Ben-Saadon, 2004).

Substrates can be mono-ubiquitylated on different residues at the same time, resulting in multiple mono-ubiquitylation. Besides mono-ubiquitylation, ubiquitin molecules can also bind to other ubiquitin molecules attached to a substrate, forming ubiquitin chains (Figure 1.3). The chain formation can happen through the lysine residues of the ubiquitin molecules (K6, K11, K27, K29, K33, K48, K63 linkages) or through the N-terminal amino group of another ubiquitin molecule, forming linear (head-to-tail or M1) ubiquitin chains. Besides this eight different homotypic linkage types, heterotypic and mixed ubiquitin chain formations are also possible (Peng et al., 2003). Different cellular function can also be related to specific chain formations. The most characterized ubiquitin chains are K48-linked, involved in proteasomal degradation, and K63-linked ubiquitin polymers, which are implicated in the DNA

damage response, signalling and trafficking (Hicke et al., 2005, Grabbe and Dikic, 2009). K11-linked ubiquitin chains have also been associated with different biological processes, such as cell cycle regulation (Jin et al., 2008, Matsumoto et al., 2010), endoplasmic reticulum-associated degradation (ERAD) and TNFα signalling (Dynek et al., 2010).

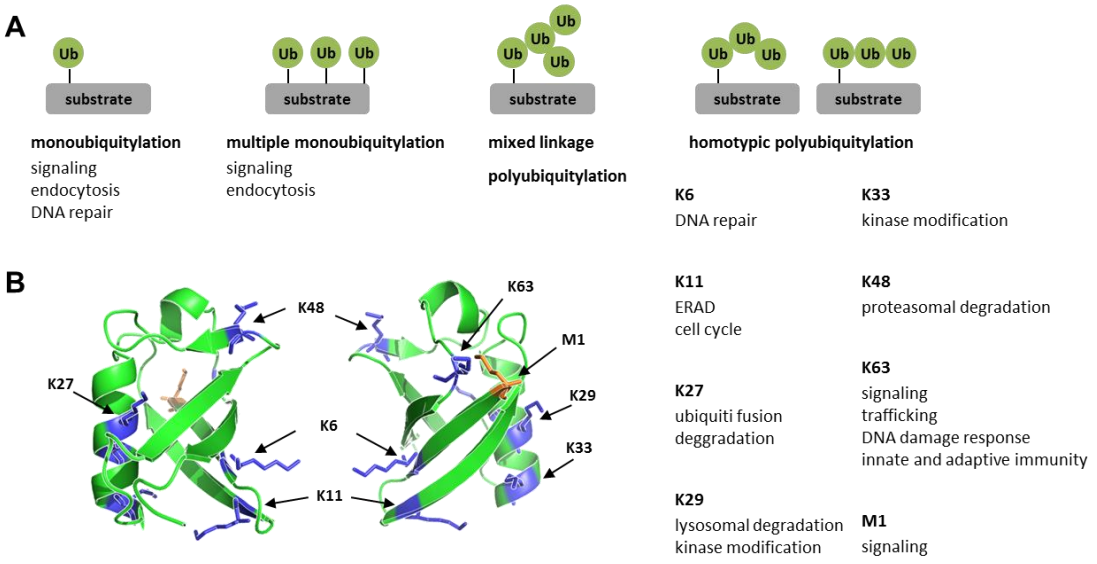

Figure 1.3: Schematic representation of different ubiquitin modifications and linkages. A) Different mono- and polyubiquitylations can be linked with various cellular processes. B) Structure of ubiquitin molecule with the seven lysine and one methionine residues highlighted. Adapted from (Husnjak and Dikic, 2012).

Ubiquitylation is a reversible process, where deubiquitinating enzymes (DUBs) are able to remove ubiquitin from target proteins.

1.3. RING finger domain E3 ligases

The RING (Really Interesting New Gene) family constitutes the vast majority of E3 ligases, containing over 600 proteins. The domain itself was first described in 1991 (Freemont et al., 1991). A typical RING finger binding platform for E2 conjugases in most cases contains a Cys-X_2-Cys-$X_{[9-39]}$-Cys-$X_{[1-3]}$-His-$X_{[2-3]}$-His/Cys-X2-Cys-$X_{[4-48]}$-Cys-X_2-Cys sequence, where X represents any amino acid and the fifth histidine residue can be replaced by cysteine. Based on this, RING domains can be classified as H2- or HC-type RINGs (Borden and Freemont, 1996). The structure of this RING finger is stabilised with the binding of two Zn^{2+} in a cross-braced arrangement. Proteins can also contain more than one RING domain like Mind bomb with three

RINGs (Itoh et al., 2003, Barsi et al., 2005) and the members of the RING-IBR-RING (RBR) class for example Parkin, HHARI and two members of the Linear Ubiquitin Chain Assembly Complex (LUBAC) HOIP and HOIL-1L. These proteins have a consensus RING sequence (RING1) followed by an in between RING (IBR) region which is Cys-rich and a third RING domain (RING2). RBRs are found to have a RING-HECT hybrid mechanism where after the initial binding of E2 by the RING1 domain ubiquitin is transferred to a Cys residue within the RING2 domain before conjugating it to the substrate (Wenzel et al., 2011a, Smit et al., 2012, Stieglitz et al., 2012, Lazarou et al., 2013).

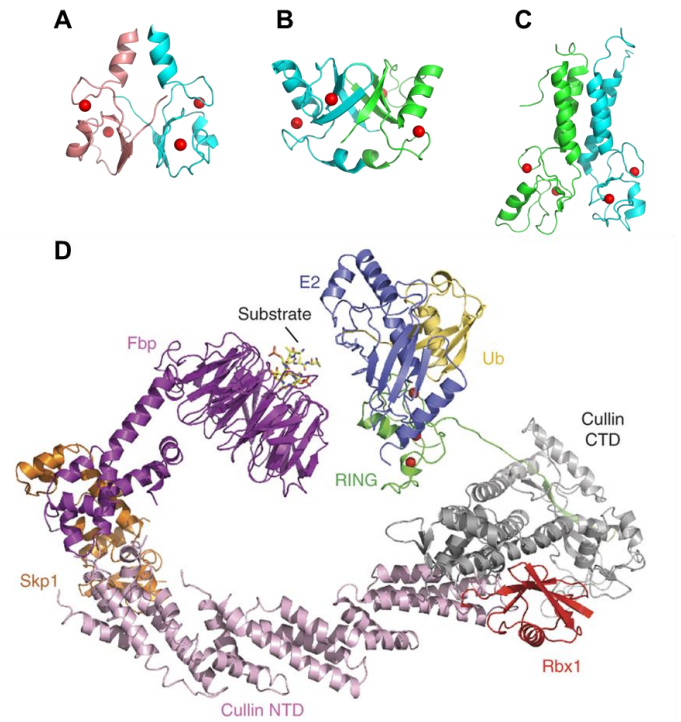

Figure 1.4: RING finger E3 ligases. Different types of RING dimers and a multi-subunit complex. A) BIRC7 homodimer B) Mdm2-MdmX heterodimer C) BRCA1-BARD1 heterodimer D) Cullin E3 ligase composite model adapted from (Berndsen and Wolberger, 2014)

RING type proteins are known to form monomers, but most notably they tend to form hetero- or homodimers and can also be part of a multi-subunit complex (Figure 1.4). While most of the homodimeric RINGs have the capacity to interact with E2 ligases with both RING proteins (cIAP, RNF4, BIRC7), heterodimeric pairs tend to just have one E2 binding RING and an enhancer, such as the BRCA1-BARD1 dimer (Metzger et al., 2012). Dimers can be formed using sequences outside of the RING domain, or the RING itself can be responsible for the dimerization as well. In either

case, the E2 binding surface is facing away from the complex. Generally E3s with N- or C-terminal RING domains tend to interact with their α–helical regions flanking the RINGs like Rad18, BRCA1-BARD1 and RING1B-Bmi1 (Brzovic et al., 2001, Li et al., 2006, Huang et al., 2011). In contrast E3s with RINGs in their extreme C-terminal regions tend to dimerise through their interleaved C-terminus for example Mdm2-MdmX and RNF4, IDOL, BIRC7 and cIAP homodimers (Linke et al., 2008, Mace et al., 2008, Liew et al., 2010, Zhang et al., 2011a, Dou et al., 2012). These preferences are not exclusive and E3s can dimerise through other domains as well (Bartkiewicz et al., 1999, Vander Kooi et al., 2006, Xu et al., 2008). There are also other RING E3s which act as a part of a multi-subunit complex. For example the Cullin Ring Ligase (CRL) superfamily typically contains a cullin protein, a small RING protein, an adaptor protein and interchangeable substrate recognition elements (Sarikas et al., 2011). An even more complex multi-subunit E3 is the anaphase promoting complex/cyclosome (APC/C) which contains 13 core subunits including a cullin-like and a RING protein (Schreiber et al., 2011). Some multi-subunit RING E3 complexes found in yeast can also contain multiple RING proteins, such as the glucose-induced degradation deficient (GID) or the PEX ligase (Platta et al., 2009, Menssen et al., 2012).

1.4. Deubiquitylation

During proteasomal or lysosomal degradation the substrate is degraded to small peptides while ubiquitin molecules are recycled (Clague and Urbe, 2006, Cohen-Kaplan et al., 2016, Collins and Goldberg, 2017). This recycling of ubiquitin molecules prior to protein degradation facilitates a longer half-life of ubiquitin *in vivo* (Lam et al., 1997, Liu and Jacobson, 2013). The disruption of ubiquitin cleavage prior to degradation was suggested to cause imbalance in free and substrate conjugated ubiquitin ratio (Hanna et al., 2006, Chen et al., 2011). Besides the aforementioned processes however, ubiquitylation is a reversible process, counterbalanced by deubiquitylating enzymes (DUBs) restoring the substrate's unmodified state (Ventii and Wilkinson, 2008).

DUBs belong to the protease superfamily and can be further divided into six subfamilies based on sequence similarities and their likely mechanisms of action (USP, UCH, OTU, MJD, MINDY and JAMM) (Reyes-Turcu et al., 2009, Abdul

Rehman et al., 2016). Four of the subfamilies are cysteine proteases, which perform their enzymatic activity through a covalent intermediate formation with the ubiquitin molecule and the release of the substrate. Further reaction of the intermediate with a water molecule then separates the enzyme and the ubiquitin (Nijman et al., 2005). The sub classification of these proteases is based on their ubiquitin protease domains. The largest and most diverse subfamily of all are the ubiquitin-specific proteases (USPs) which comprise over 60 proteins in humans. USPs have a conserved catalytical Cys and His box motif, where the cysteine and histidine alongside with an aspartate residue make up the catalytic triad which is essential for the protease activity (Hu et al., 2002). The ubiquitin C-terminal hydrolase (UCH) group has 4 human protein members which have been found to favour relatively small (up to 20–30 amino acids) protein substrates (Amerik and Hochstrasser, 2004). They are thought to act in ubiquitin recycling and in the processing of newly synthesized ubiquitin (Larsen et al., 1998). The Otubain protease (OTU) group contains 14 human proteins and has an incomplete catalytic triad which is stabilized by a hydrogen bonding network (Nanao et al., 2004). Although their physiological role is unclear research on an OTU member showed that it probably interacts with polyubiquitin (Evans et al., 2003, Wang et al., 2009, Mevissen et al., 2013). The Machado-Joseph disease (MJD) protease group has five identified human protein members. So far only one Ataxin-3 has been shown to harbour deubiquitylase activity (Burnett et al., 2003) and CAG instability in its gene leads to Machado-Joseph disease (Berke et al., 2004). A new subfamily, MINDY (motif interacting with Ub-containing novel DUB family) containing four proteins, has been recently identified and shown to be highly selective at cleaving K48-linked polyubiquitin. These proteins have a distinct folding variant of the cysteine protease catalytic domain and might possess diverse functional roles (Abdul Rehman et al., 2016). The sixth subfamily is the JAB1/MPN/Mov34 (JAMM) zinc-dependent metalloprotease group with 14 human protein members. Metalloproteases differ from cysteine proteases in using a Zn^{2+} bound polarized water molecule to generate a noncovalent intermediate with the substrate (Ambroggio et al., 2004, Nijman et al., 2005). The members of this group seemingly adopted new protease functions through evolution suggesting that some of the human JAMM proteases might be involved in other, not ubiquitin related processes (Burns et al., 2005, Nijman et al., 2005).

1.5. The MSL complex

1.5.1. The MSL complex in *Drosophila*

Heteromorphic sex chromosomes controls sex determination in different taxa, such as nematodes, fruitflies and mammals and dosage compensation is a way to deal with male (XY) and female (XX) sex chromosome imbalance (Straub and Becker, 2007). These organisms evolved to compensate for the disequilibrium through dosage compensation in different ways and to different extents (Dementyeva and Zakian, 2010). In *Drosophila*, male flies upregulate their X chromosome linked gene transcription twofold. This highly specific regulation is achieved through the activity of the MSL (Male specific lethal) complex (Hamada et al., 2005, Straub et al., 2005, Prestel et al., 2010). The *Drosophila* MSL or dosage compensation complex (DCC) itself consists of five proteins (Figure 1.5), MSL1 (Male specific lethal 1), MSL2 (Male specific lethal 2), MSL3 (male specific lethal 3), MOF (Males absent on the first), and MLE (Maleless) and two noncoding RNAs *roX1* (RNA on the X 1) and *roX2* (RNA on the X 2) (Belote and Lucchesi, 1980a, Hilfiker et al., 1997, Park and Kuroda, 2001, Quinn et al., 2014). All MSL proteins, with the exception of MSL2, are expressed in both sexes. It was found that *Msl2* transcripts in females retain a 133 nucleotides intron sequence, which is spliced from the male transcripts. In females SXL (Sex lethal) inhibits the 5' and 3' UTR splicing and translation (Kelley et al., 1995) and promotes the nuclear retention of the *Msl2* mRNA.(Graindorge et al., 2013). Thus the expression of MSL2 is crucial to maintain proper dosage compensation and ectopic expression of the protein in female flies is lethal (Kelley et al., 1995). However, several studies support the hypothesis that the MSL complex is not the direct mediator of X chromosome dosage compensation, but that binding of the MSL complex actually reduces the transcriptional activation mediated by H4K16ac down to twofold (Prestel et al., 2010, Schiemann et al., 2010, Conrad and Akhtar, 2012, Sun et al., 2013).

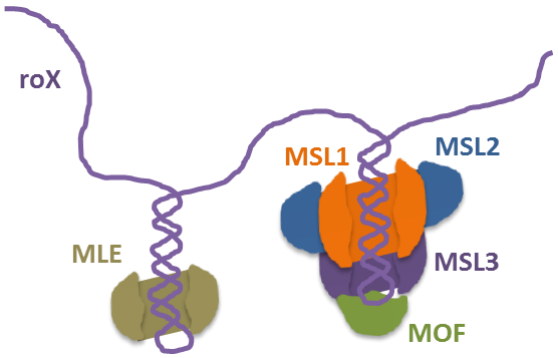

Figure 1.5: The *Drosophila* MSL complex. The complex consists of MSL1, MSL2, MSL3, MOF, a loosely attached MLE protein and two noncoding RNAs *roX1* and *roX2* (Quinn et al., 2014)

The way the MSL complex binds and regulates X chromosome linked genes is understood as follows. In the absence of other MSL proteins MSL1 and MSL2 assemble the core of the complex and recognize around 140 binding sites including the two *roX* genes across the X chromosome. These regions are called high-affinity sites (HASs) or chromatin entry sites (Palmer et al., 1994, Lyman et al., 1997, Alekseyenko et al., 2008, Straub et al., 2008). The incorporation of *roX* RNAs contributes to the stabilisation of the MSL complex and promotes further specificity to the HAS sites (Li et al., 2008a). Binding of *roX* RNAs are aided by the ATP-dependent DEXH box RNA and DNA helicase MLE which is peripherally associated with the complex by RNA interactions (Gu et al., 2000, Meller et al., 2000). From here, MSL spreads to lower affinity sites to coat the X chromosome (Kelley et al., 1999, Meller and Rattner, 2002, Park et al., 2002, Demakova et al., 2003). It was suggested that interactions through r*oX*'s bridges between multiple MSLs could stabilize chromatin binding (Conrad and Akhtar, 2012). Also, the RNA helicase activity of MLE is required for spreading along the X chromosome (Morra et al., 2008). Transcriptional activation is achieved through the acetylation of H4K16 in the coding regions which is mediated by the acetyltransferase MOF (Hilfiker et al., 1997, Akhtar and Becker, 2000). *In vitro* experiments suggest that the binding of MOF with MSL1 leads to its sequestration on the X chromosome, while the association of MSL3 to the MSL complex mediates the H4K16 specific acetylation (Morales et al., 2005). It has been shown that MSL3 contributes to substrate specificity by binding to trimethylated H3K36, which overlaps with HAS sites and is enriched in the transcribed regions of active genes (Larschan et al., 2007). However, other studies

with human MSL proteins point towards potential H4K20me1 and H4K20me2 binding instead of a direct MSL3-H3K36me3 interaction. (Kim et al., 2010, Moore et al., 2010).

In the context of dosage compensation, the MSL complex was found to interact with nuclear pore components Megator (Mtor) and Nucleoporin 153 (Nup153) which affect the X chromosome localization of the complex (Mendjan et al., 2006). Nucleoporin associated regions (NARs) are found on the male X chromosome and are proposed to promote opened chromatin environment thus stimulating transcription (Vaquerizas et al., 2010). In addition, heterochromatin proteins suppressor of variegation 3-7 (Su(var)3-7) was shown to be required for X chromosome-restricted DCC targeting. Su(var)3-7 and heterochromatin protein 1 (HP1) affect male X chromosome morphology through the enhancement or suppression of the PEV (position effect variegation) in a dose dependent manner. (Spierer et al., 2005, Spierer et al., 2008). Furthermore DNA supercoiling factor (SCF) in conjunction with topoisomerase II generates negative supercoils in the DNA and affects the expression level of X chromosome linked genes. Moreover, the knockdown of SCF leads to male lethality and SCF showed a co-localization as well as a weak interaction with the MSL complex (Furuhashi et al., 2006). In previous studies it was observed, that mutations in ISWI (imitation SWI) and NURF301 (nucleosome-remodeling factor 301), subunits of the NURF complex cause X chromosomal defects in male files, which suggests a counteracting activity against H4K16 acetylation helping to achieve a balanced chromatin state (Deuring et al., 2000, Corona et al., 2002). Another histone modification, H3S10 phosphorylation was shown to be up-regulated on the male X chromosome and its kinase JIL-1was found to interact with the MSL complex suggesting a role in dosage compensation (Jin et al., 1999, Jin et al., 2000, Johansen and Johansen, 2006).

In summary, the DCC plays important role mediating dosage compensation in *Drosophila* by regulating X chromosome linked global gene expression. Within the complex MSL2 expression is vital and allows the assembly of the DCC only in male flies (Kelley et al., 1995).

1.5.2. The MSL complex in humans

The MSL complex is evolutionary conserved from flies to humans, and MSL orthologues from yeast to humans exist (Sanjuan and Marin, 2001).

	Domains	% of similarity	Function
MSL1	Coiled-coil PEHE	21.8% 23.6%	interaction with MSL2, MSL3 and MOF
MSL2	RING CXC	32.5% 40.5%	E3 ubiquitin ligase, homeostasis, DNA binding, X targeting
MSL3	Chromo MRG	43.3% 22.4%	H3K36me3, H4K20me, DNA binding?, stimulates HAT activity
MOF	Chromobarrel HAT	32.9% 63%	modulates HAT activity, histone acetyltransferase
MLE	RB1/2/ ATPase/ Helicase/ G-rich	-	dsRNA binding, ATP hydrolisis, rox RNA unwinding, modulates RNA binding specificity

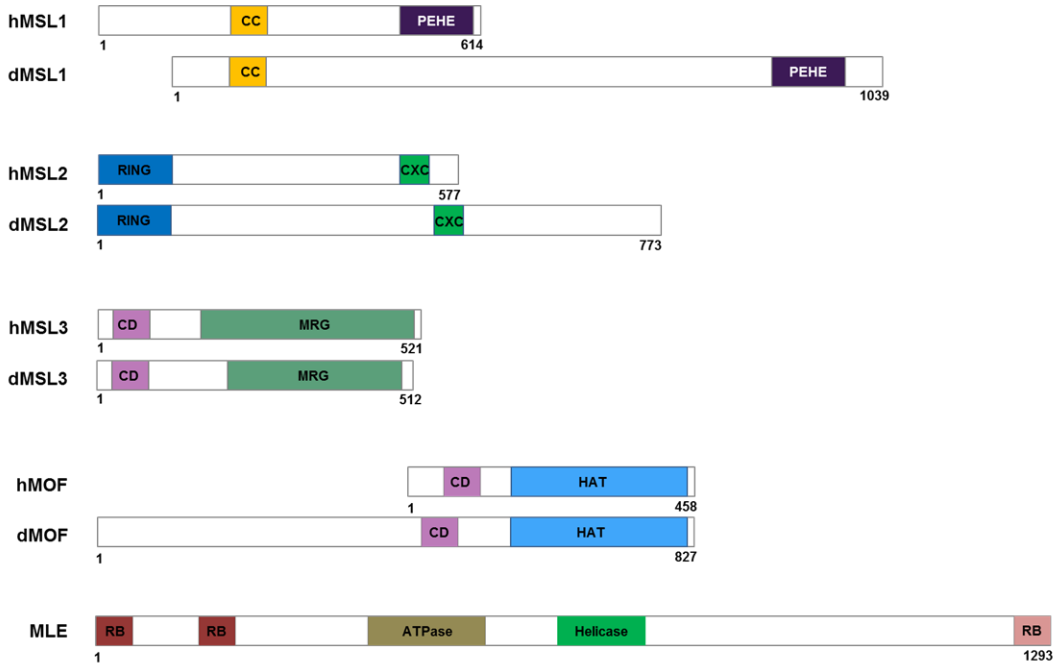

Figure 1.6: Overview of the domain architecture and functions of the human and *Drosophila* MSL complex proteins. CC: coiled-coil, PEHE: proline - glutamic acid – histidine - glutamic acid, RING: really interesting new gene, CXC: cysteine-rich domain, CD: chromodomain, MRG: morf-related gene, CB: chromobarrel domain, HAT: histone acetyltransferase, RB: double-stranded RNA binding domain, G: glycine-rich C-terminus. Adapted from (Keller and Akhtar, 2015).

However, there is relatively little known about the human complex and no evidence was found for a role in dosage compensation, which is fundamentally different to the *Drosophila* strategy (Mendjan et al., 2006, Chow and Heard, 2009). So far all five of the human MSL proteins have been identified but only four has been shown to form the human complex, MSL1, MSL2, MSL3 and MOF (Smith et al., 2005, Li et al.,

2009) (Figure 1.6). The involvement of the MLE orthologue RNA helicase A (RHA) to the other human MSL proteins is still unclear (Lee and Hurwitz, 1993, Robb and Rana, 2007). Also, there is no evidence of any RNA component in the complex. However, similar to the *Drosophila* MSL complex, the human proteins also exhibit H4K16 acetylation activity through MOF (Smith et al., 2005, Taipale et al., 2005). In recent years the structural background of the MSL complex was investigated and partial crystal structures related to the interacting parts of the subunits were solved (Kadlec et al., 2011, Hallacli et al., 2012) (Figure 1.7). Moreover, evidence from *Drosophila*, mouse and human studies have shown that the MSL complex is implicated in the DNA damage response, replication and transcription (Schwaiger et al., 2009, Wu et al., 2014a). Details on the involvement of the human proteins in these cellular processes are discussed in the following sections.

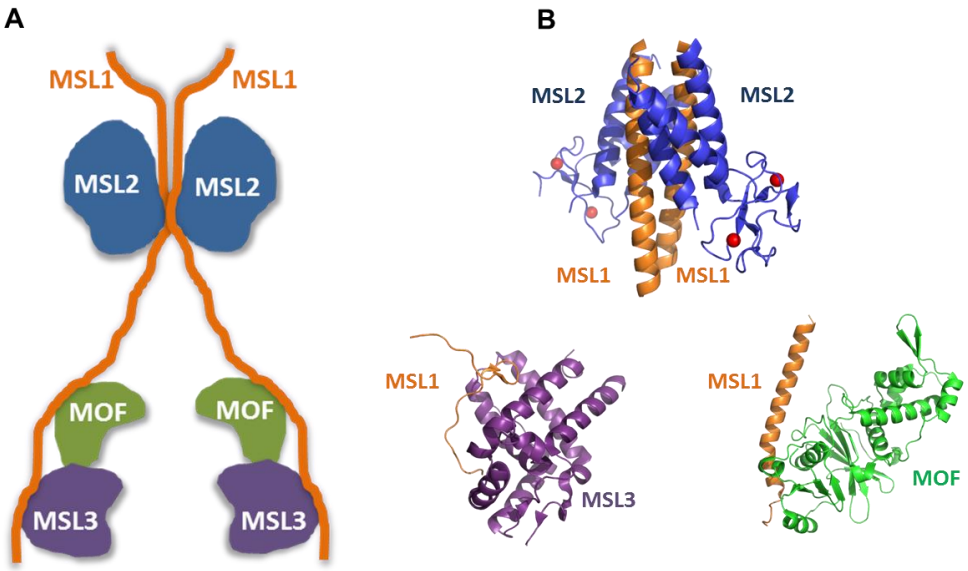

Figure 1.7: The human MSL complex. The complex consists of MSL1, MSL2, MSL3 and MOF. A) Proposed model of the MSL complex B) Structure of the MSL subunits binding sites, adapted from (Kadlec et al., 2011, Hallacli et al., 2012)

1.5.2.1. MSL1

The human male specific lethal 1 (MSL1) protein consist of 614 amino acids and contains an N-terminal coiled-coil domain, a Pro-rich region and a C-terminal PEHE domain (Marin, 2003, Dmitriev et al., 2005) (Figure 1.6). The coiled-coil domain is responsible for the interaction with MSL2 (Li et al., 2005, Hallacli et al., 2012) while the PEHE domain and the following region mediates MOF and MSL3 interaction

(Morales et al., 2004, Smith et al., 2005, Kadlec et al., 2011). In mice there are five known Msl1 isoforms and where isoform A-C are ubiquitously expressed, isoform D and E are testis specific (Dmitriev et al., 2005). It has also been found that MSL1 has two nuclear localization signals (NLSs). The presence of both NLS allows intra-nuclear focal accumulation of the protein. The recently discovered NLS1 is present in all isoforms and is highly conservative in mammals, whereas the NLS BP which is localised in the PEHE domain, is specific to isoform A, B, and D (Dmitriev et al., 2014).

While MSL1 plays an important role in the assembly of the MSL complex, so far there is no evidence about any enzymatic activity of the protein. However, it has been found that MSL1 interacts with different proteins and possibly plays a role in several cellular processes. For example, it was discovered that through negative regulation by p8 MSL1 interacts with 53BP1 which serves as a scaffold in a potential MSL1-dependent HAT DNA-repair activity (Gironella et al., 2009). Interaction with pancreatic cancer related Nupr1 is induced by DNA damage and their recruitment on DNA regulated by MSL1 facilitates the expression of DNA repair genes. (Aguado-Llera et al., 2013). All these findings suggest a potential role for MSL1 in the DNA damage response. It has also been indicated that MSL1 plays a role in the recruitment of tissue specific transcription factors through interactions with NOP17/Pih1d1, TTC4 a TPR-containing molecular co-chaperone (Dmitriev et al., 2007, Dmitriev et al., 2009) and Foxp3 (Rudra et al., 2012). Furthermore, MSL1 seems to be involved in the regulation of nucleo-cytoplasmic transport of molecular co-chaperones (Crevel et al., 2001, Crevel et al., 2008).

1.5.2.2. MSL2

The male specific lethal 2 (MSL2) protein comprises 577 amino acids and contains a CXC and an N terminal RING domain (Figure 1.6). It has been first identified in *Drosophila* (Belote and Lucchesi, 1980b) as part of the MSL (Male specific lethal) complex and it was characterized in 1998 (Copps et al., 1998). Through two long helices (α1 and α3) surrounding the RING domain it interacts with MSL1 forming a heterodimer, resulting in conformational changes facilitating its enzymatic activity (Hallacli et al., 2012). MSL2 itself acts through a RING finger domain which has E3 ubiquitin ligase activity (Kruse and Gu, 2009, Wu et al., 2011). While the CXC

domain is known as a DNA binding motif structural studies revealed, that it has an unusual zinc-cysteine cluster and shows structural homology to histone lysine methyltransferase pre-SET motifs (Zheng et al., 2012).

In *Drosophila* MSL2 plays a key part in the MSL complex assembly. It is only expressed in male flies and its ectopic expression in females is lethal due to overexpression of X chromosomal genes (Kelley et al., 1995). MSL2 also sustains MSL complex stoichiometry by poly-ubiquitylating itself and the other subunits (Villa et al., 2012). Other findings also propose that the ubiquitylation activity of MSL2 towards H2B at lysine 31 might play a role in *Drosophila* dosage compensation, since point mutations, that disrupt this activity in flies, lead to male lethality (Copps et al., 1998).

Studies in mouse embryonic stem cells (ESCs) suggest that MSL2 and the MSL complex could also play a role in mammalian dosage compensation through X chromosome inactivation. MSL1 and MSL2 have been identified among the key regulators of *Tsix* transcription and the depletion of either proteins in differentiating cells led to enhanced accumulation of *Xist* accompanied by increased number of cells with two inactive X chromosomes (Chelmicki et al., 2014).

Although there is not much known about the human protein, it has been shown that when overexpressed MSL2 can monoubiquitylate p53 at lysine 351. This promotes the translocation of p53 to the cytoplasm where it induces mitochondrial-dependent apoptosis (Muscolini et al., 2011). It was shown to regulate H2B lysine 120 ubiquitylation as well as H3K4 and K79 methylation via crosstalk and by promoting chromatin association of the RNF20/40 complex. It has also been found that MSL2 directly binds to the *HOXA9* and *MEIS1* loci, activating their transcription (Wu et al., 2011). Experiments using human and chicken DT40 cells indicate that MSL2 is involved in the DNA damage response (Lai et al., 2013). Furthermore, it has been reported that MSL2, in tandem with MSL1, monoubiquitylates histone protein H2B at lysine 34 and it also binds directly to PAF1 promoting stalled RNA polymerase II processing (Wu et al., 2014a). A recent study using transgenic mice and clinical samples showed the potential involvement of MSL2 in maintaining HBV (hepatitis B virus) cccDNA (closed circular DNA) stability through degradation of APOBEC3B (Apolipoprotein B mRNA editing enzyme catalytic subunit 3B) by ubiquitylation in

hepatoma cells. This finding suggests a role for MSL2 as a promotion factor which can selectively activate extrachromosomal DNA (Gao et al., 2017).

1.5.2.3. MSL3

Male specific lethal 3 (MSL3) protein consists of 521 amino acids and contains an N terminal Chromo (Chromatin Organization Modifier) domain and a C terminal MRG domain (Figure 1.6). Through the MRG domain it interacts with MSL1 (Kadlec et al., 2011). In *Drosophila* the Chromo domain is known to contribute to the nucleic acid and nucleosome binding of the MSL complex as well as its proper targeting and spreading (Buscaino et al., 2006, Sural et al., 2008). *In vitro* and structural studies suggest that the chromatin targeting of MSL3 is achieved by binding to H4 lysine 20 mono methylation (H4K20me1) in both humans and flies (Kim et al., 2010, Moore et al., 2010).

1.5.2.4. MOF

Males absent on the first (MOF) protein consists of 458 amino acids and contains an N terminal MYST HAT (histone acetyltransferase) domain and a C terminal Chromo domain (Figure 1.6). Through the HAT domain it interacts with MSL1 (Kadlec et al., 2011). It has been first identified as a member of the dosage compensation MSL complex in *Drosophila* (Hilfiker et al., 1997, Akhtar and Becker, 2000). This complex is responsible for the upregulation of X chromosome linked genes in male flies through direct activation (Straub et al., 2005). The MSL complex only forms in male flies since the expression of the member MSL2 is prevented by the SXL protein in female flies through RNA intron splicing inhibition (Kelley et al., 1997, Forch et al., 2001, Penalva and Sanchez, 2003). MOF however also associates with the NSL (Nonspecific lethal) complex (NSL1, NSL2, NSL3, MCRS2, MBD-R2, and WDS) which in contrast is ubiquitously expressed in both sexes and plays a major role in the regulation of transcription in *Drosophila* (Raja et al., 2010). It has also been shown that MOF is able to acetylate MSL3 at lysine 116 in *Drosophila* disrupting its interaction with RNA which contributes to the regulation of the MSL complex (Buscaino et al., 2003).

MOF is the most well studied member of the MSL complex and, having a wide range of interactors, plays an important role in several cellular processes. As part of the human MSL complex it is responsible for the bulk acetylation of H4K16. Besides it

has been shown to acetylate several non-histone proteins such as p53, TIP5 and Nrf2 (Sykes et al., 2006, Zhou et al., 2009, Chen et al., 2014). *In vitro* studies showed acetylation activity and protein substrate binding of MOF depends on autoacetylation at K274 (Yuan et al., 2012). H4K16ac is the most abundant acetylation in humans affecting chromatin structure and chromatin protein interaction (Munks et al., 1991, Smith et al., 2005, Shogren-Knaak et al., 2006, Shogren-Knaak and Peterson, 2006). Loss of MOF and H4K16 acetylation are also identified as common hallmarks of cancer and MOF dependent H4K16ac might be involved in the regulation of certain oncogenes or tumour suppressor genes (Fraga et al., 2005, Kapoor-Vazirani et al., 2008, Luo et al., 2016, Su et al., 2016). MOF was shown to play an important role in embryogenesis and in the maintenance of stem cell identity (Gupta et al., 2008, Chelmicki et al., 2014). The loss of MOF in mice is lethal in both genders at an early embryonic stage (Thomas et al., 2008).

Furthermore, MOF plays a role in the DNA damage response by preventing the binding of 53BP1 to chromatin thus promoting homologous recombination mediated (HR) repair (Hsiao and Mizzen, 2013, Tang et al., 2013) It has also been shown that the crosstalk between H3K36me3 and H4K16ac at DNA damage sites enhances HR repair protein recruitment. While H3K36me3 plays a role in the recruitment of CtIP (CtBP-interacting protein), H4K16ac relaxes the chromatin and facilitates BRCA1 recruitment. Also, MOF is involved in the activation of ATM via acetylation at T392 (Gupta et al., 2005). In addition, conditional MOF knock-out experiments showed that cells had defects in IR induced DNA repair and the recruitment of MDC1, BRCA1 and 53BP1 was completely abolished (Li et al., 2010).

1.6. DNA damage

1.6.1. The DNA damage response

Preservation of genomic integrity is essential for proper cell function and reproduction. The replication of damaged DNA can lead to genomic instability, mutation and carcinogenesis. It has been estimated that up to 10^5 spontaneous DNA lesions can occur in each cell each day (Hoeijmakers, 2009). These can be the result of single-strand breaks and spontaneous base losses or reactive oxygen species (ROS) from normal cellular metabolism and spontaneous hydrolysis of nucleotide residues, inducing abasic sites and deamination (Lindahl and Barnes, 2000). However,

environmental factors and the chemical properties of DNA can also affect its stability and its proper function. The main sources of DNA lesions are physical and chemical environmental agents. It has been shown that physical agents such as ultraviolet light (UV) and ionizing radiation (IR) can induce up to 10^5 DNA lesions per cell per day. Genotoxic chemicals used in cancer therapy such as methyl methanesulfonate (MMS), mitomycin C (MMC), cisplatin, psoralen, and nitrogen mustard, camptothecin (CPT) and etoposide are also a source of DNA lesions (Ciccia and Elledge, 2010).

To prevent these genomic erosions, eukaryotic cells evolved a network system called the DNA damage response (DDR). This system has different mechanisms to repair the various types of lesions. Mispaired DNA bases are replaced by the mismatch repair (MMR) while chemical alterations of bases are repaired through either the base excision repair (BER) or the nucleotide excision repair (NER) based on the complexity of the damage (Jiricny, 2006, Kim and Wilson, 2012, Scharer, 2013). Single strand break repair is mediated by the single-strand break repair (SSBR) pathway. The potentially more severe double-strand breaks activate either the nonhomologous end joining (NHEJ) or homologous recombination (HR) repair mechanisms depending on whether there is an available repair template for HR (Caldecott, 2008, Li and Heyer, 2008, Davis and Chen, 2013).

1.6.2. DNA damage signalling

Different types of DNA damages have their own set of molecules taking up similar roles in a damage signalling pathway and can be grouped into four categories: sensor, transducer, mediator and effector proteins (Harper and Elledge, 2007, Blanpain et al., 2011) (Figure 1.8). The final outcome of this signalling pathway depends on the severity of the damage and can result in apoptosis, senescence (permanent cell cycle arrest) or DNA damage repair which resumes normal cell cycle and proliferation (Norbury and Zhivotovsky, 2004, d'Adda di Fagagna, 2008). Chromatin modifications involved in the DNA repair also promote transcriptional silencing around the lesion to prevent interference from other DNA related processes (Shanbhag et al., 2010).

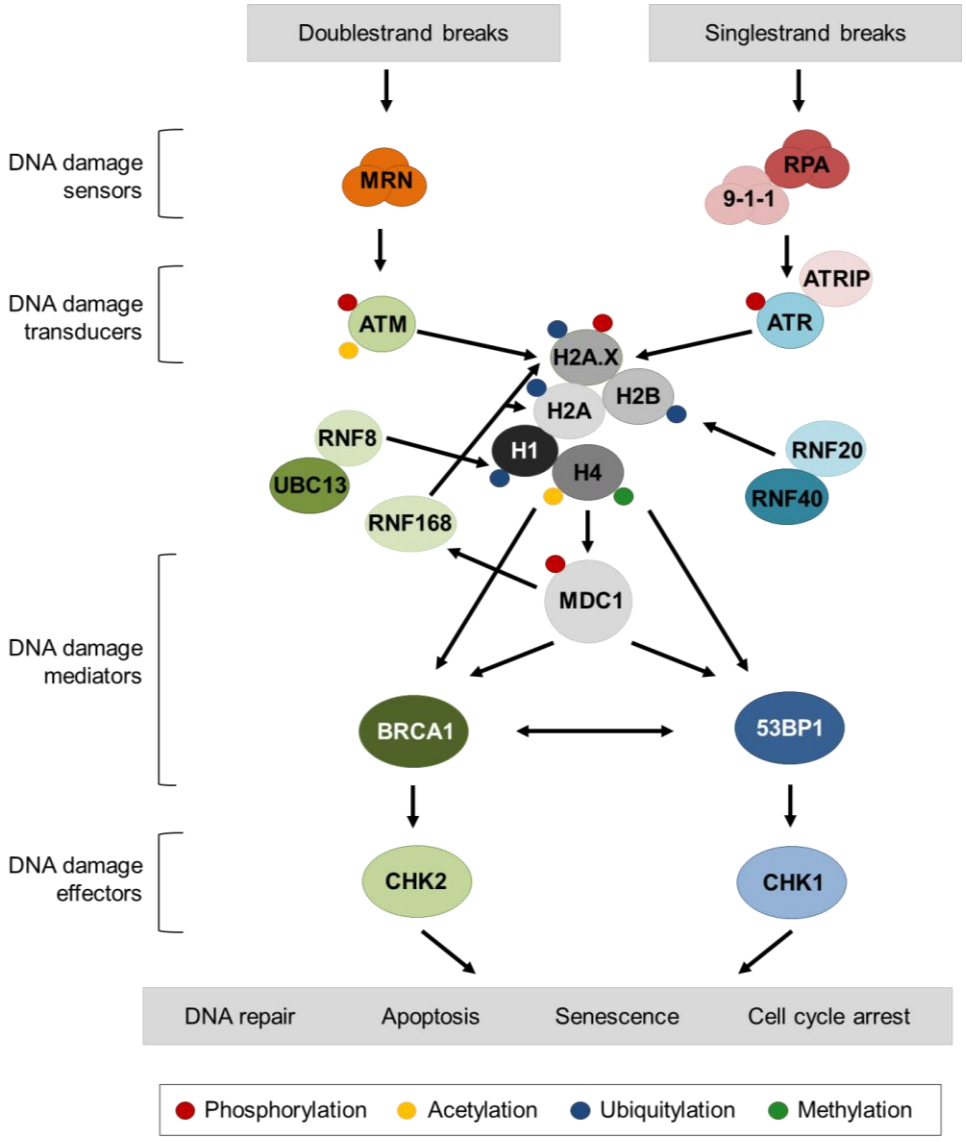

Figure 1.8: Schematic representation of the DNA damage signalling pathway. Symbols of posttranslational modifications only indicate the event due to the limitations of representation. Symbols in green are part of the ATM-CHK2 pathway and symbols in blue are part of the ATR- CHK1 pathway.

Different types of damage have independent molecular complexes for sensing and signalling, such as the MRN (Mre11-Rad50-Nbs1) complex, RPA (replication protein A) complex (RPA70, RPA32, RPA14), ATRIP (ATR-interacting protein) and the 9-1-1 (RAD9-RAD1-HUS1) complex (Sulli et al., 2012). The MRN complex specifically detects DNA double-strand breaks while RPA/9-1-1 recognises single stranded DNA for repair (Figure 1.8). After sensing specific DNA lesions these proteins recruit two different PI3K-like kinase (PIKK) transducers, which will determine the main signalling pathways. The MRN complex recruits ATM (ataxia

telangiectasia mutated) while the RPA/9-1-1 complex recruits ATR (ataxia telangiectasia and Rad3-related) bound by ATRIP (Zou and Elledge, 2003). While ATM and ATR have distinct DNA damage specificities, they are known to influence each other's localization to DNA lesions (Marechal and Zou, 2013). ATM can promote ATR activation by enhancing DNA end resection and replication stress induced phosphorylation of H2A.X by ATR can recruit ATM to the chromatin adjacent to stressed replication forks (Ward and Chen, 2001, Jazayeri et al., 2006, Myers and Cortez, 2006, Shiotani and Zou, 2009). Besides, it was found that replication stress can induce the phosphorylation of ATM at S1981 by ATR and possibly ATM can phosphorylate ATR as well (Stiff et al., 2006).

1.6.2.1. ATM -CHK2 signalling pathway

ATM is activated at the DNA damage site by dissociating from its dimeric form interacting with PP2A (protein phosphatase 2A) (Goodarzi et al., 2004) and undergoing autophosphorylation on four sites (S367, S1893, S1981 and S2996) and acetylation on K3016 (Bakkenist and Kastan, 2003, Kozlov et al., 2011). The activation of ATM also depends on its acetylation by MOF, Tip60 (60 kDa trans-acting regulatory protein of HIV type 1 (Tat) – interacting protein) acetyltransferases and phosphorylation via PP5 (serine-threonine phosphatase 5) (Gupta et al., 2005, Sun et al., 2005, Zhang et al., 2005, Sun et al., 2007, Sun et al., 2009). In addition ATM mediated phosphorylation of MOF at T392 supports its role in the repair pathway choice by facilitating HR (Gupta et al., 2014b). Furthermore MOF and Tip60 also affect cell fate decision by acetylating p53 at K120 thus enhancing proapoptotic gene transcription (Sykes et al., 2006, Tang et al., 2006). After autophosphorylation ATM, DNA-PKcs or ATR then phosphorylates H2A.X at S139 (γH2A.X) (Burma et al., 2001a, Ward et al., 2004, An et al., 2010). This serves as a direct binding site for MDC1 (mediator of DNA damage checkpoint protein 1) which recognises γH2A.X through its phospho-binding BRCT (BRCA1 carboxyl terminus) domains (Stewart et al., 2003, Stucki et al., 2005, Lou et al., 2006). MDC1 then undergoes ATM-mediated phosphorylation and dimerization (Jungmichel et al., 2012). This DNA damage-induced phosphorylation of MDC1 recruits RNF8 which binds the phosphorylation site of MDC1 via its forkhead-associated (FHA) domain (Huen et al., 2007). RNF8 promotes the RNF8–UBC13 complex formation through direct interaction with HERC2 (HECT-type E3 ligase) (Bekker-Jensen et al., 2010).

RNF8-UBC13 then polyubiquitylates H1 generating a K63-linked ubiquitin chain. These events then facilitate the recruitment of RNF168 which recognises the modification through its N-terminal UBD-containing region and ubiquitylates H2A at K13 and K15 (Gatti et al., 2012, Mattiroli et al., 2012). Together with RNF8 RNF168 is reported to be involved polyubiquitylation on histones H2A and H2A.X (Mailand et al., 2007, Doil et al., 2009, Thorslund et al., 2015, Stadler and Richly, 2017). Recent findings indicate that besides K63-linked ubiquitin chain formation RNF8 can promote Lys48- and RNF168 Lys27-linked polyubiquitination (Feng and Chen, 2012, Gatti et al., 2015) and RNF8 was also found to participate in K11-linkage conjugates on damaged chromatin, including H2A and H2A.X (Paul and Wang, 2017). RNF168 mediated ubiquitylation can be targeted by the C-terminal UBD domain of the protein to further propagate ubiquitylation which then alongside MDC1 facilitates the recruitment of downstream mediator proteins such as BRCA1 (breast cancer type 1 susceptibility protein) and 53BP1 (p53 binding protein 1) to the break sites (Stewart et al., 2009, Bohgaki et al., 2013, Hodge et al., 2016). 53BP1 foci formation at damage sites is aided by H2AK15ub and H4K20me2, serving as anchor sites (Fradet-Turcotte et al., 2013, Wilson et al., 2016). The recruitment of 53BP1 restrains end resection and propagates non-homologous end joining mediated repair and fosters error-free RAD51-mediated gene conversion (GC) in G2, S phase (Bunting et al., 2010, Zimmermann et al., 2013, Ochs et al., 2016). Particularly interesting is that the dilution of the H4K20me2 mark from early to late S phase decreases the accumulation of 53BP1 at damage sites preventing its binding to replicating DNA (Pellegrino et al., 2017) and (progressively) allowing for BRCA1 binding. The recruitment of BRCA1 is further supported by MOF dependent H4K16 acetylation, which prevents binding of 53BP1 to the H4K20me2 sites (Hsiao and Mizzen, 2013, Tang et al., 2013). 53BP1 and BRCA1 then transfer DNA damage signals to downstream effectors through CHK1 and CHK2 kinases as well as CK2, p38 and MK2 (Reinhardt et al., 2007). These two mediators are known to play a key role in the pathway choice between NHEJ and HR repair (Lowndes, 2010, Escribano-Diaz et al., 2013).

1.6.2.2. ATR -CHK1 signalling pathway

During the recruitment of ATR, first the Rad17-RFC2-5 clamp loader recognises the single stranded/double stranded DNA junctions and with RPA loads the 9-1-

1complex to the double-stranded DNA (Ellison and Stillman, 2003, Zou and Elledge, 2003, Zou et al., 2003). During DNA end resection ATR also progressively phosphorylates RPA32 at S33 prior to the phosphorylation of Ser4/Ser8 by DNA-PKcs (Liu et al., 2012a). ATR is then autophosphorylated at S428, S435, T1989 and possibly at S436 and S437 (Liu et al., 2011). TopBP1 is recruited to the damage sites by ATR binding which facilitates the substrate recognition of ATR via stimulation of its kinase activity (Kumagai et al., 2006, Liu et al., 2011). In case of stalled replication forks however Mre11 (member of the MRN complex) activates ATR in the absence of BRCA1/2 and Fanconi anemia proteins (Lee and Dunphy, 2013). ATR phosphorylates a DNA replication protein, Claspin which in turn binds and recruits CHK1 to sites near ATR to facilitate CHK1 activation (Sorensen et al., 2004). This activation is promoted by the interaction between the carboxyl terminus of Rad9 and the conserved carboxyl terminus of Claspin (Liu et al., 2012b). The ATR-mediated phosphorylation of And-1 (replisome component) at T826 after replication stress also promotes the interaction between Claspin and CHK1(Hao et al., 2015). After its recruitment, CHK1 is rapidly phosphorylated by ATR at multiple S/T-Q sites within its C-terminus, most importantly at S317 and S345 which are essential for the biological activity of CHK1 (Liu et al., 2000, Niida et al., 2007, Walker et al., 2009). Following activation CHK1 dissociates from Claspin and acts on both nuclear and cytoplasmic substrates (Lukas et al., 2003).

While these signalling pathways show specificity towards certain types of DNA lesions diverse genotoxic stress can result in the simultaneous activation of ATM–CHK2 and ATR–CHK1 pathways (Smith et al., 2010).

1.6.3. DNA double-strand break repair

There are at least four different DNA repair pathways which can deal with double-strand breaks (DSBs): NHEJ (Non-homologous end joining), alt-NHEJ (alternative-NHEJ), SSA (single-strand annealing) and HR (homologous recombination). The choice between these pathways depends on the resection of the free DNA ends at the break site. While alt-NHEJ depends on a shorter (5–25 nt) DNA end processing, SSA and HR can deal with more extensive resection (Hartlerode and Scully, 2009). The NHEJ in contrast does not need DNA end resection and is the dominant DNA repair pathway in mammalians. While it is an error prone process it does not require a

homologue template for the repair and can happen at any stage of the cell cycle. On the contrary homology-mediated repair is only available through S and G2 phase utilising error-free homologous recombination using sister-chromatid sequences (San Filippo et al., 2008). This study is focusing on the two main double-strand break repair mechanism, NHEJ and HR (Figure 1.9).

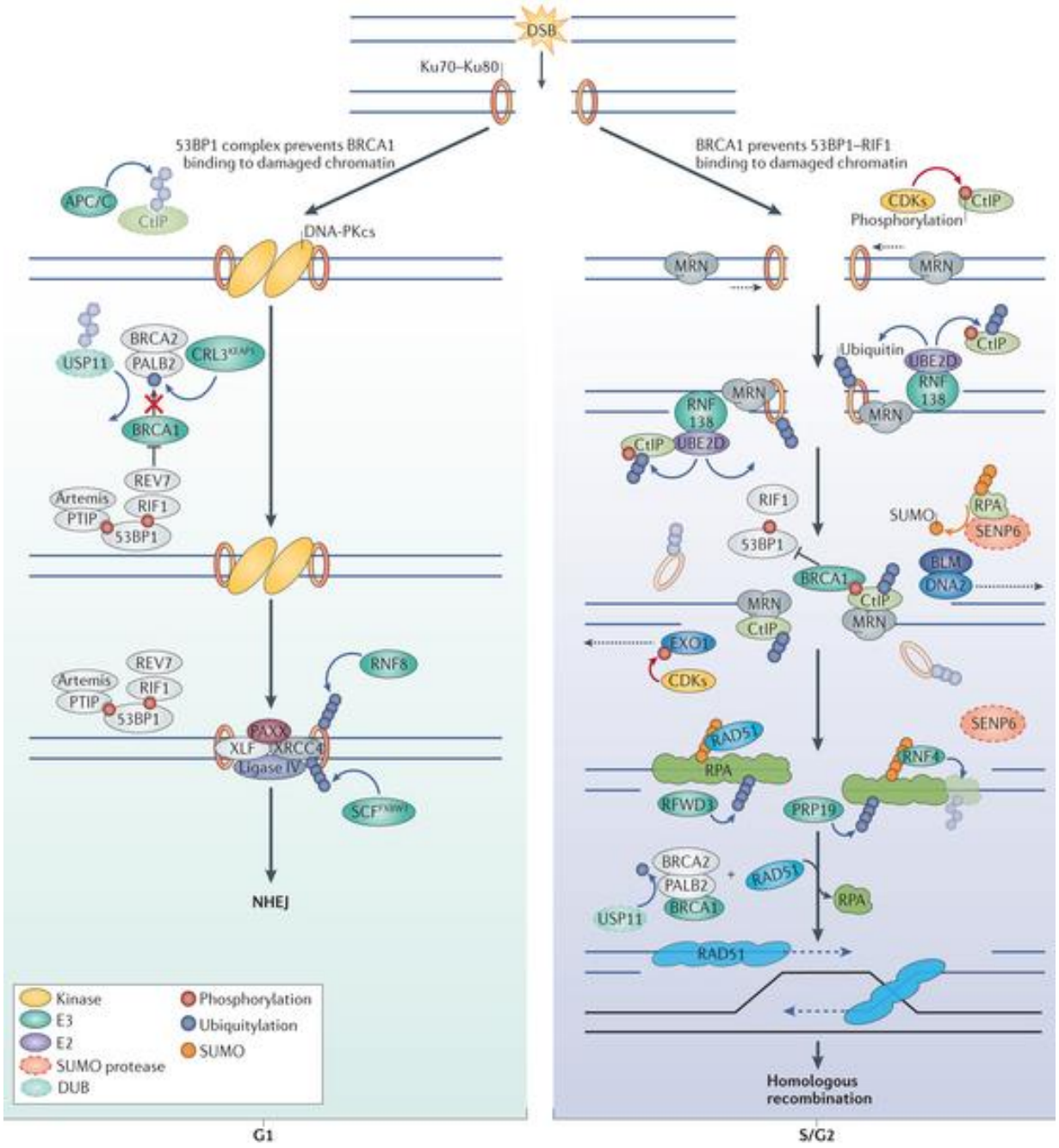

Figure 1.9: NHEJ and HR repair pathways. Non-homologous end joining and homologous recombination double-strand break repair pathways. Figure taken from (Schwertman et al., 2016).

1.6.3.1. Non-homologous end joining pathway (NHEJ)

In case of NHEJ repair first the Ku70/80 complex (Ku) binds the broken DNA ends by forming a quasisymmetrical ring structure which can envelope up to two helical turns of DNA ends (Walker et al., 2001). Ku then recruits DNA-PKcs (DNA-dependent protein kinase catalytic subunit) through interaction with the C-terminus of Ku80 (Singleton et al., 1999) and the two forms DNA-PK (Sibanda et al., 2017). DNA-PKcs also phosphorylates itself and other proteins. The N-terminal von Willebrand A (vWA) domain of Ku70 has been shown to play a role in signalling linkage between DNA repair machinery to DNA damage signalling regulators (Fell and Schild-Poulter, 2012). Besides, ATR is recruited and activated through autophosphorylation which enables the engagement of MDC1 through its BRTC domain. 53BP1 gets recruited through the recognition of H2AK15ub and H4K20me2 via its UDR (ubiquitylation-dependent recruitment) motif (Fradet-Turcotte et al., 2013). After the recruitment 53BP1 binds RIF1 and PTIP in a phosphorylated ATM dependent manner. 53BP1–RIF1 then together with REV7 prevents recruitment of BRCA1 to double-strand breaks by inhibiting extensive end resection and thus facilitating non-homologous end joining (Chapman et al., 2013, Schwertman et al., 2016, Chang et al., 2017). PTIP recruits and DNA-PKcs activates the Artemis end-processing nuclease by phosphorylation to process broken DNA ends and facilitate NHEJ repair (Davis and Chen, 2013, Moscariello et al., 2015). (Moshous et al., 2001) (Figure 1.9). Also, to further suppress HR $CRL3^{KEAP1}$ (cullin–RING E3 ligase 3) ubiquitylates PALB2 (partner and localizer of BRCA2) preventing its interaction with BRCA1 (Orthwein et al., 2015). The ligation of the broken DNA ends is performed by phosphorylated XRCC4/DNA ligase IV complex which is recruited to the damage site through interaction with Ku (Costantini et al., 2007). The DNA ligase activity of the complex is strictly dependent on DNA-PKcs/Ku assembly and XRCC4 in the complex plays a role in stabilizing and stimulating the activity of DNA ligase IV (Calsou et al., 2003). XLF (XRCC4-like factor) also known as Cernunnos is recruited to the break site where it contacts, stabilizes, and assists the other NHEJ components to assemble a functional NHEJ machinery (Yano et al., 2009). XLF can form hetero-oligomers with XRCC4 to form filaments proposedly bridging DNA prior ligation (Andres et al., 2012).

1.6.3.2. Homologous recombination pathway (HR)

HR repair of DNA double-strand breaks in cells is active during S phase at replication forks or in G2 phase after replication (Marechal and Zou, 2013). In the HR pathway the RNF8-RNF168 mediated ubiquitylation recruits the BRCA1-A complex containing BRCA1 and RAP80 which binds through a UBD containing member (Sobhian et al., 2007, Wu et al., 2009). Phosphorylated ATM recruits the CtIP exonuclease to perform DNA end resection generating 3' single-stranded DNA overhangs at the DSB (Sartori et al., 2007). Retention of CtIP at double-strand break sites is promoted by its RNF138-mediated ubiquitylation (Schmidt et al., 2015). RNF138 also ubiquitylates Ku80, a member of the double-strand break end-binding Ku70–Ku80 heterodimer thus relocating it from the ends to facilitate resection (Ismail et al., 2015). To prevent NHEJ BRCA1 impairs retention of RIF1 at the break sites in a CtIP-dependent manner. To facilitate repair RPA (Replication protein A) complex (RPA70/RPA32/RPA14) is phosphorylated by ATR and binds the exposed single stranded DNA (Figure 1.9). The RPA complex also interacts with BRCA1 (Choudhary and Li, 2002) and BRCA2 (Wong et al., 2003). In case of replication block the binding of ATR is preceded by DNA polymerase stalling and a continued DNA unwinding by MCM replicative helicases ahead of the replication fork (Byun et al., 2005). RAD52 stimulates DNA strand exchange by binding ssDNA and targeting RAD51 to RPA (Park et al., 1996, McIlwraith et al., 2000, Sugiyama and Kowalczykowski, 2002, Stauffer and Chazin, 2004). RAD51 then forms a presynaptic nucleoprotein filament and pairs the undamaged homologous sequence to the single stranded lesion leading to the formation of the displacement loop (D-loop). Through Watson–Crick base pairing the nucleoprotein filament forms a metastable paranemic joint structure (Sung et al., 2003). The other damaged single stranded DNA can align with the extended D-loop to form a double holliday junction (DHJ) which is a key pathway in meiotic cells (Heyer et al., 2010). This DHJ then can be resolved through the BLM (Sgs1)/TOP3α/RMI1 complex to prevent crossover product formation (Wu and Hickson, 2003). In mitotic cells however the newly synthesized DNA strand dissociates from the D-loop and anneals to the other DNA end resulting in a non-crossover product (Ferguson and Holloman, 1996). While in meiotic cells crossovers increase genetic diversity it is essential to avoid crossover events in mitotic cells to preserve genomic integrity.

1.7. Replication

Before each cell division cells need to faithfully replicate their DNA in a precisely regulated manner. To ensure accuracy and proper integration of the process into the cell cycle, cells evolved an intricate DNA replication machinery (Fragkos et al., 2015).

Replication occurs in the S phase of the cell cycle and takes approximately 10 hours to accomplish (Rew and Wilson, 2000). The initiation starts at specific genomic loci known as replication origins (ORI). Unlike in *E. coli*, metazoan genome does not contain a consensus ORI sequence and only a subset of the potential ORI loci are activated within each cell cycle (Cayrou et al., 2011). The number of replication origins scales with the size of the genome to ensure a manageable replication timeframe (Leonard and Mechali, 2013, Wu et al., 2014b, Gao, 2015). Accordingly, the human genome possesses about 50000 origins (Huberman and Riggs, 1966, Dellino et al., 2013).

Replication origins are recognised and bound by the pre-replication complex (pre-RC) (Sun and Kong, 2010, Yeeles et al., 2015). Since replication initiation happens on diverse sequences the origin recognition complex (ORC) consisting of six members (ORC1-6) binds DNA promiscuously (Vashee et al., 2003) (Figure 1.10). While not sequence-specific, ORC binding shows preference towards certain loci in the genome, for example newly fired replication sites (NFR), G-rich sequences and CpG islands suggesting that DNA structure might play role in the identification of these sites (Delgado et al., 1998, Kuo et al., 2012, Hoshina et al., 2013, Valton et al., 2014, Parker et al., 2017). H4K20me2 and H4K20me3 also play an important role in the recruitment of the ORC (Jorgensen et al., 2013). The loss of the Suv4 H4K20me2 methyltransferase results in a phenotype similar to ones observed in ORC1 knockdown mice and in S phase entry delay (Schotta et al., 2008, Beck et al., 2012). ORC recruits CDC6 (Cell division cycle 6) and CDT1 (CDC10‑dependent transcript 1) which load the mini-chromosome maintenance (MCM) helicase complex (MCM2-7) (Forsburg, 2004, Ferenbach et al., 2005, Remus et al., 2009, Wei et al., 2010, Frigola et al., 2017) which unwind the double-stranded DNA.

The pre-RC recruitment is followed by origin activation with the formation of a pre-initiation complex (pre-IC) (Roeder, 1991, Louder et al., 2016). Pre-RC includes

several replication factors such as MCM10, CDC45, ATP-dependent DNA helicase Q4 (RECQL4), Treslin, GINS (Sld5, Psf1, Psf2, and Psf3), DNA topoisomerase 2-binding protein 1 (TOPBP1) and DNA polymerase ε (Pol ε) (Heller et al., 2011, Fragkos et al., 2015, Larasati and Duncker, 2016). After DNA unwinding performed by the MCM2-7 helicase (Figure 1.10) (Quan et al., 2015, Yeeles et al., 2015, Deegan et al., 2016, Larasati and Duncker, 2016) further replication factors and DNA polymerases are recruited (Pacek et al., 2006, Ilves et al., 2010, Fragkos et al., 2015). These turn the pre-RC into two functional replication forks moving in opposite directions from the activated origin with a replisome (MCM 2-7, TOPBP1, GINS, CDC45 and Treslin) at each fork (Ilves et al., 2010, Kumagai et al., 2010) (Figure 1.10). Replication takes place in a 5'- 3' direction and the generated two strands are called leading and lagging strand respectively (Leman and Noguchi, 2013). Polymerization of new DNA strands is aided by PCNA which tethers DNA polymerases to the DNA. For the polymerization process first Pol α is recruited for primer synthesis which facilitates the binding of Pol ε for leading strand and Pol δ for Okazaki fragment replication (Schauer and O'Donnell, 2017). While the leading strand replication is continuous, during the lagging strand polymerization the Okazaki fragments generated by Pol δ are joined together after a maturation period by DNA ligase I (Sparks et al., 2012, Williams et al., 2016).

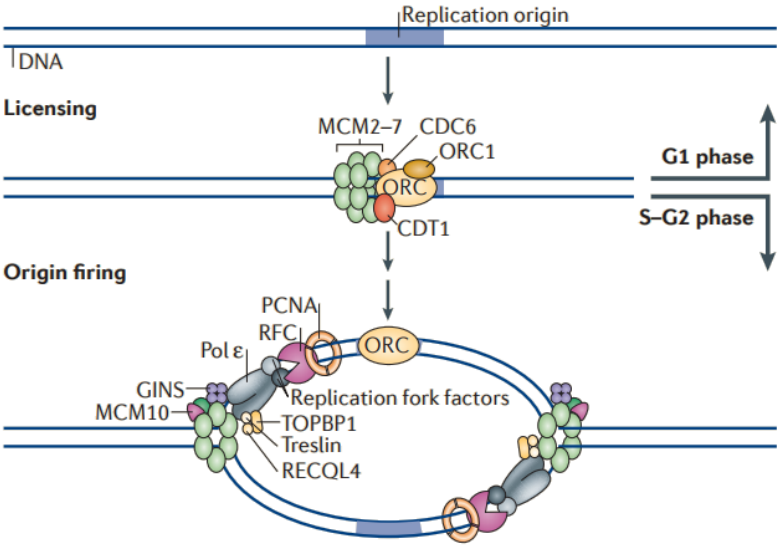

Figure 1.10: Formation and activation of DNA replication origins. Licensing of replication origins is restricted to G1 phase followed by origin activation involving the formation of a pre-initiation complex (pre-IC). Figure taken from: (Fragkos et al., 2015).

Replication stress caused by different DNA damage factors or abnormal DNA structures generally result in stalled replication forks (Minca and Kowalski, 2011, Mazouzi et al., 2014). The ATM/ATR-CHK1/CHK2 checkpoint signalling inhibits CDC25A-C via phosphorylation resulting in CDK1 inhibition and the mitotic entry is delayed until successful repair and the restart of the replication (Takizawa and Morgan, 2000, Boutros et al., 2006, Chen and Poon, 2008, Petermann and Helleday, 2010, Ma and Poon, 2011). It leads to a global origin activation inhibition triggered by the checkpoint and activation of alternative origins close to the stalled fork to complete DNA replication (Mechali, 2010, Karnani and Dutta, 2011, Fragkos et al., 2015). In replication fork restarting, BLM (Bloom syndrome protein) and WRN (Werner syndrome ATP-dependent helicase) play an important role, BLM by promoting restart and WRN by aiding efficient fork progression (Davies et al., 2007, Mao et al., 2010, Kehrli et al., 2016). Depending on the severity and complexity of the damage replicating DNA can be repaired and the replication can restart through dormant origin firing (Blow and Ge, 2009), replication repriming, stalled fork reversion or activation of the DNA damage tolerance (DDT) pathways (Mouron et al., 2013, Zeman and Cimprich, 2014, Branzei and Szakal, 2016). If replication forks cannot restart a fork collapse occurs leading to incomplete DNA replication (Cortez, 2015). 53BP1 nuclear body formation has been linked to underreplicated, damaged DNA shielding it from further erosion or an error-prone NHEJ pathway (Lukas et al., 2011).

1.8. Aims of the thesis

The aim of this study is to further characterise and understand the functions of human MSL1 and MSL2. Within this overall aim this work is focusing on three sub aims: firstly, deciphering the function of MSL2 and MSL1 in the MSL complex; secondly, based on previous findings further characterise their role in the DNA damage response and finally to identify novel interactors and possible substrates of the E3 ubiquitin ligase MSL2.

2. Materials and Methods

2.1. Materials

2.1.1. Reagents and buffers

General chemicals used in the experiments were purchased from Sigma, Fisher Scientific or GE Healthcare. Frequently used solutions and buffers are listed in Table 2.1. The solutions were prepared with either distilled H_2O (dH_2O), double-distilled H_2O (ddH_2O) or MilliQ-H_2O (PURELAB flex, Elga).

Table 2.1: Reagents and buffers

DNA works	
Name	**Composition**
6× DNA loading dye	20% Sucrose, 0.1 M EDTA pH 8.0, 1% SDS, 0.25% Bromophenol blue, 0.25% Xylene cyanol.d
1× TAE	40 mM Tris-acetate pH 8.0, 1 mM EDTA
TAIL buffer	100 mM Tris pH8.0, 5 mM EDTA, 0.2% SDS, 200 mM NaCl
Protein works	
Name	**Composition**
4× Laemmli buffer	150mM Tris pH 6.8, 4% SDS, 0.03% bromophenol blue, 10% β-mercaptoethanol , 20% glycerol
2× Laemmli buffer	150mM Tris pH 6.8, 2% SDS, 0.03% bromophenol blue, 10% β-mercaptoethanol, 20% glycerol
Stacking gel buffer	0.5M Tris pH 6.8
Separating gel buffer	1.5M Tris pH 8.8
1× Running buffer	25 mM Tris, 192 mM glycine, 1% SDS
Coomassie brilliant blue	0.5% Coomassie, 35% methanol, 14% acetic acid
Coomassie destain solution	30% methanol, 10% acetic acid
Tris-glycine buffer	25 mM Tris, 192 mM gycine, pH 8
Silver stain fixing solution	50% ethanol, 10% acetic acid
1× Transfer buffer	25 mM Tris, 192 mM glycine, 5% methanol
Ponceau S solution	0.5% Ponceau S, 5% acetic acid
Blocking solution	1 x PBS, 0.1% Tween 20, 2-5% skimmed milk or 1% BSA
Blocking solution for streptavidin-HRP	1 x PBS, 0.1% Triton X, 1% BSA (overnight)
Membrane pre-treatment for VU-1 antibody	1 x PBS, 0.5% glutaraldehyde

PBST	1× PBS, 0.1% Tween 20
TBST	1× TBS, 0.1% Tween 21
Primary antibody dilution buffer	2% BSA, 0.1% sodium azide, 25mM Tris-HCl pH 7.5, 150mM NaCl
1× Phosphate buffer saline (PBS)	137 mM NaCl, 2.7 mM KCl, 1.4 mM NaH2PO4, 4.3 mM Na2HPO4, pH 7.4
1× Tris buffer saline (TBS)	1M Tris, 1.5M NaCl
RIPA buffer	50 mM Tris-HCl pH 8, 150 mM NaCl,1% NP-40, 0.5% sodium deoxycholate, 0.1% SDS
Benzonase lysis buffer	50mM Tris-HCl pH 8, 0.5% Triton-X, 150 mM NaCl, 20% glycerol, benzonase, 100mM MgCl2
Lysis buffer (baculoviral protein expression)	3 mM HEPES pH7.8, 150 mM NaCL
Streptavidin elution buffer	95% formamide, 10 mM EDTA pH 8
Nickel beads elution buffer	50 mM Na_2PO_4 pH8, 0.3 M NaCl, 250 mM imidazole
Buffer A	10 mM HEPES pH7.5, 1.5 mM $MgCl_2$,10 mM KCl, 0.5 mM DTT, 1x PI
5xLysis Buffer	250 mM Tris pH 7.5, 750 mM $NaCl_2$, 50% glycerol, 2.5% NP-40, 1x PI
Sucrose 1	0.25 M sucrose, 10 mM $MgCl_2$, 1x PI
Sucrose 3	0.88 M sucrose, 0.5 mM $MgCl_2$, 1x PI
Isotonic lysis buffer	10 mM Tris-HCl pH7.4, 50 mM NaCl, 0.5 M sucrose, 0.5% Triton X-100, 0.1 mM EDTA, 1mM DTT, 1xPI
Nuclear extraction buffer	10 mM Tris-HCl pH7.4, 500 mM NaCl, 0.5% NP-40, 0.1 mM EDTA, 1 mM DTT, 1xPI
Crystal violet solution	6.0% v/v glutaraldehyde, 0.5% w/v crystal violet
Immunofluorescence	
Name	**Composition**
CSK pre-extraction buffer	100 mM NaCl, 300 mM $MgCl_2$, 10 mM PIPES pH 6.8, 0.5 µg/ml Rnase A
Fixation solution	100% methanol or 3% Paraformaldehyde (PFA) in PBS
Permeabilization solution (for PFA fixation)	0.125% Triton-X in 1xPBS
Blocking solution	1× PBS, 1% BSA
Mounting media	3% w/v N-propyl-gallate, 80% v/v glycerol in PBS
Spreading buffer	0.5% SDS, 200 mM Tris pH 7.4, 50 mM EDTA
***E.coli* growth**	
Name	**Composition**
Luria-Bertani (LB) Broth	1% tryptone, 0.5% yeast extract, 1% NaCl, pH adjusted to 7.0 with 4 M NaOH
Luria-Bertani (LB) Agar	1.5% agar, 1% tryptone, 0.5% yeast extract, 0.5% NaCl

SOC broth	0.5% yeast extract, 2% tryptone, 10 mM NaCl, 2.5 mM KCl, 20 mM $MgSO_4$
$CaCl_2$ solution	60 mM $CaCl_2$, 15% glycerol, 10 mM PIPES pH 6.8, final pH adjusted to 7 with KOH

2.1.2. Molecular biology kits

Molecular biology kits used in this study are listed in Table 2.2.

Table 2.2: Molecular biology kits

Name	Description	Source
High Pure PCR Cleanup Micro Kit	Purification of DNA fragments	Roche
SmartPure PCR Kit	Purification of DNA fragments	Eurogentec
QIAquick Gel Extraction Kit	Extraction of DNA bands from agarose gel	Qiagen
SmartPure Gel Kit	Extraction of DNA bands from agarose gel	Eurogentec
SmartExtract - DNA Extraction Kit	Genomic DNA extraction	Eurogentec
NucleoBond Xtra Midi Plus	Large scale extraction of plasmid DNA	Macherey-Nagel
ISOLATE RNA Mini kit	RNA extraction	Bioline
High Capacity RNA-to-cDNA Kit	cDNA synthesis	Applied Biosystems
Fast SYBR Green Master Mix	Real-time PCR	Applied Biosystems
pGEM-T Easy Vector kit	TA cloning and blue-white selection	Promega
ProteoSilver Plus Silver Stain Kit	SDS-PAGE gel silver staining	Sigma

2.1.3. Primers and oligos

Primers and oligos used for cloning, sequencing, PCR and qPCR are purchased from Sigma and listed in Table 2.3.

Table 2.3: Primers and oligos

Name	Sequence
guide sequence for targeting MSL2 ex.1	AAA CCG AGC CGC CTA GTG CTC AAC
	CAC CGT TGA GCA CTA GGC GGC TCG
guide sequence for targeting MSL2 ex.2	AAA CGT AGC TGG TGC AAA GAC TAT C
	CAC CGA TAG TCT TTG CAC CAG CTA C
guide sequence for targeting hMSL2 ex.2 for nickase Cas9	CAC CGC TAT TTC CCT ACC AGG AGT
	AAA CAC TCC TGG TAG GGA AAT AGC

Name	Sequence
guide sequence for targeting MSL2 ex.2 for nickase Cas9	CAC CGT ACG GCA GCT ATG GTT CTG T
	AAA CAC AGA ACC ATA GCT GCC GTA C
guide sequence for targeting MSL2 ex.2 for HR repair	CAC CGA TTC GAC TGT TAA ATC AGT
	AAA CAC TGA TTT AAC AGT CGA ATC
guide sequence for targeting MSL1 ex.1	CACCTGCTCAGGATTGCCGCCGGC
	AAACGCCGGCGGCAATCCTGAGCA
primers for MSL2 CRISPR clone identification ex.2 target	ATG ACA TTT GCT ACA AGA TCC TAT TGC A
	ATG CTT CCA AGT TCG GCT GCA
primers for MSL2 CRISPR clone identification ex.1 target	ATG GCT AGA CTG AGC TCC GAG TCC
	ATC GCC GTA GGT ACG TAA TCA GCT
MSL2 ex.2 –AID-GFP for HR template (800bp)	TTA GCC ATA ATG TTT TTA TGT CC
	CTC CAC TGC CCT TGT ACA GCT CGT CCA TG
MSL2 T2A-Puro. for HR template (800bp)	GCT GTA CAA GGG CAG TGG AGA GGG CAG AG
	GCA AGT TAA ATC AGG CAC CGG GCT TGC G
MSL2 3' UTR for HR template (800bp)	CGG TGC CTG ATT TAA CTT GCC GGA GCT C
	AAG TAC AAT ACA CAA ATC TGG G
MSL2 ex.2 for HR template (2500bp)	GCC ATG GCG GCC GCG GGA ATT CGA TCC CGG TTA ATT TTT TTG TAT TTT TAA TAG AAA TGG GGT TTT AC
	CAC TGC CCA TCA TAC AGT CGA ATC TCA TGT CTA TAG CTT CAT CCA AAC TTT TA
MSL2 AID-GFP for HR template (2500bp)	GAG ATT CGA CTG TAT GAT GGG CAG TGT CGA GCT GAA TCT GAG GGA GAC TGA GC
	CCG GCA AGT TAA ATT ACT TGT ACA GCT CGT CCA TGC CGA GAG TGA TCC CGG CG
MSL2 3' UTR for HR template (2500bp)	GCT GTA CAA GTA ATT TAA CTT GCC GGA GCT CCT GCA TAT AGA TCA CTT GTA TC
	AGG CGG CCG CGA ATT CAC TAG TGA TTA AGG CTA ACC AAA AAG ATA AAA TTG TCA GCT CTA AAA CTA TTA CC

primers for MSL2 insertion into pFastBac-6His plasmid	CATGGAATTCATGAACCCCGT
	ATGCCTCGAGTTAACAGTCGAAT
primers for MSL2 insertion into pIDC plasmid	TAC GTC GAC CAT CAC CAT CAC CAT
	GCT CTA GAT TAA CAG TCG AAT CTC AT
primers for MOF insertion into pIDK plasmid	GTG CTA GCT ACC CAT ACG ATG TT
	TAC CGG TAC CTC ACT TCT TGG AGA G
Q-PCR primer for *Xist*	GCT CCT CGG ACA GCT GTA AA
	CAC ATG CAG CGT GGT ATC TT
Q-PCR primer for *Tsix*	CCT ATC AGG CAG GGG TTA GG
	GCA AGT GTA CGT GTG TGT GT
Q-PCR primer for *Elav1*	CCA ACT TGT ACA TCA GCG GG
	AAA CCG GAT AAA CGC AAC CC

Name	Sequence
Q-PCR primer for *MSL1*	CAG GCC AAG GAA AAG GAG AT
	CGC CTT TCC ATA CGT TCA AT
Q-PCR primer for *MSL2*	GTC CCT TTC GTG CTG TGT TT
	GTT GGT GGG TGC AAT AGG AT
Q-PCR primer for *MSL3*	GAA GAA GCA GCT GGA GGA TG
	GTT GGT CTG GCA TGG AAG TT
Q-PCR primer for *KAT8*	AGA TCT ACC GCA AGA GCA ACA
	CAG CAG ACA CAG GTT CTG ACA
Q-PCR primer for *PPIA*	AGG GTT CCT GCT TTC ACA GA
	CTT GCC ACC AGT GCC ATT AT
Q-PCR primer for *GAPDH*	ATT CCA CCC ATG GCA AAT TC
	TCT CGC TCC TGG AAG ATG GT
Q-PCR primer for *HPRT*	TGT AGC CCT CTG TGT GCT CAA G
	CCT GTT GAC TGG TCA TTA CAA TAG CT
Q-PCR primer for *HOXA9*	GCA AAC GGA GAG AAA CCA CAC
	AAA CTC CTT CTC CAG TTC CAG
Q-PCR primer for *MEIS1*	TGT AGC TTC CCC CAG CAC AG
	TAG TGA GCC CTG TGT CTT GTG C
Q-PCR primer for *TMS1*	GCA CTT TAT AGA CCA GCA
	TCC AGC AGC CAC TCA ACG
MSL2 fragment 1 (86-226aa) for Ab binding identification, bacterial cloning	ATC CAT GGA CTA TGA GCA GTT TGA GGA AAA C
	ATC TCG AGC TAT ATG TCA ACA GTA TTA CAT ACG TCA ATC
MSL2 fragment 2 (156-296aa) for Ab binding identification, bacterial cloning	ATC CAT GGG AAC ACA TTC CCC TTT ACC TTC AA
	ATC TCG AGC TAG CTT CCA AGT TCG GCT GC
MSL2 fragment 3 (226-366aa) for Ab binding identification, bacterial cloning	ATC CAT GGA TAT AAA AAC TGA GGA TCT GTC TGA CAG
	ATC TCG AGC TAC AGT GTT GGG CCT CGG AT
MSL2 fragment 4 (296-412aa) for Ab binding identification, bacterial cloning	ATC CAT GGA TGC CAC TGT ATC CAA TGG ACC T
	ATC TCG AGC TAA TGA CTC TTT TTC ATG CTT TTA GTA GA
HA-2F primer with XhoI-BbsI restriction site for cloning	ATC TCG AGT TAC CAA GCT TGT CAT C
	TAT GAA GAC ACC GGG TAC CCA TA
Puromycin res. casette primer with T2A sequence and FseI-EcoRI restriction site for cloning	AAG GCC GGC CAG GCA AAA AAG AAA AAG GAA TTC GGC AGT GGA GAG GGC AGA GGA AGT CTG CTA ACA TGC GGT GAC GTC GAG GAG AAT CCT GGC CCA ATG ACC GAG
	TAG AAT TCT CAG GCA CCG GGC
PFastBac sequencing primer	TTG TTC GCC CAG GAC TCT AG

2.1.4. Vectors and plasmids

Vectors and plasmids used in this study for cloning, gene targeting and protein expression in prokaryotic or eukaryotic cells are listed in Table 2.4.

Table 2.4: Vectors and plasmids

Name	Use	Source
pFastBac-6His-mMsl1	Plasmid for Bacmid recombination	Dr. Stephen Rea
pFastBac-6His-hMSL2	Plasmid for Bacmid recombination	This study
pFastBac-HA-hMSL3	Plasmid for Bacmid recombination	Dr. Stephen Rea
pFastBac-FLAG-MOF	Plasmid for Bacmid recombination	Dr. Stephen Rea
pFastBac-6His	Plasmid for Bacmid recombination	Dr. Stephen Rea
pIDS	Plasmid for MultiBac system	Nasheuer Lab
pIDK	Plasmid for MultiBac system	Nasheuer Lab
pIDC	Plasmid for MultiBac system	Nasheuer Lab
pACEBac1	Plasmid for MultiBac system	Nasheuer Lab
pACEBac2	Plasmid for MultiBac system	Nasheuer Lab
pIDS-Flag-MSL3	Plasmid for MultiBac system	This study
pIDK-HA-MOF	Plasmid for MultiBac system	This study
pIDC-His-hMSL2	Plasmid for MultiBac system	This study
pACEBAC1-His-mMsl1	Plasmid for MultiBac system	This study
pACEBAC1-His-mMsl1-His-hMSL2	Plasmid for MultiBac system	This study
pACEBAC1-His-mMsl1-His-hMSL2-HA-MOF	Plasmid for MultiBac system	This study
pACEBAC1-His-mMsl1-His-MSL2-HA-MOF-Flag-MSL3	Plasmid for MultiBac system	This study
pACEBac2-HA-MOF	Plasmid for MultiBac system	This study
pcDNA3.1(+)	Cloning	Invitrogen
His-Ub	In vivo ubiquitylation assay	Dr.Gaelle Legube
pDEST-HA-2F-MSL2	Expression plasmid for mammalian cells	Dr. Simona Moravcová
HA-2F-MSL2	Expression plasmid for mammalian cells	Dr. Mikko Taipale
HA-2F-MOF	Expression plasmid for mammalian cells	Dr. Mikko Taipale
pLOX-Puro	Selection in mammalian cells	Morrison Lab
pLOX-Neo	Selection in mammalian cells	Morrison Lab
px330	CRISPR plasmid	Lowndes Lab
px335	CRISPR plasmid (Cas9n) nickase	Lowndes Lab

Name	Use	Source
px330-puro	CRISPR plasmid with puro resistance	This study
px330-S73	CRISPR plasmid with MSL2 ex2 guide	This study
px330-S90	CRISPR plasmid with MSL2 ex1 guide	This study
px335_gA1	CRISPR plasmid with MSL2 ex2 guide for DNA nicking	This study
px335_gB1	CRISPR plasmid with MSL2 ex2 guide for DNA nicking	This study
px330-puro_g4	CRISPR plasmid with MSL2 ex2 guide for HR template	This study
px330-M1_2	CRISPR plasmid with MSL1 ex1 guide	This study
pGEM-T Easy-HR 800	Repair template plasmid for endogenous tagginig	This study
pGEM-T Easy-HR	Repair template plasmid for endogenous tagginig	This study
pcDNA3.1 Myc-BirA(R118G)	C-terminal tag for BioID	Santocanale Lab
pcDNA3.1 Myc-BirA(R118G)-hMSL2	Expression plasmid for modified BioID	This study
pcDNA3.1 Myc-BirA(R118G)	Expression plasmid control for modified BioID	This study
Cerulean	FACS GFP ligation assay transfection control	Lowndes Lab
I-I-SceI	FACS GFP ligation assay	Lowndes Lab
HA-Ub	Expression plasmid for mammalian cells	Lowndes Lab
His-Ub	Expression plasmid for mammalian cells	Dr. Gaelle Legube
Flag-53BP1	Expression plasmid for mammalian cells	Lowndes Lab
GFP-53BP1	Expression plasmid for mammalian cells	Lowndes Lab
HA-2Flag-hMSL2	Expression plasmid for mammalian cells	Dr. Simona Moravcová
HA-2Flag-hMSL2-ΔRING	Expression plasmid for mammalian cells	Dr. Simona Moravcová
HA-2Flag-hMSL2-C44A	Expression plasmid for mammalian cells	Dr. Simona Moravcová
pCMV 3Tag 2A-6His-mMsl1	Expression plasmid for mammalian cells	This study

2.1.5. Bacterial strains

Bacterial strains for cloning or protein expression used in this study are listed in Table 2.5.

Table 2.5: *E. coli* strains used in this study

***E. coli* strains**	**Genotype**	**Use**
Top10 (Invitrogen)	F- *mcrAΔ (mrr-hsdRNS-mcrBC) φ80lacZΔM15 ΔlacX74deoR recA1 araD139 Δ(araleu) 7697 galU galK rpsL(StrR) endA1 nupG*	Cloning
DH5α	F- Φ80*lac*ZΔM15 Δ(*lac*ZYA-*arg*F) U169 *rec*A1 *end*A1 *hsd*R17 (rk-, mk+) *pho*A*sup*E44 λ-*thi*-1 *gyr*A96 *rel*A1	Cloning
One Shot ccdB Survival 2 T1 (Invitrogen)	F-*mcr*A Δ(*mrr-hsd*RMS-*mcr*BC) Φ80*lac*ZΔM15 Δ*lac*X74 *rec*A1 *ara*Δ139 Δ(*ara-leu*)7697 *gal*U *gal*K *rps*L(StrR) *end*A1 *nup*G *fhu*A::*IS2*	Cloning of plasmids containing the ccdB gene
BL21-CodonPlus-RIL (Stratagene)	*E. coli B F– omp T hsdS(rB – mB –) dcm+ Tetr gal endA Hte [argU ileY leuW Camr]*	Recombinant protein expression
BL21-AI (Invitrogen)	F- *ompT hsdS*$_B$ ($r_B^-m_B^-$) *gal dcm araB* : : *T7RNAP- tetA*	Recombinant protein expression
DH10Bac	F-*mcr*A Δ(*mrr*-hsdRMS-*mcr*BC) Φ80*lac*ZΔM15 Δ*lac*X74 *rec*A1 *end*A1 *ara*D139Δ(*ara, leu*)7 697 *gal*U *gal*K λ- *rps*L *nup*G/pMON14272/pMON7124	Production of recombinant bacmids (Bac-to-Bac)
PIR1	F- Δ*lac*169 *rpo*S(am) *rob*A1 *cre*C510 *hsd*R51 4 *end*A *rec*A1 *uidA(ΔMlu I)::pir-116*	Production of recombinant plasmids (MultiBac)
DH10EmBacY	B strain derivative: F-mcrA Δ(*mrr-hsd*RMS-*mcr*BC) Θ80*lac*ZΔM15 Δ*lac*X74 *rec*A1 *end*A1 *ara*D139 Δ(*ara leu*)7697 *gal*U *gal*K *rps*L *nup*G λ- *ton*A + helper plasmid for Tn7 transposon enzyme + *yfp* reporter gene ($K^RTet^RCam^R$)	Production of recombinant bacmids (MultiBac)

2.1.6. Cell lines

Cell lines used in this study are listed in Table 2.6. DR-Hela and H1299 cell lines used in GFP ligation assay for monitoring homologous recombination (HR) or non-homologous end joining (NHEJ) repair were a generous gift of Dr. Maria Jasin. Sf21 cell line for MultiBac protein expression was a generous gift of Dr. Imre Berger.

Table 2.6: Cell lines used in this study

Cell type	**Description**	**Source**
RPE-1	Retinal pigment epithelial cell line (female)	ATCC
RPE-1 (90D4) *MSL2* $^{-/-}$	MSL2 knock-out RPE-1 cell line (clone 90D4)	This study
RPE-1 73C4	MSL2 knock-out RPE-1 cell line (clone 73C4)	This study
RPE-1 *MSL1* $^{-/-}$	MSL1 knock-out RPE-1 cell line (clone M1_7)	This study

Cell type	Description	Source
RPE-1 *TP53*$^{-/-}$ *MOF*$^{-/-}$	p53 and MOF knock-out RPE-1 cell line	Karen Lane
ARPE-19	Retinal pigment epithelia cell line (male)	ATCC
HEK293T	Embryonic kidney cell line	ATCC
U2OS	Osteosarcoma cell line	ATCC
HeLa CCL2	Cervical adenocarcinoma cell line	ATCC
NHDF	Dermal fibroblast cell line	ATCC
MRC5	Fetal lung fibroblast cell line	ATCC
BJ	Foreskin fibroblast cell line	ATCC
DR-Hela	Cervical adenocarcinoma cell line containing a single stably integrated GFP repair site at a transcriptionally active genomic locus	M. Jasin, 1999
DR-Hela *MSL2*$^{-/-}$	MSL2 knock-out DR-Hela cell line (clone)	This study
H1299	Lung cancer cell line containing a single stably integrated GFP repair site at a transcriptionally active genomic locus	H. Ogiwara, 2007
H1299 *MSL2*$^{-/-}$	MSL2 knock-out H1299 cell line (clone)	This study
High Five	*Trichopulsia ni* (cabbage looper) ovary cell line	ATCC
Sf9	*Spodoptera frugiperda* (fall armyworm) ovary cell line	ATCC
Sf21	*Spodoptera frugiperda* (fall armyworm) ovary cell line	Nasheuer Lab

2.1.7. Tissue culture consumables and reagents

Tissue culture plastic ware was purchased from Sarstedt, Corning, Cruinn, Fisher or Sigma. Mediums used for cell culture and transfection are listed in Table 2.7. Fetal bovine serum (FBS), Dimethyl sulfoxide (DMSO), penicillin and streptomycin antibiotics were purchased from Sigma.

Table 2.7: Mediums used in this study

Name	Description	Source
DMEM	Dulbecco's Modified Eagle Medium	Sigma
DMEM F-12	1:1 mix of Dulbecco's Modified Eagle Medium and Ham's F-12 Medium	Lonza
RPMI 1640	Roswell Park Memorial Institute 1640 Medium	Sigma
TC100	Modified Grace's Insect Medium	Lonza
Opti-MEM	Reduced Serum Medium	Sigma

Drugs used for selection in bacteria ad stable cell line selection or culture of human cells were purchased from Invivogen are listed in Table 2.8.

Table 2.8: Antibiotics used in this study

Name	Concentration	Name	Concentration
Puromycin	5 µg/ml	**Ampicillin**	100 µg/ml
G418	1 mg/ml	**Kanamycin**	50 µg/ml
Blasticidin	15 µg/ml	**Gentamycin**	7 µg/ml
Hygromicin	15 µg/ml	**Chloramphenicol**	25 µg/ml
Zeocin	100 µg/ml	**Spectinomycin**	50 µg/ml

Inhibitors and nucleotide analogues for cell cycle arrest and analysis are listed in Table 2.9.

Table 2.9: Drugs and nucleotide analogues used in this study

Name	Working concentration	Name	Working concentration
Aphidicolin	0.2 µM	**BrdU**	20 µM
Nocodazole	0.1 µg/ml	**IdU**	20 µM
Hydroxyurea	2 mM	**CldU**	200 µM
Biotin	50 µM		

2.1.8. Antibodies

Primary and secondary antibodies used in this study are listed in Table 2.10. In general, antibodies were probed in 2% milk with the exception of antibodies against histone modifications where 1% BSA was used. All primary antibodies were probed overnight while secondary antibodies for 1 h.

Table 2.10: Antibodies used in this study

Name	Host species	Dilution for WB	Dilution for IF/FACS	Reference
53BP1 (NB100-904)	Rabbit polyclonal	1:1000	1:1000	Novus Bio
BRCA1 (D-9) (sc-6954)	Mouse	1:1000	1:200	Santa Cruz
BrdU (347 580)	Mouse monoclonal		1:50	BD Biosciences

Name	Host species	Dilution for WB	Dilution for IF/FACS	Reference
BrdU (MA1-82088) IgG2A	Rat monoclonal		1:100	Thermo Scientific
FLAG (F 1804)	Mouse monoclonal	1:1000		Sigma
GFP (11814460001)	Mouse monoclonal	1:1000	1:1000	Roche
GST (G 7781)	Rabbit monoclonal	1:5000		Sigma
H3 (ab1791)	Rabbit polyclonal	1:10000		Abcam
H3K27me3 (C36B11)(#9733)	Rabbit polyclonal	1:1000	1:1000	Cell Signaling
H3K9me3 (#9754S)	Rabbit polyclonal	1:1000		Cell Signaling
H3Ser10ph (06-570)	Rabbit polyclonal	1:1000		Millipore
H4K16ac (07-329)	Rabbit polyclonal	1:1000	1:1000	Millipore
H4K20me2 (07-367)	Rabbit monoclonal	1:1000		Millipore
H4K20me3 (07-463)	Rabbit monoclonal	1:1000		Millipore
His (27-4710-01)	Mouse monoclonal	1:2000		GE Healthcare
MOF (7D1)	Mouse monoclonal	1:5		Dundee Cell
MSL2 (4F12)	Mouse monoclonal	1:5		Dundee Cell
MSL3 (ab38382)	Rabbit polyclonal	1:300		Abcam
HRP-streptavidin (#3999)	Mouse antiserum	1:2000		Cell Signaling
HRP-β-actin (A3854)	Mouse monoclonal	1:10000		Sigma
Lamin B1 (ab133741)	Rabbit polyclonal	1:5000		Abcam
MDC1 (A300-053A)	Rabbit monoclonal	1:1000	1:1000	Bethyl
Myc (9E10)	Mouse monoclonal	1:5000		Thermo Scientific
SCC1 (2109)	Rabbit polyclonal	1:3000		Sigma Genosys
Ub (P4D1)	Mouse monoclonal	1:500		Santa Cruz
Ub (VU-1)	Mouse monoclonal	1:1000		Tebu-Bio
V5 (2F11F7)	Mouse monoclonal	1:1000		Invitrogen
α-tubulin (T 6074)	Mouse monoclonal	1:5000		Sigma
β-actin (ab8227)	Rabbit polyclonal	1:5000		Abcam
γH2A.X (05-636)	Mouse monoclonal	1:5000	1:1000	Millipore
Alexa Fluor-488 (A21202)	Donkey anti mouse monoclonal		1:800	Molecular Probes
Alexa Fluor-488 (A21470)	Chicken anti rat monoclonal		1:300	Invitrogen
Alexa Fluor-488 (A21208)	Donkey anti rat monoclonal		1:300	Invitrogen

Name	Host species	Dilution for WB	Dilution for IF/FACS	Reference
Alexa Fluor-594 (A21203)	Donkey anti mouse monoclonal		1:800	Molecular Probes
Alexa Fluor-594 (A21123)	Goat anti mouse IgG1 monoclonal		1:300	Invitrogen
Alexa Fluor-594 (A21207)	Donkey anti rabbit monoclonal		1:800	Molecular Probes
FITC (715-095-150)	Donkey anti mouse		1:50	Jackson
HRP-Anti-mouse (NA931)	Sheep monoclonal	1:10000		Amersham
HRP-Anti-rabbit (NA934)	Donkey monoclonal	1:10000		Amersham

2.1.9. Computer programmes

DNA sequencing data was viewed and DNA plasmid maps were created using SnapGene Viewer 3.1.1 (GSL Biotech). DNA and protein alignments were created in CLC Sequence Viewer (Qiagen). For primer design Primer3web (http://primer3.ut.ee/) or Primer Premiere 5 (http://www.premierbiosoft.com/) was used. Gene and protein sequences were obtained from Ensembl (http://www.ensembl.org) or National Center for Biotechnology Information (https://www.ncbi.nlm.nih.gov/). For CRISPR/Cas9 guide RNA sequence design the Zhang Lab online tool (http://crispr.mit.edu/) was used. Graph Pad Prism 7.00 (GraphPad Software) was used for graphs and statistical analysis.

2.2. Methods

2.2.1. Nucleic acid methods

2.2.1.1. RNA extraction

RNA extraction was carried out according to the manufacturer's instructions using Isolate RNA Mini Kit (Bioline). Briefly, $3x10^6$ cells were harvested and disrupted in lysis buffer. The released RNA was then bound to the column provided in the Kit. After washing, the RNA was eluted in 50 µl RNase-free water and stored at -80^{o}C.

2.2.1.2. cDNA synthesis

Following RNA extraction reverse transcription was performed using 0.5µg total RNA using the High capacity RNA-to-cDNA kit (Applied Biosystems). The conditions and the programme used are as in Table 2.11.

Table 2.11: Reverse transcription protocol

Reagents	Final concentration	RT PCR programme		
RNA	0.5µg	Reverse transcription	37°C	60 min
2x RT buffer	1x	Enzyme inactivation	95°C	5 min
20x Enzyme Mix	1x	Hold	4°C	
H_2O	up to 10 µl			

2.2.1.1. Genomic DNA extraction

Genomic DNA was extracted using SmartExtract - DNA Extraction Kit (Eurogentec) or by using the following protocol. Pelleted cells were resuspended in 500 µl TAIL Buffer, containing 20 mg/ml Proteinase K solution and incubated overnight at 37°C. Samples were then incubated at room temperature with shaking at 1400 rpm for 5 min. 240 µl 5M NaCl was added to them and incubated again at room temperature with shaking at 1400 rpm for 5 min. Genomic DNA was separated by centrifugation at 13300 rpm at 4°C for 30 min. The supernatant was then saved and the DNA was precipitated with 700 µl isopropanol. The solution was centrifuged at 13300 rpm at 4°C for 10 min and the pellet was washed with 300µl 70% ethanol. After centrifugation at 13300 rpm at room temperature for 5 min the ethanol was removed, the pellet was air dried and redissolved in 60 µl of Qiagen Elution Buffer.

2.2.1.2. RNA and DNA concentration estimation

The concentration of RNA and DNA was determined by using NanoDrop 2000c spectrophotometer (Thermo Scientific). 1µl of RNA or DNA was loaded and the absorbance was measured at 260 nm. Samples with an OD 260/280 ratio between 1.8 and 2 were used for further experiments.

2.2.1.3. Polymerase chain reaction

Polymerase chain reaction was performed on an Eppendorf Mastercycler epgradient or an Eppendorf Mastercycler epgradient S PCR machine (Eppendorf) using KOD Hot Start (Novagen) polymerase. The PCR was set up according to the manufacturer's instructions, the primers melting temperature and the predicted size of the PCR product. The general PCR programme used in this study is shown in Table 2.12.

Table 2.12: Polymerase chain reaction protocol

Reagents	Final concentration	PCR programme			
DNA	50 ng	Hot start	95°C	45 sec	
10x KOD Hot start buffer	1x	Denaturation	95°C	30 sec	
dNTPs	200 µM	Annealing	60-65°C	20 sec	30x
25mM $MgSO_4$	1 mM	Elongation	70°C	20 sec-2 min	
10mM Forward primer	0.5 µM	Final elongation	70°C	5 min	
10mM Reverse primer	0.5 µM	Hold	4°C		
KOD polymerase	1 U				
DMSO	5 %				
H_2O	up to 20 µl				

2.2.1.4. Fusion PCR

With this method two to three PCR fragments were fused together using the primers from the original reactions. First, each fragment was amplified separately using outer primers containing specific restriction sites and inner primers containing overlapping regions with the other PCR products. Then these products were used as templates in a subsequent PCR reaction using the same outer primers as for the fragment amplifications. For an easier assembly of three fragments only two PCR products were used at a time and the reaction was repeated with the previously assembled two products and the third fragment.

2.2.1.5. Quantitative real-time PCR

Quantitative real-time PCR (Q-PCR) was used to predict gene expression based on the amount of specific RNA transcribed. To measure the newly synthesised DNA in this PCR reaction SYBR Green fluorescent dye was used. SYBR Green can integrate into the synthesised DNA and the accumulation of the amplified product can be measured. The Q-PCR mix was made following the manufacturer's instruction using Fast SYBR Green Master Mix Kit (Applied Biosystems). As template, cDNA was used. After reverse transcription, it was diluted 1:50 and amplified using gene specific primers and normalised to the expression of housekeeping genes (*GAPDH*, *PPIA* and *HPRT*). Primer sequences are listed in Table 2.3. The reactions were run in Optical 96-well Reaction Plates using the 7500 Real Time PCR System (Applied

Biosystems). Each reaction was run in duplicates or triplicates. Each primer pair was tested with a melting curve analysis to confirm their specificity. The results were analysed using the Applied Biosystems detection System 7500 Software version 2.0.6. The PCR conditions are shown in Table 2.13.

Table 2.13: Quantitative real-time PCR protocol

Reagents	Final concentration	PCR programme			
2x Mastermix	1x	Hot start	95°C	20 sec	
cDNA	1:50 dil.	Denaturation	95°C	30 sec	
10mM Forward primer	0.5 µM	Annealing	60°C	30 sec	30x
10mM Reverse primer	0.5 µM	Elongation	60°C	30 sec	
H_2O	up to 10 µl				

2.2.1.6. Restriction digestion of DNA

Enzymes used in this study were purchased from New England Biolabs (NEB) and the digestion conditions were followed as provided by the manufacturer. The digested DNA was visualised on agarose gel using SybrSafe (Invitrogen).

2.2.1.7. Alkaline phosphatase treatment of DNA

In certain cases alkaline phosphatase treatment was used on restriction digested plasmids to prevent re-ligation. Digested samples were treated with Shrimp Alkaline Phosphatase (SAP) (Promega). This reaction removes 5' phosphate group from the ends of the DNA. The reaction was performed following the manufacturer's instructions. Briefly 1unit/µg DNA of SAP was incubated with the restriction digested vector at 37°C for 1 h in 1x SAP reaction buffer. The SAP treated plasmid was then purified using High Pure PCR Cleanup Micro Kit (Roche) or SmartPure PCR Kit (Eurogentec).

2.2.1.8. Agarose gel electrophoresis

Agarose gel electrophoresis was performed to visualise DNA fragments and separate them by size. For size determination the DNA fragments were compared to a 1kb DNA ladder (Fermentas) molecular weight marker ran alongside the samples. Samples were loaded with 6x Sample loading dye (New England Biolabs). 0.75-1% agarose gels were prepared using agarose (Sigma) dissolved in 1xTAE with 0.01% SybrSafe (Invitrogen) DNA dye. The electrophoresis was performed at 80V for 1h

using Bio-Rad PowerPac Basic power supply and was visualised using ChemiImager 5500 (Alpha Innotech) ultraviolet (UV) trans- illuminator.

2.2.1.9. DNA extraction and purification

DNA bands were excised from the agarose gel using a scalpel blade. Samples were placed into a 1.5ml Eppendorf tube and weighed. Using the QIAquick Gel Extraction Kit (Qiagen) or the SmartPure Gel Kit (Eurogentec) DNA was extracted from the agarose gel and redissolved following the manufacturer's instructions.

If gel extraction was not necessary, DNA was purified directly after PCR or restriction digest using High Pure PCR Cleanup Micro Kit (Roche) or SmartPure PCR Kit (Eurogentec) following the manufacturer's instructions.

2.2.1.10. A tailing of DNA for ligation

To insert DNA into a T vector, PCR products generated by KOD enzyme were treated with Taq polymerase to attach A (Adenine) overhangs to the end of the DNA. Briefly, the DNA was incubated with Taq enzyme, 10X Buffer and $MgCl_2$ at 72^{o}C for 10 min. The product was then either used directly in a ligation reaction or purified using High Pure PCR Cleanup Micro Kit (Roche) or SmartPure PCR Kit (Eurogentec) following the manufacturer's instructions.

2.2.1.11. DNA ligation

DNA ligation was performed using T4 DNA ligase enzyme and buffer (NEB) in 10 µl final volume. Depending on the size of the fragments and the nature of the ligation (blunt- or sticky-end) the reaction was kept at room temperature (RT) for 1h or at 4^{o}C overnight.

2.2.1.12. MultiBac plasmid generation with Cre-LoxP recombination

Acceptor (pACEBac1, pACEBac2) and donor (pIDC, pIDK, pIDS) vectors were used to generate plasmid fusion containing different genes. The multigene fusion was performed in a stepwise manner using one acceptor and one donor construct at a time. Briefly approximately equal amount of acceptor and donor vectors were combined with Cre recombinase enzyme (NEB) in a 20 µl reaction following the instructions described in the ACEMBL MultiBac User Manual (Version 3.0). The reaction was incubated at 37^{o}C for 1 h.

2.2.1.13. Preparation of chemically competent *E. coli*

Chemically competent *E. coli* cells were prepared with $CaCl_2$ method. Cells were grown without antibiotics overnight at 37°C in 5ml LB broth with shaking at 650 rpm. Then cells were diluted in 1:50 in 100ml LB broth and were grown again with shaking at 37°C to an OD600 between 0.5 and 0.6. Then they were aliquoted into 50 ml Falcon tubes and chilled on ice for 5 min. After that they were centrifuged at 6000g for 10 min at 4°C. The cell pellets were then resuspended in 50 ml ice cold 0.1M $CaCl_2$, incubated on ice for 30 min and pelleted again. After that cells were resuspended in 0.1M $CaCl_2$ containing 15% glycerol and aliquoted into 1.5 ml Eppendorf tubes. The aliquots were snap frozen in liquid nitrogen or on dry ice and stored at -80°C.

Chemically competent *E. coli* cells containing a bacmid backbone were prepared with a different $CaCl_2$ method. Cells were grown without antibiotics overnight at 37°C in 500ml LB broth with shaking at 650 rpm. Then they were diluted in 1:4 in 2l LB broth and were grown again with shaking at 37°C to an OD600 between 0.4 and 0.5. After that cells were aliquoted into 500ml centrifuge tubes and incubated on ice for 15 min. Cells were then pelleted at 4000g for 10 min. They were resuspended in 200 ml $CaCl_2$ solution and were pelleted again at 4000g for 10 min. The pellet was resuspended in 200 ml $CaCl_2$ solution and was incubated on ice for 30 min. Following incubation cell were pelleted again at 4000g for 10 min and resuspended in 8 ml $CaCl_2$ solution. The suspension was aliquoted into 1.5 ml Eppendorf tubes and the aliquots were snap frozen in liquid nitrogen or on dry ice and stored at -80°C.

2.2.1.14. *E. coli* transformation

Competent cells were mixed with DNA and incubated on ice for 30 min. After that cells were heat shocked at 42°C for 30 sec and then placed back on ice for 5 min. 500-1500 µl LB broth or SOC media was added to the transformation and cells were allowed to recover at 37°C with shaking at 650 rpm for 30 min or overnight. Cells then were pelleted at 2000 rpm for 3 min, resuspended in 50 µl LB broth and spread onto LB agar plates containing appropriate antibiotics and incubated overnight at 37°C.

For blue-white screening, plates were treated with 50 µl of 20mg/ml X-gal solution and 100 µl of 100 mM IPTG. After growing the cells overnight, white colonies were

picked and streaked onto a second X-gal and IPTG containing plate for double selection. For Bacmid transformation colonies were picked after 48h incubation at 37^{o}C.

2.2.1.15. Plasmid DNA preparation

Plasmid DNA was extracted using NucleoBond Xtra Midi Plus Kit (Marcherey-Nagel) following the manufacturer's instruction. The same solutions were used for miniprep extraction as well. Briefly, 4 ml of cell culture was pelleted in a tabletop centrifuge at 14000 rpm for 1 min. The pellet was resuspended in 200 µl Resuspension Buffer and lysed with 200 µl Lysis Buffer. After 2 min incubation 200 µl Neutralization Buffer was added to the lysis and the mixture was incubated on ice for 5 min. The mixture was then centrifuged at 13000 rpm for 30 min at 4^{o}C. The supernatant containing the plasmid DNA was transferred to a new Eppendorf tube and the DNA was precipitated using 200 µl 100% isopropanol. The DNA was pelleted at 13000 rpm for 30 min at 4^{o}C. The supernatant was removed and the pellet was washed with 70% ethanol and centrifuged again at 13000 rpm for 15 min at 4^{o}C. The ethanol was then carefully removed. The pellet was air dried for 10 min and resuspended in 30-50 µl Resuspension Buffer.

2.2.1.16. Bacmid DNA extraction

Bacmid DNA was extracted using reagents from NucleoBond Xtra Midi Plus Kit (Marcherey-Nagel) with the following protocol. Briefly, 2 ml DH10Bac cell culture was pelleted in a tabletop centrifuge at 14000 rpm for 1 min. After removing the media, cells were resuspended in 300 µl Resuspension Buffer. Cells were then lysed using 300 µl Lysis Buffer (without blue lysis indicator dye) and incubated at room temperature for 5 min. Following the incubation, 300 µl Neutralization Buffer was added to the lysate and mixed gently. After precipitate formation the samples were incubated on ice for 10 min and pelleted at 14000 rpm for 10 min. The supernatant was then transferred to a new Eppendorf tube containing 800 µl isopropanol. After gentle mixing the samples were incubated on ice for 10 min, then pelleted at 14000 rpm for 15 min. The supernatant was then removed and 500 µl 70% ethanol was added to the pellet and washed by inverting the tube several times. Samples were then centrifuged at 14000 rpm for 10 min and the washing step was repeated one more time. The ethanol was then removed and the pellets were air dried for 10 min.

The DNA was then resuspended in 40 µl of Resuspension Buffer. Samples were stored at 4°C until transfection and then transferred to -20°C.

2.2.2. Protein methods

2.2.2.1. Whole cellular protein extraction

For protein extract preparation cells were harvested, pelleted at 1200 rpm for 5 min and washed with 1xPBS. Cell pellets were then resuspended in either RIPA lysis buffer or Benzonase lysis buffer supplemented with Complete EDTA free Protease Inhibitor Cocktail (Roche) and PhosSTOP Phosphatase Inhibitor Cocktail Tablets (Roche). The lysates were then incubated on ice for 1 h. Then the samples were centrifuged at 13000 rpm for 15 min and the supernatant was transferred to a new tube. The pellet was discarded. The protein concentration was determined using Bradford method.

For baculoviral protein expression High Five cells were harvested, pelleted at 1000 rpm for 5 min and washed with 1xPBS. Cell pellets were then resuspended in Lysis buffer supplemented with Complete EDTA free Protease Inhibitor Cocktail (Roche). Lysates were incubated on ice for 45 min, centrifuged at 13000 rpm for 15 min and the supernatant was transferred to a new tube and saved as soluble protein fraction. The pellet was then again resuspended in Lysis buffer, incubated on ice for 45 min and saved as insoluble fraction.

2.2.2.2. Subcellular protein fractionation

4x 10 cm confluent dishes were harvested, pelleted at 1200 rpm for 5 min and washed with 1xPBS. The cell pellets were then resuspended in 750 µl Buffer A and incubated on ice for 5 min. After that cells were broken open with a pre-chilled 1 ml dounce homogenizer (20 times with a tight pestle) and pelleted at 1500 rpm for 5 min at 4°C. Pellet and supernatant were both saved. The supernatant was transferred into a new 1.5 ml Eppendorf tube, lysed with 5xLysis Buffer on ice for 10 min. The lysate was centrifuged at 12000 rpm at 4°C and the supernatant was saved as cytoplasmic fraction. The pellet saved was resuspended in 600 µl Sucrose 1, carefully layered over a 600 µl cushion of Sucrose 3 and centrifuged at 6000 rpm for 10 min at 4°C. The supernatant was discarded and the pellet was washed 2 times with 500 µl 1xLysis Buffer. After that it was resuspended in 300 µl 1xLysis Buffer and incubated on ice for 10 min. The lysate was then centrifuged at 600 rpm for 10 min at 4°C. The

supernatant was transferred to a new tube and saved as nuclear fraction. The pellet was then lysed in 150 µl Benzonase lysis buffer and incubated on ice for 1h. The lysate was centrifuged at 13000 rpm for 15 min and the supernatant was saved as chromatin bound fraction.

2.2.2.3. Cytoplasmic and nuclear protein fractionation

10 cm confluent dish/sample was harvested and pelleted at 1200 rpm for 5 min and washed with 1xPBS. Cell pellets were then resuspended in 300 µl Isotonic lysis buffer and incubated on ice for 15 min. After incubation 10% IGEPAL CA-630 was added to the lysate in a final concentration of 0.3%. Cells were vortexed and further incubated on ice for 5 min. Lysates were pelleted at 1500 rpm for 20 min at4^{o}C. The supernatant was transferred to a fresh tube and pelleted again at 14000 rpm for 15 min at 4^{o}C. The supernatant was saved as cytoplasmic fraction. The pellet was resuspended in Nuclear extraction buffer and agitated on a mixer first at 700 rpm for 10 min at 4^{o}C, then at 1400 rpm for an additional 10 min at 4^{o}C. Lysates were then pelleted at 14000 rpm for 10 min at 4^{o}C. Supernatant was saved as nuclear fraction.

2.2.2.4. Bradford assay

To determine the protein concentration of cell lysates the Bradford method was used. 1 µl of protein extract was mixed with 500 µl Bradford Reagent (Sigma) and 500 µl H_2O. The mixture was incubated for 5 min and loaded into a cuvette. The absorbance was measured against a blank sample at 595 nm with NanoDrop 2000c spectrophotometer (Thermo Scientific). To generate a calibration curve bovine serum albumin (BSA) was used. A stepwise dilution was made using a 2 mg/ml BSA stock solution (Bio-Rad) and the absorbance was measured as mentioned before. Using the absorbance and the concentration of these samples a linear standard was generated.

2.2.2.1. His-tagged protein co-immunoprecipitation

HEK293T cell were seeded to reach 70% confluency the next day. Cells were transfected with 4.5 µg DNA (2.5 µg myc-BioID/myc-BioID-MSL2 and 01 µg His-Ub constructs) and were harvested after 24 h. 10 hours prior harvest culture media was supplemented with 50 µM biotin. Cell pellets were lysed using benzonase lysis buffer. 10 µl slurry of HIS-Select HF Nickel Affinity Gel beads (H0537) (Sigma) per sample were pre-incubated in the same lysis buffer. 1 mg protein extract was then added to the beads and the final volume was adjusted to 500 µl. The affinity binding

was performed at 4°C with gentle rotation overnight. Beads were then pelleted at 1500 rpm 2 min and the supernatant was saved as unbound fraction. Samples were washed with lysis buffer and eluted with nickel bead elution buffer. Recovered samples were then used in a second immunoprecipitation using streptavidin beads.

2.2.2.2. Biotinylated protein co-immunoprecipitation

HEK293T cell were seeded to reach 70% confluency the next day. Cells were transfected with 4.5 µg DNA (2.5 µg myc-BioID/myc-BioID-MSL2 and 01 µg His-Ub constructs) and were harvested after 24 h. 10 hours prior harvest culture media was supplemented with 50 µM biotin. Cell pellets were lysed using benzonase lysis buffer. 60 µl slurry of magnetic MyOne Streptavidin C1 dynabeads (Invitrogen) per sample were pre-incubated in the same lysis buffer. 1.5 mg protein extract was then added to the beads and the final volume was adjusted to 500 µl. The affinity binding was performed at 4°C with gentle rotation for 4 h. Beads were then separated using magnetic force and the supernatant was saved as unbound fraction. Samples were washed with lysis buffer and eluted with streptavidin elution buffer at 65°C 2 min. The recovered protein was then subjected to SDS-PAGE.

2.2.2.3. GFP-tagged protein co-immunoprecipitation

HEK293T cell were seeded to reach 70% confluency the next day. Cells were transfected with 3 µg DNA (1 µg GFP-53BP1, 1.5 µg Flag-MSL2 and 0.5 µg His-Ub constructs) and were harvested after 24 h. Cell pellets were lysed using benzonase lysis buffer. 10 µl slurry of magnetic GFP-trap beads (Serotec) per sample were pre-incubated in the same lysis buffer. 700 µg protein extract was then added to the beads and the final volume was adjusted to 400 µl. The beads were then incubated with the extracts at 4°C with rotation for 2 h. The supernatant was then removed and the beads were washed and boiled in 10 µl 2xLSB. The recovered protein was then subjected to SDS-PAGE.

2.2.2.4. SDS-polyacrylamide gel electrophoresis

For visualisation and protein separation SDS polyacrylamide gel electrophoresis (SDS-PAGE) was used. For optimal separation, different percentage of gels (6-15%) were used according to the size of the protein of interest shown in Table 2.14. Briefly, protein extracts were mixed with 4x Laemmli buffer containing 1.25% β-mercaptoethanol. Samples were boiled at 95°C for 5 min for complete denaturation.

After, they were loaded on a gel alongside a Precision Plus Protein All Blue Prestained Protein Standard (Bio-Rad) or PageRuler Plus Prestained Protein Ladder (Thermo Scientific) protein weight marker and run at 100V in 1x Running buffer.

Table 2.14: SDS-polyacrylamide gel protocol

	Separating gel					Stacking gel
Gel percentage	**6%**	**8%**	**10%**	**12%**	**15%**	**5%**
H2O (ml)	5.4	4.7	4.1	3.3	2.3	3.05
30% Bis-Acrylamide (ml)	2	2.7	3.3	4.1	5.1	0.65
1.5 M Tris-HCl pH 8.8 (ml)	2.5					-
0.5 M Tris-HCl pH6.8 (ml)	-					1.25
10% SDS (µl)	100					50
10% APS (µl)	50					25
TEMED (µl)	5					5

2.2.2.5. Coomassie staining

Protein visualisation without the use of antibodies was mainly used for bacterial protein expression. After SDS-PAGE, gels were stained with Coomassie brillant blue stain for 30 min with gentle agitation. Gels were then destained using Coomassie destain solution until the background became clear. Approximate sensitivity: 100 and 500 ng/protein band.

2.2.2.6. Negative zinc staining

To visualise protein on an SDS-PAGE gel negative zinc staining was used as it shows higher sensitivity compared to coomassie straining. Gels were washed in deionised water for 5 sec and incubated in 200 mM imidazole for 20 min (12%gel). Following incubation imidazole solution was replaced by 200 mM $ZnCl_2$ solution and incubated until bands appeared. Staining results in white precipitation in the regions of the gel that does not contain proteins. Protein bands appear clear. Destaining was performed using Tris-glycine buffer. Approximate sensitivity: 10 and 100 ng/protein band.

2.2.2.7. Silver staining

For immunoprecipitated protein visualization the highly sensitive silver staining method was performed using the ProteoSilver Plus Silver Stain Kit (Sigma). Staining was performed following the manufacturer's instructions. Briefly SDS-PAGE gel

was fixed usinf Fixing solution for 20 min at room temperature. After 10 min wash in 30% ethanol solution gels were washed in MilliQ-H_2O for an additional 10 min. Gels were then senitized for 10 min using Senitizer Solution followed by 2x 10 min MilliQ-H_2O wash. Gels were then equilibrated in Silver Solution for 10 min and washed in MilliQ-H_2O for 1 min. Gels were developed using Developer solution for 10 min and the development was stopped by the addition of Stop Solution. Finally gels were washed in MilliQ-H_2O for 15 min. Approximate sensitivity: 1 and 10 ng/protein band.

2.2.2.8. Protein transfer to membrane

Before immunoblotting, proteins were transferred to nitrocellulose or PVDF membrane (GE Healthcare) in 1x Transfer buffer. For wet transfer Mini Trans-Blot Cell (Bio-Rad) was used and the transfer was run at 100V for 1 h. For semi-dry transfer Trans-Blot SD Semi-dry Transfer Cell (Bio-Rad) was used at a constant 300 mA for 45 min. The assembly of both transfer systems was performed according to the manufacturer's instructions. After the transfer, the membrane was stained with Ponceau S solution to determine the quality of the transfer for 5 min and washed with ddH_2O.

2.2.2.9. Immunoblotting

Following protein transfer the membrane was blocked with 2-5% milk or 1% BSA in 1x PBST or 1x TBST at room temperature for 30 min with gentle agitation. After that, membranes were incubated with primary antibodies listed in ... overnight at 4^{o}C. The excess antibody was washed off with 1x PBST or 1x TBST three times, then the membrane was incubated with horseradish peroxidase (HRP) conjugated secondary antibody listed in ... for 1 h at room temperature. The excess antibody was washed again as described previously and the proteins were detected using Pierce ECL Plus Western Blotting Substrate (Thermo Fisher) according to the manufacturer's instructions. The chemiluminescence signal was then captured using X-ray film (Konica Minolta) and CP1000 Automatic Film Processor (AGFA, Belgium). The signal intensity was analysed using ImageJ software (NIH).

2.2.3. Immunofluorescent microscopy

2.2.3.1. Sample fixation

Immunofluorescence was used to visualise subcellular protein localisation and foci formation after γ-irradiation (IR). Cells were seeded on 18 mm square micro cover glasses (VWR) and fixed with 100% ice cold methanol or 4% paraformaldehyde (PFA). Methanol fixed cell were then placed into -20^{o}C for at least 20 min before further proceeding to blocking and staining. PFA fixed cells were incubated at room temperature for 5 min in the PFA solution. Fixed cells were then washed twice with 1x PBS and permeabilised with 0.125% Triton-X in 1xPBS for 5 min.

2.2.3.2. Pre-extraction

Prior PFA fixation, in certain cases pre-extraction was performed. Cells were seeded on 18 mm coverslips were washed with 1x PBS twice and incubated with CSK buffer for 10 min. Then cells were washed with 1xPBS three times and fixed with 4% PFA solution.

2.2.3.3. Immunoblotting and mounting

After fixation cells were washed with 1x PBS four times for 4 min and blocked with 1% BSA/PBS for 30 min at room temperature. Samples were then incubated with 1% BSA/PBS containing primary antibody for 1 h at room temperature in a humid chamber. Coverslips were then washed three times is 1x PBS and incubated with fluorescent dye conjugated secondary antibody and 10 µg/ml Hoechst (Sigma) DNA staining solution for 1 h at room temperature in a humid chamber. Samples were then washed three times again with 1x PBS and dipped into MQ-H_2O before mounting them with mounting media on Superfrost microscope slides (Thermo Scientific). The slides were sealed with clear nail polish and stored at 4^{o}C until imaging.

2.2.3.4. Image capture

Immunofluorescent images were captured using Orca AG camera (Hamamatsu Photonics) on an Olympus IX51 inverted microscope (Olympus) under oil at room temperature. 100× oil objective, NA 1.35 and Volocity 6.0.1 software (PerkinElmer) was used. For γ-irradiation experiments z-stacks were collected using 0.4 µm distance between adjacent images. These were then merged into a 2D stack and individual channel images were exported as TIFF files for publication. Images for Figure 4.11 were captured using Olympus IX-71 (Olympus) on a DeltaVision Elite

high resolution microscope (GE Healthcare) under oil at room temperature. 100x oil objective and SWoRx version 6.5.2 software was used. Deconvolution was performed using Hygens Professional.

2.2.3.5. DNA fibre assay

DNA fibre analysis was performed as described previously (Merrick et al., 2004). Briefly, Cells were incubated in 20 µM IdU nucleotide analogue containing media for 30 min, then treated with 2 mM hydroxyurea for 2 h. The culture media was then replaced with fresh media containing 20 µM CldU nucleotide analogue and incubated for 30 min. Cells were trypsinised and resuspended in ice cold 1xPBS, counted and diluted to $2.5x10^5$ cells/ml. Nucleotide analogue labelled samples were diluted in 1:6 ratio with unlabelled samples and 2.5 µl was spread on a glass coverslip. 7.5 µl Spreading buffer was added to the cells and incubated for 8 min. Coverslips were then tilted 15^o to allow slow spreading of fibres. Once dried samples were immersed in 3:1 methanol/acetic acid solution for fixation overnight at 4^oC. Following day coverslips were treated with 2.5 M HCl for 1 h at room temperature and washed 3x with 1x PBS. Samples were blocked in 1% BSA in 1xPBST for 30 min. Then coverslips were incubated with primary antibody against CldU for 30 min, then washed with 1xPBS and blocking solution. Following the washing steps samples were incubated with the appropriate secondary antibody for 30 min. After incubation samples were washed, blocked and probed with primary antibody against IdU for 30 min followed by secondary antibody incubation as described before. Finally Coverslips were washed 3x in 1xPBS and mounted onto microscope slides with mounting media.

2.2.4. Cell biology techniques

2.2.4.1. Cell culture

Human cells were maintained in appropriate media supplemented with 10% fetal bovine serum (FBS) (Sigma) without antibiotics at 37^oC with 5% CO_2 in 95% humidity. At 90% confluency cells were trypsinised and split in 1:10 or 1:5 ratio.

Adherent insect cells were maintained in TC100 media with 10% FBS at 27^oC. Cells at 90% confluency were physically disrupted from their adherent state and split in 1:2 (Sf9 and Sf21) or 1:5 (High Five) ratio. Suspension Sf21 cells were cultured in

250 ml flasks in 20 ml media and were split 1:2 ratio when reached a confluency of $5x10^5$ cells/ml.

2.2.4.1. Freezing and thawing cells

90% confluent human cells in 10 cm dishes were trypsinised, resuspended in media, pelleted and washed with 1x PBS. Cell pellets were then resuspended in 900 µl freezing media (10% DMSO in FBS) and aliquots of 300 µl were transferred into Nalgene Cryogenic Vials (Thermo Fisher). Cells were frozen in a Mr. Frosty Freezing Container (Thermo Fisher) at -80°C overnight. Frozen samples were then transferred to liquid nitrogen tanks for long term storage or kept at -80°C.

2.2.4.2. Cell proliferation assay

RPE-1 cells were counted using a Neubauer haemocytometer (Marienfeld Superior) as described before (Strober, 2001). 20000 cells were then seeded in triplicates into 6-well dishes and counted every 24 h. Each experiment was repeated three times.

2.2.4.3. Clonogenic survival assay

RPE-1 cells were counted and seeded in numbers depending on treatment applied into 6 cm dishes in duplicates. 11-14 days after seeding the media was removed and cells were washed with 1xPBS. Colonies were then fixed with crystal violet solution for 30 min, then washed with 1x PBS twice and left for drying for 24 h. Colonies were then counted and the percentage of survival was calculated as described before (Franken et al., 2006).

2.2.5. Cell transfection

Plasmids used for transfection are listed in Table 2.4.

2.2.5.1. Transient transfection

Transient transfection of human cells was performed using Lipofectamine 2000 transfection reagent (Invitrogen). The day before transfection cells were seeded in 6-well plates to reach 70-80% confluency the next day. Plasmid DNA and Lipofectamine 2000 was mixed with Opti-MEM media separately and incubated for 30 min at room temperature. After that the two solutions were mixed and further incubated for 30 min. The cell culture media was then aspirated and the transfection mixture was added on to the cells dropwise. Followed by a 4 h incubation at 37°C the

transfection complex was replaced by culture media and the cells were further grown for 24-48 h.

2.2.5.2. Stable transfection

Stable transfection of human cells was performed using Lipofectamine 2000 transfection reagent (Invitrogen). The day before transfection cells were seeded in 10 cm dishes to reach 70-80% confluency the next day. The transfection complex was prepared as described before and was added dropwise to the cells without removing the culture media. 24 h after transfections cells were re-seeded with serial dilution (1:5) into 10 cm dishes containing selective antibiotics listed in Table 2.8. After colony formation separate clones were transferred into 24-well plates. Once confluent, cells were further scaled up to 6-well plates, 6 cm dishes and 10 cm dishes. Clones were then harvested for western blot analysis.

2.2.5.3. Bacmid transfection

Transfection of Sf9 and Sf21 insect cells was performed using Escort IV transfection reagent (Sigma). The day before transfection cells were seeded in T25 flasks to reach 70-80% confluency the next day. Bacmid DNA and Escort IV was mixed with serum free culture media separately, then mixed together and incubated for 30 min. The cells were washed with serum free media and the transfection mixture was added to them. After 4 h incubation at 27^{o}C the transfection complex was replaced by culture media and the cells were further grown for 48 h. The virus containing media was then removed and centrifuged at 1500 rpm for 5 min. The supernatant was transferred to a new tube and saved for further infections as passage 1 (P1) viral stock.

2.2.5.4. Baculoviral infection

To generate viral stocks for infection Sf9 ans Sf21 cells were seeded in T25 flasks to reach 70-80% confluency the next day. The following day 500 µl P1 viral stock was added to the culture media and the cells were further grown for 48 h. After that, the media was collected and centrifuged at 1500 rpm for 5 min. The supernatant was transferred to a new tube and saved for further infections as passage 2 (P2) viral stock. The procedure was repeated until the seventh passage of viral stock was collected. The viruses were then tested for protein expression and the infection method described before was repeated using High Five cells as host organisms

instead of Sf9 cells. 48 h post infection the cells were harvested for western blot analysis.

2.2.6. Flow cytometry

Cell cycle analysis was performed using BD Accuri C6 Flow Cytometer (BD Biosciences). 1x 10^6 cells were incubated with 20 µM BrdU for 20 min, harvested, resuspended in 1x PBS and filtered with CellTrics 30 µm cell filters (Sysmex). Cells were then pelleted at 1500 rpm for 5 min and resuspended in 300 µl 1x PBS. Fixation was performed by the addition of 700 µl of 100% ethanol with constant mixing by vortexing. Samples were stored at -20°C until further processing. Prior staining, 3 ml 1x PBS was added to the fixed cells, mixed and pelleted at 1200 rpm for 5 min. The pellets were then resuspended again in 1 ml 1x PBS. 1ml 4N HCl was added to the suspension and incubated for 15 min at room temperature. Cells were pelleted at 1200 rpm for 5 min, resuspended in 1x PBS and pelleted again. After that, the samples were resuspended in 1 ml 0.5% BSA in 1x PBST and pelleted again. The pellets were then incubated in 50 µl 0.5% BSA in 1x PBST containing anti BrdU primary antibody for 30 min at room temperature in the dark. 1 ml 1x PBS was the added to the cells and the suspension was centrifuged at 1200 rpm for 5 min. After that, the pellets were incubated in 50 µl 0.5% BSA in 1x PBST containing FITC conjugated secondary antibody for 30 min at room temperature in the dark. Cells were then pelleted and resuspended in 1 ml 1% BBSA in 1x PBS containing 40 µg/ml propidium iodide (PI) and 200 µg/ml RNase A at room temperature for 30 min.

For in vivo NHEJ and HR GFP ligation assays BD FACS Canto II (BD Biosciences) was used. Cells transfected with Cerulean and *I-SceI* encoding plasmids were harvested after 24 h, 48 h and 72 h filtered and resuspended in 1 ml 1x PBS.

Data was analysed using BD FACS Diva Software version 6.1.2 (BD Biosciences), BD Accuri C6 Plus version 9.4.11 (BD Biosciences) or Flowing Software version 2.0 (Cell Imaging Core, Turku Centre for Biotechnology).

2.2.7. γ-irradiation (IR)

For DNA damage experiments γ-irradiation was used as damaging agent. Briefly, cells were seeded into 10 or 6 cm dishes for western blot analysis or 3 cm dishes with

coverslips for immunofluorescence experiments to reach the required confluency the next day. The irradiation was performed using a γ-irradiator with a ^{137}Cs source at 9.52 Gy/min (Mainance Engineering, Hampshire, UK).

2.2.8. Ultraviolet radiation (UV)

For UV induced DNA damage experiments were performed using UVItec UV lamp (LF 106S) UV radiation was monitored using UVItec RS radiometer (SX 254) Briefly cells were seeded into 6 cm dishes to the required confluency and were treated directly after attachment. The culture media was removed from the cells and was replaced after UV treatment.

3. Generation and functional analysis of human MSL2 and MSL1 knock-out cell lines

3.1. Introduction

MSL2 and MSL1 were initially discovered in *Drosophila*. They are part of the MSL complex which plays a critical role in *Drosophila* dosage compensation equalising the expression of X chromosome linked genes (Palmer et al., 1994, Kelley et al., 1995). This complex is responsible for the acetylation of lysine 16 at histone H4 (H4K16ac) whose modification enables the recruitment of different transcriptional factors to facilitate a twofold increase in expression of X chromosomal genes in male (XY) flies thus balancing their expression relative to females (XX) (Prestel et al., 2010, Schiemann et al., 2010, Conrad and Akhtar, 2012, Sun et al., 2013).

The members of the MSL complex are well conserved across species and have orthologues from yeast to humans (Sanjuan and Marin, 2001, Rea et al., 2007). MSL2 is known to possess E3 ubiquitin ligase activity and was found to specifically ubiquitylate H2B at lysine 34 (H2BK34ub) which plays a role in restarting the stalled RNA polymerase II at promoter regions (Wu et al., 2011). It was also shown that the knockdown of MSL2 affects X chromosome inactivation in mammals suggesting a role in human dosage compensation (Chelmicki et al., 2014). Although MSL1 was not found to possess enzymatic activity it is essential for the complex stability. The dimerization of MSL1 provides binding platform for MSL2 which is required for the correct conformation of the MSL2 protein facilitating the function of its RING domain (Hallacli et al., 2012). It has been shown that MSL2 is only enzimatically active in tandem with MSL1 and is only able to bind to a previously formed MSL1 dimer (Hallacli et al., 2012). While there are more extensive studies in *Drosophila* deciphering the role of the MSL complex, there is little known about the function of the human proteins, especially in a context outside of dosage compensation. To study the effect of human MSL2 and MSL1 on the other complex members a loss of function approach was selected and human knock-out cells were generated using the novel CRISPR/Cas9 genome editing technique.

3.2. CRISPR/Cas9 mediated gene editing

Previously obtained results showed that knock-down experiments using RNA interference (RNAi) has a low efficiency and for certain investigations it also limits the timescale of the assays. The partial knockdown of MSL2 could also result in a depletion level not strong enough to show a phenotype which could lead to difficulties in further investigations. To overcome these difficulties in functional analysis of both MSL2 and MSL1 a CRISPR/Cas9 mediated knock-out approach was selected.

The CRISPR (clustered regularly interspaced short palindromic repeats)/Cas9 system is based on a prokaryotic adaptive immune system that enables the targeted cleavage of foreign genetic elements (Deveau et al., 2010). The system itself is based on RNA-guided nucleases. There are three types of CRISPR systems across bacterias and archaeas and each system comprise a cluster of CRISPR-associated (Cas) genes. The most commonly used Cas enzyme is derived from *S. pyogenes* (Cas9) and it has been codon optimised for mammalian cell expression (Cong et al., 2013). This DNA cleaving enzyme can be targeted to specific sites in the genome by a 20 bp guide nucleotide preceded by an NGG trinucleotide. The latter is a requisite protospacer-adjacent motif (PAM) which Cas9 recognises and binds to. After PAM recognition and binding the guide sequence is matched to the following nucleotide sequences in the genome and in case of a match it cleaves the DNA 3 bp upstream of the PAM sequence.

To generate knock-out cell lines a single guide sequence is introduced to the cells for site specific cleavage. After the introduction of a double-strand break (DSB) in the target sequence the method relied on the error-prone NHEJ (nonhomologous end joining) repair system to introduce indels (insertions or deletions) generating a frameshift mutation after the targeted site resulting in a truncated, mutant protein (Ran et al., 2013, Rodgers and McVey, 2016). For more efficient targeting, a mutant version of the Cas9 enzyme, Cas9n can be used. In this case an aspartate-to-alanine mutation in the RuvC catalytic domain of the enzyme allows the Cas9n to nick rather than cleave DNA resulting in single-strand breaks and the subsequent preferential repair through HR. Efficient gene targeting with Cas9n requires a pair of gRNA sites to generate double-strand breaks with 5’ overhangs (Ran et al., 2013). This method

can be used to generate specific insertions for various purposes. In parallel to the knock-out cell line generation this work made attempts to use this technique for an endogenously tagged MSL2 cell line generation however due to time limitations the project was discontinued (**Appendix 4** – Endogenously tagged conditional MSL2 cell line generation).

3.2.1. MSL2 knock-out target strategy and screening

To study MSL2 and MSL1 functions in the least transformed cellular background in tissue culture conditions a cell line with close to normal karyotype was proposed to be used. So as a model system the non-transformed near-diploid hTERT RPE-1 (RPE-1) cell line was chosen.

The human *MSL2* gene is located on the autosomal chromosome 3 and contains two exons encoding a 577 amino acid protein. The RING domain, which is responsible for the enzymatic activity of MSL2 is located at the N terminal of the protein, therefore the main target for generating a null cell line was this region (Figure 3.1). For the knock-out strategy a CRISPR/Cas9 genome editing approach was used. With this method the aim was to introduce an indel (insertion/deletion) causing a frameshift mutation and resulting in a premature stop codon. To target the genomic locus of the MSL2 protein a wild type *S. pyogenes* Cas9 encoding plasmid (px330) was used and two guide sequences were designed in the RING encoding region. For target site selection the Zhang Lab online tool (zlab.mit.edu) was used, where a score system is applied to the potential target sequences within the region of interest. The online tool takes into consideration potential offtargets both within gene coding and non-coding regions in the genome and provides the potential guide sequences with a score (higher score corresponds to lower offtarget effect). From among these results the highest scored ones targeting either exon 1 or the beginning of exon 2 were chosen. These two sequences were called S90 and S73 respectively (Figure 3.1).

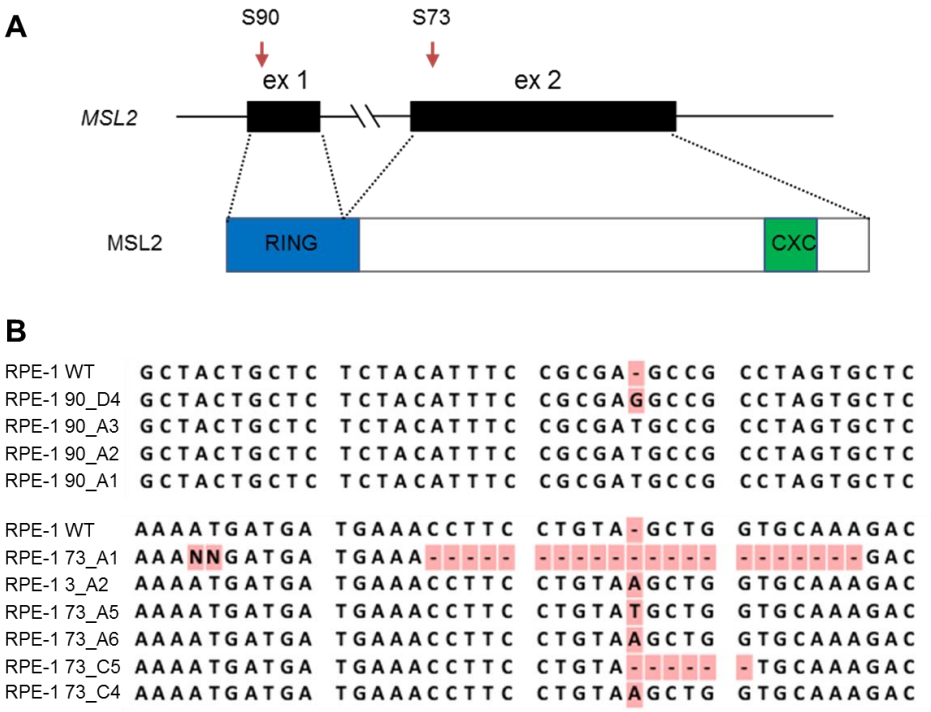

Figure 3.1: MSL2 coding region and CRISPR target strategy. A) Two target sites were selected to induce frameshift mutation in both exons disrupting the RING finger domain formation. B) Sequence alignment of wild type RPE-1 cells and mutated clones from the two target sites. Highlighted nucleotides show difference in the mutated sequence compared to the wild type (WT).

To target the Cas9 nuclease to the selected regions, the guide sequences were inserted into the px330 plasmid separately and RPE-1 cells were transfected along with a puromycin resistance coding plasmid (pLOX-Puro) using lipid transfusion. Since to date there is no reliable antibody for *in vivo* detection of MSL2 an alternative method was used to identify knock-outs. Clones from either strategy were selected and screened using restriction enzyme digest (figure not shown) and sequencing (Figure 3.1).

For pre-screening with restriction enzyme digest PCR primers were designed for the surrounding genomic region of the target sequences. The amplified region was then subjected to enzymatic digest and the digested product was visualised on agarose gel. Restriction enzymes were chosen to recognise the wild type sequence at the expected cut site. For the S90 target site *SfcI* and for the S73 *Cac8I* enzymes were used. Mutation generated in this region via CRISPR/Cas9 edition would abolish the restriction enzyme binding site and prevent it from cutting. The positive samples were sent for sequencing to identify the nature of the mutation (Figure 3.1).

Unfortunately this method only worked for the S90 target strategy and screens performed with the *Cac8I* enzyme did not give a conclusive result. Clones from the latter target strategy were thus sent directly for sequencing after PCR amplification. Both target strategies proved to be very efficient in generating mutations. In targeting exon 1 14 out of 24 clones screened proved to have some sort of indel mutation while the sequencing data from the exon 2 target site revealed 4 mutations out of 6 clones screened showing 58% and 67% efficiency respectively. Among these, clone 90D4 and 73C4 were chosen for further investigations. 90D4 contains one basepair insertion which results in a premature stop codon after the 30th amino acid. 73C4 also contains a one basepair insertion resulting in a premature stop codon after the 76th amino acid. Since both of these clones showed similar phenotypes during the initial analysis. Data is only presented for the 90D4 clone (*MSL2*$^{-/-}$).

3.2.2. MSL1 knock-out target strategy and screening

The human *MSL1* gene is located on the autosomal chromosome 17 and contains nine exons encoding a 614 amino acid protein. Similar to the MSL2 knock-out strategy, the CRISPR/Cas9 genome editing tool was used to introduce a frameshift mutation via indel generation which would result in a truncated mutant form of the protein. To generate a knock-out cell line the N-terminal coding region of the protein was targeted in exon 1 which also enabled the elimination of the MSL2 interacting region (Figure 3.2).

Detection of MSL1 via western blot proved to be challenging and while the antibody generated in house was able to detect recombinant MSL1 it was not specific enough in cellular extracts (**Appendix 1** - MSL2 and MSL1 antibody optimization). Thus, based on the success of the MSL2 knock-out strategy, the potential MSL1 clones were screened with a similar method. A pre-screening with restriction digest was not possible, since there was no available enzyme recognition site overlapping with the chosen target region. The surrounding genomic region of the expected mutation site was PCR amplified and the PCR products were sent directly for sequencing (Figure 3.2). Among the screened clones M1_7 was chosen for further investigations (*MSL1*$^{-/-}$). It contains a one basepair insertion which results in a frameshift mutation and a premature stop codon after the 19th amino acid.

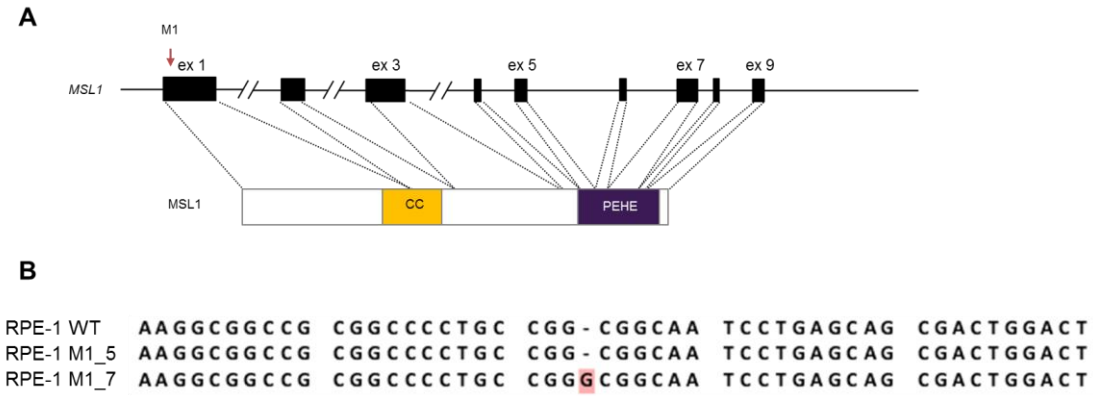

Figure 3.2: MSL1 coding region and CRISPR target strategy. A) One target site at the beginning of exon 1 was selected to induce frameshift mutation and disrupt the expression of a full length MSL1 protein. B) Sequence alignment of wild type RPE-1 cells and mutated clones from the MSL1 target site. Highlighted nucleotide shows insertion in the mutated sequence.

3.3. Human MSL2 and MSL1 are not essential for cell viability

After the generation of MSL2 and MSL1 knock-out cell lines the effect of their absence on viability and proliferation was tested. Observations showed that both *MSL2*$^{-/-}$ and *MSL1*$^{-/-}$ cells were viable and had similar morphology to wild type cells indicating that these genes are not essential for cell survival. To investigate if their proliferative ability is affected a growth assay was performed. Cells lacking either MSL2 or MSL1 had similar proliferation rate to the wild type RPE-1 cells with only a slight delay after 72h and so the loss of these proteins did not affect cell growth (Figure 3.3 A). This result was different from previously described observations in chicken DT40 cells, where *MSL2*$^{-/-}$ cells showed approximately 20% delay in proliferation (Lai, 2013). This could be due to the difference within cell types, since the doubling time for DT40 cells is approximately 8 hours as oppose to RPE-1 cells which double about every 24 hours. So the observed slight difference in proliferation rate might have been enhanced in the faster growing chicken cell line.

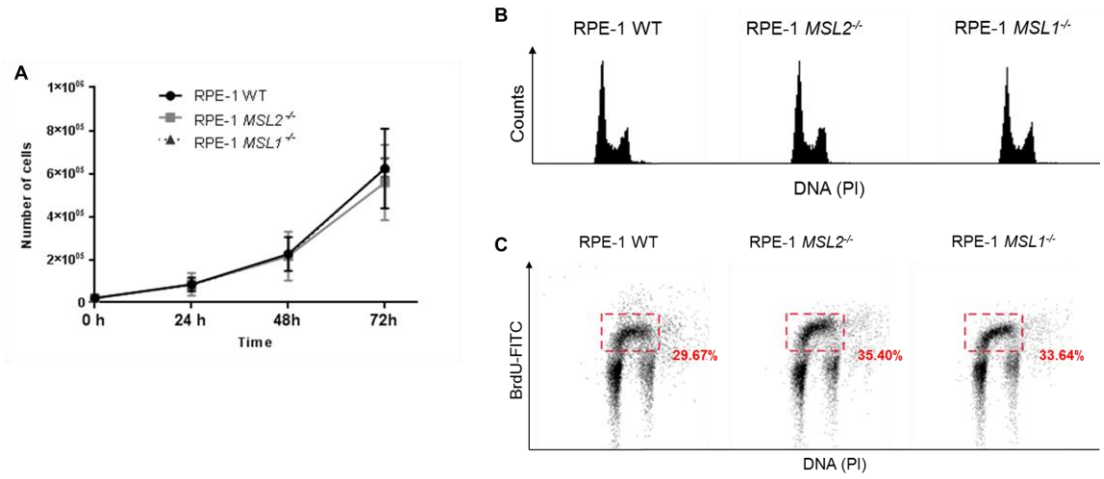

Figure 3.3: Cell proliferation analysis of RPE-1 WT, *MSL2*$^{-/-}$ and *MSL1*$^{-/-}$ cell lines. A) Growth curve of wild type, *MSL2*$^{-/-}$ and *MSL1*$^{-/-}$ RPE-1 cells. Error bars represent standard deviation (n=3). B) Cell cycle profile with propidium iodide (PI) of the indicated cells. C) Cell population in S phase of wild type, *MSL2*$^{-/-}$ and *MSL1*$^{-/-}$ RPE-1 cells. Cells were treated with BrdU, stained with FITC-anti BrdU antibody and propidium iodide (PI).

To further investigate if cell cycle progression is affected by the loss of either MSL2 or MSL1, the cell cycle distribution was analysed in each cell line by flow cytometry. $1x10^6$ asynchronous cells were treated with 20µM BrdU and harvested after 20 minutes. The cells were then trypsinised, washed and fixed in 70% ethanol. For DNA staining propidium iodide (PI) was used and the BrdU incorporation was visualised by anti-BrdU primary and FITC secondary antibody (Figure 3.3 A, B). In the assay shown, both *MSL2*$^{-/-}$ and *MSL1*$^{-/-}$ cells seem to have a slight (3.9% and 5.7%) increase in cell number in S phase compared to the wild type cells which could indicate a mild S phase arrest and a slower progression into mitosis. However, further repeats should be carried out to confirm this phenotype.

The obtained results show that wild type RPE-1, *MSL2*$^{-/-}$ and *MSL1*$^{-/-}$ cell lines grow and proliferate similarly under normal conditions.

3.4. The loss of human MSL2 and MSL1 does not affect the expression of the other MSL complex members

As reported before in Drosophila studies, the loss of MSL2 resulted in a decrease in both MSL1 and MSL3 protein levels while MOF expression did not change (Hamada et al., 2005). To address the question if the loss of either MSL2 or MSL1 has a

similar effect on the expression of the other members of the complex, first a quantitative PCR (Q-PCR) was performed (Figure 3.4).

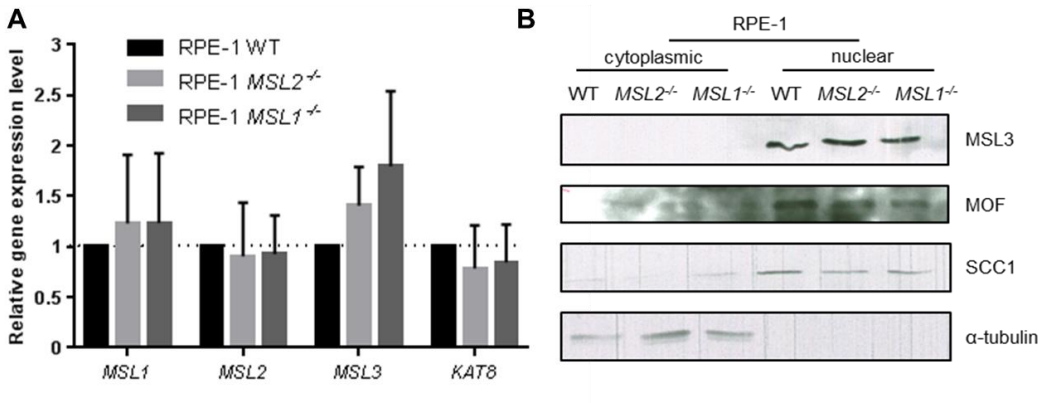

Figure 3.4: Relative gene expression levels of the human MSL complex members in wild type, *MSL2*$^{-/-}$ and *MSL1*$^{-/-}$ RPE-1 cell lines. A) Q-PCR analysis of the MSL complex member genes (*KAT8* is the MOF encoding gene.). The expression level was relative to the wild type cells and was normalised to *PPIA* and *HPRT* controls. Error bars represent standard deviation (n=3). B) Western blot using cytoplasmic and nuclear protein fractions for MSL3 and MOF protein expression in wild type, *MSL2*$^{-/-}$ and *MSL1*$^{-/-}$ RPE-1 cell lines. The control for cytoplasmic fractions was α-tubulin and for nuclear protein control SCC1 was used.

The results show that the loss of either MSL2 or MSL1 does not significantly affect the gene expression of the other members (Figure 3.4 A). Since the CRISPR/Cas9 genome editing affects proteins at the translational level it is not expected to see a decrease in the *MSL2* or *MSL1* RNA expression in the respective *MSL2*$^{-/-}$ and *MSL1*$^{-/-}$ cell lines. While a slight increase was observed in the *MSL3* gene expression western blot analysis using nuclear protein extracts revealed, that the levels of MSL3 protein are the same in the two knock-out cell lines as in the wild type RPE-1 (Figure 3.4 B). Protein levels of MOF were also compared in the three cell lines and showed similar levels suggesting that the loss of MSL2 or MSL1 did not impact MOF protein expression (Figure 3.5).

3.5. Loss of MSL2 or MSL1 affects MSL related gene expression

To see if known target genes of MSL2/1 and MOF are affected Q-PCR experiment was carried out (Figure 3.5).

It has previously been shown in mouse embryonic stem cells that the loss of MSL1/2 affects the expression of *Tsix,* a long non coding RNA (lnRNA). *Tsix* is an antagonist for the *Xist* lnRNA and represses its general transcriptional activation role on the X

chromosome in facilitating proper X inactivation (Chelmicki et al., 2014). Thus, *Tsix* and *Xist* were included in the Q-PCR screen to test the idea that the loss of MSL2 or MSL1 can affect the expression of these two lnRNAs and from that the X chromosome condensation in somatic cells.

The RNA recognition motif of the ELAV family shows close relation to the one in the SXL protein (Good, 1995, Koushika et al., 1996). SXL in *Drosophila* is known to regulate *MSL2* expression (Kelley et al., 1995, Graindorge et al., 2013), thus *ELAV1* expression was investigated in the context of a possible regulation of MSL2 in humans. Using Q-PCR analysis the potential effect on the expression of *ELAVL1* was studied in response to the loss of MSL2 or MSL1. ELAVL1 (also known as HuR) is an RNA binding protein, which through regulating mRNA stability was shown to play a role in proliferation and cell growth in mammals (King et al., 2000).

It is known that the *HOX* (homeobox) loci encoding transcription factor proteins transcriptional activation is regulated by the methylation of H3K4 and H4K16ac, latter performed by MOF (Milne et al., 2002, Dou et al., 2005). It has also been reported previously that MSL2/MSL1 play an important role in transcription activation at *HOXA9* (Homeobox A9) and *MEIS1* loci (Wu et al., 2011). HOXA9 is known to play role in hematopoietic stem cell expansion and is also linked to acute leukemias (Collins and Hess, 2016). MEIS1 is known to have an important role in normal development and together with HOXA9 its overexpression is linked to acute myeloid leukemia (Thorsteinsdottir et al., 2001, Mohr et al., 2017).

Since the acetylation of H4K16 was shown to be perturbed in the *MSL2*$^{-/-}$ DT40 cells (Lai et al., 2013), an additional Q-PCR analysis was carried out to test if the expression of MOF related genes are affected in the human knck-outs. For this experiment *TMS1* proapoptotic gene was chosen since it is known to be silenced in a H4K16ac dependent manner upon the depletion of MOF (Kapoor-Vazirani et al., 2008) (Figure 3.5).

Results showed that both *Tsix* and *Xist* RNA expression decreased in the MSL2 knock out cells, while the levels in the *MSL1*$^{-/-}$ cell line did not change (Figure 3.5). It is known that MSL2 mediates *Tsi*x expression and thus repression of *Xist* RNA spreading on inactive X chromosomes in embryonic cells. However, the obtained results show a decrease in both RNA levels. Since RPE-1 cells are already

differentiated a milder effect was expected. However, the loss of MSL2 possibly disrupter the overall expression of these two genes.

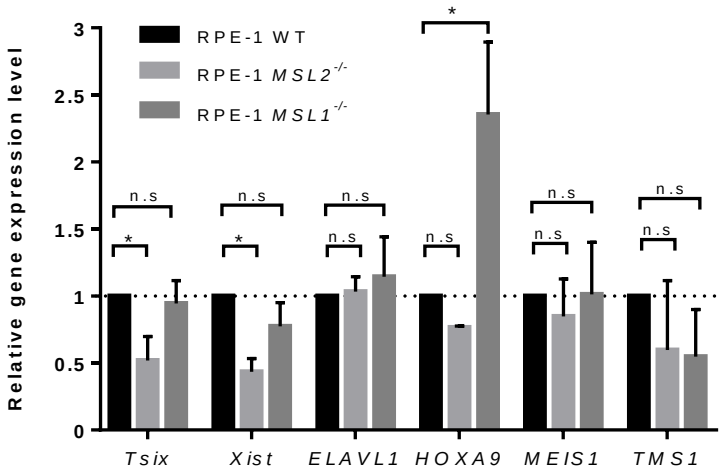

Figure 3.5: Relative expression levels of indicated genes in wild type, *MSL2*$^{-/-}$ and *MSL1*$^{-/-}$ RPE-1 cell lines. Q-PCR analysis of MSL affected genes. The expression levels are relative to the wild type cells and the expression was normalised against *PPIA* and *HPRT*. Error bars represent standard deviation. Statistical analysis was performed using one-way ANOVA and Fisher's LSD test. P value: (0.0332)* (n=2).

RNA expression levels of *ELAVL1* did not show a difference in the knock-outs compared to the wild type cells. This supports previous results on *MSL2* RNA expression levels in the MSL2 and MSL1 knock-out cells (Figure 3.4) which did not show an increase compared to wild type cells. *HOXA9* gene expression level similarly to what has been reported before (Wu et al., 2014a) showed a moderate decrease in the *MSL2*$^{-/-}$ cells. However, *HOXA9* expression in the MSL1 knock-out cells showed a significant increase. Gene expression level of *MEIS1* did not change in either *MSL2*$^{-/-}$ or *MSL1*$^{-/-}$ cell lines in comparison to wild type RPE-1 cells (Figure 3.5). RNA levels of *TMS1*, a gene activated by MOF, also showed a mild decrease in expression in both knock-out cell lines. While MSL2 knock-out cells had a higher standard deviation this experiment should be repeated to support this data. The observed change could suggest that the loss of MSL2 or MSL1 affects the activity of MOF and the subsequent transcriptional activation of *TMS1* by MOF.

3.6. Perturbed histone modification in the *MSL2*$^{-/-}$ and *MSL1*$^{-/-}$ cell lines

As mentioned before human MSL2 and MSL1 are members of the MSL complex with two other proteins, MSL3 and MOF. It has previously been shown in *Drosophila*, that MSL2 maintains the stoichiometry of the MSL complex by ubiquitylating its members (Villa et al., 2012) while MSL1 forms the physical core of the complex (Hallacli et al., 2012). These finding led to the hypothesis that the loss of human MSL2 or MSL1 could affect the stability of the complex. The function of the MSL complex and its possible disruption was studied through its main enzymatic activity which is the acetylation of histone 4 at lysine 16 (H4K16ac) performed by MOF (Akhtar and Becker, 2000, Smith et al., 2005, Taipale et al., 2005). The relative amount of this modification was compared in the wild type, *MSL2*$^{-/-}$ and *MSL1*$^{-/-}$ cell lines (Figure 3.6).

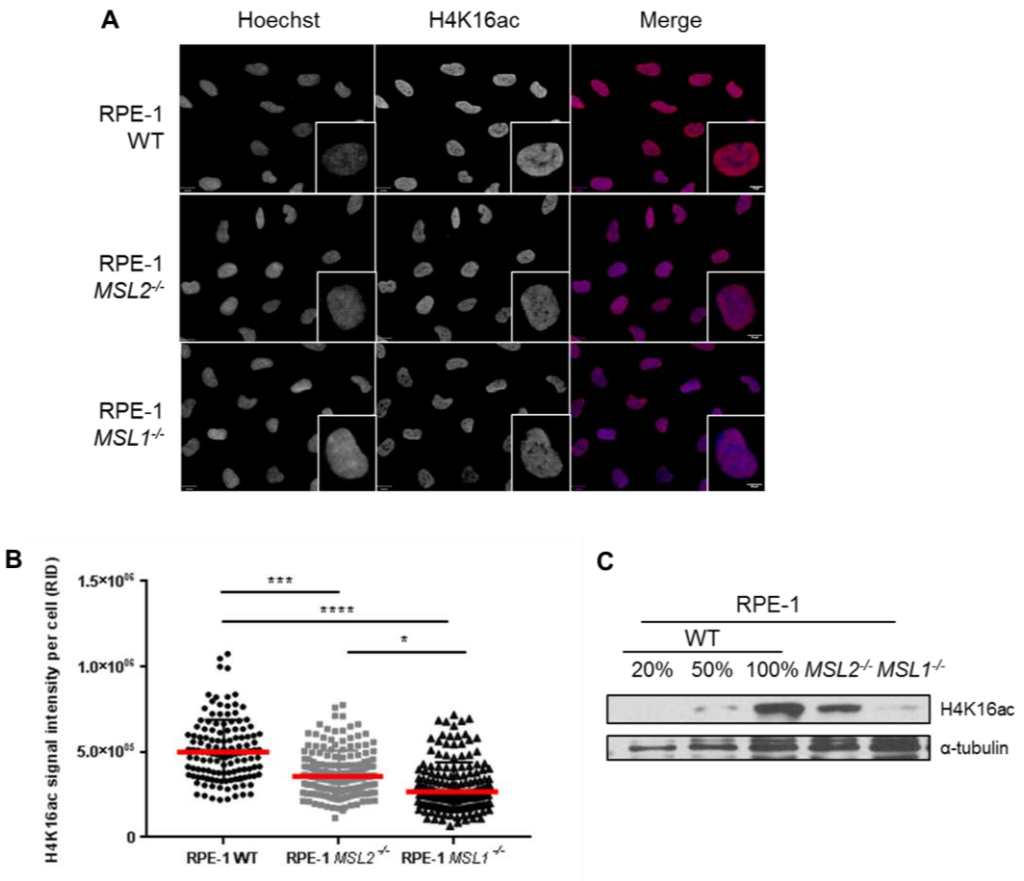

Figure 3.6: H4K16ac level in wild type, *MSL2*$^{-/-}$ and *MSL1*$^{-/-}$ RPE-1 cells. A) H4K16ac immunofluorescence microscopy in wild type, *MSL2*$^{-/-}$ and *MSL1*$^{-/-}$ RPE-1 cells. Scale bar indicates 5 µm. B) Quantification of the relative integrated density (RID) signals of H4K16ac in wild type, *MSL2*$^{-/-}$ and *MSL1*$^{-/-}$ RPE-1 cells. Statistical analysis was performed using one-wayANOVA and Tukey's muliple comparison test. P value: (0.0332) * , (0.0002)***, (<0.0001) ****. C) Visualization of H4K16ac levels with western blot analysis in wild type, *MSL2*$^{-/-}$ and *MSL1*$^{-/-}$ RPE-1 cells.

Consistent with previous findings both in *Drosophila* and DT40 cells, the level of H4K16ac was reduced in the *MSL2*$^{-/-}$ cells (Gelbart et al., 2009, Lai et al., 2013). which supports the hypothesis about the role of MSL2 in regulating the stability of the human complex. The acetylation phenotype was observed to be even more perturbed in case of the depletion of MSL1 suggesting that the stability of the MSL complex greatly affects the histone acetylation ability of MOF (Figure 3.6).

Other histone modification related to MOF, global transcriptional activation or inactive chromatin markers were also investigated including some which has already been reported to be affected by the loss of MSL2 in DT40 cells (Lai et al., 2013) (Figure 3.7).

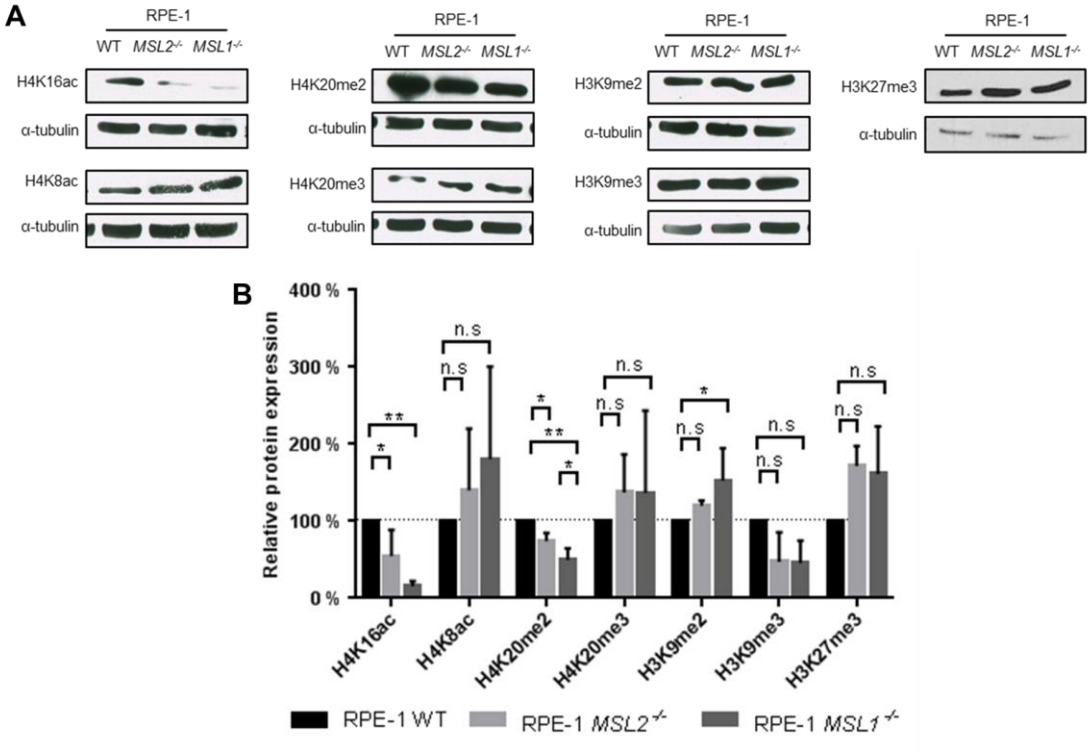

Figure 3.7: Perturbed histone modifications in *MSL2*$^{-/-}$ and *MSL1*$^{-/-}$ cells. A) Histone modifications affected by the loss of either MSL2 or MSL1. B) Quantification of the western blot data. Signal intensity was measured and normalised to α–tubulin expression. Levels are shown as relative to the wild type levels. Error bars represent standard deviation. Statistical analysis was performed using one-wayANOVA and Fisher's LSD test. P value: (0.0332) *, (0.0021) ** (n=3).

Besides H4K16ac, the levels of another transcription related modification H4K8 acetylation was chosen to be observed. H4K8ac is known to mediate the recruitment of the chromatin remodelling SWI/SNF complex which after recruiting other factors

enables transcriptional initiation (Agalioti et al., 2002). A slight increase in the level of acetylation was observed, but the difference in protein levels was not significant (Figure 3.7).

Inactive heterochromatin markers such as H3K9me2 and H3K9me3 and H3K27me3 were also investigated (Figure 3.7). Levels of H3K9me2 were investigated previously in DT40 cells, but no significant difference was found in the Msl2 knock-outs in comparison to wild type cells (Lai et al., 2013). H3K9me2 and H3K9me3 are known to mark constitutive heterochromatin while H3K27me3 is a general facultative heterochromatic marker (Rea et al., 2000, Beisel and Paro, 2011). The results show that the level of H3K9me3 decreased which could indicate a more active chromatin state. However, both H3K9me2 and H3K27me3 was found to be increased in both knock-out cell lines probably indicating that the loss of either MSL2 or MSL1 affects either chromatin compaction or structure and thus the access of other chromatin modifying enzymes.

As reported previously, the loss of MSL2 resulted in decreased H4K20me2 (Lai et al., 2013) and in the MSL1 knock-out cells a similar decrease was observed here as well (Figure 3.7). H4K20me2 mark is particularly interesting as this modification is involved in the DNA damage response, in particular the recruitment of 53BP1 to damage sites (Wilson et al., 2016). In case of H4K20me3 a previously reported decrease was not observed, H4K20me3 level was found to be similar to wild type levels in both knock-out cell lines. H4K20me3 is known to be present at promoter regions is associated with transcriptional repression (Wang et al., 2008, Kuo et al., 2012).

3.7. In the absence of MSL2 or MSL1 the chromatin binding affinity of MOF is affected

Since the loss of either MSL2 or MSL1 affected the general H4K16ac, further investigation was carried out to identify if the absence of these proteins could alter the chromatin binding ability of MOF by affecting the stability of the MSL complex. In *Drosophila* studies it has been found that MSL3 and MOF mutations lead to decreased chromatin binding of the other members, where mutation of MSL1 or MSL2 lead to a complete loss of chromatin binding (Lyman et al., 1997, Gu et al.,

1998). To estimate the chromatin bound fraction of MOF in RPE-1 cells, cellular fractionation was carried out to separate cytoplasmic, nuclear and chromatin bound protein fractions (Figure 3.8).

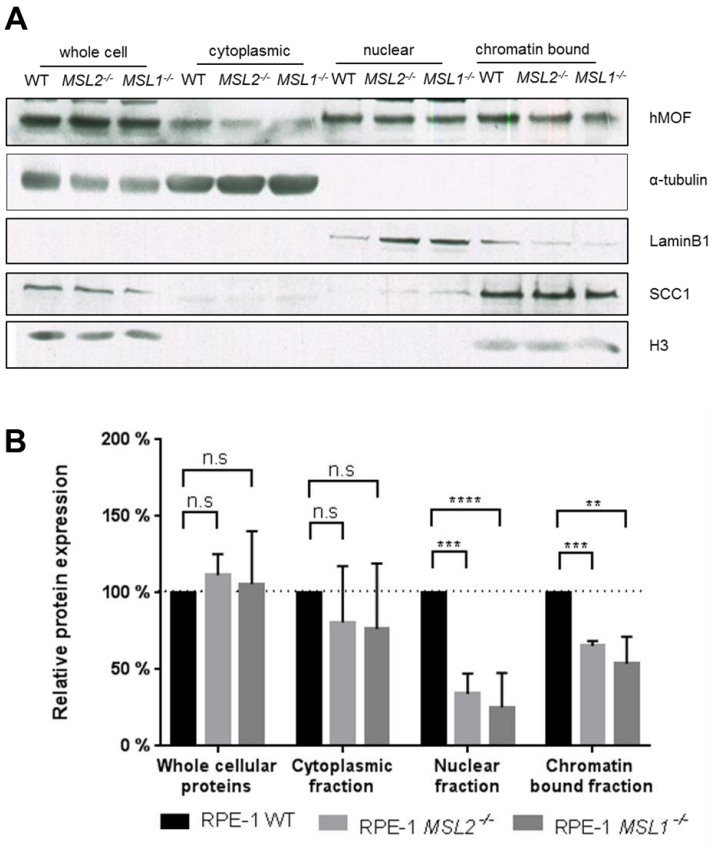

Figure 3.8: Cellular localization of MOF in wild type, *MSL2*$^{-/-}$ and *MSL1*$^{-/-}$ RPE-1 cells. A) Western blot showing that the cellular localization of MOF is perturbed both in the *MSL2*$^{-/-}$ and *MSL1*$^{-/-}$ RPE-1 cells showing decreased chromatin binding. B) Quantification of the western blot data. Signal intensity was measured and normalised to Lamin B1, α–tubulin and H3 expressions in the different fractions. Error bars represent standard deviation (n=4). Levels are shown as relative to the wild type levels. Statistical analysis was performed using one-wayANOVA and Fisher's LSD test. P value: (0.0021) **, (0.0002)***, (0.0001)****

The result shows that compared to wild type both *MSL2*$^{-/-}$ and *MSL1*$^{-/-}$ cells have perturbed MOF localization to the chromatin. This means that the presence of MOF in the chromatin bound protein fraction is reduced and in parallel an even greater decrease of MOF presence was observed in the nuclear MOF pool, while the cytoplasmic fraction did not seem to be affected. However, the fractionation had its own limitations and during fractionation soluble proteins could be lost affecting the amount of captured proteins in each fraction.

3.8. Re-introduction of MSL1 partially rescues H4K16ac

To investigate whether the acetyltransferase activity could be restored by providing the physical structure of the complex a rescue experiment was carried out (Figure 3.9). For this experiment already available mouse *Msl1* cDNA was used as mouse Msl1 protein has a 95.44 % similarity to human MSL1. Full length mMsl1 cDNA was inserted into an expression plasmid and transiently transfected into *MSL1*$^{-/-}$ RPE-1 cell line.

Full length mMsl1 cDNA with 6His tag has been digested from pACEBAC1-6His-mMsl1 plasmid and inserted into pEGFP-C1 plasmid using *XhoI* restriction site. Two different clones from the same construct were transfected into RPE-1 *MSL1*$^{-/-}$ cells and GFP-MSL1 protein expression was observed in G6 while G4 likely contained a mutation preventing expression. This construct however was unable to rescue the phenotype probably due to the large N-terminal GFP tag which could have interfered with binding or conformation (Figure 3.9 A).

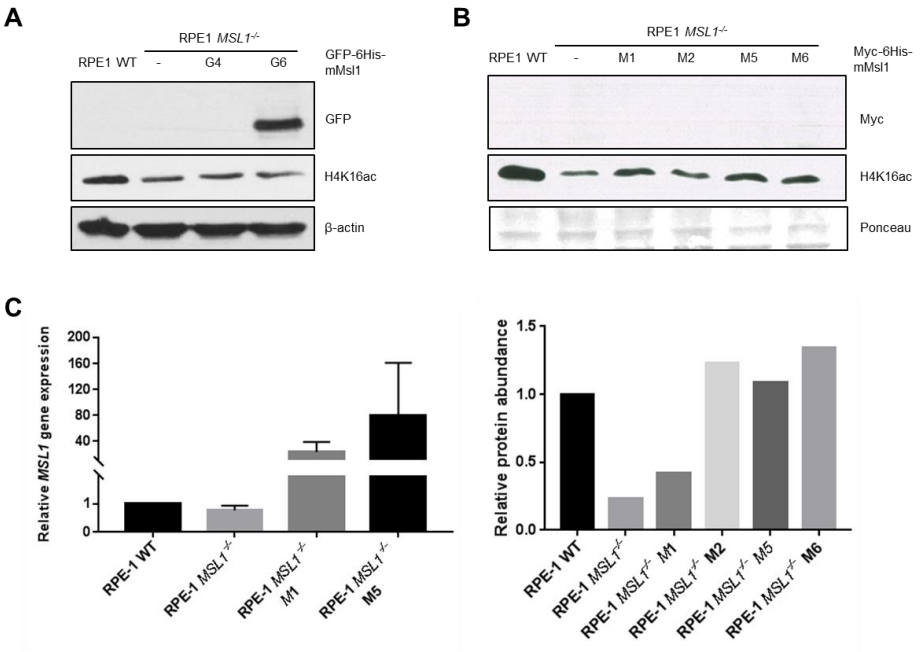

Figure 3.9: Transient MSL1 rescue expression. A) Transient GFP-6His-mMsl1 plasmid expression and H4K16ac levels show that the addback of MSL1 could not rescue the acetylation on H4K16. B) Transient Myc-6His-mMsl1 plasmid expression and expression and H4K16ac levels and quantification of the western blot data shown above. Signal intensity was measured and normalised to Ponceau. C) Q-PCR analysis of transient MSL1 rescue using Myc-6His-mMsl11 plasmid Error bars show standard deviation (n=2).

To generate a smaller epitope tagged construct 6His-mMsl1 sequence was inserted into pCMV-3Tag-Myc-2A plasmid using *BamHI* and *HindIII* restriction sites. Four different clones from the same construct were transfected into RPE-1 *MSL1*$^{-/-}$ cells and different levels of H4K16ac were observed in each transfection (Figure 3.9 B). While this construct partially restored the H4K16ac level in the RPE-1 *MSL1*$^{-/-}$ cell line, the level of exogenous MSL1 could not be detected by western blot (Figure 3.9). As previous studies also experienced difficulties with the detection of ectopic MSL1 protein (Cai et al., 2010), Q-PCR experiment was carried out to look at MSL1 RNA expression in the transfected cells (Figure 3.9 C). The results showed that indeed the mouse *Msl1* RNA is expressed in the cells and the observed increase of H4K16ac was due to the re-introduction of the protein. As MSL1 seemed to be sensitive to epitope tag size and possibly location even the smaller tag could have disrupted its proper functioning as a core protein.

3.9. Discussion

After successfully generating human MSL2 and MSL1 knock-out cell lines using the CRISPR/Cas9 genome editing tool, effects on cell growth and proliferation were studied. It was found that while neither the *MSL2*$^{-/-}$ nor the *MSL1*$^{-/-}$ RPE-1 cells showed a growth defect compared to wild type cells, cell cycle profile analysis completed with BrdU incorporation revealed a slight increase in S/G2 population (Figure 3.3).

Gene expression of the other MSL complex subunits in the absence of MSL2 or MSL1 was also studied and found to be unperturbed. This data was further supported by western blot analysis probing against MSL3 and MOF proteins which abundance also did not show a difference in the two knock-out cell lines compared to wild type cells.

Further investigation was performed to study the effect of the loss of MSL2 or MSL1 on gene expression by looking at known target genes of MSL1/2 and MOF. As MSL2 related lnRNAs *Tsix* and *Xist* expression was studied. While *Xist* contributes to X chromosome inactivation and compaction *Tsix* has an antagonising effect on *Xist*. However, results showed a decrease in expression in both knock-outs. To follow up on this finding RNA FISH experiment could be performed to address if the

loss of MSL2 affected the compaction or inactive status of the inactive X chromosome. In accordance with previous findings MSL2 related *HOXA9* and gene expression was found to be decreased (Wu et al., 2011), but *MEIS1* expression did not change in the *MSL2*$^{-/-}$ or *MSL1*$^{-/-}$ cells. Significant increase in *HOXA9* expression was observed in the MSL1 knock-out, which could suggest that MSL1 is involved in the activation of this gene different to MSL2. However, further studies are required to support this hypothesis. As MOF related gene, *TMS1* RNA levels were studied and found decreased in both MSL2 and MSL1 knock-out cell lines. This result might be due to a possible disruption in the MSL complex which could affect MOF functions. This hypothesis could be further studied using co-immunoprecipitation assay in the *MSL2*$^{-/-}$ and *MSL1*$^{-/-}$ cell lines using MOF as bait.

To address the effects of the loss of either MSL2 or MSL1 on the MSL complex, its specific H4K16ac was studied and found to be decreased to 70% and 50% respectively which was consistent with previous observations (Smith et al., 2005, Lai et al., 2013). The acetylation itself is performed by the catalytic subunit MOF and the decrease in acetylation could be an indirect effect caused by the structural disruption of the MSL complex. Supporting evidence from *Drosophila* experiments showed that *Drosophila* MSL2 can maintain the stoichiometry of the complex and human structural studies revealed that MSL1 serves as a backbone and binding platform for the other members (Kadlec et al., 2011, Hallacli et al., 2012). While it is possible that human MSL2 through ubiquitylating MOF affects its mediated H4K16ac activity, so far there is no evidence for this hypothesis. In parallel, a moderate increase in H4K8ac was observed which is known to be involved in transcriptional initiation (Agalioti et al., 2002). It is possible that H4K8ac plays a role in counterbalancing the effect of the decreased H4K16ac along with other transcriptional activating modification but further investigation are required to study genome wide gene activation.

As observed before in DT40 cells the loss of MSL2 (Lai et al., 2013) and in this study also MSL1 affected other chromatin modifications as well. Constitutive and facultative heterochromatic markers such as H3K9me2 and H3K27me3 were found to be increased which might indicates a more compacted chromatin status. However, decrease in H3K9me3 might indicate an increase in actively transcribed regions in the chromatin, which could also suggest a balancing effect on compacted regions. To

gain information on the status global gene expression RNA sequencing assay could be performed. The decreased level in H4K20me2 was particularly interesting since it plays a role in replication and helps the recruitment of 53BP1 to DNA damage sites (Botuyan et al., 2006, Kuo et al., 2012). It has been shown before that the loss of MSL2 affects DNA repair, particularly the NHEJ pathway (Lai et al., 2013).

To investigate if the loss of MSL2 and MSL1 affects MOF mediated H4K16ac via disrupting its association with chromatin previously reported in *Drosophila* (Lyman et al., 1997, Gu et al., 1998) the chromatin binding affinity of MOF was studied through subcellular fractionation. Results revealed that the loss of either MSL2 or MSL1 decrease the amount of chromatin bound MOF. This result indicates that MOF is only able to properly associate with the chromatin within a stable complex in humans, and this stability is likely to affect the levels of MOF present in the nucleus as well. The less severe effect on chromatin binding observed in cells lacking either MSL2 or MSL1 could mean that an incomplete MSL complex is still able to bind chromatin with a lower efficiency. Alternatively the MOF containing NSL complex can also contribute to the observed level of chromatin bound MOF, which could conceal the actual severity of a disrupted MSL complex on the binding of MOF to chromatin. Also, since the quantification of the western blot shows a 35-47% decrease in the presence of MOF in the chromatin bound fraction compared to the wild type cells, a large portion of MOF is likely to be associated with the MSL complex in human cells. In addition, chromatin immunoprecipitation (ChIP) assay could also be performed to study MOF binding and gene specific association to chromatin in the absence of either MSL2 or MSL1.

In general, the disruption of the MSL complex via the knock-out of either MSL2 or MSL1 led to changes in several posttranslational modifications, affected MSL mediated gene expression and affected the chromatin binding ability of MOF.

4. The role of MSL2 and MSL1 in DNA damage repair and replication

4.1. Introduction

Different physical or chemical agents as well as endogenous damage happening during normal cellular metabolism can affect the stability of the genome most importantly by introducing breakage in the DNA. Faithful transmission of genetic information is very important and DNA damage occurring during replication can cause replication fork stalling which can lead to mitotic entry delay or incomplete DNA replication (Petermann and Helleday, 2010, Minca and Kowalski, 2011, Cortez, 2015). Eukaryotes evolved a complex repair mechanism called the DNA damage response to overcome these potentially dangerous effects (Ciccia and Elledge, 2010).

The human MSL complex has previously been shown to play a role in the DNA damage response. The acetylation of histone H4 at lysine 16 (H4K16ac) is required for the recruitment of MDC1 (Li et al., 2010). Through trans-tail crosstalk with H4K20me2 it is also involved in the establishment of BRCA1 recruitment sites simultaneously preventing the formation of 53BP1 foci at damage sites (Tang et al., 2013). Furthermore, MOF through its acetyltransferase activity is known to be involved in the activation of ATM in response to γ-irradiation induced double-strand breaks (Gupta et al., 2005, Sykes et al., 2006, Gupta et al., 2014b). The depletion of MOF also affected the DNA damage repair in both the non-homologous end joining (NHEJ) and the homologous recombination (HR) pathways (Li et al., 2010). Experiments in human cell lines and in chicken DT40 MSL2 knock-out cells have also shown that MSL2 is involved in the DNA damage response. Histone modifications related to the recruitment of different mediators and repair proteins such as 53BP1 or MDC1 were decreased and cells depleted of MSL2 showed defects in DNA repair suggesting a role in the NHEJ repair pathway (Lai et al., 2013). Human MSL1 protein was shown to interact with 53BP1 (Gironella et al., 2009). These results suggested that MSL2 and MSL1 besides the initiation of H4K16ac might be involved in promoting recruitment and DNA binding of key DDR mediators such as MDC1 and 53BP1 to damage sites. 53BP1 is also known to form nuclear bodies around damaged or underreplicated DNA. It is thought to shield exposed DNA from further damage or to protect the DNA ends from the error prone

NHEJ repair mechanism until the S phase of cell cycle where HR repair is available (Rothkamm et al., 2003, Saleh-Gohari and Helleday, 2004, Lukas et al., 2011). Studies in *Drosophila* showed that mutation in *mof* lead to mitotic cell cycle progression without DNA repair causing centrosomal inactivation through *checkpoint kinase 2* homologue (*DmChk2*) activation (Pushpavalli et al., 2013). Also MSL2 and MSL1 were shown to interact with PAF1 protein which is known to be involved in recovery from hydroxyurea induced replication stress (Poli et al., 2016).

This chapter describes work aiming to follow up on these findings and better understand the role of MSL2 and MSL1 in the DNA damage response and DNA double-strand break repair.

4.2. MSL2 and MSL1 are required for efficient DNA damage repair

To study the general involvement of human MSL2 and MSL1 in different types of DNA damage response pathways such as NHEJ, HR, NER and stalled replication fork induced damage repair. RPE-1 WT, *MSL2*$^{-/-}$ and *MSL1*$^{-/-}$ cells were subjected to increasing doses of three different DNA damaging agents, γ-irradiation (IR), ultraviolet radiation (UV) and hydroxyurea (HU) treatment (Figure 4.1).

IR induced DNA damage can result in various lesions including the most severe type, DNA double-strand breaks activating mainly the NHEJ and HR repair pathways (Vignard et al., 2013). It has been previously shown, that the loss of MSL2 in chicken cells contributed to increased sensitivity to IR (Lai et al., 2013). Experiments with human knock-out cells performed here showed significant difference in clonogenic survival rate supporting the aforementioned observations (Figure 4.1 A, B). Both *MSL2*$^{-/-}$ and *MSL1*$^{-/-}$ cell lines had decreased colony formation ability, *MSL2*$^{-/-}$ cells showing a more severe phenotype compared to *MSL1*$^{-/-}$.

To investigate if the loss of MSL2 or MSL1 affects nucleotide excision repair (NER) a survival assay using UV induced DNA damage was performed. UV induced damage mainly results in bulky adduct formation by cyclobutane pyrimidine dimers (CPDs) or pyrimidine-pyrimidone (6-4) photoproducts (Hu et al., 2017). A colony formation assay after UV induced damage revealed that both *MSL2*$^{-/-}$ and *MSL1*$^{-/-}$ cells showed similar sensitivity and had a deceased survival rate compared to wild

type RPE-1 (Figure 4.1 C, D). However, this assay should be repeated using UV doses smaller than 5J, as the number of colonies had a great decrease compared to untreated cells which could affect correct interpretation of the data.

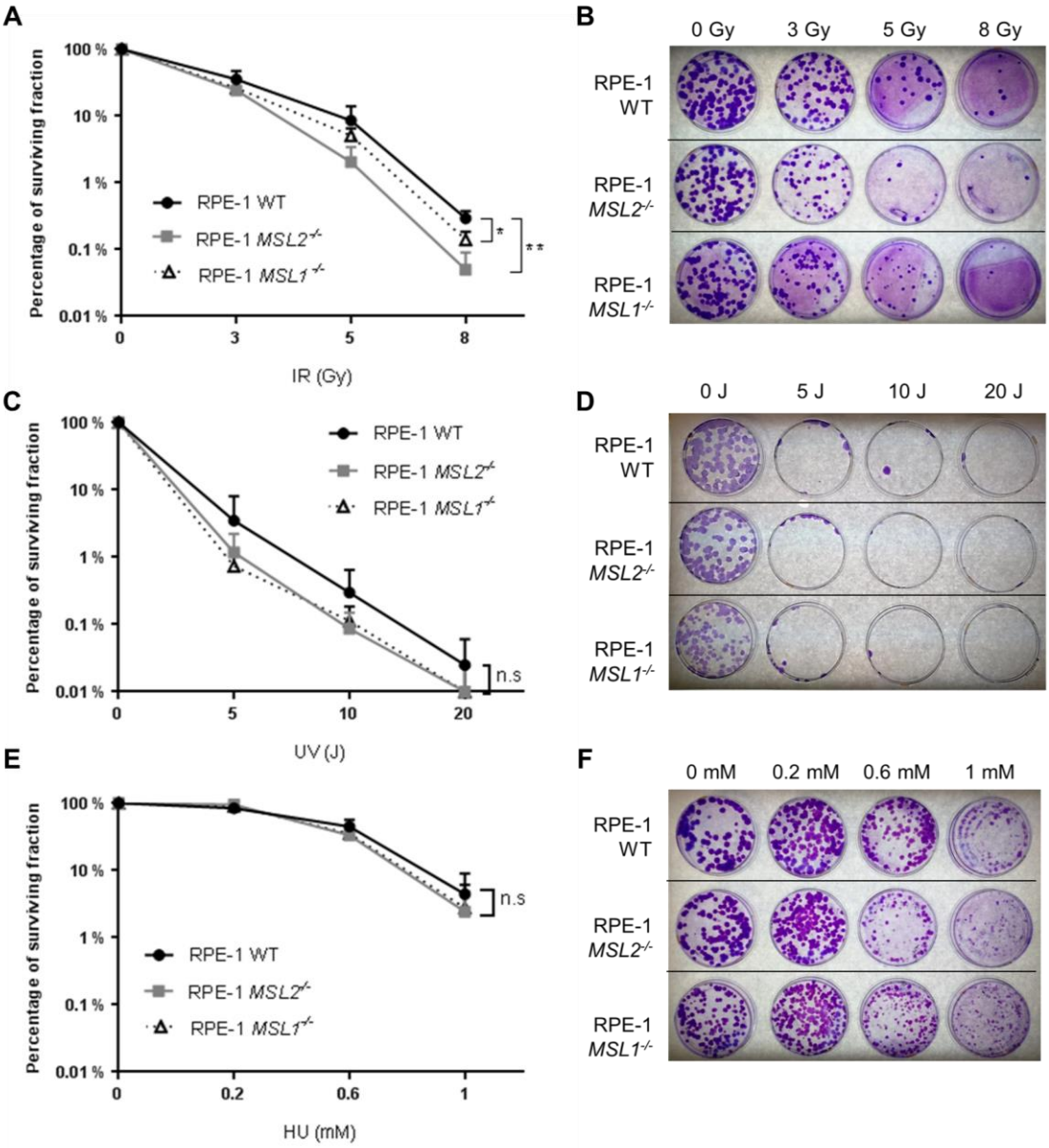

Figure 4.1: Clonogenic survival assay. RPE-1 WT, *MSL2*$^{-/-}$ and *MSL1*$^{-/-}$ were treated with indicated types of DNA damaging agents in increasing doses. A-B) Colony formation after IR treatment. C-D) Colony formation after UV treatment. E-F) Colony formation after HU tratment. Surviving percentage was normalised to untreated control population. Error bars represent standard deviation. Statistical analysis was performed using nonpaparametric one-wayANOVA and Tukey's multiple comparison test. P value: (0.0332) *, (0.0021) **

To better understand if repair mechanisms related to replication induced stress were also affected HU survival assay was performed (Figure 4.1 E, F). Hydroxyurea

treatment blocks replication via nucleotide starvation in a reversible manner (Kurose et al., 2006). The obtained results showed that the loss of MSL2 or MSL1 did not show a significant difference in recovery in response to HU induced repair in comparison to wild type cells.

In conclusion both MSL2 and MSL1 depleted cells showed increased sensitivity towards IR and to a lesser extent to UV induced DNA damage while HU treatment did not affect colony formation and growth. This data suggests that both proteins are required for efficient DNA damage repair, and might play a role in various repair mechanisms. To further characterise how pathways might be affected, this chapter focused on MSL2 using *in vivo* reporter assays.

4.3. *In vivo* NHEJ and HR DNA damage repair assays

It has previously been shown that MSL2 is involved in NHEJ repair (Lai et al., 2013). However, whether if it has a role in the HR pathway has not been investigated yet. To study if human MSL2 knock-out cells show a similar defect in the NHEJ repair pathway and also to investigate the effect on HR repair two specific *in vivo* GFP ligation assays were performed. These systems enable the study of the involvement of MSL2 in the DNA damage response by using different GFP reporter constructs.

4.3.1. Generation of *MSL2*$^{-/-}$ H1299 and DR-HeLa cell lines

To study the effect of MSL2 in the NHEJ repair mechanism, a previously established GFP reporter cell line (H1299) was used (Ogiwara and Kohno, 2011). In order to utilise this system MSL2 knock-out cell line was generated using the CRISPR/Cas9 target strategy in the H1299 cells. Since the gene targeting has already been successfully established in RPE-1 cells, for this cell line the same guide sequence, targeting exon 1 (S90) was used (Figure 4.2 A). For antibiotic selection a neomycin resistance cassette containing plasmid (pLOX-Neo) was chosen, since puromycin had previously been used to establish the assay system. Screening was performed by PCR amplification of the Cas9 target site surrounding genomic region followed by sequencing (Figure 4.2 B). To perform the *in vivo* assay clone H1299 S90_2 was chosen (referred to as H1299 *MSL2*$^{-/-}$ now onward).

For investigating the involvement of MSL2 in HR repair *in vivo* the DR-HeLa GFP reporter cell line was used (Pierce et al., 1999). Similar to the H1299 cell line

described above an *MSL2*$^{-/-}$ cell line was generated in the DR-HeLa cells as well. For screening, the target site and its surrounding region was PCR amplified and sent directly for sequencing (Figure 4.2 C). To perform the HR assay the DR-HeLa S90_2 clone was chosen (referred to as DR-HeLa *MSL2*$^{-/-}$ now onward).

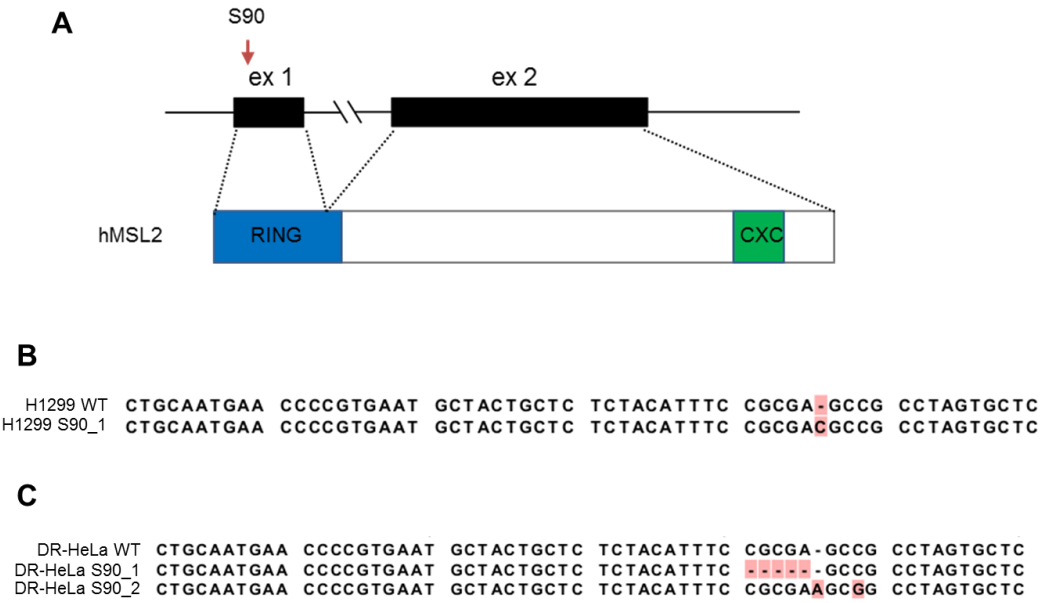

Figure 4.2: Schematic representation of the MSL2 target strategy. A) MSL2 target site for CRISPR/Cas9 mediated gene editing. The Cas9 cut site was designed to target the enzymatic domain (RING) encoding region of the MSL2 protein. B) Sequence alignment of wild type H1299 cells and the selected clone at the MSL2 target site. C) Sequence alignment of wild type DR-HeLa cells and two clones at the MSL2 target site.

The chosen *in vivo* repair assays knock-out clones contain a one basepair insertion to mimic a similar mutation to the previously generated RPE-1 clone (90_D4).

4.3.2. The loss of MSL2 negatively affects NHEJ repair

The H1299 cell line contains a stably integrated reporter construct consisting of eGFP cDNA separated from a CMV promoter by a HSV-TK (Herpes simplex virus-thymidine kinase) sequence. Before and after the HSV-TK coding region *I-SceI* restriction enzyme sites have been inserted (Figure 4.3).

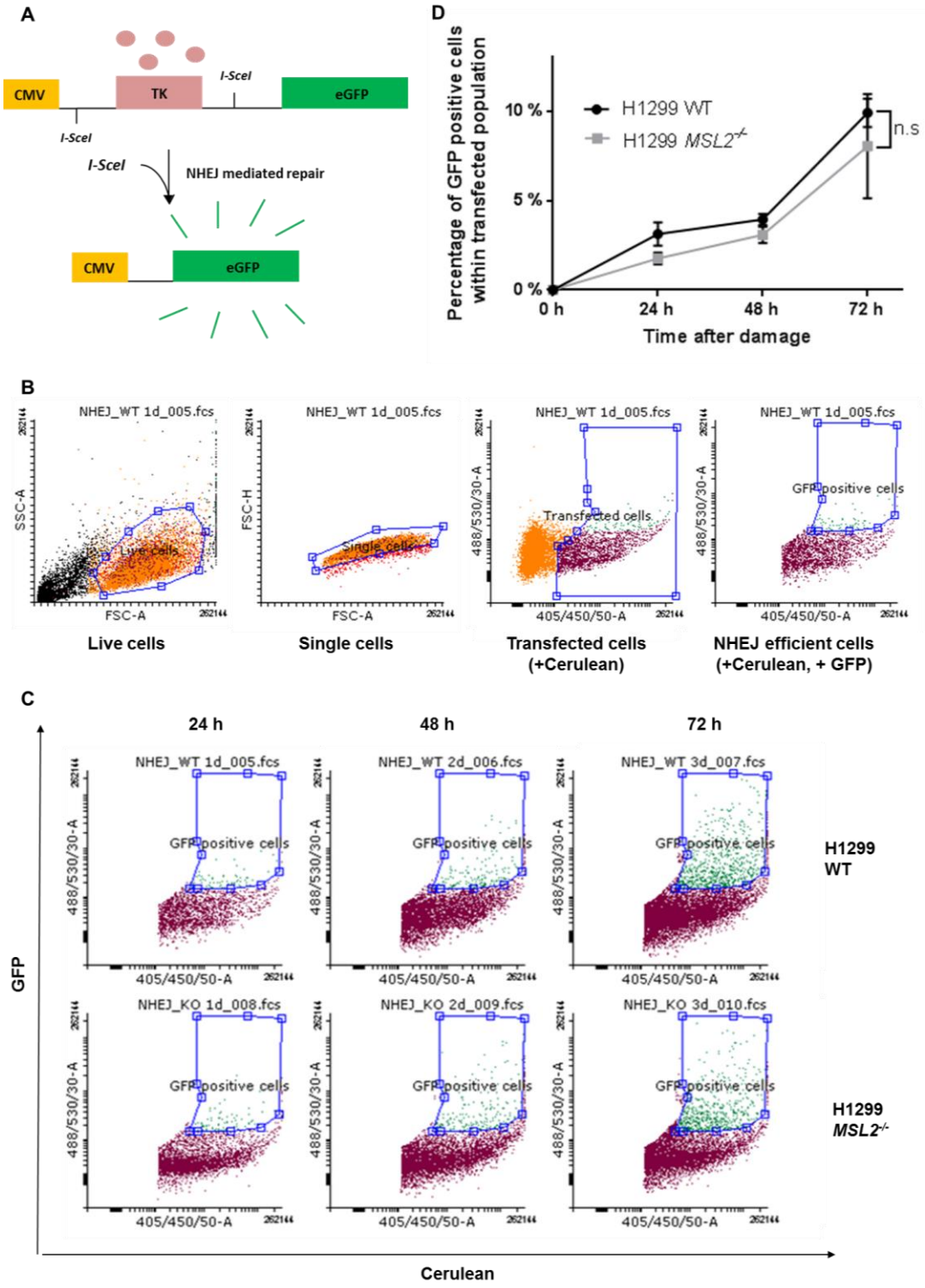

Figure 4.3: *In vivo* NHEJ repair assay. NHEJ repair efficiency was monitored through *in vivo* GFP expression. A) *In vivo* NHEJ assay schematics. The *I-SceI* generated double-strand break in the TK surrounding genomic region results in a functional eGFP sequence upon NHEJ repair. B) Gating strategy for GFP expressing cells within the transfected population. The percentage of GFP expressing cells was calculated from the transfected population indicated by Cerulean expression. C) Representative image of the GFP positive population at the indicated timepoints in H1299 WT and *MSL2*$^{-/-}$ cells. D) Quantification of GFP positive cells. Statistical analysis was performed using two-wayANOVA and Fisher's LSD test (n=3). Error bars represent standard error of the mean (SEM).

In normal conditions the eGFP is not expressed in the cells. However, the introduction of the *I-SceI* endonuclease results in the excision of the HSV-TK open reading frame (ORF) and following successful ligation, the eGFP sequence can be transcribed since it is now in close proximity to the CMV promoter (Figure 4.3 A). Thus, if the *I-SceI* digested sequence is repaired through NHEJ it facilitates the expression of eGFP and the level of repair activity can be evaluated by the proportion of eGFP-positive cells using flow cytometry.

To analyse the repair efficiency in the *MSL2*$^{-/-}$ H1299 cells a flow cytometric assay was carried out. 10^5 cells were seeded into 6-well dishes and co-transfected with an *I-SceI* and a Cerulean coding plasmid to facilitate the gating of the transfected population. Cells were analysed at 24h, 48h and 72h post transfection using BD FACS Canto II (BD Biosciences) flow cytometer (Figure 4.3 C).

The gating strategy used for the analysis is shown on Figure 4.3 B. Unfortunately, the assay seemed less reliable than expected in terms of GFP expression, since the wild type cell population already expressed a considerable amount of GFP. This could be the result of endogenous removal of the HSV-TK, due to its high toxicity. While time limitation prevented the setup of a new system with a knock-out cell line generation, additional controls were included to correct for the GFP positive population. Each assay contained Cerulean only controls both for the H1299 and the H1299 *MSL2*$^{-/-}$ cell lines. From these samples the GFP and Cerulean positive cells were used as a correction base. The successful repair via NHEJ was measured by counting the number of GFP positive cells in the MSL2 knock-out and the wild type transfected population. As transfection and repair efficiency was variable between repeats instead of standard deviation error bars were chosen to represent the standard error of the mean. While the results did not show a significant difference, they indicated a trend that human cells lacking MSL2 had a lower repair efficiency (in average 4.2% of GFP positive cells) compared to wild type cells (in average 5.6% of GFP positive cells) (Figure 4.3 D).

This result suggests that human cells lacking MSL2 have impaired NHEJ repair mechanism which supports previous findings using chicken DT40 cells and RNAi treated human U2OS cells (Lai et al., 2013). Data obtained from previous results also showed that following IR induced DNA damage the MSL2 protein accumulated and

this dynamics of accumulation mirror that of γH2A.X suggesting that it might plays a role at the first part of the signalling pathway (Lai et al., 2013).

4.3.3. The loss of MSL2 negatively affects HR repair

DR-HeLa cells contain a non-functional eGFP sequence which was mutated by the insertion of an *I-SceI* restriction site (SceGFP). Further along the sequence also contains an incomplete eGFP (iGFP) cDNA with the correct eGFP ORF. Upon introduction of the *I-SceI* enzyme a double-strand break is generated in the SceGFP sequence. If its repair is facilitated by the HR mechanism, the iGFP sequence is used as repair template and the corrected eGFP sequence is able to be translated into a functional eGFP protein (Figure 4.4).

To perform the *in vivo* HR assay, DR-HeLa and DR-HeLa cells were transfected with an *I-SceI* coding plasmid. The selection and gating for transfected cells was done using Cerulean fluorescent protein, and the encoding plasmid was co-transfected alongside the *I-SceI* plasmid. This system was not compromised by non *I-SceI* induced GFP expression so no additional corrections were included in the analysis. Gating strategy for GFP positive transfected population is shown on Figure 4.4 B. Cells were harvested at 24h, 48h and 72h after transfection and analysed using BD FACS Canto II (BD Biosciences) flow cytometer (Figure 4.4 C).

Results show a trend of decreased GFP expression in the *MSL2*$^{-/-}$ cells(in average 4% of GFP positive cells) suggesting that the have a lower HR repair efficiency compared to wild type DR-HeLa (in average 12% of GFP positive cells) (Figure 4.4 D). However, to address whether this defect is a direct effect due to the loss of MSL2 or whether MSL2 plays a role in cellular processes upstream of the HR mechanism requires further investigations.

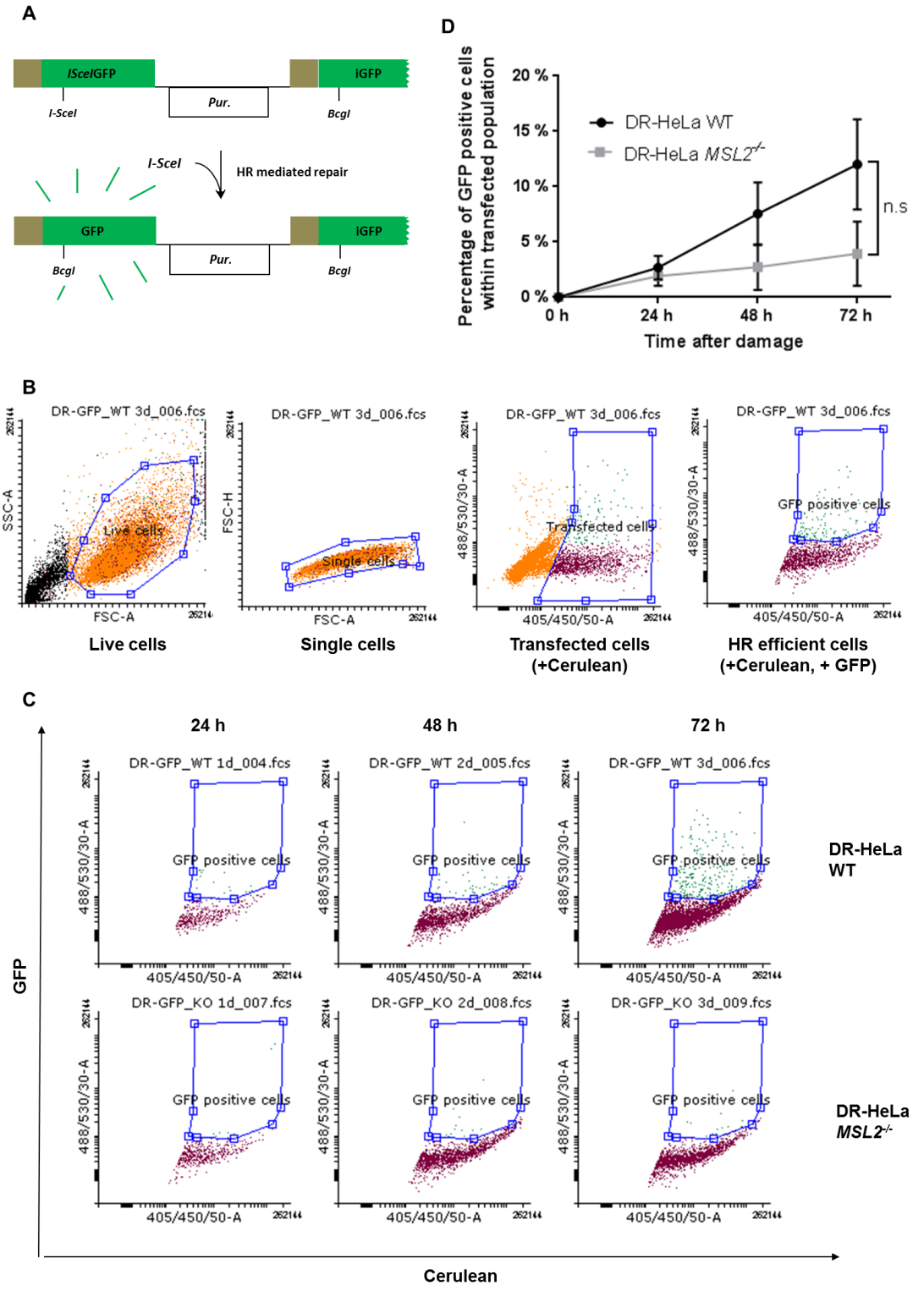

Figure 4.4: *In vivo* HR repair assay. HR repair efficiency was monitored through *in vivo* GFP expression. A) *In vivo* HR assay schematics. The *I-SceI* generated double-strand break in the mutant SceGFP region results in a functional eGFP sequence upon HR repair. B) Gating strategy for GFP expressing cells within the transfected population. The percentage of GFP positive cells was calculated from the transfected papulation indicated by Cerulean expression. C) Representative image of the GFP positive population at the indicated timepoints.in DR-HeLa WT and *MSL2*$^{-/-}$ cells. D) Quantification of GFP positive cells. Statistical analysis was performed using two-wayANOVA and Fisher's LSD test (n=3). Error bars represent standard error of the mean (SEM).

4.4. Focal recruitment of DNA damage and repair proteins

Result described previously showed that the loss of MSL2 or MSL1, potentially affect various types of DDR pathways, particularly the NHEJ and HR repair mechanisms and MSL2 was also shown to accumulate in response to DNA damage (Lai et al., 2013). In combination with the previously obtained data showing that the absence of either MSL2 or MSL1 affects histone modifications involved in the DNA damage response (Figure 3.7), further investigation was carried out to see if the different mediators linked to these histone modifications have a defect in recruitment or foci formation.

To generate a more homogenous population for IRIF assays cells were synchronised by 48h serum starvation to enrich in G0 prior to being subjected to γ-irradiation. G0 arrest was achieved by serum starvation using no serum containing culture media.

The efficiency of the cell cycle arrest was analysed using flow cytometry. The asynchronous and arrested cells were labelled with propidium iodide (PI) as DNA stain (Figure 4.5 A) and the percentage of cells in each stage of the cell cycle (G0/G1, S, G2/M) was quantified (Figure 4.5 B). While different levels of arrest was observed in the RPE-1 WT, *MSL2*$^{-/-}$ and *MSL1*$^{-/-}$ cell lines the serum starvation increased the G0/G1 population in each cell line 48h after synchronisation compared to the asynchronous population. In parallel, the percentage of cells in S and G2/M phase after arrest showed a decrease in all cell lines compared to the unsynchronised cells. (Figure 4.5 B).

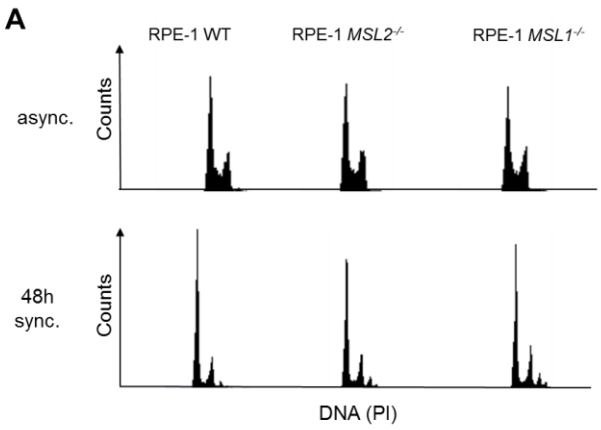

B

	asynchronous cells			48h serum starved cells		
	G0/G1	S	G2/M	G0/G1	S	G2/M
RPE-1 WT	56.30%	17.78%	27.24%	69.53%	6.94%	18.72%
RPE-1 *MSL2*$^{-/-}$	58.15%	15.50%	31.06%	63.19%	9.09%	21.56%
RPE-1 *MSL1*$^{-/-}$	48.19%	13.63%	25.91%	61.14%	4.89%	22.99%

Figure 4.5: Cell cycle profile of asynchronous and G0 arrested cells. A) RPE-1 WT, *MSL2*$^{-/-}$ and *MSL1*$^{-/-}$ cells were either fixed without any treatment or synchronised in G0 by 48h serum starvation, released and fixed at 0h. Cells were stained with propidium iodide (PI). B) Quantification of cell population at different stages of cell cycle in asynchronous and 48 h arrested cells.

4.4.1. γH2A.X foci formation after DNA damage

The phosphorylation of H2A.X at S139 (γH2A.X) at damaged DNA sites is one of the first DNA strand break recognition and signalling event (Rogakou et al., 1998, Firsanov et al., 2011). DNA breaks are first recognised by DNA damage sensor complexes such as MRN, RPA, ATRIP and 9-1-1 (Sulli et al., 2012). These, then recruit transducer protein ATM and ATR which perform phosphorylation on different molecules including H2A.X (An et al., 2010, Marechal and Zou, 2013). γH2A.X then serves as a recruitment factor and binding platform for the DNA damage response mediator proteins for example MDC1 (Stewart et al., 2003, Stucki et al., 2005). To study if the foci formation of γH2A.X was affected in the *MSL2*$^{-/-}$ and *MSL1*$^{-/-}$ cell lines IR-induced nuclear foci (IRIF) experiment was carried out (Figure 4.6). The layout of the experiment and the timepoints taken are indicated on Figure 4.6 A. (Expanded figure in **Appendix 2** – Expanded IRIF foci formation images)

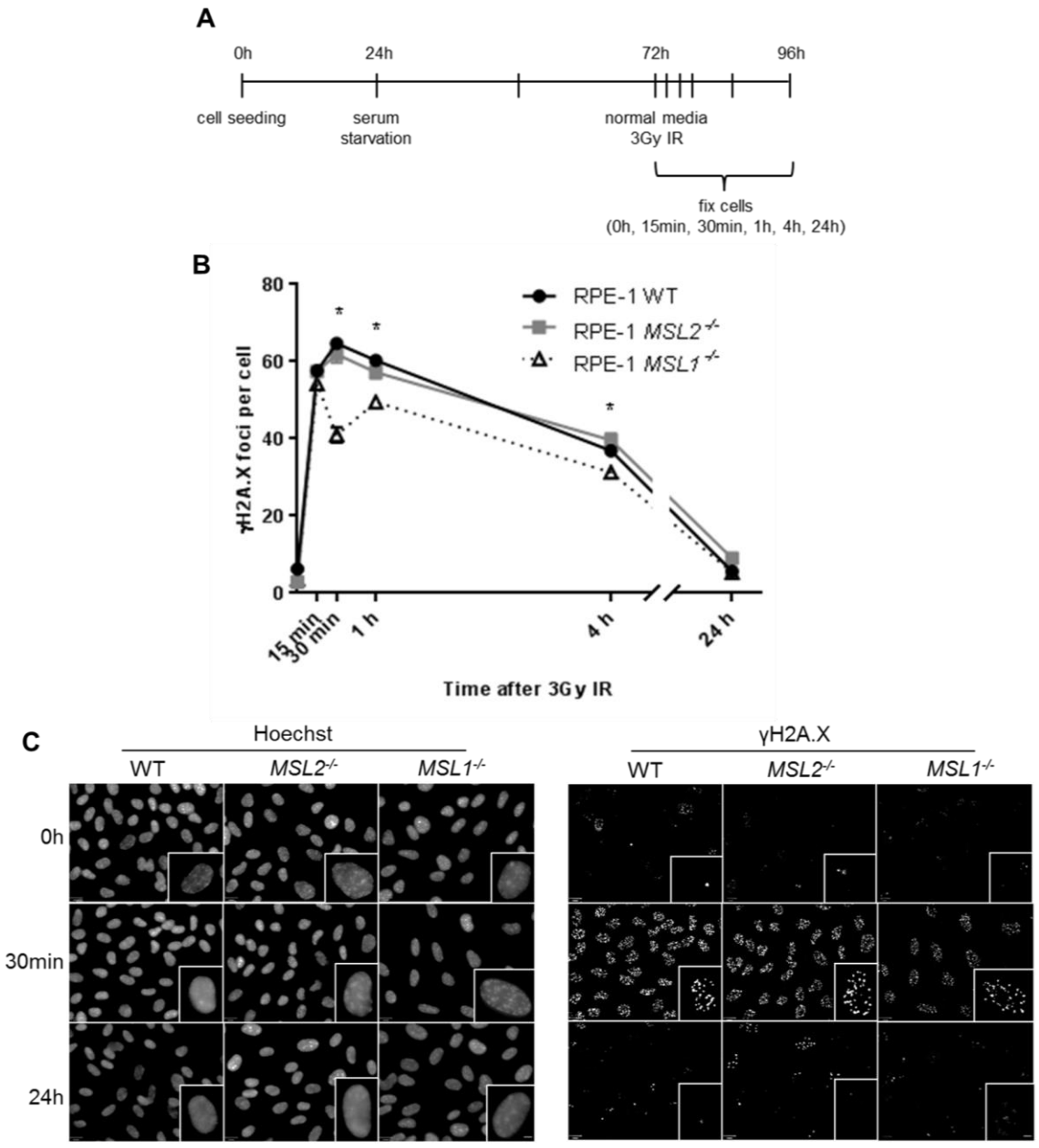

Figure 4.6: γH2A.X foci formation after 3Gy irradiation. A) Schematic representation of the IRIF experimental setup. B) Quantification of the number of γH2A.X foci per cell after 3Gy IR (n=3). Error bars represent standard error of the mean. Asterix represents significant difference between measurements. Statistical analysis was performed using one-way ANOVA and Dunn's multiple comparison tests. Detailed significances are as followed: 30min: WT vs. *MSL1*$^{-/-}$ ****, *MSL2*$^{-/-}$ vs. *MSL1*$^{-/-}$ ****; 1h: WT vs. *MSL1*$^{-/-}$ ****, *MSL2*$^{-/-}$ vs. *MSL1*$^{-/-}$**; 4h: WT vs. *MSL1*$^{-/-}$ *, *MSL2*$^{-/-}$ vs. *MSL1*$^{-/-}$ **. P value: (0.0332)*, (0.0021)**, (<0.0001)****. C) γH2A.X foci formation in wild type and *MSL2*$^{-/-}$ RPE-1 cells. Scale bar indicates 5 µm.

The obtained results show that γH2A.X foci formation in case of the RPE-1 *MSL2*$^{-/-}$ cells is similar to the wild type. However, compared to the wild type RPE-1 in the *MSL1*$^{-/-}$ cell line 30min, 1h and 4h after irradiation there is significantly less foci

(Figure 4.6 B) and these foci seem to be less bright and defined as well (Figure 4.6 C). Since it is known that acetylation by MOF plays a role in ATM activation (Gupta et al., 2005), the observed phenotype in the *MSL1*$^{-/-}$ cells could indicate that the disruption of the MSL complex partially affects ATM mediated phosphorylation of H2A.X. There is no evidence though for this MSL1 related indirect effect on ATM activation. The suggested explanation for the observed perturbed foci formation in the RPE-1 *MSL1*$^{-/-}$ cell line needs further investigations involving ATM activation experiments in the absence of MSL1. The recovery time after IR showed a similar trend in all three cell lines and 24h post irradiation there is no difference in the number of foci between RPE-1 WT, *MSL2*$^{-/-}$ and *MSL1*$^{-/-}$ (Figure 4.6 B). This suggests that neither MSL2 nor MSL1 are essential for the general repair of DNA double-strand breaks, but the general γH2A.X foci formation is affected by the loss of MSL1.

To follow the later events of the DDR, the focal recruitment of three different DNA damage mediators (MDC1, BRCA1 and 53BP1) were studied as well.

4.4.2. MDC1 foci formation after DNA damage

MDC1 is recruited to DNA damage sites through binding γH2A.X via its BRCT domain (Stewart et al., 2003, Stucki et al., 2005). This event is followed by the activation of MDC1 through phosphorylation and dimerization (Jungmichel et al., 2012). Activation of MDC1 and RNF168 mediated ubiquitylation of H2A at K13 and K15 facilitates the recruitment of important downstream mediators such as BRCA1 and 53BP1 (Lou et al., 2006, Stewart et al., 2009, Mattiroli et al., 2012).

While the relation between MSL2 and MDC1 has not been studied yet, it has also been reported that the knockdown of MSL1 in human U2OS cells leads to the downregulation of MDC1 (Lai, 2013).

To see if the loss of MSL1 or MSL2 could affect the focal recruitment of MDC1 an IRIF experiment was carried out (Figure 4.7). The layout of the experiment and the timepoints taken are indicated on (Figure 4.7 A). (Expanded figure in **Appendix 2** – Expanded IRIF foci formation images)

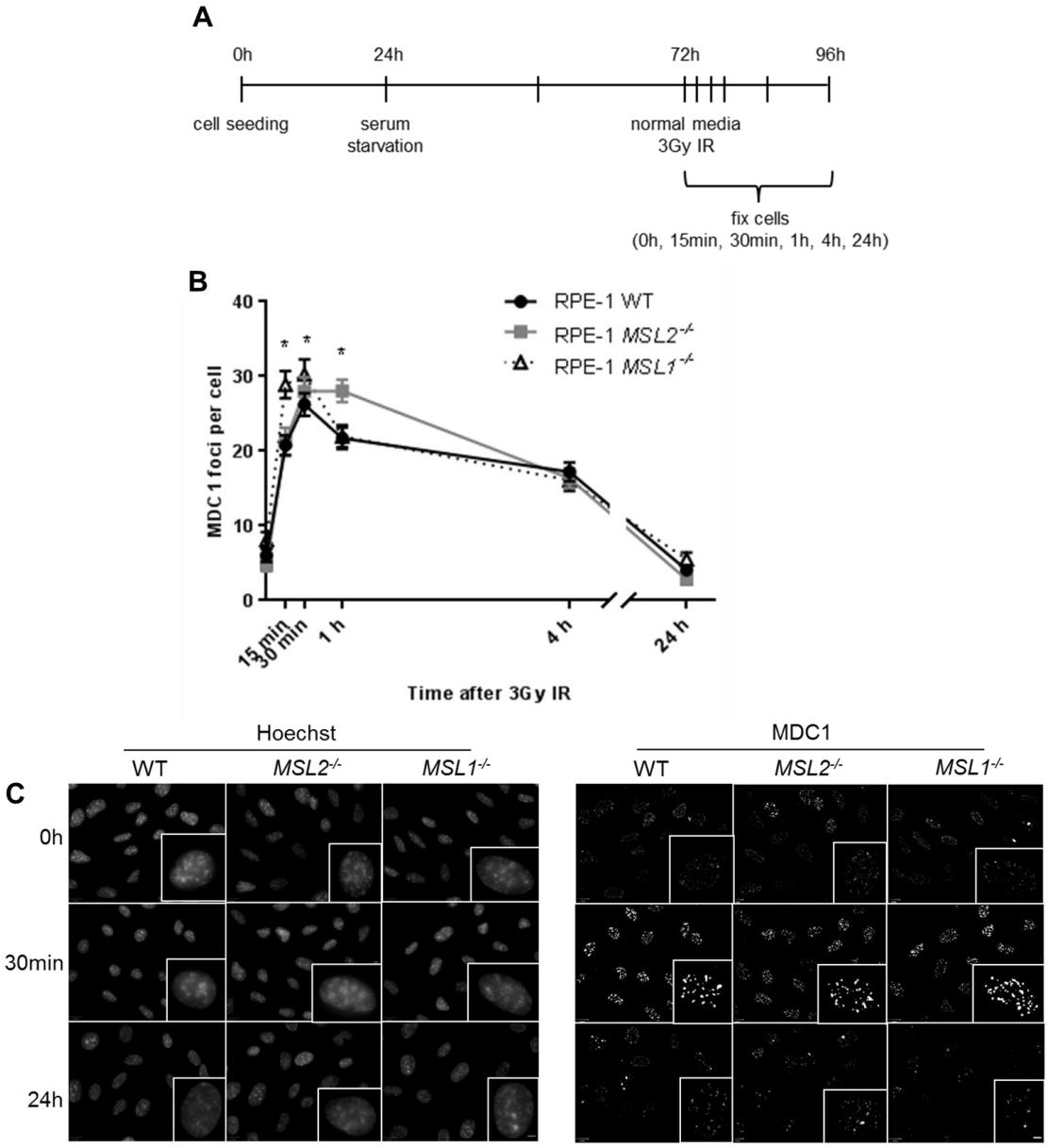

Figure 4.7: MDC1 foci formation after 3Gy irradiation. A) Schematic representation of the IRIF experimental setup. B) MDC1 foci formation after IR (n=3). Error bars represent standard error of the mean. Asterix represents significant difference between measurements. Statistical analysis was performed using one-way ANOVA and Dunn's multiple comparison tests. Detailed significances are as followed: 15min: WT vs. *MSL1*$^{-/-}$ ****, *MSL2*$^{-/-}$ vs. *MSL1*$^{-/-}$ ****; 30min: WT vs. *MSL1*$^{-/-}$ **, 1h: WT vs. *MSL2*$^{-/-}$ ****, *MSL2*$^{-/-}$ vs. *MSL1*$^{-/-}$ ****. P value: (0.0021)**, (<0.0001)****. C) IRIF of MDC1 foci formation in wild type, *MSL2*$^{-/-}$ and *MSL1*$^{-/-}$ RPE-1 cells. Scale bar indicates 5 µm.

The results show that the loss of MSL1 significantly increased the number of foci at 15min and 30min after IR compared to wild type RPE-1 cells (Figure 4.7 B). The recruitment of MDC1 to DNA damage sites partially depends on H4K16ac and γH2A.X binding (Taipale et al., 2005, Sharma et al., 2010) and these modifications in previously performed experiments were found to be perturbed (Figure 3.7 and

Figure 4.6). The increased number of MDC1 foci formation observed (Figure 4.7 C) could indicate a recruitment defect at the early time points after irradiation in the *MSL1*$^{-/-}$ cells compared to wild type. However, the same increase was not observed in the *MSL2*$^{-/-}$ cells suggesting that there might be a threshold level of DDR related histone modifications to affect the recruitment of MDC1 and the loss of MSL2 did not result in a decrease great enough to affect the foci formation at 15min and 30min post IR. In the RPE-1 *MSL2*$^{-/-}$ cell line significant difference in MDC1 foci number was observed 1h after IR compared to wild type cells, showing similar level as the 30min timepoint (Figure 4.7 B). This prolonged presence of MDC1 IRIF foci could either suggest an impaired dissociation of MDC1 from the repair sites or a temporarily slowed repair. However, in the number of MDC1 foci at the later timepoints after IR there was no difference between the three cell lines.

This data indicates that while the overall repair was not affected by the loss of either MSL2 or MSL1, they possibly had an indirect effect on the early timepoint recruitment of MDC1.

4.4.3. BRCA1 foci formation after DNA damage

BRCA1 is an important DDR mediator protein recruited to DNA damage sites and plays a key role in the choice between NHEJ and HR repair pathways (Lowndes, 2010, Daley and Sung, 2014). The recruitment of BRCA1 depends mainly on MDC1, the MOF mediated acetylation of H4K16 and the RNF8-RNF168 mediated ubiquitylation of H2A and H2A.X (Mailand et al., 2007, Li et al., 2010, Gatti et al., 2012, Mattiroli et al., 2012).

To investigate how the loss of MSL2 or MSL1 affects the recruitment of BRCA1, and the promotion of HR repair, immunofluorescent experiment was carried out to look at foci formation after IR (Figure 4.8). The layout of the experiment and the timepoints taken are indicated on Figure 4.8 A.

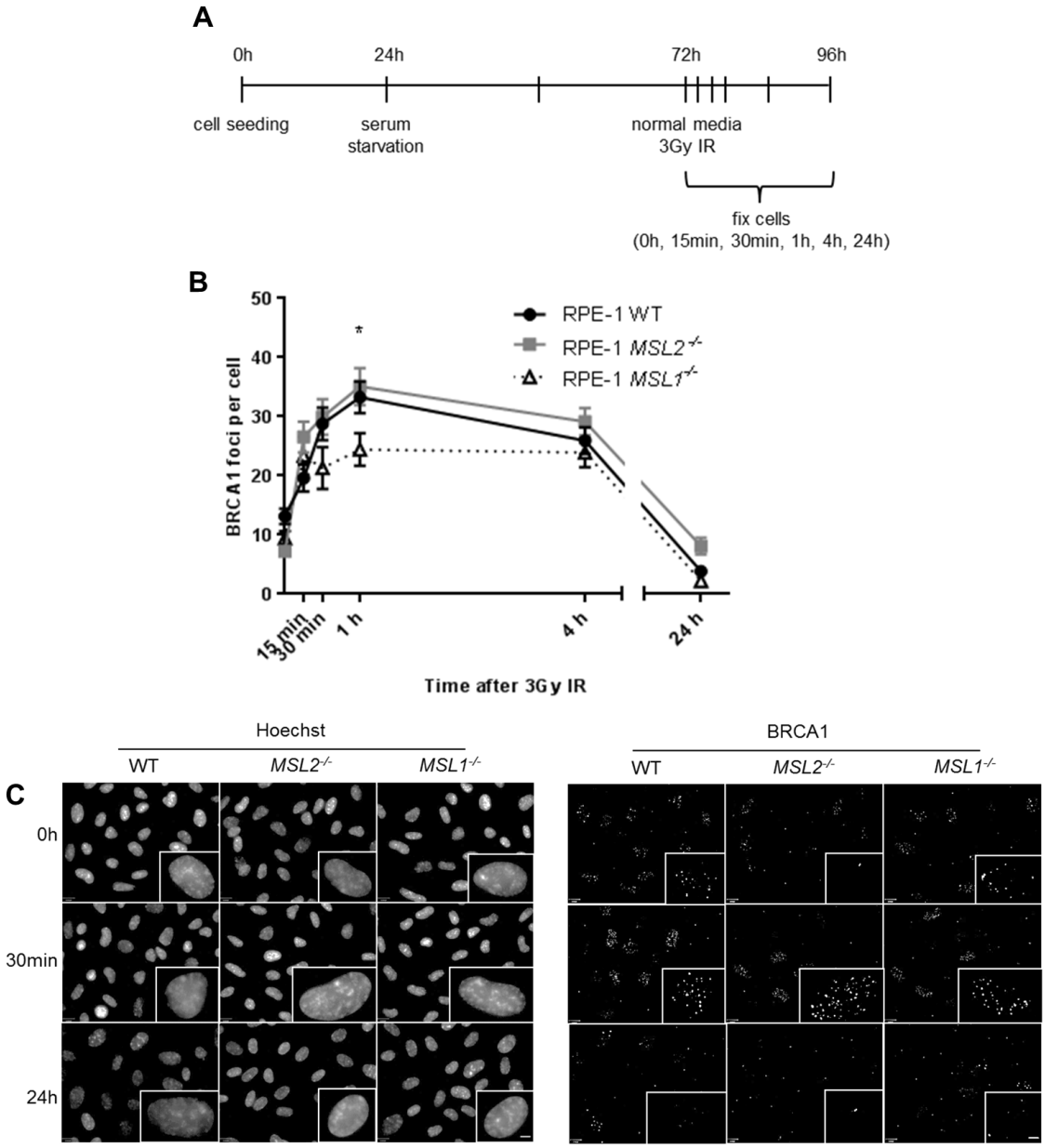

Figure 4.8: BRCA1 foci formation after 3Gy irradiation. A) Schematic representation of the IRIF experimental setup. B) BRCA1 foci formation after IR. (n=2). Error bars represent standard error of the mean. Asterix represents significant difference between measurements. Statistical analysis was performed using one-way ANOVA (nonparametric) and Dunn's multiple comparison tests. Detailed significances are as followed: 1h: WT vs. *MSL1*$^{-/-}$ **, *MSL2*$^{-/-}$ vs. *MSL1*$^{-/-}$ **. P value: (0.0021)**. C) IRIF of BRCA1 foci formation in wild type, *MSL2*$^{-/-}$ and *MSL1*$^{-/-}$ RPE-1 cells. Scale bar indicates 5 μm.

The results show that RPE-1 *MSL2*$^{-/-}$ cells had slightly elevated number of BRCA1 foci 4h and 24h after DNA damage compared to the wild type cells. While this difference is not statistically significant it could indicate a moderately impaired HR repair. The difference in BRCA1 foci number in case of the *MSL1*$^{-/-}$ cells compared

to wild type RPE-1 30min and 1h after IR show a trend of decreased number of foci with the 1h timepoint being significantly different. This result suggests that the loss of either MSL2 or MSL1 has no or very mild effect on BRCA1 recruitment.

4.4.4. 53BP1 foci formation after DNA damage

53BP1 is the main mediator of the NHEJ repair pathway (Gupta et al., 2014a). It is recruited to the DNA damage sites by MDC1 and RNF168 and binds H2AK15ub and H4K20me2 as anchor sites (Bohgaki et al., 2013, Fradet-Turcotte et al., 2013, Wilson et al., 2016). The concentration of H4K20me2 is particularly important for its recruitment and dilution of this modification can prevent the binding of 53BP1 to DNA (Pellegrino et al., 2017). Similarly, the loss of p53 also contributes to defective 53BP1 foci formation in G1 and early S phase of the cell cycle (Moureau et al., 2016). Following recruitment 53BP1 binds RIF1 and together with REV7 prevents DNA end resection thus BRCA1 recruitment to damage sites facilitating NHEJ repair (Bunting et al., 2010, Chapman et al., 2013, Zimmermann et al., 2013). In contrast H4K16ac at DNA damage sites prevents 53BP1 binding to H4K20me2 marks and promotes HR repair (Tang et al., 2013).

While MSL2 so far has not been implicated in 53BP1 mediated recruitment, but it has previously been shown that MSL1 interacts with 53BP1 (Gironella et al., 2009) suggesting that other MSL proteins might be involved as interactors as well.

The IRIF foci formation of 53BP1was studied to investigate the role of MSL2 or MSL1 in the NHEJ pathway (Figure 4.9). The experimental layout and timepoints taken are indicated on Figure 4.9 A. (Expanded figure in **Appendix 3** – 53BP1 nuclear body definition)

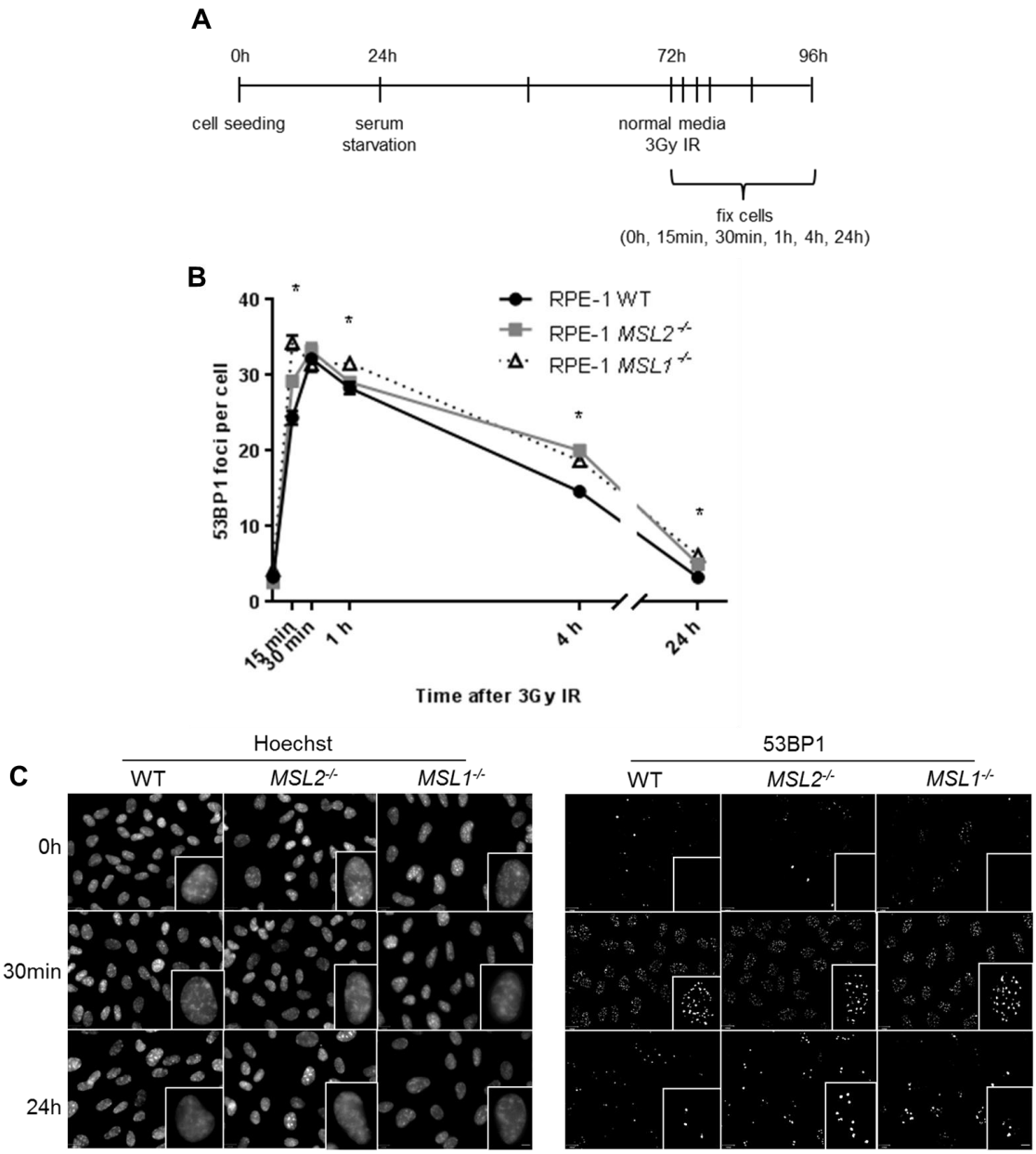

Figure 4.9: 53BP1 foci formation after 3Gy irradiation. A) Schematic representation of the IR IF experimental setup. 53BP1 foci formation after IR (n=3). Error bars represent standard error of the mean. Asterix represents significant difference between measurements. Statistical analysis was performed using one-way ANOVA and Dunn's multiple comparison tests. Detailed significances are as followed: 15min: WT vs. *MSL2*$^{-/-}$ ****, WT vs. *MSL1*$^{-/-}$ ****, *MSL2*$^{-/-}$ vs. *MSL1*$^{-/-}$ ***; 1h: WT vs. *MSL1*$^{-/-}$ **, *MSL2*$^{-/-}$ vs. *MSL1*$^{-/-}$ *; 4h: WT vs. *MSL2*$^{-/-}$ ****, WT vs. *MSL1*$^{-/-}$ ****; 24h: WT vs. *MSL2*$^{-/-}$ **, WT vs. *MSL1*$^{-/-}$ ****. P value: (0,0332)*, (0.0021)**, (<0.0001)****. C) IRIF of MDC1 foci formation in wild type, *MSL2*$^{-/-}$ and *MSL1*$^{-/-}$ RPE-1 cells. Scale bar indicates 5 µm.

The results show that the recruitment of 53BP1 to damage sites was affected significantly 15min, 1h, 4h and 24h after IR in the *MSL2*$^{-/-}$ and *MSL1*$^{-/-}$ RPE-1 cells compared to the wild type cells (Figure 4.9 B). Previously discussed perturbed H4K20me2 and H4K16ac (Figure 3.7) could contribute to the observed increase in

foci number as both posttranslational modifications have an important role in localising 53BP1 to damage sites. While decrease alone in H4K20me2 can prevent 53BP1 binding at DNA damage sites potentially resulting in a lower number of IRIF foci, similar change in H4K16ac mark would rather propagate NHEJ and 53BP1 recruitment. So the observed phenotype could point towards a counteracting effect, where decrease of H4K16ac enables 53BP1 recruitment to damage sites but the reduction of H4K20me2 prevents its proper association to chromatin. However, further investigation is required to address this hypothesis.

In addition, 24h post irradiation more 53BP1 sites with larger foci were observed in the *MSL2*$^{-/-}$ cells (Figure 4.9 C). These foci have previously been described as 53BP1 nuclear bodies which are thought to shield DNA lesions generated by mitotic transmission and remain underreplicated (Lukas et al., 2011). Underreplicated DNA regions (generally late replicating genomic regions) are repressed for replication through different mechanisms, for example Fob1 (Fork blocking less) in *S. cerevisiae* physically prevents replication while SUUR (suppressor of underreplication) in *Drosophila* inhibits fork progression (Kobayashi and Horiuchi, 1996, Di Felice et al., 2005, Sher et al., 2012). These regions in general tend to replicate slower or fail to finish replication before the end of S-phase (Wallace and Orr-Weaver, 2005, Andreyeva et al., 2008, Nordman and Orr-Weaver, 2015). DNA lesions sequestered in these 53BP1 nuclear bodies accumulate in G1 phase of the cell cycle (Lukas et al., 2011).

To quantify the phenotype observed after IRIF further analysis was performed (Figure 4.10). The number of nuclear bodies were counted in RPE-1 wild type, *MSL2*$^{-/-}$ and *MSL1*$^{-/-}$ cells using a size exclusion quantification analysis (Detailed explanation on threshold settings are explained in **Appendix 3** – 53BP1 nuclear body definition).

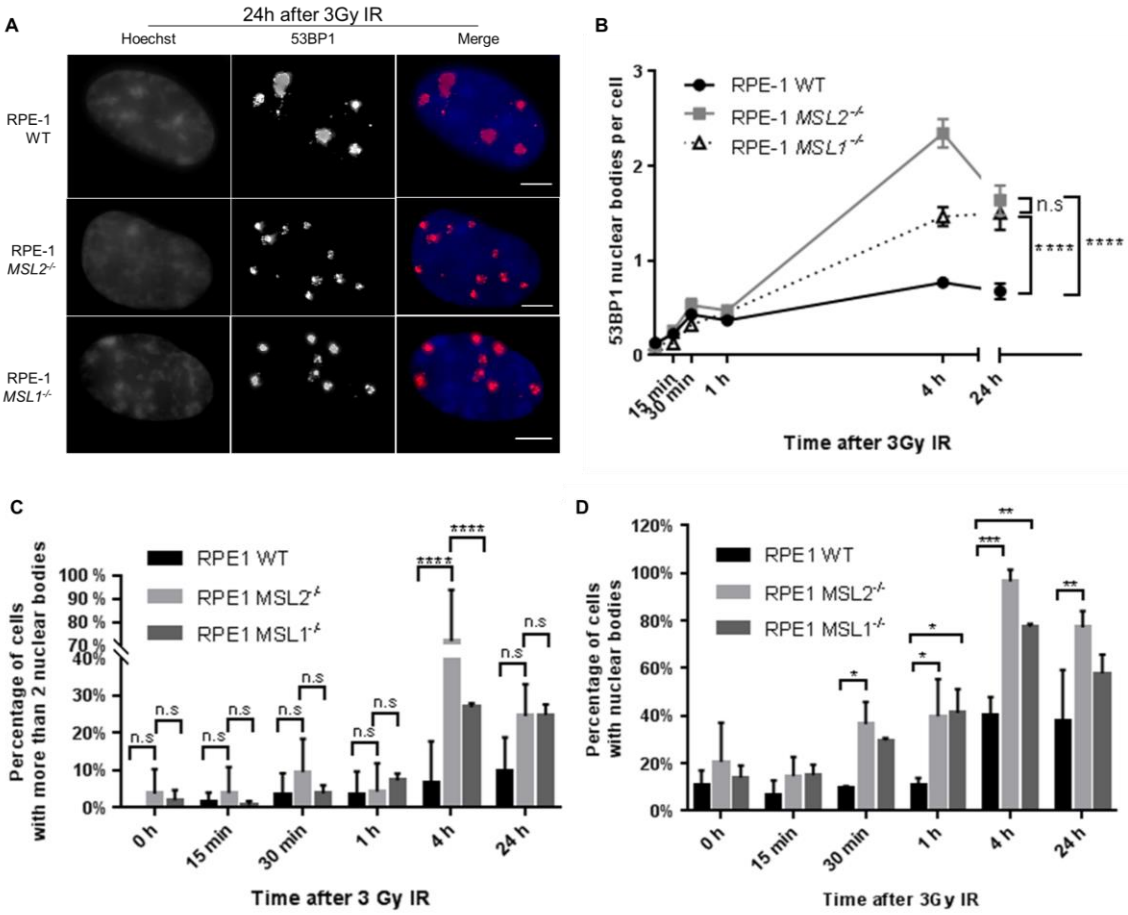

Figure 4.10: 53BP1 nuclear body presence after 3Gy IR. A) Representative images of 53BP1 nuclear body formation in wild type and *MSL2*$^{-/-}$ RPE-1 cells 24h after 3 Gy IR. Scale bar indicates 10 µm. B) Number of nuclear bodies present in wild type, *MSL2*$^{-/-}$ and *MSL1*$^{-/-}$ RPE-1 cells after 3Gy IR. Error bars represent standard error of the mean. Statistical analysis was performed using Kruskal-Wallis and Dunn's multiple comparison tests (n=3). P value: (0.0001)**** C) Percentage of cells with more than 2 nuclear bodies in wild type, *MSL2*$^{-/-}$ and *MSL1*$^{-/-}$ RPE-1 cells after 3Gy IR. D) Percentage of cells with nuclear bodies in wild type, *MSL2*$^{-/-}$ and *MSL1*$^{-/-}$ RPE-1 cells after 3Gy IR. Statistical analysis was performed using two-wayANOVA and Tukey's muliple comparison test. P value: (0.0332) * , (0.0021)**, (0.0002)***, (<0.0001) ****.

The number of nuclear bodies after IR (Figure 4.10 A) were counted in wild type, *MSL2*$^{-/-}$ and *MSL1*$^{-/-}$ RPE-1 cell. (Figure 4.10 B) and the results show an increased number of nuclear bodies peaking at 4h and 24h. Since most cells only contained one or two nuclear bodies, the percentage of cells with more than 2 nuclear bodies was also calculated. The obtained data showed a larger number of *MSL2*$^{-/-}$ and *MSL1*$^{-/-}$ cells with more than two nuclear bodies compared to wild type RPE-1 cells (Figure 4.10 C). These observation could suggest either 53BP1 localization defect as shown before with foci formation (Figure 4.9) or an increased number of damaged, underreplicated DNA. To address this question the number of cells with 53BP1

nuclear bodies was counted and found to be increased in cells lacking either MSL2 or MSL1 (Figure 4.10 D). This result could indicate that it is more likely to have an increase in damaged, underreplicated DNA in both *MSL2*$^{-/-}$ and *MSL1*$^{-/-}$ cell lines, given that this quantification is not biased by foci number.

Overall, these findings point towards that the loss of MSL2 or MSL1 might causes prolonged 53BP1 nuclear bodies shielding unresolved DNA damage and that these damages were probably occurred during mitosis.

4.5. The loss of MSL2 and MSL1 affects replication related DNA damage recovery

4.5.1. γH2A.X foci formation in mitotic cells

To study if the loss of MSL2 or MSL1 results in an increase in mitosis related damage immunofluorescent analysis was performed using exponentially growing wild type RPE-1, RPE-1 *MSL2*$^{-/-}$ and RPE-1 *MSL1*$^{-/-}$ cells. To monitor DNA damage occurring in mitotic cells γH2A.X was used as a marker (Figure 4.11). Cells in different stages of mitotic division were imaged and the number of γH2A.X foci present was counted. As oppose to an expected increase in DNA breaks in *MSL2*$^{-/-}$ and *MSL1*$^{-/-}$ cells the γH2A.X foci formation showed no significant difference to the wild type cells in number (Figure 4.11 B). However, interestingly in the RPE-1 WT cells less defined foci formation was observed compared to the two knock-out cell lines (Figure 4.11 A).

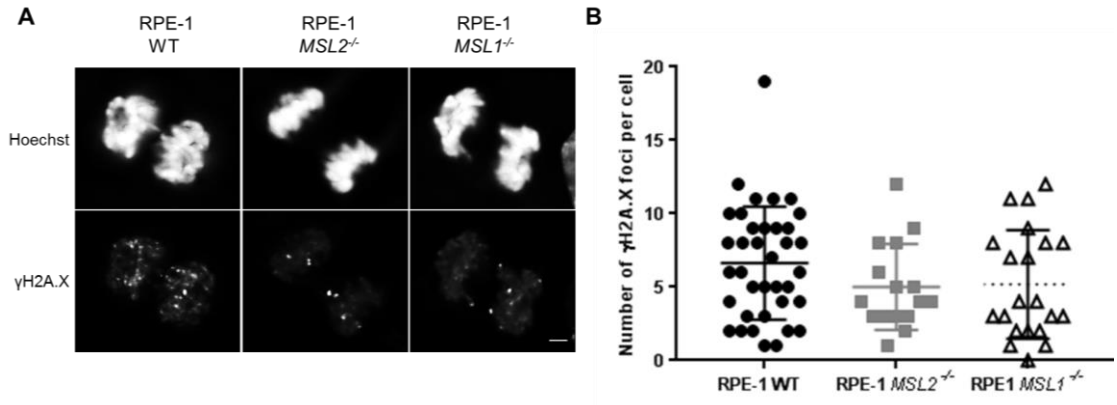

Figure 4.11: γH2A.X foci formation in mitotic cells. A) γH2A.X foci formation in wild type and *MSL2*$^{-/-}$ RPE-1 cells. Scale bar indicates 5µm. Images were taken by Dr. Muriel Voisin. B) Quantification of IF image analysis showing average γH2A.X foci formation per cell in the indicated samples.

This observation could indicate a different role in γH2A.X foci formation in mitosis for MSL2 and MSL1 which might affect the redundancy of this histone modification. Upon the loss of either MSL2 or MSL1 proteins the phosphorylation of H2A.X foci could remain more redundant. However, this hypothesis needs further investigation such as immunofluorescent detection of ATM and ATR recruitment and quantification at DNA damage sites.

4.5.2. Replication restart after fork stalling

To investigate if the prolonged presence and increased number of 53BP1 nuclear bodies in both *MSL2*$^{-/-}$ and *MSL1*$^{-/-}$ cell lines is related to a replication defect induced by fork stalling DNA fibre assay was performed. As the depletion of MOF via RNAi was previously shown to cause defect in replication restart after HU damage (Rea Lab-Dr. Jennifer Chubb unpublished data), *TP53*$^{-/-}$ *KAT8*$^{-/-}$ double knock-out cells were also included in these experiments. Results presented before showed that the loss of either MSL2 or MSL1 affect the activity of MOF (Figure 3.8) and it is likely that the removal of either of these proteins from the cells will result in a MOF mimicking, but less severe phenotype. It has also been reported previously that PAF1, an MSL2 and MSL1 interacting protein, is involved in recovery from hydroxyurea induced replication stress (Poli et al., 2016) which can indicate the involvement of these two MSL proteins in replication related DNA damage as well.

To see if the loss of MSL2 or MSL1 can affect replication recovery after hydroxyurea induced stress DNA fibre assay was performed (Figure 4.12). Cells were treated first with IdU (5-Iodo-2′-deoxyuridine) nucleotide analogue for 30 min. The media was then completed with hydroxyurea to induce replication arrest by nucleotide starvation. Cells were released into CldU (5-chloro-2'-deoxyuridine) analogue containing fresh media and the incorporation of newly synthesised DNA was labelled for 30 min (Figure 4.12 A). DNA fibres were visualised using immunofluorescent microscopy (Figure 4.12 B).

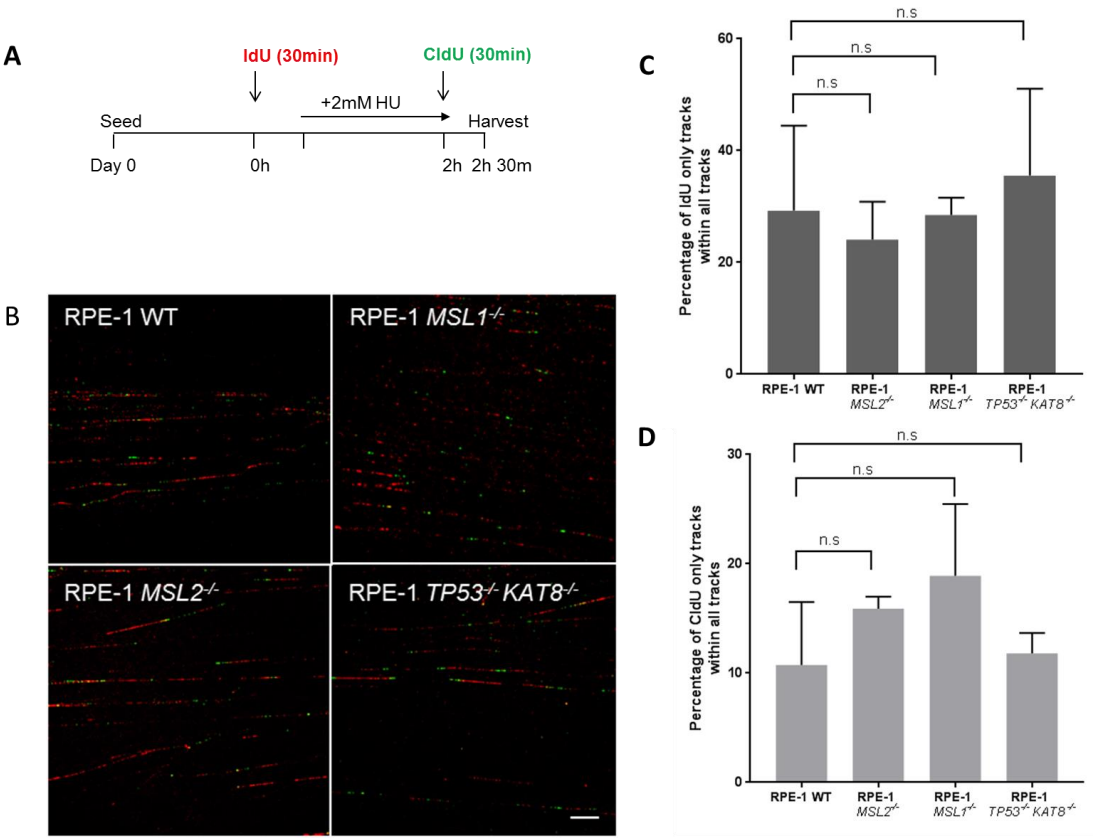

Figure 4.12: Replication fork progression after hydroxyurea treatment. A) Schematic representation of the pulse-chase experimental setup. Scale bar represents 20µM. B) DNA fibres with IdU and CldU tracks representing ongoing, newly fired and stalled replication sites after hydroxyurea treatment. IdU-red, CldU-green. C) Percentage of DNA fibres representing replication termination and fork collapse events. Data is represented as percentage of tracks within all counted tracks. D) Percentage of DNA fibres representing new origin firing. Data is represented as percentage of tracks within all counted tracks. Error bars represent standard deviation. Statistical analysis was performed using two-wayANOVA and Tukey's muliple comparison test.

The results show that cells depleted of MSL2 or MSL1 have a decrease in the percentage of replication termination/fork collapse events (indicated by IdU only tracks) after hydroxyurea treatment (Figure 4.12 B). Also, both RPE-1 *MSL2*$^{-/-}$ and *MSL1*$^{-/-}$ cells had a larger number of newly fired origins (indicated by CldU only tracks) compared to wild type cells suggesting an increase in silent replication origin site activation (Figure 4.12 C). On the contrary, RPE-1 *TP53*$^{-/-}$ *KAT8*$^{-/-}$ showed similar phenotype to wild type cells both in fork termination/collapse and newly fired origin track events. This suggests that the MSL2/1 complex might act outside of the MSL complex in replication.

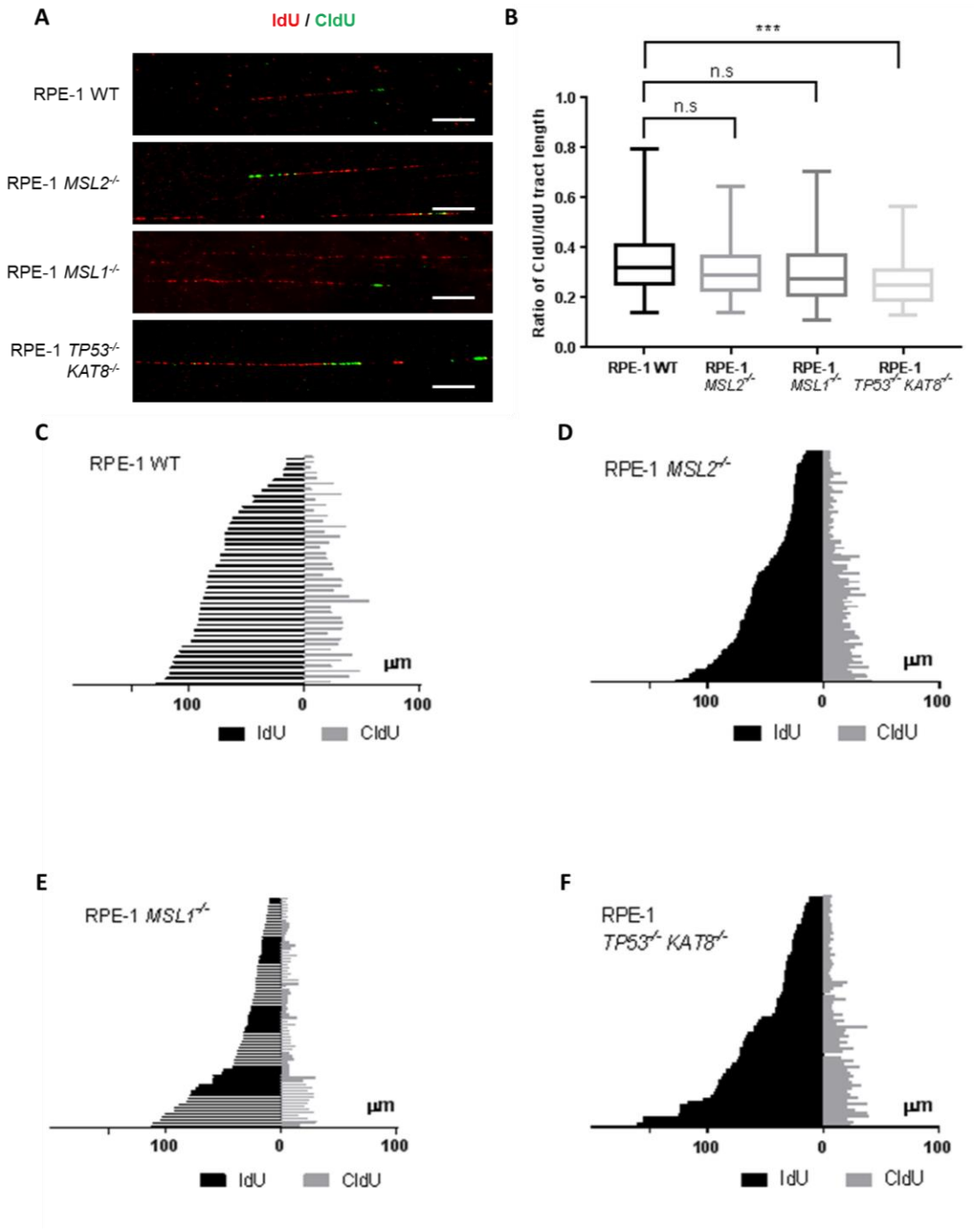

Figure 4.13: Idu/CldU ratio in ongoing replication. A) Representative image of ongoing replication forks in RPE-1 WT, MSL2$^{-/-}$, *MSL1*$^{-/-}$ and *TP53*$^{-/-}$ *KAT8*$^{-/-}$ cell lines. IdU treatment was performed for 30 min without replication stress and an additional 2 h with 2 mM HU treatment, then replaced by CldU for an additional 30 min for recovery without HU. Scale bar represents 20 µm. B) Ratio of IdU and CldU length measured in ongoing replication, recovered after HU treatment. C-F) Individual IdU and CldU labelled DNA fibre tracks of RPE-1 WT, MSL2$^{-/-}$, *MSL1*$^{-/-}$ and *TP53*$^{-/-}$ *KAT8*$^{-/-}$ representing ongoing replications are shown as tree bar graph. Fibre lengths were plotted in µm. Statistical analysis was performed using two-wayANOVA and Tukey's muliple comparison test. P value: (0.0002)**.

While stretching DNA in a uniform manner cannot be achieved using DNA fibre assay, preliminary data was obtained in relation with replication speed before and after HU treatment (Figure 4.12).

Recovered/ongoing replication tracks containing both IdU and CldU label were measured using ImageJ programme (Figure 4.13 A). The ratio between IdU and CldU track length was plotted on Figure 4.13 B. The obtained results show that all cell lines had slowed replication after recovery with the *TP53*$^{-/-}$ *KAT8*$^{-/-}$ RPE-1 cells having significantly lower recovery rate compared to the wild type cells. This data suggests that replication forks which were able to recover progress in a similar rate in the MSL2 and MSL1 knock-out cell lines as wild type cells while cells depleted of MOF and p53 might have difficulty in fork progress after HU release.

The overall distribution of IdU and CldU track length was plotted to look at the distribution of different track length measured as well (Figure 4.13 C-F). RPE-1 WT, *MSL2*$^{-/-}$ and *TP53*$^{-/-}$ *KAT8*$^{-/-}$ cell lines show normal distribution of varying length of replicating fibres, while the *MSL1*$^{-/-}$ population seemed to have a larger number of short IdU and CldU tracks. However, due to the limitations of the DNA fibre technique, the observed difference could be the result of more condensed DNA fibres in the sample population. For more accurate measurements of labelled track length DNA combing method is suggested where DNA fibres are stretched along the sample slide in a uniform manner.

4.6. Discussion

To investigate the involvement of human MSL2 and MSL1 in the DNA damage response a series of experiments were carried out. To see what type of DNA damaging agents affect proliferation the knock-out cell lines clonogenic colony formation assay was performed and RPE-1 *MSL2*$^{-/-}$ and *MSL1*$^{-/-}$ cells both showed increased sensitivity towards IR and UV induced damage (Figure 4.1). Similar to what has been previously reported (Lai et al., 2013) using an *in vivo* reporter assay, the loss of human MSL2 showed impaired NHEJ repair efficiency (Figure 4.3). In addition MSL2 knock-out cells also showed lower efficiency in an *in vivo* HR repair experiment compared to the wild type cells (Figure 4.4).

Based on these findings and earlier observations on perturbed histone modifications related to DNA damage mediator protein recruitment (Figure 3.7), the foci formation of early stage DDR factors was investigated. As a general DNA break marker γH2A.X foci formation was studied in an IRIF (ionizing radiation-induced foci) experiment (Figure 4.6) and in the case of the RPE-1 *MSL2*$^{-/-}$, found to be similar to wild type cells. However, in the RPE-1 *MSL1*$^{-/-}$ cells a significant decrease was observed 30min, 1h and 4h after IR. A possible explanation for the observed phenotype could be that the disruption of the MSL complex by the loss of MSL1 affects DDR related MOF functions. MOF is known to play role in ATM activation (Gupta et al., 2005, Gupta et al., 2014b) which is a key H2A.X phosphorylating kinase (Burma et al., 2001b, Ward and Chen, 2001, An et al., 2010). While previous studies showed the depletion of MOF leads to prolonged γH2A.X foci formation (Gupta et al., 2014b), the overall trend of recovery after damage was not affected in this experiment and all three cell lines showed the same level of γH2A.X foci 24h after IR induced damage.

Since previous experiments suggested the involvement of MSL1 in MDC1 expression (Lai, 2013). IRIF foci formation of MDC1 was studied using the RPE-1 *MSL2*$^{-/-}$ and *MSL1*$^{-/-}$ cells to investigate a potential effect on MDC1 foci formation. The results showed that the loss of either MSL2 or MSL1 affected the early recruitment of MDC1 to the damage sites (Figure 4.7). The number of MDC1 foci per cell showed significant increase at 15min and 30min in the *MSL1*$^{-/-}$ cells and at 1h in the *MSL2*$^{-/-}$ cells after IR compared to the wild type cells. Since the recruitment of MDC1 is partially dependent on its binding to γH2A.X (Stewart et al., 2003, Stucki et al., 2005), the obtained result could suggest an early time recruitment defect indirectly promoted by the loss of either MSL2 or MSL1.

To study how the loss of MSL2 or MSL1 effects HR repair, BRCA1, a key mediator protein was investigated in an IRIF experiment (Li and Yu, 2013). However, the foci formation in both *MSL2*$^{-/-}$ and *MSL1*$^{-/-}$ cells showed similar levels as wild type RPE-1 cells and the only significant difference was observed at 1h after IR in the MSL1 knock-out cells (Figure 4.8). This suggests that the previously observed HR repair defect (Figure 4.4) in cells lacking MSL2 is not related to BRCA1 foci formation. Similarly, the loss of MSL1 did not affect the recruitment of BRCA1 to damage sites.

Overall the aforementioned DNA damage response mediators or γH2A.X showed a mild foci formation phenotype suggesting that neither MSL2 nor MSL1 is essential for their localization.

Since previous findings suggested that MSL1 is involved 53BP1 foci formation (Gironella et al., 2009) and two histone modification (H4K20me2 and H4K16ac) related to its recruitment was observed to be decreased in both MSL2 and MSL1 knock-outs (Figure 3.7) the foci formation of this NHEJ mediator was also studied in an IRIF experiment (Figure 4.9). In both RPE-1 *MSL2*$^{-/-}$ and *MSL1*$^{-/-}$ cell lines the number of 53BP1 foci showed significant increase in all investigated timepoints (with the exception of the 30min IRIF foci) but the initial recovery of the cells was not affected. While the decrease of H4K16ac would suggest propagation of NHEJ and 53BP1 binding to chromatin, the reduced H4K20me2 mark should negatively affect this recruitment (Fradet-Turcotte et al., 2013, Pellegrino et al., 2017). So it is possible that while the recruitment of 53BP1 was propagated at DNA damage sites, the decrease in H4K20me2 affected its proper localization.

In addition, increased 53BP1 nuclear body formation was observed 24h after damage (Figure 4.9 C). 53BP1 nuclear bodies are believed to shield DNA lesions generated during mitosis resulting in unresolved replication intermediates and incomplete replication (underreplicated DNA sites). While the exact role of this nuclear body formation is unclear, it was proposed that they protect the DNA form further damage during mitosis or to prevent repair through the error prone NHEJ pathway (Lukas et al., 2011). Quantification of 53BP1 nuclear bodies showed an increase in number peaking at 4h and 24h after irradiation (Figure 4.10). This observation could suggest that the loss of either MSL2 or MSL1 might affect replication or DNA damage repair during mitosis. To further investigate this hypothesis γH2A.X foci formation (as a marker for DNA breaks) was studied in untreated mitotic RPE-1 WT, *MSL2*$^{-/-}$ *and* *MSL1*$^{-/-}$ cells (Figure 4.11). While there was no significant difference in foci number within the three cell lines, RPE-1 wild type cells showed less defined γH2A.X foci compared to the knock-out cells. This result suggests that the loss of MSL2 or MSL1 did not increase DNA breaks during mitosis, but might contribute to the stabilization of H2A.X phosphorylation during cell division.

To address the other hypothesis about the involvement of MSL2 or MSL1 in replication related DNA damage a fibre assay was performed (Figure 4.12). The loss of MSL2 and MSL1 was found to affect MOF activity (Figure 3.7) and previous results from the lab (Dr. Jennifer Chubb unpublished) using RNAi mediated knock-down of the MSL member MOF showed severe defects in recovery from stalled replication. Thus, a recently generated RPE-1 *TP53*$^{-/-}$ *KAT8*$^{-/-}$ cell line was also included in the experiment as control. Replication restart after stalling was studied in a pulse-chase experimental setup using hydroxyurea as fork progression blocking agent. Results showed that all four cell lines have similar levels of replication recovery while termination or fork collapse events were less frequent in the *MSL2*$^{-/-}$ and *MSL1*$^{-/-}$ cell lines (Figure 4.12 C). They also showed a slight increase in newly fired replication origins compared to the wild type and p53-MOF double knock-out cells (Figure 4.12 D). This data suggest that the loss of either MSL2 or MSL1 moderately affects replication recovery in a way that it activates more silent origins but the mechanism or the mode of act is currently unknown.

In summary, results obtained from investigating the role of MSL2 and MSL1 in the DNA damage response show that the loss of either proteins result in the disruption in foci formation of early DDR mediator proteins but does not affect the overall repair. Thus, while MSL2 and MSL1 are required, not essential for any of the investigated damage types. Elevated levels of 53BP1 nuclear body formation in the RPE-1 *MSL2*$^{-/-}$ and *MSL1*$^{-/-}$ cell lines and replication stress recovery suggest a potential role for the MSL1/2 dimer in replication possibly independent of MOF functions.

5. Identification of novel human MSL2 interacting proteins and potential substrates

5.1. Introduction

So far there is little known about MSL2 and its role in human cells thus a specific assay to identify interacting proteins and substrates would provide useful information about its potential functions. Since MSL2 is a known E3 ubiquitin ligase it is important to address the existence of potential substrates within the group of interactors. MSL2 is known to ubiquitylate H2B at lysine 34 (Wu et al., 2011) and its loss affects both the NHEJ (Lai et al., 2013) and HR DNA repair pathways (Figure 4.4). Moreover, results from this study show that the loss of MSL2 results in perturbed histone modifications mainly related to replication and DNA damage (Figure 3.7). In order to broaden the available information on MSL2 interactors and substrates and explore what other pathways it could potentially play a role in, this chapter aims to generate new data from a novel immunoprecipitation-based assay.

Protein-protein interactions can be validated or identified with different methods, most commonly by co-immunoprecipitation (Co-IP) or pull-down assays, but these methods have certain limitations. They require a good quality antibody or an epitope tagged fusion of the protein of interest and a strong enough interaction between the bait and the protein captured (Phizicky and Fields, 1995, Berggard et al., 2007). However, in recent years technological advances in high-throughput protein analysis lead to the establishment of novel techniques mainly focusing on affinity-based purifications (Carneiro et al., 2016). For example, using BioID approach made it possible to capture weak and transient interactions by using a biotin ligase fusion construct which can label molecules in close proximity of the protein investigated, facilitating their pulldown (Roux et al., 2013).

Identifying ubiquitylated substrates of certain E3 ligases still proves to be a challenge provided by the dynamic nature of ubiquitylation, weak/transient interactions between ligase and substrate, significant degrees of redundancy and multiplicity and the rapid destruction of many ubiquitylated proteins targeted by the proteasome (Iconomou and Saunders, 2016). Except for a few E3 ligases, conserved substrate

targeting motifs are also not available (Tasaki et al., 2005, Jiang et al., 2011) making it difficult to identify ligase specific substrates.

To overcome the aforementioned challenges for MSL2 interactor identification a simple, high-throughput, proximity biotin ligation based method known as BioID was chosen. While this approach uses a sensitive capture the disadvantage of a protein fusion construct causing interference with some of the interactions and functions was kept in mind as well. Furthermore, after careful consideration the assay was combined with a co-immunoprecipitation technique using epitope labelled ubiquitin to capture and identify potential substrates.

5.2. BioID

The BioID system itself is based on a fusion construct between the protein of interest (in this case MSL2) and a promiscuous biotin ligase enzyme BirA (Bifunctional ligase/repressor BirA) mutant (BirA*). BirA is a 35kDa highly specific biotin ligase originally derived from *E. coli* (Beckett et al., 1999, Chapman-Smith and Cronan, 1999). As biotinylation in mammalian cells is a rare occurrence it makes the BioID system ideal for interaction assays. While the wild type BirA has a strong affinity to a minimal peptide sequence of LX§IFEAQKIEWR (X = any and § = any but not L, V, I, W, F or Y) (Choi-Rhee et al., 2004, Fairhead and Howarth, 2015), the R118G mutation introduced causes the protein to lose its specificity and perform its activity on any substrate with lysine residues within close proximity (Couzens et al., 2013, Lambert et al., 2015). Thus, the expression of this fusion with the addition of biotin (vitamin H) enables permanent and specific tagging of interacting molecules. Proteins labelled with biotin can then be subjected to immunoprecipitation by using immobilised streptavidin and then analysed using mass spectrometry. The system uses a specific HEK293TRex Flp-In cell line (O'Gorman et al., 1991) containing a single stably integrated FRT (Flp Recombination Target) site within its genome. Using a Flp-In expression and a pOG44 recombinase vector enables the integration of the expression vector to the FRT locus. Transient expression of the inserted cDNA coding region is achieved by a tetracycline inducible system. With this, stable integration of a BirA* fusion construct can be achieved and protein–protein interactions can be captured under various conditions such as replication stress or DNA damage induction.

5.1. Modified BioID

To successfully identify human MSL2 interacting proteins and possible substrates the above described BioID method was adapted and modified for the purposes of this work. In the modified BioID assay a Myc-BirA*-MSL2 construct is transiently transfected into HEK293T cells alongside His-Ub. Cells are then treated with biotin to allow proximity labelling via BirA* ligase activity (Figure 5.1). Biotinylated potential interactors are then captured in an immunoprecipitation assay (IP) using streptavidin conjugated beads. The molecules pulled down with this method are then identified using mass spectrometry. For potential substrate identification, in a separate assay nickel beads are used for immunoprecipitation. Ubiquitin labelled with histidine tag is covalently conjugated to substrate proteins facilitating the pulldown. The elution is then subjected to a second IP using streptavidin as bait to select potential interactors (biotinylated proteins) from the ubiquitylated molecules. The recovered proteins from this second IP can then be identified and analysed using mass spectrometry.

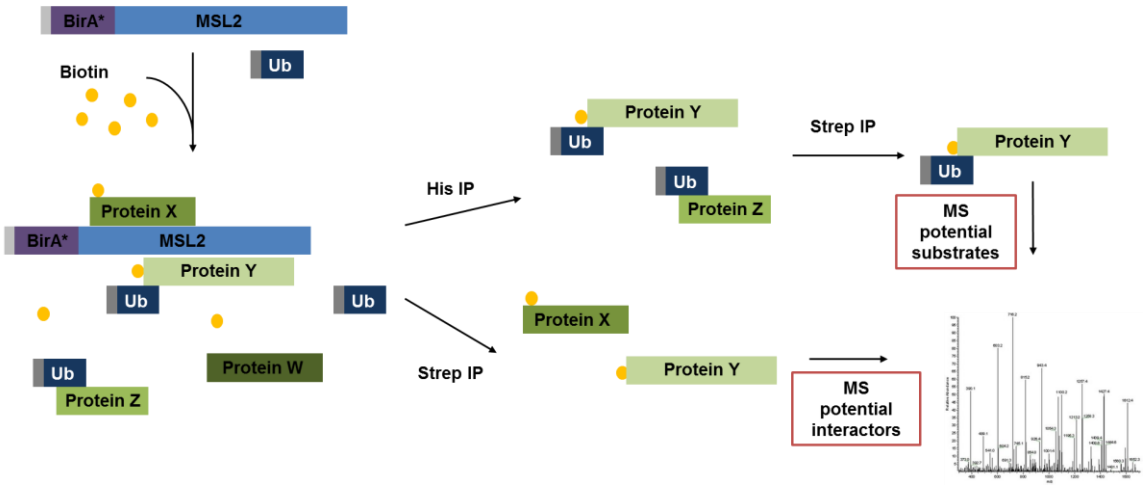

Figure 5.1: Schematic representation of the modified BioID assay. Generation of Myc-BirA*-MSL2 fusion protein enables *in vivo* labelling of interacting proteins via BirA* mediated biotin ligation. The addition of histidine (His) epitope tagged ubiquitin molecules to the system provides further selectivity towards ubiquitylated interactors as potential substrates. Interacting protein identification relies on immunoprecipitation of His-Ub labelled molecules followed by biotinylated protein pulldown. Potential interactor identification is based on biotinylated protein immunoprecipitation. Molecules recovered from either analysis are identified using mass spectrometric analysis. Ub- ubiquitin. BirA* - mutant BirA protein, Strep IP – streptavidine coupled immunoprecipitation, His IP – nickel beads coupled immunoprecipitation for histidine tagged molecules.

5.1.1. Assay optimization for mass spectrometry analysis

5.1.1.1. Test biotinylation and expression of BirA* fusion construct

Before performing the immunoprecipitation assays the level of biotinylation and expression of the BirA* fusion constructs was tested (Figure 5.2).

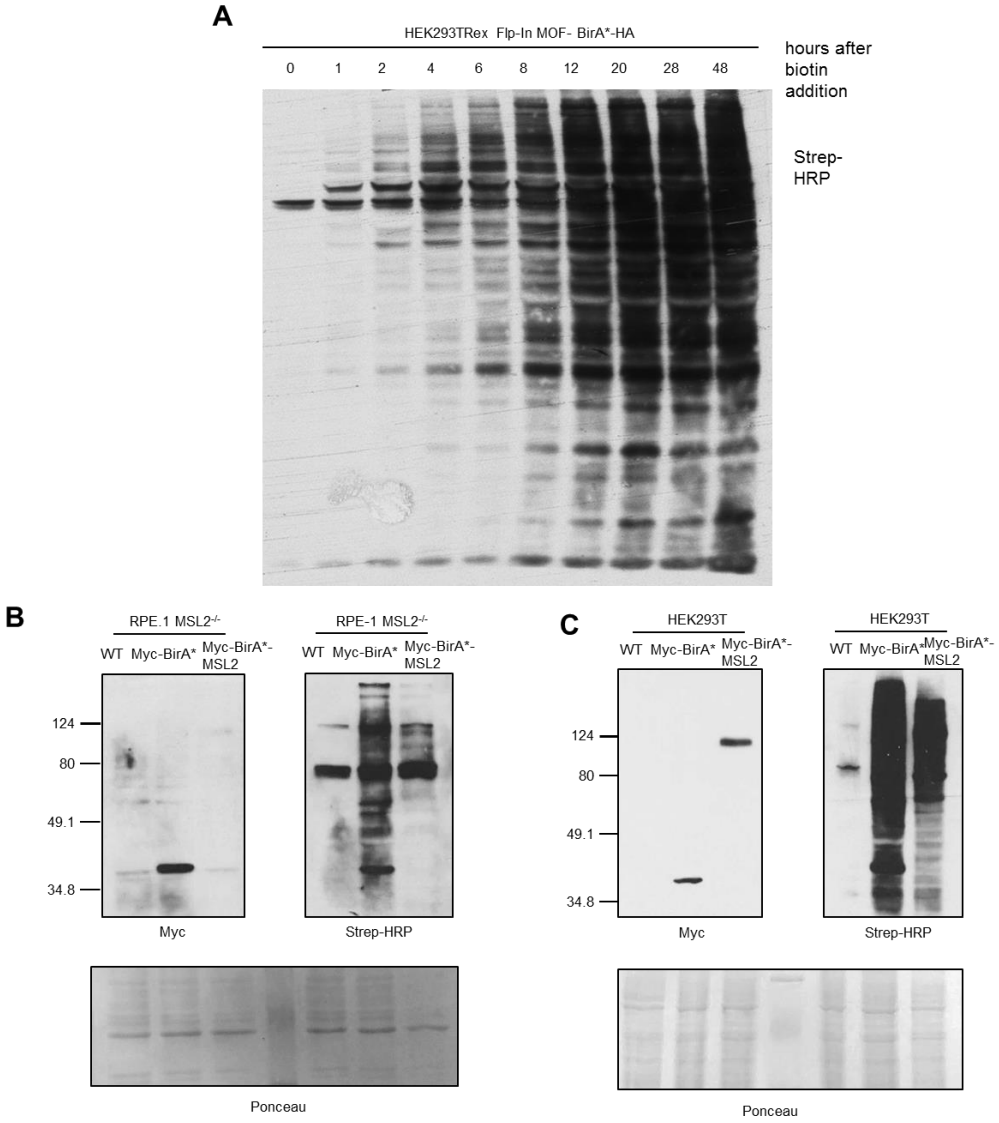

Figure 5.2: Test biotinylation and expression of Myc-BirA* and Myc-BirA-MSL2 fusion proteins. A) Biotinylation timecourse experiment. 50µM biotin was added to the culture media of HEK293TRex Flp-In MOF-BirA*-HA cells and at the indicated timepoits cells were harvested and whole cell protein extracts were subjected to western bolt analysis. For biotinylated protein visualization HRP conjugated streptavidin was used. The experiment was performed by Karen Lane. B-C) RPE-1 *MSL2*$^{-/-}$ and HEK293T cells were transiently transfected with Myc-BirA* and Myc-BirA*-MSL2 and probed for biotinylation and protein expression using antibody against Myc tag.

To determine the timing for sufficient biotinylation in BirA* expressing cells a timecourse experiment was set up. Cells were harvested at the indicated hours after

the addition of biotin and whole cellular protein extracts were probed with HRP conjugated streptavidin (Figure 5.2 A). This experiment was carried out by Karen Lane in a MOF-BorA*-HA expressing HEK293TRex Flp-In cell line. For the proposed modified BioID experiment the time between 8 and 12h was chosen to provide sufficient time for labelling. All further biotinylation experiments were carried out with cells cultured in biotin supplemented media for 10h.

A Myc-BirA*-MSL2 construct was generated using pcDNA3.1 as backbone. To test the expression of the construct and the efficiency of biotinylation, the Myc-BirA*-MSL2 and the control Myc-BirA* only constructs were transiently transfected into RPE-1 *MSL2*$^{-/-}$ and HEK293T cells. To facilitate biotinylation 100 mM biotin was added to the culture media10h prior to harvest. The results show that both fusion constructs express in cells and BirA* is able to biotinylate potential interactors (Figure 5.2 B, C). The RPE-1 *MSL2*$^{-/-}$ cell line was planned to be used instead of the original HEK293TRex Flp-In cell line to avoid the interference of endogenous MSL2. However, test expression of the BirA*-MSL2 construct showed very low protein levels in this cell line (Figure 5.2 B) so the assay was changed to use HEK293T cells instead (Figure 5.2 C).

5.1.1.2. Optimization of modified BioID pulldown

To perform a test pulldown assay HEK293T cells were co-transfected with Myc-BirA*-MSL2 or Myc-BirA* (control) and His-Ub, cultured for 24h and the culture media was supplemented with biotin (Figure 5.3 A). Protein lysates were then subjected to immunoprecipitation using streptavidin conjugated and nickel beads. The nickel-histidine IP was followed by a streptavidin IP the following day. To see the efficiency of the pulldown western blot analysis was carried out probing against ubiquitylated proteins and biotinylated molecules.

Since it has been shown that MSL2 can ubiquitylate MOF in *Drosophila* in *in vitro* conditions (Schunter et al., 2017) the efficiency of the assay was also tested by probing against MOF (Figure 5.3 B). Immunoprecipitation of histidine tagged molecules was efficient indicated by the lack of signal in the flowthrough lanes, but the streptavidin IP still contained uncaptured biotinylated molecules (Figure 5.3 C) so for the final analysis the amount of beads and the incubation time was increased (4h). Western blot against MOF shows enrichment in the histidine pulldown and to a

lesser extent in the streptavidin IP possibly due to the lower immunoprecipitation efficiency.

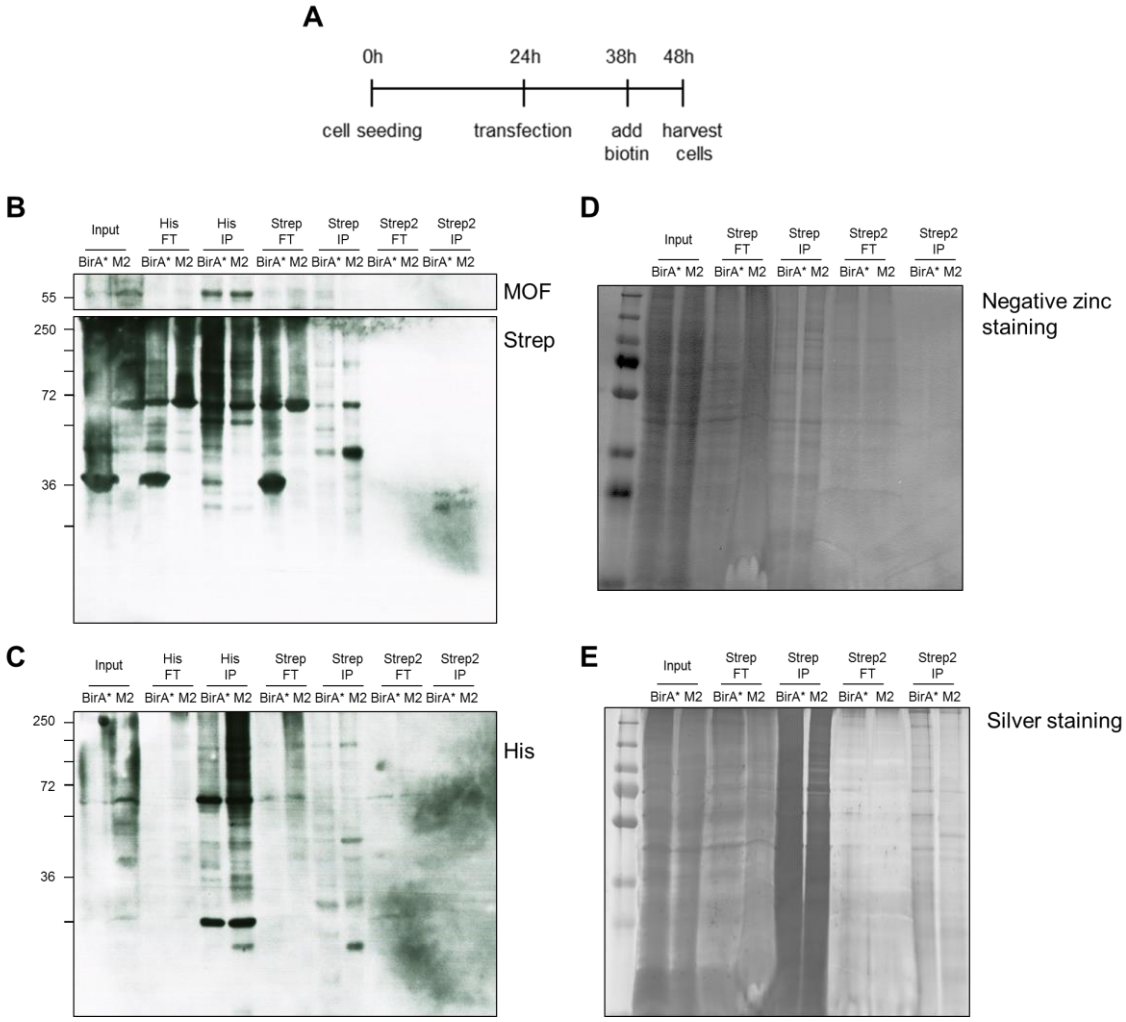

Figure 5.3: Pulldown assay for biotinylated and ubiquitylated molecules. A) Schematic representation of the assay setup. Cell were seeded 24h prior transfection to reach optimal confluency the next day. 14h after transfection the culture media was completed with 100mM biotin. Cells were harvested 10h after biotin addition. B-C) Western blot analysis of BioID immunoprecipitation. Whole cell protein extracts were divided into two fractions and pulldown assays were performed using either nickel beads to capture histidine tagged (ubiquitylated substrates) proteins or streptavidin beads to capture biotinylated substrates (interactors). The histidine pulldown was then followed by a second immunoprecipitation using streptavidin beads to capture ubiquitylated potential interactors. HRP conjugated streptavidin and histidine antibodies were used to visualise pulldown efficiency. Western blot was also probed for MOF as potential interactor. D-E) Visualization of immunoprecipitated proteins using negative zinc staining and silver staining for higher sensitivity. His FT/His IP: immunoprecipitation performed using nickel beads for His-Ub pulldown on whole cell protein extracts, Strep FT/ Strep IP: immunoprecipitation performed using streptavidin beads for biotinylated protein pulldown on whole cell protein extracts, Strep2 FT/Strep2 IP: immunoprecipitation performed using streptavidin beads for biotinylated protein pulldown on His IP selected protein extracts.

While there was visible amounts of protein in the histidine IP, the subsequent pulldown did not contain enough molecules for detection using western blot. To overcome this limitation in detection, immunoprecipitated proteins were also visualised using negative zinc staining which revealed some proteins in the flowthrough of the second IP performed on ubiquitylated proteins (Strep2 FT) (Figure 5.3 D). However, the staining was still not sensitive enough to visualise the final IP products so silver staining was also performed on the same SDS-PAGE gel. This method was able to detect ubiquitylated and biotinylated molecules in the Strep2 IP (Figure 5.3 E). Based on these results, for the final assay further adjustments were made and the amount of input material was doubled for the histidine-streptavidin IP.

The pulldown was performed in two replicates for each sample and a small amount of protein extract was silver stained for a final control. Immunoprecipitated protein extracts were then sent for mass spectrometry analysis to the University of Bristol Proteomics Facility, Bristol to Dr. Kate Heesom.

5.2. Computational analysis of the modified BioID data

Following the mass spectrometry analysis the obtained lists of potential interactors and substrates with their respective controls were further analysed. Firstly the two biological replicates for each condition were merged into a single file using Galaxy version 17.09 (Galaxy Project) online tool. The peptide spectrum match values corresponding to the total number of identified peptide sequences of the captured proteins were then averaged.

To exclude background contamination from the results beside the Myc-BirA* control samples external controls were also included as there are false positive interactions which usually present in every affinity purification dataset (for example proteins interacting with the epitope tag, the solid-phase support or the affinity reagent). For this the CRAPome (Contaminant Repository for Affinity Purification Mass Spectrometry Data) online tool was used in two rounds (Mellacheruvu et al., 2013).

During the CRAPome analysis a computational probability scoring was also implemented using SAINTexpress (Significance Analysis of INTeractome) software (Teo et al., 2014). SAINTexpress analysis is an objective statistical method

providing a probability score based on the likelihood of true interactions captured via co-immunoprecipitation. The CRAPome and SAINTexpress analysis was performed separately on the two datasets (potential MSL2 interactors and potential MSL2 substrates). Firstly the two datasets were analysed using the Myc-BirA* control alone. After this primary selection a second round of CRAPome analysis including 13 external BirA* controls from the CRAPome database were used on the already selected datasets.

As quality control known MSL2 interacors were searched and identified in the dataset such as MOF and PAF1. The filtered protein lists were then further analysed and true interactors were considered with a false discovery rate (FDR) lower than 0.05. The two datasets were compared using ProHits-viz (Protein High-throughput Solution, Gingras lab, LTRI) online tool (Figure 5.4 A).

Prey specificity was also investigated in the MSL2 interacting protein list using a scatter plot analysis from the same resource (Figure 5.4 B). In this analysis the prey specificity scores are calculated for each bait in the dataset. In this case the fold enrichment score was calculated for each prey gene and the bait it was detected with, relative to the entire dataset using the average spectral counts (the data was not normalised against protein size). This preliminary representation was used to see if known interactors such as MOF (*KAT8*) would be detected to be MSL2 specific. Alongside MOF three potential interactors NSL1 (*KANSL1*), CDK2 (*CDK2*) and DGCR14 (*DGCR14*) were highlighted as well. The data analysis showed that while MOF and NSL1 showed infinite specificity CDK2 and DGCR14 were below treshold and might not be specific enough. This result shows that utilising strict gating some true interactors might get excluded from the analysis but it also gives higher confidence value to the genes labelled with infinite specificity.

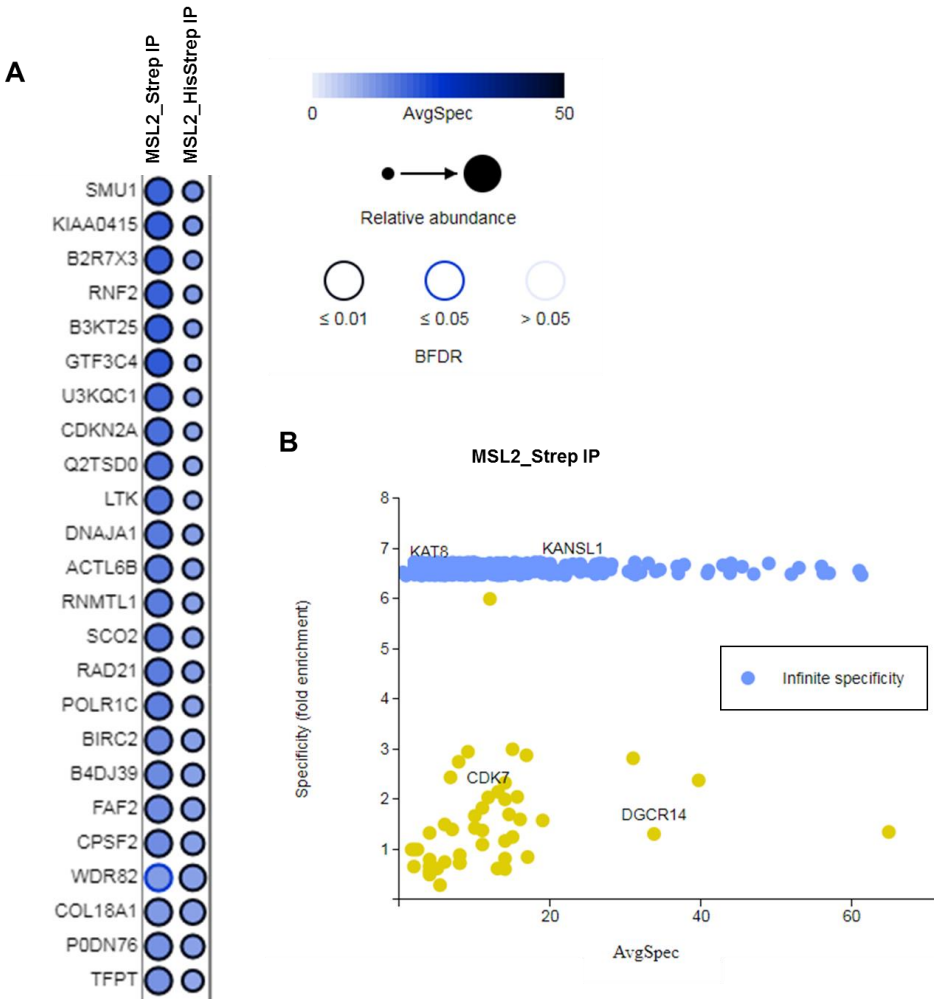

Figure 5.4:Dotplot and scatterplot of MSL2 interacting proteins and ubiquitylated MSL2 interacting proteins. A) Dotplot visualization of protein abundance in the MSL2 interactome and the ubiquitylated MSL2 interacting protein lists. The spectral count was visualised by colour intensity using light blue for low and dark for high number of spectral counts. The size of the dots for each genes (corresponding to a protein) corresponds to their relative abundance, while the outline colour corresponds to their false discovery rate. B) Scatter plot of MSL2 interacting proteins showing specificity scores for each identified protein are plotted relative to their abundance (fold change). Only genes that pass the specified filter were plotted. Blue dots indicate genes with infinit specificity.

With this method altogether 972 hits were identified as potential MSL2 interactors or substrates. However, there was no available additional control in the CRAPome database for nickel coupled agarose beads or histidine affinity tag. The two lists of potential MSL2 interactomes were then further filtered for the most common contaminants such as keratin and the proteins identified using the Most frequently detected proteins(reduced) CRAPome reference list (www.crapome.org/?q=suppdata) were manually removed from the dataset. To overcome this potentially bias the list of captured proteins from the MSL2 streptavidin IP (MSL2_Strep, MSL2) was

plotted against the MSL2 histidine-streptavidin IP (MSL2_HisStrep, MSL2 Ub) and hits not present in the streptavidin IP were removed from the histidine-streptavidin IP. Using this selection method 296 proteins were identified in the MSL2_Strep IP, while from the MSL2_HisStrep IP 351 proteins were found. From these lists 15 protein hits were identified as common for both datasets using BioVenn diagram online tool (Hulsen et al., 2008) (Figure 5.5). The lack of additional controls might have contributed to the high number of identified MSL2 interacting ubiquitylated genes which were not found in the MSL2 interacting genes dataset. These were considered as contaminants and they were excluded from further analysis involving potentially interesting MSL2 substrate selection.

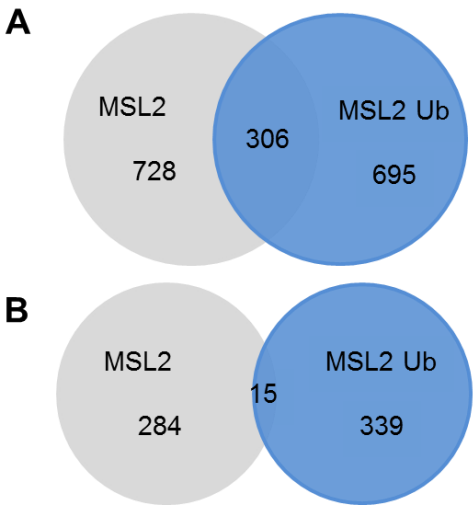

C

Prey	PreyGene	AvgSpec	ctrlCounts	FoldChange
Q5THJ4	VPS13D	48	0|0|1|0|0|0|0|0|0|0|0|0	480
A0A024RA92	GLI3	23	0|0|0|0|0|0|0|0|0|0|0|0	230
S4R2X9	MBIP	20	0|0|0|0|0|0|0|0|0|0|0|0	200
B4DDX2	B4DDX2	12	0|0|0|0|0|0|0|0|0|0|0|0	120
Q2TSD0	Q2TSD0	10	0|0|0|0|0|0|0|0|0|0|0|0	100
Q86Y79	PTRH1	8	0|0|0|0|0|0|0|0|0|0|0|0	80
B7Z6D1	B7Z6D1	7	0|0|0|0|0|0|0|0|0|0|0|0	70
F8VV56	CD63	6	0|0|0|0|0|0|0|0|0|0|0|0	60
B3KUE6	B3KUE6	5	0|0|0|0|0|0|0|0|0|0|0|0	50
L0R5A1	CSF2RB	4	0|0|0|0|0|0|0|0|0|0|0|0	40
Q96H79	ZC3HAV1L	3	0|0|0|0|0|0|0|0|0|0|0|0	30
D6RAD4	CDK7	6	0|3|0|0|0|0|0|0|0|0|0|0	20
Q5QP19	NFS1	8	0|0|0|0|0|0|5|0|0|0|0|0	16
E7EQY4	MTA3	14	1|2|3|4|5|3|2|0|4|3|4|3|5	3,89
P52655	GTF2A1	4	4|3|1|0|0|0|0|1|2|1|1|1	2,86

Figure 5.5: MSL2 interacting proteins and ubiquitylated MSL2 interacting proteins. A) Potential MSL2 interactors and B) potential ubiquitylated MSL2 interactors before and after removal of common contaminants and selection using CRAPome and SAINT analysis. C) Profile of common interactors in the MSL2 interactor dataset.

An example of the top 30 proteins identified in the streptavidin IP arranged by fold change are shown in Table 5.1. (Full list of interacting proteins is shown in Table A 1.)

Table 5.1: Filtered MSL2 interactors

Prey	PreyGene	AvgSpec	ctrlCounts	FoldChange
A6NGQ3	*OBSCN*	93	0|0|0|0|0|0|0|0|0|0|1|0	930
D3DSW5	*GPR124*	74	0|0|0|0|0|0|0|0|0|0|0|0	740
Q5THJ4	*VPS13D*	65	0|0|1|0|0|0|0|0|0|0|0|0	650
C0JYZ1	*DNAH11*	61	0|0|0|0|0|0|0|0|0|0|0|0	610
Q5XPV6	*Q5XPV6*	53	0|0|0|0|0|0|0|0|0|0|0|0	530
Q9UL03	*INTS6*	47	0|0|0|0|0|0|0|0|0|0|0|0	470
J3KNF5	*J3KNF5*	44	0|0|0|0|0|0|0|0|0|0|0|0	440
B8XCX8	*B8XCX8*	44	0|0|0|0|0|0|0|0|0|0|0|0	440
J9R021	*eIF3a*	37	0|0|0|0|0|0|0|0|0|0|0|0	370
B4DN41	*B4DN41*	34	0|0|0|0|0|0|0|0|0|0|0|0	340
Q6N022	*TENM4*	32	0|0|0|0|0|0|0|0|0|0|0|0	320
B4DN49	*B4DN49*	31	0|0|0|0|0|0|0|0|0|0|0|0	310
F4ZW65	*NF90b*	31	0|0|0|0|0|0|0|0|0|0|0|0	310
Q8WWQ8	*STAB2*	31	0|0|0|0|0|0|0|0|0|0|0|0	310
Q4LE58	*EIF4G1 variant*	28	0|0|0|0|0|0|0|0|0|0|0|0	280
A0A1S5UZ39	*HBA2*	27	0|0|0|0|0|0|0|0|0|0|0|0	270
Q4ZHG4	*FNDC1*	27	0|0|0|0|0|0|0|0|0|0|0|0	270
A0A0X1KG71	*NELFB*	27	0|0|0|0|0|0|0|0|0|0|0|0	270
Q07283	*TCHH*	27	0|0|0|0|0|0|0|0|0|0|0|0	270
B4DJ44	*B4DJ44*	26	0|0|0|0|0|0|0|0|0|0|0|0	260
Q9C0A1	*ZFHX2*	25	0|0|0|0|0|0|0|0|0|0|0|0	250
A8K5V5	*A8K5V5*	24	0|0|0|0|0|0|0|0|0|0|0|0	240
Q9P227	*ARHGAP23*	24	0|0|0|0|0|0|0|0|0|0|0|0	240
B7Z388	*B7Z388*	24	0|0|0|0|0|0|0|0|0|0|0|0	240
A0A0C4DGG8	*A0A0C4DGG8*	23	0|0|0|0|0|0|0|0|0|0|0|0	230
A0A0G2JQF5	*KANSL1*	23	0|0|0|0|0|0|0|0|0|0|0|0	230
Q6ZRS2	*SRCAP*	44	0|0|0|0|0|0|0|0|1|0|0|1	220
Q5K651	*SAMD9*	22	0|0|0|0|0|0|0|0|0|0|0|0	220
A8K2F4	*A8K2F4*	22	0|0|0|0|0|0|0|0|0|0|0|0	220
Q9NVW2	*RLIM*	22	0|0|0|0|0|0|0|0|0|0|0|0	220

Prey: Uniprot accession number, PreyGene: Corresponding protein coding gene name, AvgSpec: Average spectral counts representing the number of peptides detected in the analysis, ctrlCounts: Control counts representing the number of peptides detected in each control separately, Fold change: Protein enrichment fold change compared to the controls.

An example of the top 30 proteins identified in the histidine-streptavidin IP arranged by fold change are shown in Table 5.2. (Full list of ubiquitylated interacting proteins is shown in Table A 2.)

Table 5.2: Filtered ubiquitylated MSL2 interactors

Prey	PreyGene	AvgSpec	ctrlCounts	FoldChange
Q5THJ4	VPS13D	48	0|0|1|0|0|0|0|0|0|0|0|0	480
Q8TB01	Q8TB01	39	0|0|0|0|0|0|0|0|0|0|0|0	390
Q02224	CENPE	37	0|0|0|0|0|0|0|0|0|0|0|0	370
Q9NR48	ASH1L	32	0|0|0|0|0|0|0|0|0|0|0|0	320
B7Z8Z6	B7Z8Z6	32	0|0|0|0|0|0|0|0|0|0|0|0	320
A0A0C4DH75	MPP2	31	0|0|0|0|0|0|0|0|0|0|0|0	310
A0A0G2JPP5	SCRIB	30	0|0|0|0|0|0|0|0|0|0|0|0	300
B4DQX5	B4DQX5	28	0|0|0|0|0|0|0|0|0|0|0|0	280
B2RAH5	B2RAH5	28	0|0|0|0|0|0|0|0|0|0|0|0	280
Q9H0D2	ZNF541	27	0|0|0|0|0|0|0|0|0|0|0|0	270
A0A1K0GXZ1	GLNC1	26	0|0|0|0|0|0|0|0|0|0|0|0	260
Q58EX2	SDK2	26	0|0|0|0|0|0|0|0|0|0|0|0	260
B7Z2B5	B7Z2B5	25	0|0|0|0|0|0|0|0|0|0|0|0	250
Q96RY7	IFT140	23	0|0|0|0|0|0|0|0|0|0|0|0	230
B4E2K0	B4E2K0	23	0|0|0|0|0|0|0|0|0|0|0|0	230
A8K9P0	A8K9P0	23	0|0|0|0|0|0|0|0|0|0|0|0	230
A0A024RA92	GLI3	23	0|0|0|0|0|0|0|0|0|0|0|0	230
B4DWL1	B4DWL1	23	0|0|0|0|0|0|0|0|0|0|0|0	230
A0A087WSZ2	ACTN3	22	0|0|0|0|0|0|0|0|0|0|0|0	220
A9UF07	BCR/ABL fusion	22	0|0|0|0|0|0|0|0|0|0|0|0	220
O14924	RGS12	22	0|0|0|0|0|0|0|0|0|0|0|0	220
B1ALM3	CACNA1S	21	0|0|0|0|0|0|0|0|0|0|0|0	210
E5RJH9	SQLE	21	0|0|0|0|0|0|0|0|0|0|0|0	210
B3KTJ9	B3KTJ9	21	0|0|0|0|0|0|0|0|0|0|0|0	210
S4R2X9	S4R2X9	20	0|0|0|0|0|0|0|0|0|0|0|0	200
B3KRM2	B3KRM2	20	0|0|0|0|0|0|0|0|0|0|0|0	200
B4DSH1	B4DSH1	20	0|0|0|0|0|0|0|0|0|0|0|0	200
B7Z2Z8	B7Z2Z8	19	0|0|0|0|0|0|0|0|0|0|0|0	190
O00512	BCL9	18	0|0|0|0|0|0|0|0|0|0|0|0	180
B2RTS4	B2RTS4	18	0|0|0|0|0|0|0|0|0|0|0|0	180

Prey: Uniprot accession number, PreyGene: Corresponding protein coding gene name, AvgSpec: Average spectral counts representing the number of peptides detected in the analysis, ctrlCounts: Control counts representing the number of peptides detected in each control separately, Fold change: Protein enrichment fold change compared to the controls.

5.2.1. Gene ontology analysis

To identify biological functions related to MSL2 a gene ontology analysis was performed using DAVID (Database for Annotation, Visualization and Integrated Discovery) online database (Huang da et al., 2009b, Huang da et al., 2009a). Proteins potentially interacting with MSL2 were uploaded into the database and grouped into biological processes using the GOTERM_DIRECT classification. As the dataset proved to be quite rich only functional clusters with a P value smaller than 5E-2 (0.05) were displayed in (Table 5.3).

Table 5.3: Gene ontology enrichment for biological processes

Term	Count	%	P-Value	Fold Enrichment
nucleotide-excision repair, DNA gap filling	5	2.9	6.0E-5	22.9
translation	11	6.4	1.0E-4	4.8
transcription, DNA-templated	35	20.5	1.2E-4	2.0
snRNA transcription from RNA polymerase II promoter	6	3.5	4.3E-4	9.4
transcription-coupled nucleotide-excision repair	6	3.5	5.5E-4	8.9
nuclear-transcribed mRNA catabolic process, nonsense-mediated decay	7	4.1	7.5E-4	6.5
DNA repair (Lai et al., 2013)	9	5.3	1.4E-3	4.2
translational initiation	7	4.1	1.5E-3	5.6
SRP-dependent cotranslational protein targeting to membrane	6	3.5	1.6E-3	7.0
negative regulation of transcription, DNA-templated	13	7.6	2.0E-3	2.9
transcription from RNA polymerase II promoter	13	7.6	2.5E-3	2.8
transcription initiation from RNA polymerase II promoter	7	4.1	2.6E-3	5.1
viral transcription (Gao et al., 2017)	6	3.5	3.5E-3	5.9
DNA damage response, detection of DNA damage (Lai et al., 2013)	4	2.3	4.2E-3	12.2
white fat cell differentiation	3	1.8	5.9E-3	25.3
DNA recombination	5	2.9	6.8E-3	6.6
histone H3 acetylation	4	2.3	6.9E-3	10.2
transcription elongation from RNA polymerase II promoter	5	2.9	7.7E-3	6.4
DNA-dependent DNA replication	3	1.8	1.1E-2	18.3
error-free translesion synthesis	3	1.8	1.3E-2	17.3

Term	Count	%	P-Value	Fold Enrichment
error-prone translesion synthesis	3	1.8	1.3E-2	17.3
rRNA processing	7	4.1	1.3E-2	3.6
negative regulation of transcription from RNA polymerase II promoter	14	8.2	1.4E-2	2.1
regulation of mRNA stability	5	2.9	1.4E-2	5.3
regulation of transcription, DNA-templated	23	13.5	1.7E-2	1.7
base-excision repair, DNA ligation	2	1.2	2.7E-2	73.2
circadian rhythm	4	2.3	3.1E-2	5.9
histone acetylation (Smith et al., 2005)	3	1.8	3.8E-2	9.7
translesion synthesis	3	1.8	4.2E-2	9.1
nucleotide-excision repair, DNA incision, 5'-to lesion	3	1.8	4.4E-2	8.9
positive regulation of transcription, DNA-templated (Smith et al., 2005)	10	5.8	4.5E-2	2.1
nucleotide-excision repair, DNA incision	3	1.8	4.6E-2	8.7

Known biological processes related to MSL2 were highlighted in pink. Count: Proteins identified, %: percentage of proteins within the category compared to the total number of proteins identified.

There is very little information on what biological processes MSL2 is involved in thus the gene ontology clustering performed provided an extensive list of interesting results on where MSL2 might also play a role. For example nucleotide excision repair, translation and replication were one of the lowest P-value associated functions.

Molecular functions related to the MSL2 interactome were also analysed and showed mainly known MSL2 or MSL complex related functions (highlighted in pink) such as protein, chromatin and DNA binding (Table 5.4).

Table 5.4: Functional annotation of MSL2 interacting proteins

Term	Count	%	P-Value	Fold Enrichment
protein binding	120	69.8	1.7E-8	1.4
poly(A) RNA binding	27	15.7	2.7E-5	2.5
transcription coactivator activity	10	5.8	6.6E-4	4.2
TBP-class protein binding	4	2.3	1.0E-3	19.7
structural constituent of ribosome	9	5.2	1.4E-3	4.2
chromatin binding	12	7.0	1.4E-3	3.2
damaged DNA binding	5	2.9	3.1E-3	8.2

Term	Count	%	P-Value	Fold Enrichment
enzyme binding	10	5.8	4.9E-3	3.1
RNA binding	13	7.6	6.6E-3	2.5
nucleotide binding	9	5.2	1.9E-2	2.7
thyroid hormone receptor binding	3	1.7	2.7E-2	11.5
protein C-terminus binding	6	3.5	3.1E-2	3.4
ATPase binding	4	2.3	3.4E-2	5.6
RNA polymerase II transcription cofactor activity	3	1.7	4.7E-2	8.6
estrogen receptor binding	3	1.7	4.9E-2	8.4
DNA binding	24	14.0	5.0E-2	1.5

Known biological processes related to MSL2 were highlighted in pink. Count: Proteins identified, %: percentage of proteins within the category compared to the total number of proteis identified.

5.2.1. Potential MSL2 interacting proteins involved in different biological processes

Some known MSL2 related biological processes were expanded and the list of interactors were further analysed in more detail.

As known MSL function H4K16ac related protein hits were investigated (Table 5.5). Interestingly, other than MOF (*KAT8* gene) two members of the NSL complex were also present as interactors. It is known that MOF is a subunit in both the MSL and the NSL complexes, but it has not been reported yet that other MSL proteins would be present in the NSL complex as well (Cai et al., 2010).

Table 5.5: MSL2 interacting proteins in relation to H4K16 acetylation

UNIPROT_ACCESSION	GENE NAME
A0A0G2JQF5	KAT8 regulatory NSL complex subunit 1(*KANSL1*)
Q9H7Z6	lysine acetyltransferase 8(*KAT8*)

Known MSL2 interactors were highlighted in pink.

In DNA damage response (Table 5.6) an interesting protein coding gene *CDK2* was found. CDK2 plays important role in DNA damage response by phosphorylating BRCA2 at S3291 which prevents its interaction with Rad51 and results in HR inhibition in a cell-cycle-dependent manner (Muller-Tidow et al., 2004, Esashi et al., 2005). It has also shown to associate with Mre11 and facilitates phosphorylation of

CtIP thus restricting the HR pathway to phases of the cell cycle when a repair template is available (Buis et al., 2012).

Two other potential interactor DNA polymerase beta is involved in base excision repair (Sobol and Wilson, 2001) while PNKP plays important role in both NHEJ and base excision repair pathways (Jilani et al., 1999, Davis and Chen, 2013).

However, as the experiment did not involve DNA damage initiation the captured protein list is only indicative and possibly represents only a fraction of DDR related interactions.

Table 5.6: Captured interactors in DNA damage response and DNA repair

UNIPROT_ACCESSION	GENE NAME
P06746	DNA polymerase beta(POLB)
Q96MG7	NSE3 homolog, SMC5-SMC6 complex component(NSMCE3)
P0C1Z6	TCF3 fusion partner(TFPT)
P24941	cyclin dependent kinase 2(CDK2)
E5RGZ9	endonuclease V(ENDOV)
Q6P4R8	nuclear factor related to kappaB binding protein(NFRKB)
F6M2K3	nuclear receptor coactivator 6(NCOA6)
M0QYH2	polynucleotide kinase 3'-phosphatase(PNKP)
P40937	replication factor C subunit 5(RFC5)

Common hits with DNA replication were highlighted in blue.

While there was some overlap between potential interactor hits related to DNA replication and DNA damage response, two replication specific proteins (PCNA, DUT) were captured as well (Table 5.7).

Table 5.7: Captured interactors in DNA replication

UNIPROT_ACCESSION	GENE NAME
P24941	cyclin dependent kinase 2(CDK2)
P33316	deoxyuridine triphosphatase(DUT)
F6M2K3	nuclear receptor coactivator 6(NCOA6)
P12004	proliferating cell nuclear antigen(PCNA)
P40937	replication factor C subunit 5(RFC5)

Common hits with DNA damage response and DNA repair were highlighted in blue.

PCNA is a DNA clamp which serves as loading platform for DNA pol δ/ε and other replication proteins and moves along both leading and lagging strands (Moldovan et al., 2007, Strzalka and Ziemienowicz, 2011). It is also known to be involved in post-

replication repair recruiting for example recruitment of translesion (TLS) polymerases (Motegi et al., 2008, Burkovics et al., 2009, Cazzalini et al., 2014). DUT on the other hand plays a more general but very important role in nucleotide metabolism (Gadsden et al., 1993). It produces a thymidine precursor, dUMP, thus decreasing intracellular dUTP concentration which prevents the incorporation of uracil into DNA (Mol et al., 1996, Toth et al., 2007). The increased level of dUTP in cells and incorporation into DNA can lead to DNA fragmentation and cell death (el-Hajj et al., 1988, Pearl and Savva, 1996).

5.2.2. MSL2 and MOF interacting proteins

Since, a BioID experiment with MOF as bait molecule was also set up in the lab by Karen Lane and the obtained results from her assay were compare to the ones received here. Interacting proteins common for both MOF and MSL2 were identified using BioVenn diagram online tool (Hulsen et al., 2008) (Figure 5.6). Ubiquitylated MSL2 interactors were also included in the comparison. These common interactors could potentially reveal MSL complex related functions while non common interacting partners could indicate an MSL independent role in related cellular processes for both proteins.

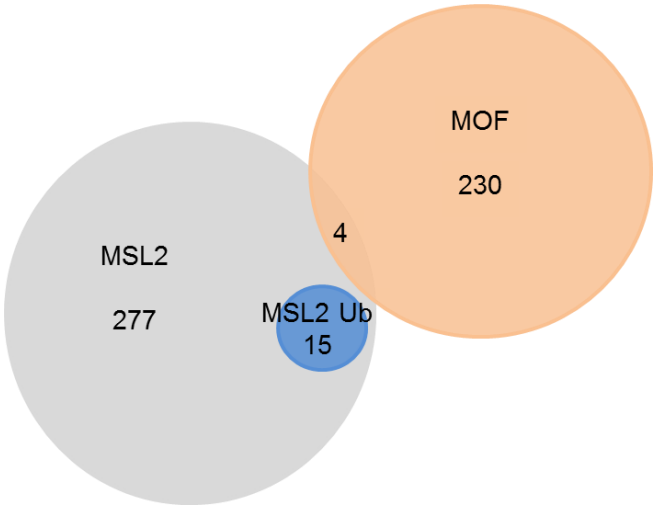

Figure 5.6: MSL2 interacting proteins, ubiquitylated MSL2 interactors and MOF interacting proteins. Potential MSL2 interactors including potential ubiquitylated MSL2 interactors compared to potential MOF interacting proteins.

The analysis revealed that the following genes: *KANSL1* (NSL1), *NCOR1* (NCOR1), *SRCAP* (SRCAP) and *YEATS2* (YEATS2) are common for both datasets and potentially interact with both MSL2 and MOF. All four proteins encoded by these genes are members of different chromatin modifying complexes responsible for either transcriptional activation or repression. The NSL complex (with NSL1 as one of its subunit) is known to be responsible for housekeeping gene expression (Lam et al., 2012) while the SRCAP complex (with SRCAP2 as subunit) is involved in histone H2AZ/H2B dimer exchange for nucleosomal H2A/H2B both acting as transcriptional activators (Monroy et al., 2003, Wong et al., 2007). The Ada2a-containing (ATAC) complex (with YEATS2 as one of its subunit) has a histone acetyltransferase activity known to stimulate nucleosome sliding by the ISWI, SWI-SNF and RSC complexes (Suganuma et al., 2008). On the other hand, the N-Cor complex (with NCOR1 as subunit) is known to promote repressive chromatin structure formation through histone deacetylation (Yoon et al., 2003).

While it is known that MOF can also be part of the NSL complex (NSL1, NSL2, NSL3, MCRS2, MBD-R2 and WDS) (Raja et al., 2010) it is interesting that MSL2 might also interact with NSL1 and could associate with the NSL complex as well. Interaction of MSL2 and MOF with other chromatin modifying complexes and the possibility of these proteins in potentially associating as subunits would be an exciting topic to further investigate.

5.3. Immunoprecipitation of 53BP1 as potential substrate

As a strong MSL2 substrate candidate the potential ubiquitylation of 53BP1 by MSL2 was investigated in an immunoprecipitation assay prior receiving data from the BioID analysis.

A previous computational analysis pointed towards that 53BP1 might be a substrate for MSL2 (Lai et al., 2013). Using the protein sequence surrounding the known H2B ubiquitylation site at lysine 34 a blast analysis was performed and besides H2B, two peptide regions of 53BBP1 were identified as well. Moreover, overexpression experiment using different 53BP1 M domain (the minimal 53BP1 domain required for foci formation) point mutants showed that MSL2 potentially monoubiquitylates 53BP1 (Lai et al., 2013). Also results obtained in this work in the DNA damage

response showed that the loss of MSL2 affects 53BP1 foci and nuclear body formation after IR (Figure 4.9 and Figure 4.10). Based on these findings and to address if MSL2 directly ubiquitylates 53BP1 or whether the observed increased number in foci formation (Figure 4.10) is only the result of an underlying different effect a pulldown assay was performed (Figure 5.7).

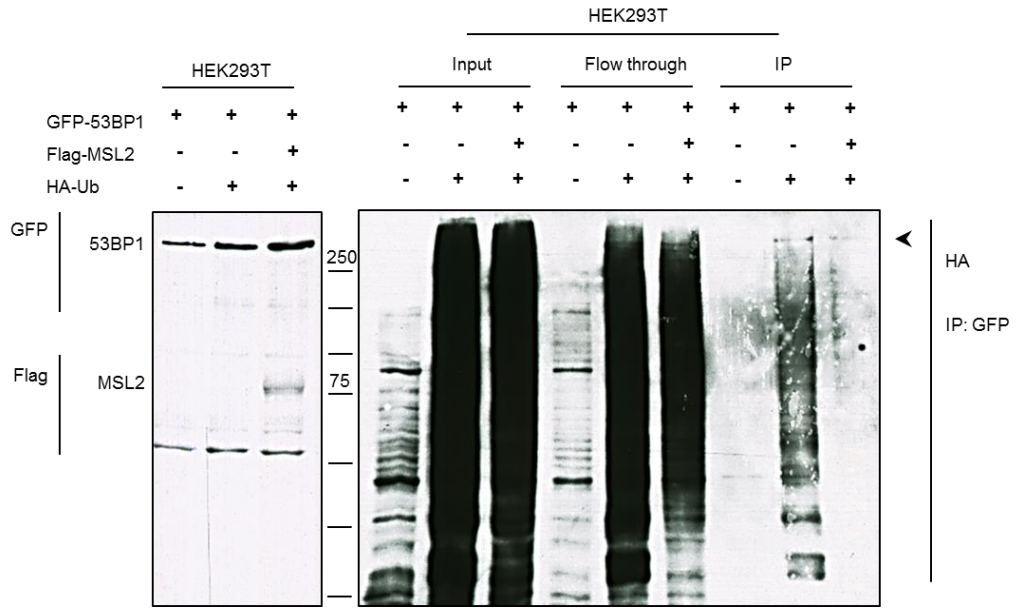

Figure 5.7: Immunoprecipitation assay for ubiquitylated 53BP1. HEK293T cells were transfected with HA-Ubiquitin, Flag-MSL2 and GFP-53BP1 constructs. Immunoprecipitation assay was performed using GFP-trap beads against GFP-53BP1. Ubiquitylated 53BP1 was visualised using antibody against HA tagged ubiquitin. Arrowhead indicates Ubiquitylated 53BP1.

HEK293T cells were co-transfected with GFP-53BP1, HA-Ub and Flag-MSL2 constructs. After 24h protein extracts were subjected to immunoprecipitation using GFP-trap magnetic beads. The expression of GFP-53BP1 and Flag-MSL2 was confirmed on a western blot and ubiquitylated proteins were visualised using HA antibody.

Results obtained from repeated experiments show that the level of ubiquitylated 53BP1 decreased after the addition of MSL2. This observation could suggest that MSL2 possibly affects the ubiquitylated status of 53BP1 but whether it is an indirect or direct effect is yet to be determined. It is also possible that MSL2 is able to polyubiquitylate 53BP1 leading to proteasomal degradation or it is not a monoubiquitylated substrate for MSL2. However, due to the limitations of the assay, a potential interaction between MSL2 and 53BP1 cannot be excluded and other

assays such as proximity ligation are to be performed to identify physical interaction between the two molecules. Results from the modified BioID data showed that 53BP1 is a potential MSL2 interactor while it was not identified as a potential substrate in the ubiquitylated interactor screen. This result supports the hypothesis that MSL2 and 53BP1 are potential interacting partners, but 53BP1 is not a direct substrate of MSL2.

5.4. Discussion

So far MSL2 was indicated to be involved in the DNA damage response and transcriptional activation, but there is little known about its interactors and substrates (Lai et al., 2013, Wu et al., 2014a). The assay performed here will be the first direct analysis to identify MSL2 interacting proteins and substrates.

To address the question of what other cellular processes MSL2 can be involved in, and through what mechanism is it possibly takes part in known pathways a modified BioID immunoprecipitation assay was set up (Figure 5.1). The generation and expression of Myc-BirA*-MSL2 fusion protein construct was successful, but for optimal expression levels the model cell line was changed from RPE-1 *MSL2*$^{-/-}$ to HEK293T cells (Figure 5.2). The BirA* mediated biotinylation was confirmed and optimised and the immunoprecipitation assay was set up successfully (Figure 5.3).

Immunoprecipitated protein extracts were sent for mass spectrometry analysis and computational analysis was performed on the datasets. After several filtering steps including both internal and external controls a number of potential MSL2 interacting proteins were identified (Table 5.1, Table 5.2). Using gene ontology the results were further divided into categories related to certain biological functions (Table 5.3) such as H4K16ac (Table 5.5), DNA damage response and replication (Table 5.6, Table 5.7). Furthermore the results were compared with a MOF BioID interactome dataset generated in the lab by Karen Lane (Figure 5.6). Proteins common for both were identified suggesting that these are potential MSL complex interactors. A few selected hits from these datasets such as NSL1 and CDK2 will be further validated using proximity ligation assay. If time allows MSL2 specific ubiquitylation sites on substrate proteins will also be identified in an *in vitro* ubiquitylation assay using the method described in **Appendix 5 -** In vitro manipulation of the human MSL complex.

As one of the strongest candidates as a potential MSL2 substrate 53BP1 was investigated in an *in vivo* overexpression ubiquitylation assay and show decreased ubiquitylation levels in the presence of MSL2 (Figure 5.7). While this observation needs further investigation, in this experiment MSL2 seemed to negatively affect the ubiquitylation of 53BP1 but whether it is a direct or indirect affect is yet to be determined.

6. Conclusions and future perspectives

In order to study the role of MSL2 and MSL1 in human cells a loss of function approach was chosen. RPE-1 *MSL2*$^{-/-}$ and *MSL1*$^{-/-}$ cell lines were successfully generated using the CRISPR/Cas9 genome editing method and a number of interesting phenotypes were observed.

Histone modifications

Results from this work showed that both MSL2 and MSL1 knock-out cells are viable and proliferate at a similar rate to wild type RPE-1 cells. However, histone modifications involved in the DNA damage response and markers for different chromatin status were perturbed. In particular, decreased H4K16ac and H4K20me2 levels were observed in both the MSL2 and MSL1 knock-out cell lines (Figure 3.7). The levels showed even more decrease in the case of MSL1 depletion possibly due to a more severe effect on MSL complex stability (MSL1 forms the physical core of the MSL complex). Unsurprisingly, MSL related gene expression was also found to be affected, which was in line with what has been reported previously (Wu et al., 2014a). The chromatin binding affinity of MOF also showed a decrease in the knock-out cell lines (Figure 3.8) similar to, but less severe than what was previously reported in *Drosophila* (Lyman et al., 1997, Gu et al., 1998). This is possibly due to the physical disruption of the MSL complex through the removal of MSL1. In addition the loss of MSL2 resulted in a similar disruption in MOF chromatin binding ability as observed in the *MSL1*$^{-/-}$ cells. This observation could imply a role in maintaining the stoichiometry of the complex possibly through its enzymatic activity as reported previously in *Drosophila* (Villa et al., 2012). The obtained results suggest that the disruption of the MSL complex by the removal of a core subunit results in the functional disturbance of MSL related MOF functions.

DNA damage response

The role of the MSL2 and MSL1 knock-outs in DNA damage response, as findings implied previously, was also investigated (Gironella et al., 2009, Lai et al., 2013). Clonogenic survival assay results showed that both *MSL2*$^{-/-}$ and *MSL1*$^{-/-}$ cells are sensitive to γ-irradiation, ultraviolet radiation and to a lesser extent hydroxyurea induced damage (Figure 4.1). These damaging agents mainly activate NHEJ, HR,

and NER repair or induce replication fork stalling. The obtained results could indicate that both MSL2 and MSL1 are involved in different DDR repair pathways while they are not essential to either. To further investigate specific repair pathways *in vivo* NHEJ and HR assays were set up with MSL2 knock-out cells and the results showed decreased repair ability in both cases (Figure 4.3 and Figure 4.4). This preliminary result was studied in more details using IRIF experiments: The foci formation of γH2A.X, as well as three main DDR mediators MDC1, BRCA1 and 53BP1 was followed in a time-course experiment in both knock-out cell lines.

Phosphorylation of H2A.X was found to be decreased in the *MSL1*$^{-/-}$ cell line (Figure 4.6), suggesting that MSL1 might have an effect on ATM mediated phosphorylation. While it was not investigated the observed mild phenotype could be an indirect effect induced by the disruption of the MSL complex and MOF functions (MOF is known to play role in ATM activation via acetylation (Gupta et al., 2005)). It would be interesting in the future to look at ATM recruitment and activity in the MSL1 knock-out cell line in response to γ-irradiation to analyse the potential underlying mechanism behind the decrease in γH2A.X foci formation.

In case of MDC1 an increased level of foci formation was observed at early timepoints in the MSL1 knock-out cells (Figure 4.7). The recruitment of MDC1 at damage sites is partially dependent on γH2A.X (Stewart et al., 2003, Stucki et al., 2005). This could suggest that maybe a lower level of H2A.X phosphorylation observed in the loss of MSL1 can affect MDC1 foci formation. The MSL2 knock-out cells showed a different phenotype with a delay in foci recovery at 1h after IR. This persistent foci formation is probably related to a different mechanism and might indicates a defect in MDC1 dissociation from the repair sites or a temporarily slowed repair. In both cases the observed phenotypes were mild and did not affect the overall repair and recovery after damage.

In addition, significant increase in 53BP1 foci formation was observed in both *MSL2*$^{-/-}$ and *MSL1*$^{-/-}$ cells compared to wild type RPE-1 (Figure 4.9). This phenotype could indicate foci formation defect due to the decreased H4K20me2 and H4K16ac in the MSL2 and MSL1 knock-out cell lines (Figure 3.7). H4K16ac prevents 53BP1 binding to H4K20me2 mark, thus its decreased level should promote 53BP1 recruitment to DNA lesions. However, the also decreased H4K20me2 which

promotes 53BP1 recruitment to damage sites is also decreased so it is possible that 53BP1 is unable to properly localise and forms more dispersed foci in the nucleus.

Nuclear bodies and replication

Further investigation showed that the number of 53BP1 nuclear bodies also increased in response to IR (Figure 4.10). These elements are thought to shield unrepaired or underreplicated DNA from the previous cell cycle (Lukas et al., 2011). Based on these observations it was speculated that the loss of MSL2 or MSL1 affects replication or replication related damage repair which might be carried over to the next cycle for repair causing an increase in 53BP1 nuclear body formation.

The possibility of a potential effect from DNA damage being carried over from an earlier mitosis was studied using immunofluorescence analysis. γH2A.X foci formation was studied in mitotic cells and no change was observed in the number of foci in the MSL2 and MSL1 knock-out cells compared to wild type RPE-1. However, the observed foci appeared to be less sharp and defined in wild type cells but the reason behind it is yet to be investigated.

To examine a potential effect on replication recovery a DNA fibre assay was performed after hydroxyurea induced fork stalling. While no difference in replication restart was observed within the investigated cell types there was a slight decrease in replication termination or fork collapse events in both MSL2 and MSL1 knock-out cell lines (Figure 4.12 A). In addition *MSL2*$^{-/-}$ and *MSL1*$^{-/-}$ cells showed an increase in the number of tracks with new origin firing after HU treatment (Figure 4.12 B). This observation could indicate a defect in recovery compensated by an increase in origin activation. However, further experiments need to be carried out to investigate replication speed as well as distance between firing origins which could give a better insight into how the loss of either MSL2 or MSL1 affects stalled replication recovery.

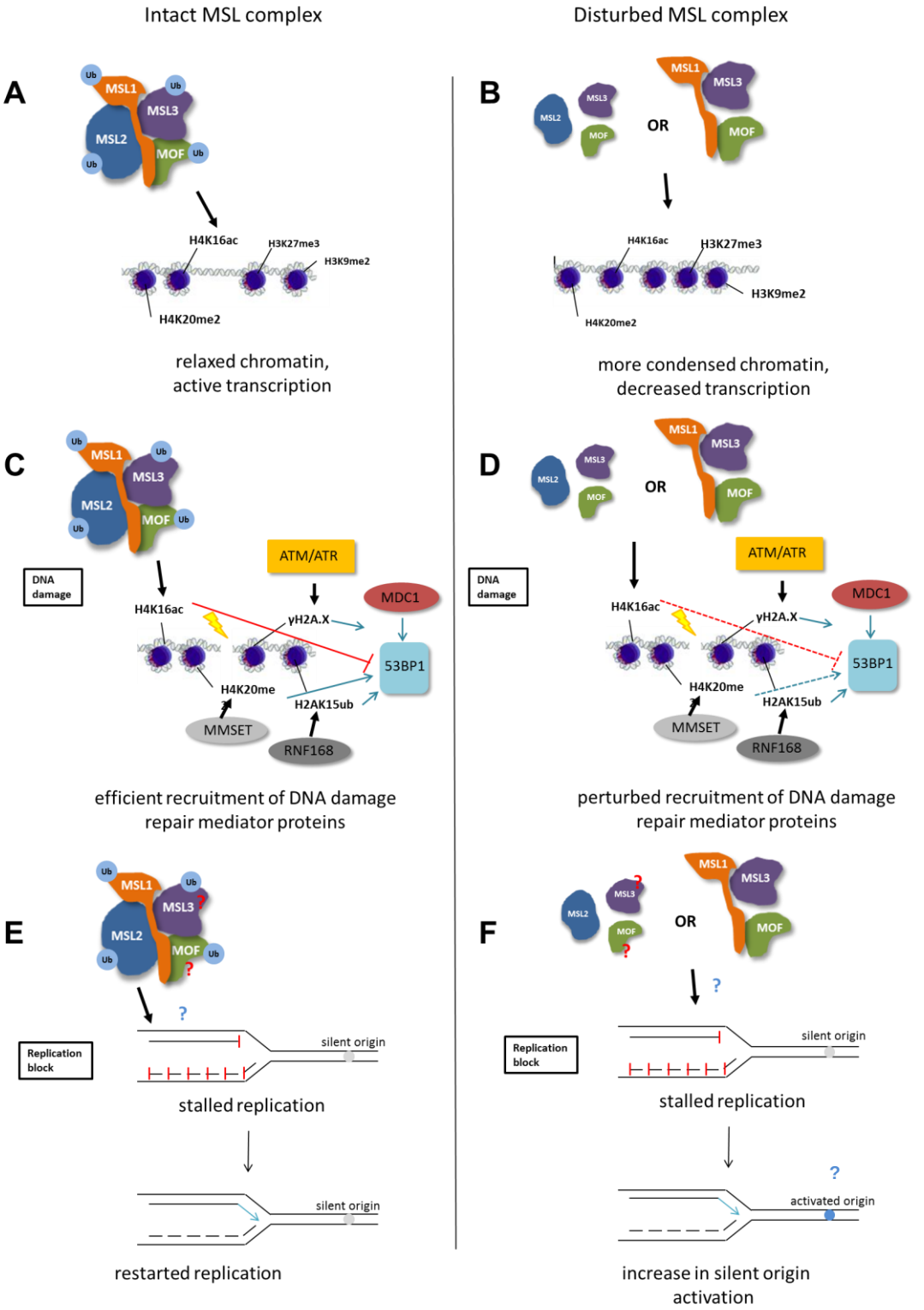

Figure 6.1: Proposed model for the effect of a perturbed MSL complex. A-B) The disruption of the MSL complex by MSL2 or MSL1 knock-out results in decreased H4K16ac and H4K20me2 as well as increase in inactive chromatin markers such as H3K9me2 and H3K27me3. C-D) The loss of MSL2 or MSL1 affects the foci formation of DNA damage repair mediator proteins at early timepoints. E-F) RPE-1 *MSL2*$^{-/-}$ and *MSL1*$^{-/-}$ cells show increased new origin firing after stalled replication, unlike wild type or MOF depleted cells.

Novel substrates and interactors

Also, a modified BioID experiment was set up (Figure 5.1) to identify potential MSL2 interactors and substrates. The results from the mass spectrometry analysis were recently obtained and computational analysis was performed. Other than potential interactors (Table 5.1), potential substrates were also identified (Table 5.2). The resulting dataset was also compared to potential MOF interactors (generated by Karen Lane using classical BioID approach) Figure 5.6). From these interesting proteins such as NSL1 and CHK2 were selected for experimental validation. The result from this work will form the base for future experiments and could indicate other pathways that MSL2 might be involved in.

Summary

Results obtained in this work suggest that the loss of either MSL2 or MSL1 affect the stability of the MSL complex similar to Drosophila and disturb MSL related MOF activity (H4K16ac) resulting in increased heterochromatic marks (H3K9me2 and H3K27me3) and gene inactivation (Figure 6.1 A, B). Disturbed foci formation in different DDR mediator proteins in response to IR could be explained with perturbed histone modifications (Figure 6.1 C, D) while the 53BP1 nuclear body formation is probably a carried on effect from unresolved damage occurred during mitosis. However, this hypothesis needs further investigations. The obtained results suggest that while MSL2 and MSL1 are involved, but not essential for the DNA damage response and a novel role in replication restart is proposed for MSL2 and MSL1 independent of MOF functions (Figure 6.1 E, F).

References

Abdul Rehman, S. A., Kristariyanto, Y. A., Choi, S. Y., Nkosi, P. J., Weidlich, S., Labib, K., Hofmann, K. and Kulathu, Y. (2016). "MINDY-1 Is a Member of an Evolutionarily Conserved and Structurally Distinct New Family of Deubiquitinating Enzymes." *Mol Cell,* 63**,** 146-55.

Agalioti, T., Chen, G. and Thanos, D. (2002). "Deciphering the transcriptional histone acetylation code for a human gene." *Cell,* 111**,** 381-92.

Aguado-Llera, D., Hamidi, T., Domenech, R., Pantoja-Uceda, D., Gironella, M., Santoro, J., Velazquez-Campoy, A., Neira, J. L. and Iovanna, J. L. (2013). "Deciphering the binding between Nupr1 and MSL1 and their DNA-repairing activity." *PLoS One,* 8**,** e78101.

Airenne, K. J., Hu, Y. C., Kost, T. A., Smith, R. H., Kotin, R. M., Ono, C., Matsuura, Y., Wang, S. and Yla-Herttuala, S. (2013). "Baculovirus: an insect-derived vector for diverse gene transfer applications." *Mol Ther,* 21**,** 739-49.

Akhtar, A. and Becker, P. B. (2000). "Activation of transcription through histone H4 acetylation by MOF, an acetyltransferase essential for dosage compensation in Drosophila." *Mol Cell,* 5**,** 367-75.

Alekseyenko, A. A., Peng, S., Larschan, E., Gorchakov, A. A., Lee, O. K., Kharchenko, P., McGrath, S. D., Wang, C. I., Mardis, E. R., Park, P. J. and Kuroda, M. I. (2008). "A sequence motif within chromatin entry sites directs MSL establishment on the Drosophila X chromosome." *Cell,* 134**,** 599-609.

Allfrey, V. G., Faulkner, R. and Mirsky, A. E. (1964). "Acetylation and Methylation of Histones and Their Possible Role in the Regulation of Rna Synthesis." *Proc Natl Acad Sci U S A,* 51**,** 786-94.

Ambroggio, X. I., Rees, D. C. and Deshaies, R. J. (2004). "JAMM: a metalloprotease-like zinc site in the proteasome and signalosome." *PLoS Biol,* 2**,** E2.

Amerik, A. Y. and Hochstrasser, M. (2004). "Mechanism and function of deubiquitinating enzymes." *Biochim Biophys Acta,* 1695**,** 189-207.

An, J., Huang, Y. C., Xu, Q. Z., Zhou, L. J., Shang, Z. F., Huang, B., Wang, Y., Liu, X. D., Wu, D. C. and Zhou, P. K. (2010). "DNA-PKcs plays a dominant role in the regulation of H2AX phosphorylation in response to DNA damage and cell cycle progression." *BMC Mol Biol,* 11**,** 18.

Andres, S. N., Vergnes, A., Ristic, D., Wyman, C., Modesti, M. and Junop, M. (2012). "A human XRCC4-XLF complex bridges DNA." *Nucleic Acids Res,* 40**,** 1868-78.

Andreyeva, E. N., Kolesnikova, T. D., Belyaeva, E. S., Glaser, R. L. and Zhimulev, I. F. (2008). "Local DNA underreplication correlates with accumulation of phosphorylated H2Av in the Drosophila melanogaster polytene chromosomes." *Chromosome Res,* 16**,** 851-62.

Avvakumov, N. and Cote, J. (2007). "The MYST family of histone acetyltransferases and their intimate links to cancer." *Oncogene,* 26**,** 5395-407.

Bakkenist, C. J. and Kastan, M. B. (2003). "DNA damage activates ATM through intermolecular autophosphorylation and dimer dissociation." *Nature,* 421**,** 499-506.

Bannister, A. J. and Kouzarides, T. (1996). "The CBP co-activator is a histone acetyltransferase." *Nature,* 384**,** 641-3.

Bannister, A. J. and Kouzarides, T. (2011). "Regulation of chromatin by histone modifications." *Cell Res,* 21**,** 381-95.

Barsi, J. C., Rajendra, R., Wu, J. I. and Artzt, K. (2005). "Mind bomb1 is a ubiquitin ligase essential for mouse embryonic development and Notch signaling." *Mech Dev,* 122**,** 1106-17.

Barski, A., Cuddapah, S., Cui, K., Roh, T. Y., Schones, D. E., Wang, Z., Wei, G., Chepelev, I. and Zhao, K. (2007). "High-resolution profiling of histone methylations in the human genome." *Cell,* 129**,** 823-37.

Barth, T. K. and Imhof, A. (2010). "Fast signals and slow marks: the dynamics of histone modifications." *Trends Biochem Sci,* 35**,** 618-26.

Bartkiewicz, M., Houghton, A. and Baron, R. (1999). "Leucine zipper-mediated homodimerization of the adaptor protein c-Cbl. A role in c-Cbl's tyrosine phosphorylation and its association with epidermal growth factor receptor." *J Biol Chem,* 274**,** 30887-95.

Beck, D. B., Burton, A., Oda, H., Ziegler-Birling, C., Torres-Padilla, M. E. and Reinberg, D. (2012). "The role of PR-Set7 in replication licensing depends on Suv4-20h." *Genes Dev,* 26**,** 2580-9.

Beckett, D., Kovaleva, E. and Schatz, P. J. (1999). "A minimal peptide substrate in biotin holoenzyme synthetase-catalyzed biotinylation." *Protein Sci,* 8**,** 921-9.

Beisel, C. and Paro, R. (2011). "Silencing chromatin: comparing modes and mechanisms." *Nat Rev Genet,* 12**,** 123-35.

Bekker-Jensen, S., Rendtlew Danielsen, J., Fugger, K., Gromova, I., Nerstedt, A., Lukas, C., Bartek, J., Lukas, J. and Mailand, N. (2010). "HERC2 coordinates ubiquitin-dependent assembly of DNA repair factors on damaged chromosomes." *Nat Cell Biol,* 12**,** 80-6; sup pp 1-12.

Belote, J. M. and Lucchesi, J. C. (1980a). "Control of X chromosome transcription by the maleless gene in Drosophila." *Nature,* 285**,** 573-5.

Belote, J. M. and Lucchesi, J. C. (1980b). "Male-specific lethal mutations of Drosophila melanogaster." *Genetics,* 96**,** 165-86.

Berggard, T., Linse, S. and James, P. (2007). "Methods for the detection and analysis of protein-protein interactions." *Proteomics,* 7**,** 2833-42.

Bergink, S., Salomons, F. A., Hoogstraten, D., Groothuis, T. A., de Waard, H., Wu, J., Yuan, L., Citterio, E., Houtsmuller, A. B., Neefjes, J., Hoeijmakers, J. H., Vermeulen, W. and Dantuma, N. P. (2006). "DNA damage triggers nucleotide excision repair-dependent monoubiquitylation of histone H2A." *Genes Dev,* 20**,** 1343-52.

Berke, S. J., Schmied, F. A., Brunt, E. R., Ellerby, L. M. and Paulson, H. L. (2004). "Caspase-mediated proteolysis of the polyglutamine disease protein ataxin-3." *J Neurochem,* 89**,** 908-18.

Berndsen, C. E. and Wolberger, C. (2014). "New insights into ubiquitin E3 ligase mechanism." *Nat Struct Mol Biol,* 21**,** 301-7.

Bhoj, V. G. and Chen, Z. J. (2009). "Ubiquitylation in innate and adaptive immunity." *Nature,* 458**,** 430-7.

Blanpain, C., Mohrin, M., Sotiropoulou, P. A. and Passegue, E. (2011). "DNA-damage response in tissue-specific and cancer stem cells." *Cell Stem Cell,* 8**,** 16-29.

Blissard, G. W. (1996). "Baculovirus--insect cell interactions." *Cytotechnology,* 20**,** 73-93.

Blow, J. J. and Ge, X. Q. (2009). "A model for DNA replication showing how dormant origins safeguard against replication fork failure." *EMBO Rep,* 10**,** 406-12.

Bohgaki, M., Bohgaki, T., El Ghamrasni, S., Srikumar, T., Maire, G., Panier, S., Fradet-Turcotte, A., Stewart, G. S., Raught, B., Hakem, A. and Hakem, R. (2013). "RNF168 ubiquitylates 53BP1 and controls its response to DNA double-strand breaks." *Proc Natl Acad Sci U S A,* 110**,** 20982-7.

Borden, K. L. and Freemont, P. S. (1996). "The RING finger domain: a recent example of a sequence-structure family." *Curr Opin Struct Biol,* 6**,** 395-401.

Botuyan, M. V., Lee, J., Ward, I. M., Kim, J. E., Thompson, J. R., Chen, J. and Mer, G. (2006). "Structural basis for the methylation state-specific recognition of histone H4-K20 by 53BP1 and Crb2 in DNA repair." *Cell,* 127**,** 1361-73.

Boutros, R., Dozier, C. and Ducommun, B. (2006). "The when and wheres of CDC25 phosphatases." *Curr Opin Cell Biol,* 18**,** 185-91.

Branzei, D. and Szakal, B. (2016). "DNA damage tolerance by recombination: Molecular pathways and DNA structures." *DNA Repair (Amst),* 44**,** 68-75.

Briggs, S. D., Xiao, T., Sun, Z. W., Caldwell, J. A., Shabanowitz, J., Hunt, D. F., Allis, C. D. and Strahl, B. D. (2002). "Gene silencing: trans-histone regulatory pathway in chromatin." *Nature,* 418**,** 498.

Brown, C. E., Lechner, T., Howe, L. and Workman, J. L. (2000). "The many HATs of transcription coactivators." *Trends Biochem Sci,* 25**,** 15-9.

Brzovic, P. S., Rajagopal, P., Hoyt, D. W., King, M. C. and Klevit, R. E. (2001). "Structure of a BRCA1-BARD1 heterodimeric RING-RING complex." *Nat Struct Biol,* 8**,** 833-7.

Buis, J., Stoneham, T., Spehalski, E. and Ferguson, D. O. (2012). "Mre11 regulates CtIP-dependent double-strand break repair by interaction with CDK2." *Nat Struct Mol Biol,* 19**,** 246-52.

Bunting, S. F., Callen, E., Wong, N., Chen, H. T., Polato, F., Gunn, A., Bothmer, A., Feldhahn, N., Fernandez-Capetillo, O., Cao, L., Xu, X., Deng, C. X., Finkel, T., Nussenzweig, M., Stark, J. M. and Nussenzweig, A. (2010). "53BP1 inhibits homologous recombination in Brca1-deficient cells by blocking resection of DNA breaks." *Cell,* 141**,** 243-54.

Burkovics, P., Hajdu, I., Szukacsov, V., Unk, I. and Haracska, L. (2009). "Role of PCNA-dependent stimulation of 3'-phosphodiesterase and 3'-5' exonuclease activities of human Ape2 in repair of oxidative DNA damage." *Nucleic Acids Res,* 37**,** 4247-55.

Burma, S., Chen, B. P., Murphy, M., Kurimasa, A. and Chen, D. J. (2001a). "ATM phosphorylates histone H2AX in response to DNA double-strand breaks." *J Biol Chem,* 276**,** 42462-7.

Burma, S., Chen, B. P., Murphy, M., Kurimasa, A. and Chen, D. J. (2001b). "ATM phosphorylates histone H2AX in response to DNA double-strand breaks." *Journal of Biological Chemistry,* 276**,** 42462-42467.

Burnett, B., Li, F. and Pittman, R. N. (2003). "The polyglutamine neurodegenerative protein ataxin-3 binds polyubiquitylated proteins and has ubiquitin protease activity." *Hum Mol Genet,* 12**,** 3195-205.

Burns, K. E., Baumgart, S., Dorrestein, P. C., Zhai, H., McLafferty, F. W. and Begley, T. P. (2005). "Reconstitution of a new cysteine biosynthetic pathway in Mycobacterium tuberculosis." *J Am Chem Soc,* 127**,** 11602-3.

Buscaino, A., Kocher, T., Kind, J. H., Holz, H., Taipale, M., Wagner, K., Wilm, M. and Akhtar, A. (2003). "MOF-regulated acetylation of MSL-3 in the Drosophila dosage compensation complex." *Mol Cell,* 11**,** 1265-77.

Buscaino, A., Legube, G. and Akhtar, A. (2006). "X-chromosome targeting and dosage compensation are mediated by distinct domains in MSL-3." *EMBO Rep,* 7**,** 531-8.

Byun, T. S., Pacek, M., Yee, M. C., Walter, J. C. and Cimprich, K. A. (2005). "Functional uncoupling of MCM helicase and DNA polymerase activities activates the ATR-dependent checkpoint." *Genes Dev,* 19**,** 1040-52.

Cadwell, K. and Coscoy, L. (2005). "Ubiquitination on nonlysine residues by a viral E3 ubiquitin ligase." *Science,* 309**,** 127-130.

Cai, Y., Jin, J., Swanson, S. K., Cole, M. D., Choi, S. H., Florens, L., Washburn, M. P., Conaway, J. W. and Conaway, R. C. (2010). "Subunit composition and substrate specificity of a MOF-containing histone acetyltransferase distinct from the male-specific lethal (MSL) complex." *J Biol Chem,* 285**,** 4268-72.

Caldecott, K. W. (2008). "Single-strand break repair and genetic disease." *Nat Rev Genet,* 9**,** 619-31.

Calsou, P., Delteil, C., Frit, P., Drouet, J. and Salles, B. (2003). "Coordinated assembly of Ku and p460 subunits of the DNA-dependent protein kinase on DNA ends is necessary for XRCC4-ligase IV recruitment." *J Mol Biol,* 326**,** 93-103.

Cao, J. and Yan, Q. (2012). "Histone ubiquitination and deubiquitination in transcription, DNA damage response, and cancer." *Front Oncol,* 2**,** 26.

Cao, R., Tsukada, Y. and Zhang, Y. (2005). "Role of Bmi-1 and Ring1A in H2A ubiquitylation and Hox gene silencing." *Mol Cell,* 20**,** 845-54.

Carneiro, D. G., Clarke, T., Davies, C. C. and Bailey, D. (2016). "Identifying novel protein interactions: Proteomic methods, optimisation approaches and data analysis pipelines." *Methods,* 95**,** 46-54.

Cayrou, C., Coulombe, P., Vigneron, A., Stanojcic, S., Ganier, O., Peiffer, I., Rivals, E., Puy, A., Laurent-Chabalier, S., Desprat, R. and Mechali, M. (2011). "Genome-scale analysis of metazoan replication origins reveals their organization in specific but flexible sites defined by conserved features." *Genome Res,* 21**,** 1438-49.

Cazzalini, O., Sommatis, S., Tillhon, M., Dutto, I., Bachi, A., Rapp, A., Nardo, T., Scovassi, A. I., Necchi, D., Cardoso, M. C., Stivala, L. A. and Prosperi, E. (2014). "CBP and p300 acetylate PCNA to link its degradation with nucleotide excision repair synthesis." *Nucleic Acids Res,* 42**,** 8433-48.

Chang, H. H. Y., Pannunzio, N. R., Adachi, N. and Lieber, M. R. (2017). "Non-homologous DNA end joining and alternative pathways to double-strand break repair." *Nat Rev Mol Cell Biol,* 18**,** 495-506.

Chapman-Smith, A. and Cronan, J. E., Jr. (1999). "Molecular biology of biotin attachment to proteins." *J Nutr,* 129**,** 477S-484S.

Chapman, J. R., Barral, P., Vannier, J. B., Borel, V., Steger, M., Tomas-Loba, A., Sartori, A. A., Adams, I. R., Batista, F. D. and Boulton, S. J. (2013). "RIF1 is essential for 53BP1-dependent nonhomologous end joining and suppression of DNA double-strand break resection." *Mol Cell,* 49**,** 858-71.

Chelmicki, T., Dundar, F., Turley, M. J., Khanam, T., Aktas, T., Ramirez, F., Gendrel, A. V., Wright, P. R., Videm, P., Backofen, R., Heard, E., Manke, T. and Akhtar, A. (2014). "MOF-associated complexes ensure stem cell identity and Xist repression." *Elife,* 3**,** e02024.

Chen, H. Y., Sun, J. M., Zhang, Y., Davie, J. R. and Meistrich, M. L. (1998). "Ubiquitination of histone H3 in elongating spermatids of rat testes." *J Biol Chem,* 273**,** 13165-9.

Chen, P. C., Bhattacharyya, B. J., Hanna, J., Minkel, H., Wilson, J. A., Finley, D., Miller, R. J. and Wilson, S. M. (2011). "Ubiquitin homeostasis is critical for synaptic development and function." *J Neurosci,* 31**,** 17505-13.

Chen, Y. and Poon, R. Y. (2008). "The multiple checkpoint functions of CHK1 and CHK2 in maintenance of genome stability." *Front Biosci,* 13**,** 5016-29.

Chen, Y., Sprung, R., Tang, Y., Ball, H., Sangras, B., Kim, S. C., Falck, J. R., Peng, J., Gu, W. and Zhao, Y. (2007). "Lysine propionylation and butyrylation are novel post-translational modifications in histones." *Mol Cell Proteomics,* 6**,** 812-9.

Chen, Z., Ye, X., Tang, N., Shen, S., Li, Z., Niu, X., Lu, S. and Xu, L. (2014). "The histone acetylranseferase hMOF acetylates Nrf2 and regulates anti-drug responses in human non-small cell lung cancer." *Br J Pharmacol,* 171**,** 3196-211.

Choi-Rhee, E., Schulman, H. and Cronan, J. E. (2004). "Promiscuous protein biotinylation by Escherichia coli biotin protein ligase." *Protein Sci,* 13**,** 3043-50.

Choudhary, S. K. and Li, R. (2002). "BRCA1 modulates ionizing radiation-induced nuclear focus formation by the replication protein A p34 subunit." *J Cell Biochem,* 84**,** 666-74.

Chow, J. and Heard, E. (2009). "X inactivation and the complexities of silencing a sex chromosome." *Curr Opin Cell Biol,* 21**,** 359-66.

Christophorou, M. A., Castelo-Branco, G., Halley-Stott, R. P., Oliveira, C. S., Loos, R., Radzisheuskaya, A., Mowen, K. A., Bertone, P., Silva, J. C., Zernicka-Goetz, M., Nielsen, M. L., Gurdon, J. B. and Kouzarides, T. (2014). "Citrullination regulates pluripotency and histone H1 binding to chromatin." *Nature,* 507**,** 104-8.

Ciccia, A. and Elledge, S. J. (2010). "The DNA Damage Response: Making It Safe to Play with Knives." *Molecular Cell,* 40**,** 179-204.

Ciechanover, A. and Ben-Saadon, R. (2004). "N-terminal ubiquitination: more protein substrates join in." *Trends Cell Biol,* 14**,** 103-6.

Ciechanover, A., Elias, S., Heller, H. and Hershko, A. (1982). ""Covalent affinity" purification of ubiquitin-activating enzyme." *J Biol Chem,* 257**,** 2537-42.

Clague, M. J. and Urbe, S. (2006). "Endocytosis: the DUB version." *Trends Cell Biol,* 16**,** 551-9.

Cohen-Kaplan, V., Livneh, I., Avni, N., Cohen-Rosenzweig, C. and Ciechanover, A. (2016). "The ubiquitin-proteasome system and autophagy: Coordinated and independent activities." *Int J Biochem Cell Biol,* 79**,** 403-418.

Cohen, P. (2002). "The origins of protein phosphorylation." *Nat Cell Biol,* 4**,** E127-30.

Collins, C. T. and Hess, J. L. (2016). "Role of HOXA9 in leukemia: dysregulation, cofactors and essential targets." *Oncogene,* 35**,** 1090-8.

Collins, G. A. and Goldberg, A. L. (2017). "The Logic of the 26S Proteasome." *Cell,* 169**,** 792-806.

Conaway, R. C., Brower, C. S. and Conaway, J. W. (2002). "Emerging roles of ubiquitin in transcription regulation." *Science,* 296**,** 1254-8.

Cong, L., Ran, F. A., Cox, D., Lin, S., Barretto, R., Habib, N., Hsu, P. D., Wu, X., Jiang, W., Marraffini, L. A. and Zhang, F. (2013). "Multiplex genome engineering using CRISPR/Cas systems." *Science,* 339**,** 819-23.

Conrad, T. and Akhtar, A. (2012). "Dosage compensation in Drosophila melanogaster: epigenetic fine-tuning of chromosome-wide transcription." *Nat Rev Genet,* 13**,** 123-34.

Copps, K., Richman, R., Lyman, L. M., Chang, K. A., Rampersad-Ammons, J. and Kuroda, M. I. (1998). "Complex formation by the Drosophila MSL proteins: role of the MSL2 RING finger in protein complex assembly." *Embo Journal,* 17**,** 5409-5417.

Corn, J. E. and Vucic, D. (2014). "Ubiquitin in inflammation: the right linkage makes all the difference." *Nat Struct Mol Biol,* 21**,** 297-300.

Corona, D. F., Clapier, C. R., Becker, P. B. and Tamkun, J. W. (2002). "Modulation of ISWI function by site-specific histone acetylation." *EMBO Rep,* 3**,** 242-7.

Cortez, D. (2015). "Preventing replication fork collapse to maintain genome integrity." *DNA Repair (Amst),* 32**,** 149-57.

Costantini, S., Woodbine, L., Andreoli, L., Jeggo, P. A. and Vindigni, A. (2007). "Interaction of the Ku heterodimer with the DNA ligase IV/Xrcc4 complex and its regulation by DNA-PK." *DNA Repair (Amst),* 6**,** 712-22.

Couzens, A. L., Knight, J. D., Kean, M. J., Teo, G., Weiss, A., Dunham, W. H., Lin, Z. Y., Bagshaw, R. D., Sicheri, F., Pawson, T., Wrana, J. L., Choi, H. and Gingras, A. C. (2013). "Protein interaction network of the mammalian Hippo pathway reveals mechanisms of kinase-phosphatase interactions." *Sci Signal,* 6**,** rs15.

Crevel, G., Bates, H., Huikeshoven, H. and Cotterill, S. (2001). "The Drosophila Dpit47 protein is a nuclear Hsp90 co-chaperone that interacts with DNA polymerase alpha." *J Cell Sci,* 114**,** 2015-25.

Crevel, G., Bennett, D. and Cotterill, S. (2008). "The human TPR protein TTC4 is a putative Hsp90 co-chaperone which interacts with CDC6 and shows alterations in transformed cells." *PLoS One,* 3**,** e0001737.

d'Adda di Fagagna, F. (2008). "Living on a break: cellular senescence as a DNA-damage response." *Nat Rev Cancer,* 8**,** 512-22.

Dai, L., Peng, C., Montellier, E., Lu, Z., Chen, Y., Ishii, H., Debernardi, A., Buchou, T., Rousseaux, S., Jin, F., Sabari, B. R., Deng, Z., Allis, C. D., Ren, B., Khochbin, S. and Zhao, Y. (2014). "Lysine 2-hydroxyisobutyrylation is a widely distributed active histone mark." *Nat Chem Biol,* 10**,** 365-70.

Daley, J. M. and Sung, P. (2014). "53BP1, BRCA1, and the choice between recombination and end joining at DNA double-strand breaks." *Mol Cell Biol,* 34**,** 1380-8.

Davies, S. L., North, P. S. and Hickson, I. D. (2007). "Role for BLM in replication-fork restart and suppression of origin firing after replicative stress." *Nat Struct Mol Biol,* 14**,** 677-9.

Davis, A. J. and Chen, D. J. (2013). "DNA double strand break repair via non-homologous end-joining." *Transl Cancer Res,* 2**,** 130-143.

de Ruijter, A. J., van Gennip, A. H., Caron, H. N., Kemp, S. and van Kuilenburg, A. B. (2003). "Histone deacetylases (HDACs): characterization of the classical HDAC family." *Biochem J,* 370**,** 737-49.

Deegan, T. D., Yeeles, J. T. and Diffley, J. F. (2016). "Phosphopeptide binding by Sld3 links Dbf4-dependent kinase to MCM replicative helicase activation." *EMBO J,* 35**,** 961-73.

Delcuve, G. P., Khan, D. H. and Davie, J. R. (2012). "Roles of histone deacetylases in epigenetic regulation: emerging paradigms from studies with inhibitors." *Clin Epigenetics,* 4**,** 5.

Delgado, S., Gomez, M., Bird, A. and Antequera, F. (1998). "Initiation of DNA replication at CpG islands in mammalian chromosomes." *EMBO J,* 17**,** 2426-35.

Dellino, G. I., Cittaro, D., Piccioni, R., Luzi, L., Banfi, S., Segalla, S., Cesaroni, M., Mendoza-Maldonado, R., Giacca, M. and Pelicci, P. G. (2013). "Genome-wide mapping of human DNA-replication origins: levels of transcription at ORC1 sites regulate origin selection and replication timing." *Genome Res,* 23**,** 1-11.

Demakova, O. V., Kotlikova, I. V., Gordadze, P. R., Alekseyenko, A. A., Kuroda, M. I. and Zhimulev, I. F. (2003). "The MSL complex levels are critical for its correct targeting to the chromosomes in Drosophila melanogaster." *Chromosoma,* 112**,** 103-15.

Dementyeva, E. V. and Zakian, S. M. (2010). "Dosage compensation of sex chromosome genes in eukaryotes." *Acta Naturae,* 2**,** 36-43.

Deubzer, H. E., Schier, M. C., Oehme, I., Lodrini, M., Haendler, B., Sommer, A. and Witt, O. (2013). "HDAC11 is a novel drug target in carcinomas." *Int J Cancer,* 132**,** 2200-8.

Deuring, R., Fanti, L., Armstrong, J. A., Sarte, M., Papoulas, O., Prestel, M., Daubresse, G., Verardo, M., Moseley, S. L., Berloco, M., Tsukiyama, T., Wu, C., Pimpinelli, S. and Tamkun, J. W. (2000). "The ISWI chromatin-remodeling protein is required for gene expression and the maintenance of higher order chromatin structure in vivo." *Mol Cell,* 5**,** 355-65.

Deveau, H., Garneau, J. E. and Moineau, S. (2010). "CRISPR/Cas system and its role in phage-bacteria interactions." *Annu Rev Microbiol,* 64**,** 475-93.

Dhalluin, C., Carlson, J. E., Zeng, L., He, C., Aggarwal, A. K. and Zhou, M. M. (1999). "Structure and ligand of a histone acetyltransferase bromodomain." *Nature,* 399**,** 491-6.

Di Felice, F., Cioci, F. and Camilloni, G. (2005). "FOB1 affects DNA topoisomerase I in vivo cleavages in the enhancer region of the Saccharomyces cerevisiae ribosomal DNA locus." *Nucleic Acids Res,* 33**,** 6327-37.

DiMaggio, P. A., Jr., Young, N. L., Baliban, R. C., Garcia, B. A. and Floudas, C. A. (2009). "A mixed integer linear optimization framework for the identification and quantification of targeted post-translational modifications of highly modified proteins using multiplexed electron transfer dissociation tandem mass spectrometry." *Mol Cell Proteomics,* 8**,** 2527-43.

Dion, M. F., Altschuler, S. J., Wu, L. F. and Rando, O. J. (2005). "Genomic characterization reveals a simple histone H4 acetylation code." *Proc Natl Acad Sci U S A,* 102**,** 5501-6.

Dmitriev, R. I., Korneenko, T. V., Bessonov, A. A., Shakhparonov, M. I., Modyanov, N. N. and Pestov, N. B. (2007). "Characterization of hampin/MSL1 as a node in the nuclear interactome." *Biochem Biophys Res Commun,* 355**,** 1051-7.

Dmitriev, R. I., Okkelman, I. A., Abdulin, R. A., Shakhparonov, M. I. and Pestov, N. B. (2009). "Nuclear transport of protein TTC4 depends on the cell cycle." *Cell Tissue Res,* 336**,** 521-7.

Dmitriev, R. I., Pestov, N. B., Korneenko, T. V., Gerasimova, A. V., Zhao, K., Modianov, N. N., Kostina, M. B. and Shakhparonov, M. I. (2005). "[Tissue specificity of alternative splicing products of mouse mRNA encoding new protein hampin homologous to the Drosophila MSL-1 protein]." *Bioorg Khim,* 31**,** 363-71.

Dmitriev, R. I., Pestov, N. B., Shakhparonov, M. I. and Okkelman, I. A. (2014). "Two distinct nuclear localization signals in mammalian MSL1 regulate its function." *J Cell Biochem,* 115**,** 1967-73.

Doil, C., Mailand, N., Bekker-Jensen, S., Menard, P., Larsen, D. H., Pepperkok, R., Ellenberg, J., Panier, S., Durocher, D., Bartek, J., Lukas, J. and Lukas, C. (2009). "RNF168 Binds and Amplifies Ubiquitin Conjugates on Damaged Chromosomes to Allow Accumulation of Repair Proteins." *Cell,* 136**,** 435-446.

Dou, H., Buetow, L., Sibbet, G. J., Cameron, K. and Huang, D. T. (2012). "BIRC7-E2 ubiquitin conjugate structure reveals the mechanism of ubiquitin transfer by a RING dimer." *Nat Struct Mol Biol,* 19**,** 876-83.

Dou, Y., Milne, T. A., Tackett, A. J., Smith, E. R., Fukuda, A., Wysocka, J., Allis, C. D., Chait, B. T., Hess, J. L. and Roeder, R. G. (2005). "Physical association and coordinate function of the H3 K4 methyltransferase MLL1 and the H4 K16 acetyltransferase MOF." *Cell,* 121**,** 873-85.

Dutnall, R. N., Tafrov, S. T., Sternglanz, R. and Ramakrishnan, V. (1998). "Structure of the histone acetyltransferase Hat1: a paradigm for the GCN5-related N-acetyltransferase superfamily." *Cell,* 94**,** 427-38.

Dynek, J. N., Goncharov, T., Dueber, E. C., Fedorova, A. V., Izrael-Tomasevic, A., Phu, L., Helgason, E., Fairbrother, W. J., Deshayes, K., Kirkpatrick, D. S. and Vucic, D. (2010). "c-IAP1 and UbcH5 promote K11-linked polyubiquitination of RIP1 in TNF signalling." *EMBO J,* 29**,** 4198-209.

el-Hajj, H. H., Zhang, H. and Weiss, B. (1988). "Lethality of a dut (deoxyuridine triphosphatase) mutation in Escherichia coli." *J Bacteriol,* 170**,** 1069-75.

Ellison, V. and Stillman, B. (2003). "Biochemical characterization of DNA damage checkpoint complexes: clamp loader and clamp complexes with specificity for 5' recessed DNA." *PLoS Biol,* 1**,** E33.

Esashi, F., Christ, N., Gannon, J., Liu, Y., Hunt, T., Jasin, M. and West, S. C. (2005). "CDK-dependent phosphorylation of BRCA2 as a regulatory mechanism for recombinational repair." *Nature,* 434**,** 598-604.

Escribano-Diaz, C., Orthwein, A., Fradet-Turcotte, A., Xing, M., Young, J. T., Tkac, J., Cook, M. A., Rosebrock, A. P., Munro, M., Canny, M. D., Xu, D. and Durocher, D. (2013). "A cell cycle-dependent regulatory circuit composed of 53BP1-RIF1 and BRCA1-CtIP controls DNA repair pathway choice." *Mol Cell,* 49**,** 872-83.

Evans, P. C., Smith, T. S., Lai, M. J., Williams, M. G., Burke, D. F., Heyninck, K., Kreike, M. M., Beyaert, R., Blundell, T. L. and Kilshaw, P. J. (2003). "A novel type of deubiquitinating enzyme." *J Biol Chem,* 278**,** 23180-6.

Fairhead, M. and Howarth, M. (2015). "Site-specific biotinylation of purified proteins using BirA." *Methods Mol Biol,* 1266**,** 171-84.

Fell, V. L. and Schild-Poulter, C. (2012). "Ku regulates signaling to DNA damage response pathways through the Ku70 von Willebrand A domain." *Mol Cell Biol,* 32**,** 76-87.

Feng, L. and Chen, J. (2012). "The E3 ligase RNF8 regulates KU80 removal and NHEJ repair." *Nat Struct Mol Biol,* 19**,** 201-6.

Ferenbach, A., Li, A., Brito-Martins, M. and Blow, J. J. (2005). "Functional domains of the Xenopus replication licensing factor Cdt1." *Nucleic Acids Res,* 33**,** 316-24.

Ferguson, D. O. and Holloman, W. K. (1996). "Recombinational repair of gaps in DNA is asymmetric in Ustilago maydis and can be explained by a migrating D-loop model." *Proc Natl Acad Sci U S A,* 93**,** 5419-24.

Fernandez, J. M. H., J.P. 1999. *Gene Expression Systems. Using nature for the art of expression,* San Diego, Academic Press.

Firsanov, D. V., Solovjeva, L. V. and Svetlova, M. P. (2011). "H2AX phosphorylation at the sites of DNA double-strand breaks in cultivated mammalian cells and tissues." *Clin Epigenetics,* 2**,** 283-97.

Forch, P., Merendino, L., Martinez, C. and Valcarcel, J. (2001). "Modulation of msl-2 5' splice site recognition by Sex-lethal." *RNA,* 7**,** 1185-91.

Forsberg, E. C. and Bresnick, E. H. (2001). "Histone acetylation beyond promoters: long-range acetylation patterns in the chromatin world." *Bioessays,* 23**,** 820-30.

Forsburg, S. L. (2004). "Eukaryotic MCM proteins: beyond replication initiation." *Microbiol Mol Biol Rev,* 68**,** 109-31.

Fradet-Turcotte, A., Canny, M. D., Escribano-Diaz, C., Orthwein, A., Leung, C. C., Huang, H., Landry, M. C., Kitevski-LeBlanc, J., Noordermeer, S. M., Sicheri, F. and Durocher, D. (2013). "53BP1 is a reader of the DNA-damage-induced H2A Lys 15 ubiquitin mark." *Nature,* 499**,** 50-4.

Fraga, M. F., Ballestar, E., Villar-Garea, A., Boix-Chornet, M., Espada, J., Schotta, G., Bonaldi, T., Haydon, C., Ropero, S., Petrie, K., Iyer, N. G., Perez-Rosado, A., Calvo, E., Lopez, J. A., Cano, A., Calasanz, M. J., Colomer, D., Piris, M. A., Ahn, N., Imhof, A., Caldas, C., Jenuwein, T. and Esteller, M. (2005). "Loss of acetylation at Lys16 and trimethylation at Lys20 of histone H4 is a common hallmark of human cancer." *Nat Genet,* 37**,** 391-400.

Fragkos, M., Ganier, O., Coulombe, P. and Mechali, M. (2015). "DNA replication origin activation in space and time." *Nat Rev Mol Cell Biol,* 16**,** 360-74.

Franken, N. A., Rodermond, H. M., Stap, J., Haveman, J. and van Bree, C. (2006). "Clonogenic assay of cells in vitro." *Nat Protoc,* 1**,** 2315-9.

Freemont, P. S., Hanson, I. M. and Trowsdale, J. (1991). "A Novel Cysteine-Rich Sequence Motif." *Cell,* 64**,** 483-484.

Frigola, J., He, J., Kinkelin, K., Pye, V. E., Renault, L., Douglas, M. E., Remus, D., Cherepanov, P., Costa, A. and Diffley, J. F. X. (2017). "Cdt1 stabilizes an open MCM ring for helicase loading." *Nat Commun,* 8**,** 15720.

Furuhashi, H., Nakajima, M. and Hirose, S. (2006). "DNA supercoiling factor contributes to dosage compensation in Drosophila." *Development,* 133**,** 4475-83.

Gadsden, M. H., McIntosh, E. M., Game, J. C., Wilson, P. J. and Haynes, R. H. (1993). "dUTP pyrophosphatase is an essential enzyme in Saccharomyces cerevisiae." *EMBO J,* 12**,** 4425-31.

Gangaraju, V. K. and Bartholomew, B. (2007). "Mechanisms of ATP dependent chromatin remodeling." *Mutat Res,* 618**,** 3-17.

Gao, F. (2015). "Bacteria may have multiple replication origins." *Front Microbiol,* 6**,** 324.

Gao, L., Cueto, M. A., Asselbergs, F. and Atadja, P. (2002). "Cloning and functional characterization of HDAC11, a novel member of the human histone deacetylase family." *J Biol Chem,* 277**,** 25748-55.

Gao, Y., Feng, J., Yang, G., Zhang, S., Liu, Y., Bu, Y., Sun, M., Zhao, M., Chen, F., Zhang, W., Ye, L. and Zhang, X. (2017). "HBx-elevated MSL2 Modulates

HBV cccDNA through Inducing Degradation of APOBEC3B to Enhance Hepatocarcinogenesis." *Hepatology*.

Garcia, B. A., Pesavento, J. J., Mizzen, C. A. and Kelleher, N. L. (2007). "Pervasive combinatorial modification of histone H3 in human cells." *Nat Methods,* 4**,** 487-9.

Gatti, M., Pinato, S., Maiolica, A., Rocchio, F., Prato, M. G., Aebersold, R. and Penengo, L. (2015). "RNF168 promotes noncanonical K27 ubiquitination to signal DNA damage." *Cell Rep,* 10**,** 226-38.

Gatti, M., Pinato, S., Maspero, E., Soffientini, P., Polo, S. and Penengo, L. (2012). "A novel ubiquitin mark at the N-terminal tail of histone H2As targeted by RNF168 ubiquitin ligase." *Cell Cycle,* 11**,** 2538-44.

Gelbart, M. E., Larschan, E., Peng, S., Park, P. J. and Kuroda, M. I. (2009). "Drosophila MSL complex globally acetylates H4K16 on the male X chromosome for dosage compensation." *Nat Struct Mol Biol,* 16**,** 825-32.

Ginjala, V., Nacerddine, K., Kulkarni, A., Oza, J., Hill, S. J., Yao, M., Citterio, E., van Lohuizen, M. and Ganesan, S. (2011). "BMI1 is recruited to DNA breaks and contributes to DNA damage-induced H2A ubiquitination and repair." *Mol Cell Biol,* 31**,** 1972-82.

Gironella, M., Malicet, C., Cano, C., Sandi, M. J., Hamidi, T., Tauil, R. M., Baston, M., Valaco, P., Moreno, S., Lopez, F., Neira, J. L., Dagorn, J. C. and Iovanna, J. L. (2009). "p8/nupr1 regulates DNA-repair activity after double-strand gamma irradiation-induced DNA damage." *J Cell Physiol,* 221**,** 594-602.

Goldknopf, I. L., Taylor, C. W., Baum, R. M., Yeoman, L. C., Olson, M. O., Prestayko, A. W. and Busch, H. (1975). "Isolation and characterization of protein A24, a "histone-like" non-histone chromosomal protein." *J Biol Chem,* 250**,** 7182-7.

Goldstein, G., Scheid, M., Hammerling, U., Schlesinger, D. H., Niall, H. D. and Boyse, E. A. (1975). "Isolation of a polypeptide that has lymphocyte-differentiating properties and is probably represented universally in living cells." *Proc Natl Acad Sci U S A,* 72**,** 11-5.

Good, P. J. (1995). "A conserved family of elav-like genes in vertebrates." *Proc Natl Acad Sci U S A,* 92**,** 4557-61.

Goodarzi, A. A., Jonnalagadda, J. C., Douglas, P., Young, D., Ye, R., Moorhead, G. B., Lees-Miller, S. P. and Khanna, K. K. (2004). "Autophosphorylation of ataxia-telangiectasia mutated is regulated by protein phosphatase 2A." *EMBO J,* 23**,** 4451-61.

Grabbe, C. and Dikic, I. (2009). "Functional roles of ubiquitin-like domain (ULD) and ubiquitin-binding domain (UBD) containing proteins." *Chem Rev,* 109**,** 1481-94.

Graindorge, A., Carre, C. and Gebauer, F. (2013). "Sex-lethal promotes nuclear retention of msl2 mRNA via interactions with the STAR protein HOW." *Genes Dev,* 27**,** 1421-33.

Gu, W., Szauter, P. and Lucchesi, J. C. (1998). "Targeting of MOF, a putative histone acetyl transferase, to the X chromosome of Drosophila melanogaster." *Dev Genet,* 22**,** 56-64.

Gu, W., Wei, X., Pannuti, A. and Lucchesi, J. C. (2000). "Targeting the chromatin-remodeling MSL complex of Drosophila to its sites of action on the X chromosome requires both acetyl transferase and ATPase activities." *EMBO J,* 19**,** 5202-11.

Gupta, A., Guerin-Peyrou, T. G., Sharma, G. G., Park, C., Agarwal, M., Ganju, R. K., Pandita, S., Choi, K., Sukumar, S., Pandita, R. K., Ludwig, T. and Pandita, T. K. (2008). "The mammalian ortholog of Drosophila MOF that acetylates histone H4 lysine 16 is essential for embryogenesis and oncogenesis." *Mol Cell Biol,* 28**,** 397-409.

Gupta, A., Hunt, C. R., Chakraborty, S., Pandita, R. K., Yordy, J., Ramnarain, D. B., Horikoshi, N. and Pandita, T. K. (2014a). "Role of 53BP1 in the regulation of DNA double-strand break repair pathway choice." *Radiat Res,* 181**,** 1-8.

Gupta, A., Hunt, C. R., Hegde, M. L., Chakraborty, S., Chakraborty, S., Udayakumar, D., Horikoshi, N., Singh, M., Ramnarain, D. B., Hittelman, W. N., Namjoshi, S., Asaithamby, A., Hazra, T. K., Ludwig, T., Pandita, R. K., Tyler, J. K. and Pandita, T. K. (2014b). "MOF phosphorylation by ATM regulates 53BP1-mediated double-strand break repair pathway choice." *Cell Rep,* 8**,** 177-89.

Gupta, A., Sharma, G. G., Young, C. S., Agarwal, M., Smith, E. R., Paull, T. T., Lucchesi, J. C., Khanna, K. K., Ludwig, T. and Pandita, T. K. (2005). "Involvement of human MOF in ATM function." *Mol Cell Biol,* 25**,** 5292-305.

Haglund, K. and Dikic, I. (2005). "Ubiquitylation and cell signaling." *EMBO J,* 24**,** 3353-9.

Hallacli, E., Lipp, M., Georgiev, P., Spielman, C., Cusack, S., Akhtar, A. and Kadlec, J. (2012). "Msl1-Mediated Dimerization of the Dosage Compensation Complex Is Essential for Male X-Chromosome Regulation in Drosophila." *Molecular Cell,* 48**,** 587-600.

Hamada, F. N., Park, P. J., Gordadze, P. R. and Kuroda, M. I. (2005). "Global regulation of X chromosomal genes by the MSL complex in Drosophila melanogaster." *Genes Dev,* 19**,** 2289-94.

Hanna, J., Hathaway, N. A., Tone, Y., Crosas, B., Elsasser, S., Kirkpatrick, D. S., Leggett, D. S., Gygi, S. P., King, R. W. and Finley, D. (2006). "Deubiquitinating enzyme Ubp6 functions noncatalytically to delay proteasomal degradation." *Cell,* 127**,** 99-111.

Hao, J., de Renty, C., Li, Y., Xiao, H., Kemp, M. G., Han, Z., DePamphilis, M. L. and Zhu, W. (2015). "And-1 coordinates with Claspin for efficient Chk1 activation in response to replication stress." *EMBO J,* 34**,** 2096-110.

Harper, J. W. and Elledge, S. J. (2007). "The DNA damage response: Ten years after." *Molecular Cell,* 28**,** 739-745.

Hartlerode, A. J. and Scully, R. (2009). "Mechanisms of double-strand break repair in somatic mammalian cells." *Biochem J,* 423**,** 157-68.

Haynes, S. R., Dollard, C., Winston, F., Beck, S., Trowsdale, J. and Dawid, I. B. (1992). "The bromodomain: a conserved sequence found in human, Drosophila and yeast proteins." *Nucleic Acids Res,* 20**,** 2603.

Heller, R. C., Kang, S., Lam, W. M., Chen, S., Chan, C. S. and Bell, S. P. (2011). "Eukaryotic origin-dependent DNA replication in vitro reveals sequential action of DDK and S-CDK kinases." *Cell,* 146**,** 80-91.

Herniou, E. A., Olszewski, J. A., Cory, J. S. and O'Reilly, D. R. (2003). "The genome sequence and evolution of baculoviruses." *Annu Rev Entomol,* 48**,** 211-34.

Hershko, A. and Ciechanover, A. (1998). "The ubiquitin system." *Annu Rev Biochem,* 67**,** 425-79.

Heyer, W. D., Ehmsen, K. T. and Liu, J. (2010). "Regulation of homologous recombination in eukaryotes." *Annu Rev Genet,* 44**,** 113-39.

Hicke, L., Schubert, H. L. and Hill, C. P. (2005). "Ubiquitin-binding domains." *Nat Rev Mol Cell Biol,* 6**,** 610-21.

Hilfiker, A., Hilfiker-Kleiner, D., Pannuti, A. and Lucchesi, J. C. (1997). "mof, a putative acetyl transferase gene related to the Tip60 and MOZ human genes and to the SAS genes of yeast, is required for dosage compensation in Drosophila." *EMBO J,* 16**,** 2054-60.

Hodge, C. D., Ismail, I. H., Edwards, R. A., Hura, G. L., Xiao, A. T., Tainer, J. A., Hendzel, M. J. and Glover, J. N. (2016). "RNF8 E3 Ubiquitin Ligase Stimulates Ubc13 E2 Conjugating Activity That Is Essential for DNA Double Strand Break Signaling and BRCA1 Tumor Suppressor Recruitment." *J Biol Chem,* 291**,** 9396-410.

Hoeijmakers, J. H. (2009). "DNA damage, aging, and cancer." *N Engl J Med,* 361**,** 1475-85.

Holland, A. J., Fachinetti, D., Han, J. S. and Cleveland, D. W. (2012). "Inducible, reversible system for the rapid and complete degradation of proteins in mammalian cells." *Proc Natl Acad Sci U S A,* 109**,** E3350-7.

Hoshina, S., Yura, K., Teranishi, H., Kiyasu, N., Tominaga, A., Kadoma, H., Nakatsuka, A., Kunichika, T., Obuse, C. and Waga, S. (2013). "Human origin recognition complex binds preferentially to G-quadruplex-preferable RNA and single-stranded DNA." *J Biol Chem,* 288**,** 30161-71.

Hsiao, K. Y. and Mizzen, C. A. (2013). "Histone H4 deacetylation facilitates 53BP1 DNA damage signaling and double-strand break repair." *J Mol Cell Biol,* 5**,** 157-65.

Hu, J., Adebali, O., Adar, S. and Sancar, A. (2017). "Dynamic maps of UV damage formation and repair for the human genome." *Proc Natl Acad Sci U S A,* 114**,** 6758-6763.

Hu, M., Li, P., Li, M., Li, W., Yao, T., Wu, J. W., Gu, W., Cohen, R. E. and Shi, Y. (2002). "Crystal structure of a UBP-family deubiquitinating enzyme in isolation and in complex with ubiquitin aldehyde." *Cell,* 111**,** 1041-54.

Huang, A., Hibbert, R. G., de Jong, R. N., Das, D., Sixma, T. K. and Boelens, R. (2011). "Symmetry and asymmetry of the RING-RING dimer of Rad18." *J Mol Biol,* 410**,** 424-35.

Huang da, W., Sherman, B. T. and Lempicki, R. A. (2009a). "Bioinformatics enrichment tools: paths toward the comprehensive functional analysis of large gene lists." *Nucleic Acids Res,* 37**,** 1-13.

Huang da, W., Sherman, B. T. and Lempicki, R. A. (2009b). "Systematic and integrative analysis of large gene lists using DAVID bioinformatics resources." *Nat Protoc,* 4**,** 44-57.

Huang, H., Sabari, B. R., Garcia, B. A., Allis, C. D. and Zhao, Y. (2014). "SnapShot: histone modifications." *Cell,* 159**,** 458-458 e1.

Huberman, J. A. and Riggs, A. D. (1966). "Autoradiography of chromosomal DNA fibers from Chinese hamster cells." *Proc Natl Acad Sci U S A,* 55**,** 599-606.

Huen, M. S., Grant, R., Manke, I., Minn, K., Yu, X., Yaffe, M. B. and Chen, J. (2007). "RNF8 transduces the DNA-damage signal via histone ubiquitylation and checkpoint protein assembly." *Cell,* 131**,** 901-14.

Huibregtse, J. M., Scheffner, M., Beaudenon, S. and Howley, P. M. (1995). "A family of proteins structurally and functionally related to the E6-AP ubiquitin-protein ligase." *Proc Natl Acad Sci U S A,* 92**,** 5249.

Hulsen, T., de Vlieg, J. and Alkema, W. (2008). "BioVenn - a web application for the comparison and visualization of biological lists using area-proportional Venn diagrams." *BMC Genomics,* 9**,** 488.

Husnjak, K. and Dikic, I. (2012). "Ubiquitin-binding proteins: decoders of ubiquitin-mediated cellular functions." *Annu Rev Biochem,* 81**,** 291-322.

Iconomou, M. and Saunders, D. N. (2016). "Systematic approaches to identify E3 ligase substrates." *Biochem J,* 473**,** 4083-4101.

Illingworth, R. S., Moffat, M., Mann, A. R., Read, D., Hunter, C. J., Pradeepa, M. M., Adams, I. R. and Bickmore, W. A. (2015). "The E3 ubiquitin ligase activity of RING1B is not essential for early mouse development." *Genes Dev,* 29**,** 1897-902.

Ilves, I., Petojevic, T., Pesavento, J. J. and Botchan, M. R. (2010). "Activation of the MCM2-7 helicase by association with Cdc45 and GINS proteins." *Mol Cell,* 37**,** 247-58.

Ismail, I. H., Andrin, C., McDonald, D. and Hendzel, M. J. (2010). "BMI1-mediated histone ubiquitylation promotes DNA double-strand break repair." *J Cell Biol,* 191**,** 45-60.

Ismail, I. H., Gagne, J. P., Genois, M. M., Strickfaden, H., McDonald, D., Xu, Z., Poirier, G. G., Masson, J. Y. and Hendzel, M. J. (2015). "The RNF138 E3 ligase displaces Ku to promote DNA end resection and regulate DNA repair pathway choice." *Nat Cell Biol,* 17**,** 1446-57.

Itoh, M., Kim, C. H., Palardy, G., Oda, T., Jiang, Y. J., Maust, D., Yeo, S. Y., Lorick, K., Wright, G. J., Ariza-McNaughton, L., Weissman, A. M., Lewis, J., Chandrasekharappa, S. C. and Chitnis, A. B. (2003). "Mind bomb is a ubiquitin ligase that is essential for efficient activation of Notch signaling by Delta." *Dev Cell,* 4**,** 67-82.

Jazayeri, A., Falck, J., Lukas, C., Bartek, J., Smith, G. C., Lukas, J. and Jackson, S. P. (2006). "ATM- and cell cycle-dependent regulation of ATR in response to DNA double-strand breaks." *Nat Cell Biol,* 8**,** 37-45.

Jenuwein, T. and Allis, C. D. (2001). "Translating the histone code." *Science,* 293**,** 1074-80.

Jiang, T., Zhou, X., Taghizadeh, K., Dong, M. and Dedon, P. C. (2007). "N-formylation of lysine in histone proteins as a secondary modification arising from oxidative DNA damage." *Proc Natl Acad Sci U S A,* 104**,** 60-5.

Jiang, W., Wang, S., Xiao, M., Lin, Y., Zhou, L., Lei, Q., Xiong, Y., Guan, K. L. and Zhao, S. (2011). "Acetylation regulates gluconeogenesis by promoting PEPCK1 degradation via recruiting the UBR5 ubiquitin ligase." *Mol Cell,* 43**,** 33-44.

Jilani, A., Ramotar, D., Slack, C., Ong, C., Yang, X. M., Scherer, S. W. and Lasko, D. D. (1999). "Molecular cloning of the human gene, PNKP, encoding a polynucleotide kinase 3'-phosphatase and evidence for its role in repair of DNA strand breaks caused by oxidative damage." *J Biol Chem,* 274**,** 24176-86.

Jin, L., Williamson, A., Banerjee, S., Philipp, I. and Rape, M. (2008). "Mechanism of ubiquitin-chain formation by the human anaphase-promoting complex." *Cell,* 133**,** 653-65.

Jin, Y., Wang, Y., Johansen, J. and Johansen, K. M. (2000). "JIL-1, a chromosomal kinase implicated in regulation of chromatin structure, associates with the male specific lethal (MSL) dosage compensation complex." *J Cell Biol,* 149**,** 1005-10.

Jin, Y., Wang, Y., Walker, D. L., Dong, H., Conley, C., Johansen, J. and Johansen, K. M. (1999). "JIL-1: a novel chromosomal tandem kinase implicated in transcriptional regulation in Drosophila." *Mol Cell,* 4**,** 129-35.

Jiricny, J. (2006). "The multifaceted mismatch-repair system." *Nat Rev Mol Cell Biol,* 7**,** 335-46.

Johansen, K. M. and Johansen, J. (2006). "Regulation of chromatin structure by histone H3S10 phosphorylation." *Chromosome Res,* 14**,** 393-404.

Jorgensen, S., Schotta, G. and Sorensen, C. S. (2013). "Histone H4 lysine 20 methylation: key player in epigenetic regulation of genomic integrity." *Nucleic Acids Res,* 41**,** 2797-806.

Jung, M., Philpott, M., Muller, S., Schulze, J., Badock, V., Eberspacher, U., Moosmayer, D., Bader, B., Schmees, N., Fernandez-Montalvan, A. and Haendler, B. (2014). "Affinity map of bromodomain protein 4 (BRD4) interactions with the histone H4 tail and the small molecule inhibitor JQ1." *J Biol Chem,* 289**,** 9304-19.

Jungmichel, S., Clapperton, J. A., Lloyd, J., Hari, F. J., Spycher, C., Pavic, L., Li, J., Haire, L. F., Bonalli, M., Larsen, D. H., Lukas, C., Lukas, J., MacMillan, D., Nielsen, M. L., Stucki, M. and Smerdon, S. J. (2012). "The molecular basis of ATM-dependent dimerization of the Mdc1 DNA damage checkpoint mediator." *Nucleic Acids Res,* 40**,** 3913-28.

Kadlec, J., Hallacli, E., Lipp, M., Holz, H., Sanchez-Weatherby, J., Cusack, S. and Akhtar, A. (2011). "Structural basis for MOF and MSL3 recruitment into the dosage compensation complex by MSL1." *Nat Struct Mol Biol,* 18**,** 142-9.

Kamadurai, H. B., Souphron, J., Scott, D. C., Duda, D. M., Miller, D. J., Stringer, D., Piper, R. C. and Schulman, B. A. (2009). "Insights into ubiquitin transfer cascades from a structure of a UbcH5B approximately ubiquitin-HECT(NEDD4L) complex." *Mol Cell,* 36**,** 1095-102.

Kapoor-Vazirani, P., Kagey, J. D., Powell, D. R. and Vertino, P. M. (2008). "Role of hMOF-dependent histone H4 lysine 16 acetylation in the maintenance of TMS1/ASC gene activity." *Cancer Research,* 68**,** 6810-6821.

Karnani, N. and Dutta, A. (2011). "The effect of the intra-S-phase checkpoint on origins of replication in human cells." *Genes Dev,* 25**,** 621-33.

Kehrli, K., Phelps, M., Lazarchuk, P., Chen, E., Monnat, R., Jr. and Sidorova, J. M. (2016). "Class I Histone Deacetylase HDAC1 and WRN RECQ Helicase Contribute Additively to Protect Replication Forks upon Hydroxyurea-induced Arrest." *J Biol Chem,* 291**,** 24487-24503.

Keller, C. I. and Akhtar, A. (2015). "The MSL complex: juggling RNA-protein interactions for dosage compensation and beyond." *Curr Opin Genet Dev,* 31**,** 1-11.

Kelley, R. L., Meller, V. H., Gordadze, P. R., Roman, G., Davis, R. L. and Kuroda, M. I. (1999). "Epigenetic spreading of the Drosophila dosage compensation complex from roX RNA genes into flanking chromatin." *Cell,* 98**,** 513-22.

Kelley, R. L., Solovyeva, I., Lyman, L. M., Richman, R., Solovyev, V. and Kuroda, M. I. (1995). "Expression of msl-2 causes assembly of dosage compensation regulators on the X chromosomes and female lethality in Drosophila." *Cell,* 81**,** 867-77.

Kelley, R. L., Wang, J., Bell, L. and Kuroda, M. I. (1997). "Sex lethal controls dosage compensation in Drosophila by a non-splicing mechanism." *Nature,* 387**,** 195-9.

Khochbin, S., Verdel, A., Lemercier, C. and Seigneurin-Berny, D. (2001). "Functional significance of histone deacetylase diversity." *Curr Opin Genet Dev,* 11**,** 162-6.

Kim, D., Blus, B. J., Chandra, V., Huang, P., Rastinejad, F. and Khorasanizadeh, S. (2010). "Corecognition of DNA and a methylated histone tail by the MSL3 chromodomain." *Nat Struct Mol Biol,* 17**,** 1027-9.

Kim, J., Guermah, M., McGinty, R. K., Lee, J. S., Tang, Z., Milne, T. A., Shilatifard, A., Muir, T. W. and Roeder, R. G. (2009). "RAD6-Mediated transcription-coupled H2B ubiquitylation directly stimulates H3K4 methylation in human cells." *Cell,* 137**,** 459-71.

Kim, J. H., Lee, S. R., Li, L. H., Park, H. J., Park, J. H., Lee, K. Y., Kim, M. K., Shin, B. A. and Choi, S. Y. (2011). "High cleavage efficiency of a 2A peptide derived from porcine teschovirus-1 in human cell lines, zebrafish and mice." *PLoS One,* 6**,** e18556.

Kim, Y. J. and Wilson, D. M., 3rd (2012). "Overview of base excision repair biochemistry." *Curr Mol Pharmacol,* 5**,** 3-13.

Kimura, Y. and Tanaka, K. (2010). "Regulatory mechanisms involved in the control of ubiquitin homeostasis." *J Biochem,* 147**,** 793-8.

King, P. H., Fuller, J. J., Nabors, L. B. and Detloff, P. J. (2000). "Analysis of the 5' end of the mouse Elavl1 (mHuA) gene reveals a transcriptional regulatory element and evidence for conserved genomic organization." *Gene,* 242**,** 125-31.

Kobayashi, T. and Horiuchi, T. (1996). "A yeast gene product, Fob1 protein, required for both replication fork blocking and recombinational hotspot activities." *Genes Cells,* 1**,** 465-74.

Kolas, N. K., Chapman, J. R., Nakada, S., Ylanko, J., Chahwan, R., Sweeney, F. D., Panier, S., Mendez, M., Wildenhain, J., Thomson, T. M., Pelletier, L., Jackson, S. P. and Durocher, D. (2007). "Orchestration of the DNA-damage response by the RNF8 ubiquitin ligase." *Science,* 318**,** 1637-40.

Komander, D. (2009). "The emerging complexity of protein ubiquitination." *Biochem Soc Trans,* 37**,** 937-53.

Kornberg, R. D. and Lorch, Y. (1999). "Twenty-five years of the nucleosome, fundamental particle of the eukaryote chromosome." *Cell,* 98**,** 285-94.

Korzus, E., Torchia, J., Rose, D. W., Xu, L., Kurokawa, R., McInerney, E. M., Mullen, T. M., Glass, C. K. and Rosenfeld, M. G. (1998). "Transcription factor-specific requirements for coactivators and their acetyltransferase functions." *Science,* 279**,** 703-7.

Koushika, S. P., Lisbin, M. J. and White, K. (1996). "ELAV, a Drosophila neuron-specific protein, mediates the generation of an alternatively spliced neural protein isoform." *Curr Biol,* 6**,** 1634-41.

Kouzarides, T. (2007). "Chromatin modifications and their function." *Cell,* 128**,** 693-705.

Kozlov, S. V., Graham, M. E., Jakob, B., Tobias, F., Kijas, A. W., Tanuji, M., Chen, P., Robinson, P. J., Taucher-Scholz, G., Suzuki, K., So, S., Chen, D. and Lavin, M. F. (2011). "Autophosphorylation and ATM activation: additional sites add to the complexity." *J Biol Chem,* 286**,** 9107-19.

Kraft, C., Peter, M. and Hofmann, K. (2010). "Selective autophagy: ubiquitin-mediated recognition and beyond." *Nat Cell Biol,* 12**,** 836-41.

Kruse, J. P. and Gu, W. (2009). "MSL2 promotes Mdm2-independent cytoplasmic localization of p53." *J Biol Chem,* 284**,** 3250-63.

Kumagai, A., Lee, J., Yoo, H. Y. and Dunphy, W. G. (2006). "TopBP1 activates the ATR-ATRIP complex." *Cell,* 124**,** 943-955.

Kumagai, A., Shevchenko, A., Shevchenko, A. and Dunphy, W. G. (2010). "Treslin collaborates with TopBP1 in triggering the initiation of DNA replication." *Cell,* 140**,** 349-59.

Kuo, A. J., Song, J., Cheung, P., Ishibe-Murakami, S., Yamazoe, S., Chen, J. K., Patel, D. J. and Gozani, O. (2012). "The BAH domain of ORC1 links H4K20me2 to DNA replication licensing and Meier-Gorlin syndrome." *Nature,* 484**,** 115-9.

Kurose, A., Tanaka, T., Huang, X., Traganos, F., Dai, W. and Darzynkiewicz, Z. (2006). "Effects of hydroxyurea and aphidicolin on phosphorylation of ataxia telangiectasia mutated on Ser 1981 and histone H2AX on Ser 139 in relation to cell cycle phase and induction of apoptosis." *Cytometry A,* 69**,** 212-21.

Lai, Z. 2013. *Functional Analysis of Vetebrate Msl2.* PhD Doctoral thesis, National University of Ireland.

Lai, Z., Moravcova, S., Canitrot, Y., Andrzejewski, L. P., Walshe, D. M. and Rea, S. (2013). "Msl2 is a novel component of the vertebrate DNA damage response." *PLoS One,* 8**,** e68549.

Lam, K. C., Muhlpfordt, F., Vaquerizas, J. M., Raja, S. J., Holz, H., Luscombe, N. M., Manke, T. and Akhtar, A. (2012). "The NSL complex regulates housekeeping genes in Drosophila." *PLoS Genet,* 8**,** e1002736.

Lam, Y. A., Xu, W., DeMartino, G. N. and Cohen, R. E. (1997). "Editing of ubiquitin conjugates by an isopeptidase in the 26S proteasome." *Nature,* 385**,** 737-40.

Lambert, J. P., Tucholska, M., Go, C., Knight, J. D. and Gingras, A. C. (2015). "Proximity biotinylation and affinity purification are complementary approaches for the interactome mapping of chromatin-associated protein complexes." *J Proteomics,* 118**,** 81-94.

Larasati and Duncker, B. P. (2016). "Mechanisms Governing DDK Regulation of the Initiation of DNA Replication." *Genes (Basel),* 8.

Larschan, E., Alekseyenko, A. A., Gortchakov, A. A., Peng, S., Li, B., Yang, P., Workman, J. L., Park, P. J. and Kuroda, M. I. (2007). "MSL complex is attracted to genes marked by H3K36 trimethylation using a sequence-independent mechanism." *Mol Cell,* 28**,** 121-33.

Larschan, E., Bishop, E. P., Kharchenko, P. V., Core, L. J., Lis, J. T., Park, P. J. and Kuroda, M. I. (2011). "X chromosome dosage compensation via enhanced transcriptional elongation in Drosophila." *Nature,* 471**,** 115-8.

Larsen, C. N., Krantz, B. A. and Wilkinson, K. D. (1998). "Substrate specificity of deubiquitinating enzymes: ubiquitin C-terminal hydrolases." *Biochemistry,* 37**,** 3358-68.

Lau, A. C., Zhu, K. P., Brouhard, E. A., Davis, M. B. and Csankovszki, G. (2016). "An H4K16 histone acetyltransferase mediates decondensation of the X chromosome in C. elegans males." *Epigenetics Chromatin,* 9**,** 44.

Lazarou, M., Narendra, D. P., Jin, S. M., Tekle, E., Banerjee, S. and Youle, R. J. (2013). "PINK1 drives Parkin self-association and HECT-like E3 activity upstream of mitochondrial binding." *J Cell Biol,* 200**,** 163-72.

Lee, C. G. and Hurwitz, J. (1993). "Human RNA helicase A is homologous to the maleless protein of Drosophila." *J Biol Chem,* 268**,** 16822-30.

Lee, J. and Dunphy, W. G. (2013). "The Mre11-Rad50-Nbs1 (MRN) complex has a specific role in the activation of Chk1 in response to stalled replication forks." *Mol Biol Cell,* 24**,** 1343-53.

Lee, J. S., Shukla, A., Schneider, J., Swanson, S. K., Washburn, M. P., Florens, L., Bhaumik, S. R. and Shilatifard, A. (2007). "Histone crosstalk between H2B monoubiquitination and H3 methylation mediated by COMPASS." *Cell,* 131**,** 1084-96.

Lee, J. S., Smith, E. and Shilatifard, A. (2010a). "The language of histone crosstalk." *Cell,* 142**,** 682-5.

Lee, J. Y., Koga, H., Kawaguchi, Y., Tang, W., Wong, E., Gao, Y. S., Pandey, U. B., Kaushik, S., Tresse, E., Lu, J., Taylor, J. P., Cuervo, A. M. and Yao, T. P. (2010b). "HDAC6 controls autophagosome maturation essential for ubiquitin-selective quality-control autophagy." *EMBO J,* 29**,** 969-80.

Leman, A. R. and Noguchi, E. (2013). "The replication fork: understanding the eukaryotic replication machinery and the challenges to genome duplication." *Genes (Basel),* 4**,** 1-32.

Leonard, A. C. and Mechali, M. (2013). "DNA replication origins." *Cold Spring Harb Perspect Biol,* 5**,** a010116.

Li, F., Parry, D. A. and Scott, M. J. (2005). "The amino-terminal region of Drosophila MSL1 contains basic, glycine-rich, and leucine zipper-like motifs that promote X chromosome binding, self-association, and MSL2 binding, respectively." *Mol Cell Biol,* 25**,** 8913-24.

Li, F., Schiemann, A. H. and Scott, M. J. (2008a). "Incorporation of the noncoding roX RNAs alters the chromatin-binding specificity of the Drosophila MSL1/MSL2 complex." *Mol Cell Biol,* 28**,** 1252-64.

Li, M. and Yu, X. (2013). "Function of BRCA1 in the DNA damage response is mediated by ADP-ribosylation." *Cancer Cell,* 23**,** 693-704.

Li, W., Bengtson, M. H., Ulbrich, A., Matsuda, A., Reddy, V. A., Orth, A., Chanda, S. K., Batalov, S. and Joazeiro, C. A. (2008b). "Genome-wide and functional annotation of human E3 ubiquitin ligases identifies MULAN, a mitochondrial E3 that regulates the organelle's dynamics and signaling." *PLoS One,* 3**,** e1487.

Li, X., Corsa, C. A., Pan, P. W., Wu, L., Ferguson, D., Yu, X., Min, J. and Dou, Y. (2010). "MOF and H4 K16 acetylation play important roles in DNA damage repair by modulating recruitment of DNA damage repair protein Mdc1." *Mol Cell Biol,* 30**,** 5335-47.

Li, X. and Heyer, W. D. (2008). "Homologous recombination in DNA repair and DNA damage tolerance." *Cell Res,* 18**,** 99-113.

Li, X. Z., Wu, L. P., Corsa, C. A. S., Kunkel, S. and Dou, Y. L. (2009). "Two Mammalian MOF Complexes Regulate Transcription Activation by Distinct Mechanisms." *Molecular Cell,* 36**,** 290-301.

Li, Z., Cao, R., Wang, M., Myers, M. P., Zhang, Y. and Xu, R. M. (2006). "Structure of a Bmi-1-Ring1B polycomb group ubiquitin ligase complex." *J Biol Chem,* 281**,** 20643-9.

Liang, J., Wan, M., Zhang, Y., Gu, P., Xin, H., Jung, S. Y., Qin, J., Wong, J., Cooney, A. J., Liu, D. and Songyang, Z. (2008). "Nanog and Oct4 associate with unique transcriptional repression complexes in embryonic stem cells." *Nat Cell Biol,* 10**,** 731-9.

Liew, C. W., Sun, H., Hunter, T. and Day, C. L. (2010). "RING domain dimerization is essential for RNF4 function." *Biochem J,* 431**,** 23-9.

Lindahl, T. and Barnes, D. E. (2000). "Repair of endogenous DNA damage." *Cold Spring Harb Symp Quant Biol,* 65**,** 127-33.

Linke, K., Mace, P. D., Smith, C. A., Vaux, D. L., Silke, J. and Day, C. L. (2008). "Structure of the MDM2/MDMX RING domain heterodimer reveals dimerization is required for their ubiquitylation in trans." *Cell Death Differ,* 15**,** 841-8.

Liu, C. W. and Jacobson, A. D. (2013). "Functions of the 19S complex in proteasomal degradation." *Trends Biochem Sci,* 38**,** 103-10.

Liu, Q., Guntuku, S., Cui, X. S., Matsuoka, S., Cortez, D., Tamai, K., Luo, G., Carattini-Rivera, S., DeMayo, F., Bradley, A., Donehower, L. A. and Elledge, S. J. (2000). "Chk1 is an essential kinase that is regulated by Atr and required for the G(2)/M DNA damage checkpoint." *Genes Dev,* 14**,** 1448-59.

Liu, S., Opiyo, S. O., Manthey, K., Glanzer, J. G., Ashley, A. K., Amerin, C., Troksa, K., Shrivastav, M., Nickoloff, J. A. and Oakley, G. G. (2012a). "Distinct roles for DNA-PK, ATM and ATR in RPA phosphorylation and checkpoint activation in response to replication stress." *Nucleic Acids Res,* 40**,** 10780-94.

Liu, S., Shiotani, B., Lahiri, M., Marechal, A., Tse, A., Leung, C. C., Glover, J. N., Yang, X. H. and Zou, L. (2011). "ATR autophosphorylation as a molecular switch for checkpoint activation." *Mol Cell,* 43**,** 192-202.

Liu, S., Song, N. and Zou, L. (2012b). "The conserved C terminus of Claspin interacts with Rad9 and promotes rapid activation of Chk1." *Cell Cycle,* 11**,** 2711-6.

Lou, Z., Minter-Dykhouse, K., Franco, S., Gostissa, M., Rivera, M. A., Celeste, A., Manis, J. P., van Deursen, J., Nussenzweig, A., Paull, T. T., Alt, F. W. and Chen, J. (2006). "MDC1 maintains genomic stability by participating in the amplification of ATM-dependent DNA damage signals." *Mol Cell,* 21**,** 187-200.

Louder, R. K., He, Y., Lopez-Blanco, J. R., Fang, J., Chacon, P. and Nogales, E. (2016). "Structure of promoter-bound TFIID and model of human pre-initiation complex assembly." *Nature,* 531**,** 604-9.

Lowndes, N. F. (2010). "The interplay between BRCA1 and 53BP1 influences death, aging, senescence and cancer." *DNA Repair (Amst),* 9**,** 1112-6.

Luckow, V. A. (1993). "Baculovirus systems for the expression of human gene products." *Curr Opin Biotechnol,* 4**,** 564-72.

Luger, K., Rechsteiner, T. J., Flaus, A. J., Waye, M. M. and Richmond, T. J. (1997). "Characterization of nucleosome core particles containing histone proteins made in bacteria." *J Mol Biol,* 272**,** 301-11.

Lukas, C., Falck, J., Bartkova, J., Bartek, J. and Lukas, J. (2003). "Distinct spatiotemporal dynamics of mammalian checkpoint regulators induced by DNA damage." *Nat Cell Biol,* 5**,** 255-60.

Lukas, C., Savic, V., Bekker-Jensen, S., Doil, C., Neumann, B., Pedersen, R. S., Grofte, M., Chan, K. L., Hickson, I. D., Bartek, J. and Lukas, J. (2011). "53BP1 nuclear bodies form around DNA lesions generated by mitotic transmission of chromosomes under replication stress." *Nat Cell Biol,* 13**,** 243-53.

Luo, H., Shenoy, A. K., Li, X., Jin, Y., Jin, L., Cai, Q., Tang, M., Liu, Y., Chen, H., Reisman, D., Wu, L., Seto, E., Qiu, Y., Dou, Y., Casero, R. A., Jr. and Lu, J. (2016). "MOF Acetylates the Histone Demethylase LSD1 to Suppress Epithelial-to-Mesenchymal Transition." *Cell Rep,* 15**,** 2665-78.

Lyman, L. M., Copps, K., Rastelli, L., Kelley, R. L. and Kuroda, M. I. (1997). "Drosophila male-specific lethal-2 protein: structure/function analysis and dependence on MSL-1 for chromosome association." *Genetics,* 147**,** 1743-53.

Ma, H. T. and Poon, R. Y. (2011). "How protein kinases co-ordinate mitosis in animal cells." *Biochem J,* 435**,** 17-31.

Mace, P. D., Linke, K., Feltham, R., Schumacher, F. R., Smith, C. A., Vaux, D. L., Silke, J. and Day, C. L. (2008). "Structures of the cIAP2 RING domain reveal conformational changes associated with ubiquitin-conjugating enzyme (E2) recruitment." *J Biol Chem,* 283**,** 31633-40.

Mailand, N., Bekker-Jensen, S., Faustrup, H., Melander, F., Bartek, J., Lukas, C. and Lukas, J. (2007). "RNF8 ubiquitylates histones at DNA double-strand breaks and promotes assembly of repair proteins." *Cell,* 131**,** 887-900.

Mao, F. J., Sidorova, J. M., Lauper, J. M., Emond, M. J. and Monnat, R. J. (2010). "The human WRN and BLM RecQ helicases differentially regulate cell proliferation and survival after chemotherapeutic DNA damage." *Cancer Res,* 70**,** 6548-55.

Marechal, A. and Zou, L. (2013). "DNA damage sensing by the ATM and ATR kinases." *Cold Spring Harb Perspect Biol,* 5.

Marin, I. (2003). "Evolution of chromatin-remodeling complexes: comparative genomics reveals the ancient origin of "novel" compensasome genes." *J Mol Evol,* 56**,** 527-39.

Martinez-Balbas, M. A., Bannister, A. J., Martin, K., Haus-Seuffert, P., Meisterernst, M. and Kouzarides, T. (1998). "The acetyltransferase activity of CBP stimulates transcription." *EMBO J,* 17**,** 2886-93.

Matsumoto, M. L., Wickliffe, K. E., Dong, K. C., Yu, C., Bosanac, I., Bustos, D., Phu, L., Kirkpatrick, D. S., Hymowitz, S. G., Rape, M., Kelley, R. F. and Dixit, V. M. (2010). "K11-linked polyubiquitination in cell cycle control revealed by a K11 linkage-specific antibody." *Mol Cell,* 39**,** 477-84.

Mattiroli, F., Vissers, J. H., van Dijk, W. J., Ikpa, P., Citterio, E., Vermeulen, W., Marteijn, J. A. and Sixma, T. K. (2012). "RNF168 ubiquitinates K13-15 on H2A/H2AX to drive DNA damage signaling." *Cell,* 150**,** 1182-95.

Matunis, M. J., Coutavas, E. and Blobel, G. (1996). "A novel ubiquitin-like modification modulates the partitioning of the Ran-GTPase-activating protein RanGAP1 between the cytosol and the nuclear pore complex." *J Cell Biol,* 135**,** 1457-70.

Mazouzi, A., Velimezi, G. and Loizou, J. I. (2014). "DNA replication stress: causes, resolution and disease." *Exp Cell Res,* 329**,** 85-93.

McGinty, R. K., Kim, J., Chatterjee, C., Roeder, R. G. and Muir, T. W. (2008). "Chemically ubiquitylated histone H2B stimulates hDot1L-mediated intranucleosomal methylation." *Nature,* 453**,** 812-6.

McIlwraith, M. J., Van Dyck, E., Masson, J. Y., Stasiak, A. Z., Stasiak, A. and West, S. C. (2000). "Reconstitution of the strand invasion step of double-strand break repair using human Rad51 Rad52 and RPA proteins." *J Mol Biol,* 304**,** 151-64.

Mechali, M. (2010). "Eukaryotic DNA replication origins: many choices for appropriate answers." *Nat Rev Mol Cell Biol,* 11**,** 728-38.

Mellacheruvu, D., Wright, Z., Couzens, A. L., Lambert, J. P., St-Denis, N. A., Li, T., Miteva, Y. V., Hauri, S., Sardiu, M. E., Low, T. Y., Halim, V. A., Bagshaw, R. D., Hubner, N. C., Al-Hakim, A., Bouchard, A., Faubert, D., Fermin, D., Dunham, W. H., Goudreault, M., Lin, Z. Y., Badillo, B. G., Pawson, T., Durocher, D., Coulombe, B., Aebersold, R., Superti-Furga, G., Colinge, J., Heck, A. J., Choi, H., Gstaiger, M., Mohammed, S., Cristea, I. M., Bennett, K. L., Washburn, M. P., Raught, B., Ewing, R. M., Gingras, A. C. and

Nesvizhskii, A. I. (2013). "The CRAPome: a contaminant repository for affinity purification-mass spectrometry data." *Nat Methods,* 10**,** 730-6.

Meller, V. H., Gordadze, P. R., Park, Y., Chu, X., Stuckenholz, C., Kelley, R. L. and Kuroda, M. I. (2000). "Ordered assembly of roX RNAs into MSL complexes on the dosage-compensated X chromosome in Drosophila." *Curr Biol,* 10**,** 136-43.

Meller, V. H. and Rattner, B. P. (2002). "The roX genes encode redundant male-specific lethal transcripts required for targeting of the MSL complex." *EMBO J,* 21**,** 1084-91.

Mendjan, S., Taipale, M., Kind, J., Holz, H., Gebhardt, P., Schelder, M., Vermeulen, M., Buscaino, A., Duncan, K., Mueller, J., Wilm, M., Stunnenberg, H. G., Saumweber, H. and Akhtar, A. (2006). "Nuclear pore components are involved in the transcriptional regulation of dosage compensation in Drosophila." *Mol Cell,* 21**,** 811-23.

Menssen, R., Schweiggert, J., Schreiner, J., Kusevic, D., Reuther, J., Braun, B. and Wolf, D. H. (2012). "Exploring the topology of the Gid complex, the E3 ubiquitin ligase involved in catabolite-induced degradation of gluconeogenic enzymes." *J Biol Chem,* 287**,** 25602-14.

Merrick, C. J., Jackson, D. and Diffley, J. F. (2004). "Visualization of altered replication dynamics after DNA damage in human cells." *J Biol Chem,* 279**,** 20067-75.

Metzger, M. B., Hristova, V. A. and Weissman, A. M. (2012). "HECT and RING finger families of E3 ubiquitin ligases at a glance." *J Cell Sci,* 125**,** 531-7.

Mevissen, T. E., Hospenthal, M. K., Geurink, P. P., Elliott, P. R., Akutsu, M., Arnaudo, N., Ekkebus, R., Kulathu, Y., Wauer, T., El Oualid, F., Freund, S. M., Ovaa, H. and Komander, D. (2013). "OTU deubiquitinases reveal mechanisms of linkage specificity and enable ubiquitin chain restriction analysis." *Cell,* 154**,** 169-84.

Milne, T. A., Briggs, S. D., Brock, H. W., Martin, M. E., Gibbs, D., Allis, C. D. and Hess, J. L. (2002). "MLL targets SET domain methyltransferase activity to Hox gene promoters." *Mol Cell,* 10**,** 1107-17.

Minca, E. C. and Kowalski, D. (2011). "Replication fork stalling by bulky DNA damage: localization at active origins and checkpoint modulation." *Nucleic Acids Res,* 39**,** 2610-23.

Miyamoto, N., Izumi, H., Noguchi, T., Nakajima, Y., Ohmiya, Y., Shiota, M., Kidani, A., Tawara, A. and Kohno, K. (2008). "Tip60 is regulated by circadian transcription factor clock and is involved in cisplatin resistance." *J Biol Chem,* 283**,** 18218-26.

Mohr, S., Doebele, C., Comoglio, F., Berg, T., Beck, J., Bohnenberger, H., Alexe, G., Corso, J., Strobel, P., Wachter, A., Beissbarth, T., Schnutgen, F., Cremer, A., Haetscher, N., Gollner, S., Rouhi, A., Palmqvist, L., Rieger, M. A., Schroeder, T., Bonig, H., Muller-Tidow, C., Kuchenbauer, F., Schutz, E., Green, A. R., Urlaub, H., Stegmaier, K., Humphries, R. K., Serve, H. and Oellerich, T. (2017). "Hoxa9 and Meis1 Cooperatively Induce Addiction to Syk Signaling by Suppressing miR-146a in Acute Myeloid Leukemia." *Cancer Cell,* 31**,** 549-562 e11.

Mol, C. D., Harris, J. M., McIntosh, E. M. and Tainer, J. A. (1996). "Human dUTP pyrophosphatase: uracil recognition by a beta hairpin and active sites formed by three separate subunits." *Structure,* 4**,** 1077-92.

Moldovan, G. L., Pfander, B. and Jentsch, S. (2007). "PCNA, the maestro of the replication fork." *Cell,* 129**,** 665-79.

Monroy, M. A., Schott, N. M., Cox, L., Chen, J. D., Ruh, M. and Chrivia, J. C. (2003). "SNF2-related CBP activator protein (SRCAP) functions as a coactivator of steroid receptor-mediated transcription through synergistic interactions with CARM-1 and GRIP-1." *Mol Endocrinol,* 17**,** 2519-28.

Moore, S. A., Ferhatoglu, Y., Jia, Y., Al-Jiab, R. A. and Scott, M. J. (2010). "Structural and biochemical studies on the chromo-barrel domain of male specific lethal 3 (MSL3) reveal a binding preference for mono- or dimethyllysine 20 on histone H4." *J Biol Chem,* 285**,** 40879-90.

Morales, V., Regnard, C., Izzo, A., Vetter, I. and Becker, P. B. (2005). "The MRG domain mediates the functional integration of MSL3 into the dosage compensation complex." *Mol Cell Biol,* 25**,** 5947-54.

Morales, V., Straub, T., Neumann, M. F., Mengus, G., Akhtar, A. and Becker, P. B. (2004). "Functional integration of the histone acetyltransferase MOF into the dosage compensation complex." *EMBO J,* 23**,** 2258-68.

Morra, R., Smith, E. R., Yokoyama, R. and Lucchesi, J. C. (2008). "The MLE subunit of the Drosophila MSL complex uses its ATPase activity for dosage compensation and its helicase activity for targeting." *Mol Cell Biol,* 28**,** 958-66.

Moscariello, M., Wieloch, R., Kurosawa, A., Li, F., Adachi, N., Mladenov, E. and Iliakis, G. (2015). "Role for Artemis nuclease in the repair of radiation-induced DNA double strand breaks by alternative end joining." *DNA Repair (Amst),* 31**,** 29-40.

Moshous, D., Callebaut, I., de Chasseval, R., Corneo, B., Cavazzana-Calvo, M., Le Deist, F., Tezcan, I., Sanal, O., Bertrand, Y., Philippe, N., Fischer, A. and de Villartay, J. P. (2001). "Artemis, a novel DNA double-strand break repair/V(D)J recombination protein, is mutated in human severe combined immune deficiency." *Cell,* 105**,** 177-86.

Motegi, A., Liaw, H. J., Lee, K. Y., Roest, H. P., Maas, A., Wu, X., Moinova, H., Markowitz, S. D., Ding, H., Hoeijmakers, J. H. and Myung, K. (2008). "Polyubiquitination of proliferating cell nuclear antigen by HLTF and SHPRH prevents genomic instability from stalled replication forks." *Proc Natl Acad Sci U S A,* 105**,** 12411-6.

Moureau, S., Luessing, J., Harte, E. C., Voisin, M. and Lowndes, N. F. (2016). "A role for the p53 tumour suppressor in regulating the balance between homologous recombination and non-homologous end joining." *Open Biol,* 6.

Mouron, S., Rodriguez-Acebes, S., Martinez-Jimenez, M. I., Garcia-Gomez, S., Chocron, S., Blanco, L. and Mendez, J. (2013). "Repriming of DNA synthesis at stalled replication forks by human PrimPol." *Nat Struct Mol Biol,* 20**,** 1383-9.

Muller-Tidow, C., Ji, P., Diederichs, S., Potratz, J., Baumer, N., Kohler, G., Cauvet, T., Choudary, C., van der Meer, T., Chan, W. Y., Nieduszynski, C., Colledge, W. H., Carrington, M., Koeffler, H. P., Restle, A., Wiesmuller, L., Sobczak-Thepot, J., Berdel, W. E. and Serve, H. (2004). "The cyclin A1-CDK2 complex regulates DNA double-strand break repair." *Mol Cell Biol,* 24**,** 8917-28.

Munks, R. J., Moore, J., O'Neill, L. P. and Turner, B. M. (1991). "Histone H4 acetylation in Drosophila. Frequency of acetylation at different sites defined by immunolabelling with site-specific antibodies." *FEBS Lett,* 284**,** 245-8.

Muscolini, M., Montagni, E., Palermo, V., Di Agostino, S., Gu, W., Abdelmoula-Souissi, S., Mazzoni, C., Blandino, G. and Tuosto, L. (2011). "The Cancer-associated K351N Mutation Affects the Ubiquitination and the Translocation to Mitochondria of p53 Protein." *Journal of Biological Chemistry,* 286**,** 39693-39702.

Myers, J. S. and Cortez, D. (2006). "Rapid activation of ATR by ionizing radiation requires ATM and Mre11." *J Biol Chem,* 281**,** 9346-50.

Nanao, M. H., Tcherniuk, S. O., Chroboczek, J., Dideberg, O., Dessen, A. and Balakirev, M. Y. (2004). "Crystal structure of human otubain 2." *EMBO Rep,* 5**,** 783-8.

Natsume, T., Kiyomitsu, T., Saga, Y. and Kanemaki, M. T. (2016). "Rapid Protein Depletion in Human Cells by Auxin-Inducible Degron Tagging with Short Homology Donors." *Cell Rep,* 15**,** 210-8.

Niida, H., Katsuno, Y., Banerjee, B., Hande, M. P. and Nakanishi, M. (2007). "Specific role of Chk1 phosphorylations in cell survival and checkpoint activation." *Mol Cell Biol,* 27**,** 2572-81.

Nijman, S. M., Luna-Vargas, M. P., Velds, A., Brummelkamp, T. R., Dirac, A. M., Sixma, T. K. and Bernards, R. (2005). "A genomic and functional inventory of deubiquitinating enzymes." *Cell,* 123**,** 773-86.

Nishimura, K., Fukagawa, T., Takisawa, H., Kakimoto, T. and Kanemaki, M. (2009). "An auxin-based degron system for the rapid depletion of proteins in nonplant cells." *Nat Methods,* 6**,** 917-22.

Nishizuka, Y., Ueda, K., Nakazawa, K. and Hayaishi, O. (1967). "Studies on the polymer of adenosine diphosphate ribose. I. Enzymic formation from nicotinamide adenine dinuclotide in mammalian nuclei." *J Biol Chem,* 242**,** 3164-71.

Norbury, C. J. and Zhivotovsky, B. (2004). "DNA damage-induced apoptosis." *Oncogene,* 23**,** 2797-808.

Nordman, J. T. and Orr-Weaver, T. L. (2015). "Understanding replication fork progression, stability, and chromosome fragility by exploiting the Suppressor of Underreplication protein." *Bioessays,* 37**,** 856-61.

O'Gorman, S., Fox, D. T. and Wahl, G. M. (1991). "Recombinase-mediated gene activation and site-specific integration in mammalian cells." *Science,* 251**,** 1351-5.

Ochs, F., Somyajit, K., Altmeyer, M., Rask, M. B., Lukas, J. and Lukas, C. (2016). "53BP1 fosters fidelity of homology-directed DNA repair." *Nat Struct Mol Biol,* 23**,** 714-21.

Ogiwara, H. and Kohno, T. (2011). "Essential factors for incompatible DNA end joining at chromosomal DNA double strand breaks in vivo." *PLoS One,* 6**,** e28756.

Ogryzko, V. V., Schiltz, R. L., Russanova, V., Howard, B. H. and Nakatani, Y. (1996). "The transcriptional coactivators p300 and CBP are histone acetyltransferases." *Cell,* 87**,** 953-9.

Oh, C., Park, S., Lee, E. K. and Yoo, Y. J. (2013). "Downregulation of ubiquitin level via knockdown of polyubiquitin gene Ubb as potential cancer therapeutic intervention." *Sci Rep,* 3**,** 2623.

Oppikofer, M., Kueng, S., Martino, F., Soeroes, S., Hancock, S. M., Chin, J. W., Fischle, W. and Gasser, S. M. (2011). "A dual role of H4K16 acetylation in the establishment of yeast silent chromatin." *EMBO J,* 30**,** 2610-21.

Orthwein, A., Noordermeer, S. M., Wilson, M. D., Landry, S., Enchev, R. I., Sherker, A., Munro, M., Pinder, J., Salsman, J., Dellaire, G., Xia, B., Peter, M. and Durocher, D. (2015). "A mechanism for the suppression of homologous recombination in G1 cells." *Nature,* 528**,** 422-6.

Osley, M. A., Fleming, A. B. and Kao, C. F. (2006). "Histone ubiquitylation and the regulation of transcription." *Results Probl Cell Differ,* 41**,** 47-75.

Ouyang, H., Ali, Y. O., Ravichandran, M., Dong, A., Qiu, W., MacKenzie, F., Dhe-Paganon, S., Arrowsmith, C. H. and Zhai, R. G. (2012). "Protein aggregates are recruited to aggresome by histone deacetylase 6 via unanchored ubiquitin C termini." *J Biol Chem,* 287**,** 2317-27.

Pacek, M., Tutter, A. V., Kubota, Y., Takisawa, H. and Walter, J. C. (2006). "Localization of MCM2-7, Cdc45, and GINS to the site of DNA unwinding during eukaryotic DNA replication." *Mol Cell,* 21**,** 581-7.

Palmer, M. J., Richman, R., Richter, L. and Kuroda, M. I. (1994). "Sex-specific regulation of the male-specific lethal-1 dosage compensation gene in Drosophila." *Genes Dev,* 8**,** 698-706.

Park, M. S., Ludwig, D. L., Stigger, E. and Lee, S. H. (1996). "Physical interaction between human RAD52 and RPA is required for homologous recombination in mammalian cells." *J Biol Chem,* 271**,** 18996-9000.

Park, Y., Kelley, R. L., Oh, H., Kuroda, M. I. and Meller, V. H. (2002). "Extent of chromatin spreading determined by roX RNA recruitment of MSL proteins." *Science,* 298**,** 1620-3.

Park, Y. and Kuroda, M. I. (2001). "Epigenetic aspects of X-chromosome dosage compensation." *Science,* 293**,** 1083-5.

Parker, M. W., Botchan, M. R. and Berger, J. M. (2017). "Mechanisms and regulation of DNA replication initiation in eukaryotes." *Crit Rev Biochem Mol Biol,* 52**,** 107-144.

Paul, A. and Wang, B. (2017). "RNF8- and Ube2S-Dependent Ubiquitin Lysine 11-Linkage Modification in Response to DNA Damage." *Mol Cell,* 66**,** 458-472 e5.

Pearl, L. H. and Savva, R. (1996). "The problem with pyrimidines." *Nat Struct Biol,* 3**,** 485-7.

Pellegrino, S., Michelena, J., Teloni, F., Imhof, R. and Altmeyer, M. (2017). "Replication-Coupled Dilution of H4K20me2 Guides 53BP1 to Pre-replicative Chromatin." *Cell Rep,* 19**,** 1819-1831.

Pelzer, C., Kassner, I., Matentzoglu, K., Singh, R. K., Wollscheid, H. P., Scheffner, M., Schmidtke, G. and Groettrup, M. (2007). "UBE1L2, a novel E1 enzyme specific for ubiquitin." *J Biol Chem,* 282**,** 23010-4.

Penalva, L. O. and Sanchez, L. (2003). "RNA binding protein sex-lethal (Sxl) and control of Drosophila sex determination and dosage compensation." *Microbiol Mol Biol Rev,* 67**,** 343-59, table of contents.

Peng, J., Schwartz, D., Elias, J., Thoreen, C., Cheng, D., Marsischky, G., Roelofs, J., Finley, D. and Gygi, S. (2003). "A proteomics approach to understanding protein ubiquitination." *Nature Biotechnology* 21**,** 921 - 926.

Petermann, E. and Helleday, T. (2010). "Pathways of mammalian replication fork restart." *Nat Rev Mol Cell Biol,* 11**,** 683-7.

Pfister, S., Rea, S., Taipale, M., Mendrzyk, F., Straub, B., Ittrich, C., Thuerigen, O., Sinn, H. P., Akhtar, A. and Lichter, P. (2008). "The histone acetyltransferase hMOF is frequently downregulated in primary breast carcinoma and

medulloblastoma and constitutes a biomarker for clinical outcome in medulloblastoma." *International Journal of Cancer,* 122**,** 1207-1213.

Pham, A. D. and Sauer, F. (2000). "Ubiquitin-activating/conjugating activity of TAFII250, a mediator of activation of gene expression in Drosophila." *Science,* 289**,** 2357-60.

Phizicky, E. M. and Fields, S. (1995). "Protein-protein interactions: methods for detection and analysis." *Microbiol Rev,* 59**,** 94-123.

Pierce, A. J., Johnson, R. D., Thompson, L. H. and Jasin, M. (1999). "XRCC3 promotes homology-directed repair of DNA damage in mammalian cells." *Genes Dev,* 13**,** 2633-8.

Platta, H. W., El Magraoui, F., Baumer, B. E., Schlee, D., Girzalsky, W. and Erdmann, R. (2009). "Pex2 and pex12 function as protein-ubiquitin ligases in peroxisomal protein import." *Mol Cell Biol,* 29**,** 5505-16.

Poli, J., Gerhold, C. B., Tosi, A., Hustedt, N., Seeber, A., Sack, R., Herzog, F., Pasero, P., Shimada, K., Hopfner, K. P. and Gasser, S. M. (2016). "Mec1, INO80, and the PAF1 complex cooperate to limit transcription replication conflicts through RNAPII removal during replication stress." *Genes Dev,* 30**,** 337-54.

Prenzel, T., Begus-Nahrmann, Y., Kramer, F., Hennion, M., Hsu, C., Gorsler, T., Hintermair, C., Eick, D., Kremmer, E., Simons, M., Beissbarth, T. and Johnsen, S. A. (2011). "Estrogen-dependent gene transcription in human breast cancer cells relies upon proteasome-dependent monoubiquitination of histone H2B." *Cancer Res,* 71**,** 5739-53.

Prestel, M., Feller, C., Straub, T., Mitlohner, H. and Becker, P. B. (2010). "The activation potential of MOF is constrained for dosage compensation." *Mol Cell,* 38**,** 815-26.

Pushpavalli, S. N., Sarkar, A., Ramaiah, M. J., Chowdhury, D. R., Bhadra, U. and Pal-Bhadra, M. (2013). "Drosophila MOF controls Checkpoint protein2 and regulates genomic stability during early embryogenesis." *BMC Mol Biol,* 14**,** 1.

Quan, Y., Xia, Y., Liu, L., Cui, J., Li, Z., Cao, Q., Chen, X. S., Campbell, J. L. and Lou, H. (2015). "Cell-Cycle-Regulated Interaction between Mcm10 and Double Hexameric Mcm2-7 Is Required for Helicase Splitting and Activation during S Phase." *Cell Rep,* 13**,** 2576-86.

Quinn, J. J., Ilik, I. A., Qu, K., Georgiev, P., Chu, C., Akhtar, A. and Chang, H. Y. (2014). "Revealing long noncoding RNA architecture and functions using domain-specific chromatin isolation by RNA purification." *Nat Biotechnol,* 32**,** 933-40.

Raja, S. J., Charapitsa, I., Conrad, T., Vaquerizas, J. M., Gebhardt, P., Holz, H., Kadlec, J., Fraterman, S., Luscombe, N. M. and Akhtar, A. (2010). "The nonspecific lethal complex is a transcriptional regulator in Drosophila." *Mol Cell,* 38**,** 827-41.

Ran, F. A., Hsu, P. D., Wright, J., Agarwala, V., Scott, D. A. and Zhang, F. (2013). "Genome engineering using the CRISPR-Cas9 system." *Nat Protoc,* 8**,** 2281-308.

Ravid, T. and Hochstrasser, M. (2007). "Autoregulation of an E2 enzyme by ubiquitin-chain assembly on its catalytic residue." *Nat Cell Biol,* 9**,** 422-7.

Rea, S., Eisenhaber, F., O'Carroll, D., Strahl, B. D., Sun, Z. W., Schmid, M., Opravil, S., Mechtler, K., Ponting, C. P., Allis, C. D. and Jenuwein, T. (2000).

"Regulation of chromatin structure by site-specific histone H3 methyltransferases." *Nature,* 406**,** 593-9.

Rea, S., Xouri, G. and Akhtar, A. (2007). "Males absent on the first (MOF): from flies to humans." *Oncogene,* 26**,** 5385-94.

Reinhardt, H. C., Aslanian, A. S., Lees, J. A. and Yaffe, M. B. (2007). "p53-deficient cells rely on ATM- and ATR-mediated checkpoint signaling through the p38MAPK/MK2 pathway for survival after DNA damage." *Cancer Cell,* 11**,** 175-89.

Remus, D., Beuron, F., Tolun, G., Griffith, J. D., Morris, E. P. and Diffley, J. F. (2009). "Concerted loading of Mcm2-7 double hexamers around DNA during DNA replication origin licensing." *Cell,* 139**,** 719-30.

Rew, D. A. and Wilson, G. D. (2000). "Cell production rates in human tissues and tumours and their significance. Part 1: an introduction to the techniques of measurement and their limitations." *Eur J Surg Oncol,* 26**,** 227-38.

Reyes-Turcu, F. E., Ventii, K. H. and Wilkinson, K. D. (2009). "Regulation and cellular roles of ubiquitin-specific deubiquitinating enzymes." *Annu Rev Biochem,* 78**,** 363-97.

Robb, G. B. and Rana, T. M. (2007). "RNA helicase A interacts with RISC in human cells and functions in RISC loading." *Mol Cell,* 26**,** 523-37.

Rodgers, K. and McVey, M. (2016). "Error-Prone Repair of DNA Double-Strand Breaks." *J Cell Physiol,* 231**,** 15-24.

Roeder, R. G. (1991). "The complexities of eukaryotic transcription initiation: regulation of preinitiation complex assembly." *Trends Biochem Sci,* 16**,** 402-8.

Rogakou, E. P., Pilch, D. R., Orr, A. H., Ivanova, V. S. and Bonner, W. M. (1998). "DNA double-stranded breaks induce histone H2AX phosphorylation on serine 139." *J Biol Chem,* 273**,** 5858-68.

Rogers, G. E., Harding, H. W. and Llewellyn-Smith, I. J. (1977). "The origin of citrulline-containing proteins in the hair follicle and the chemical nature of trichohyalin, an intracellular precursor." *Biochim Biophys Acta,* 495**,** 159-75.

Roos-Mattjus, P. and Sistonen, L. (2004). "The ubiquitin-proteasome pathway." *Ann Med,* 36**,** 285-95.

Rosano, G. L. and Ceccarelli, E. A. (2014). "Recombinant protein expression in Escherichia coli: advances and challenges." *Front Microbiol,* 5**,** 172.

Rothkamm, K., Kruger, I., Thompson, L. H. and Lobrich, M. (2003). "Pathways of DNA double-strand break repair during the mammalian cell cycle." *Molecular and cellular biology,* 23**,** 5706-15.

Roux, K. J., Kim, D. I. and Burke, B. (2013). "BioID: a screen for protein-protein interactions." *Curr Protoc Protein Sci,* 74**,** Unit 19 23.

Rudra, D., deRoos, P., Chaudhry, A., Niec, R. E., Arvey, A., Samstein, R. M., Leslie, C., Shaffer, S. A., Goodlett, D. R. and Rudensky, A. Y. (2012). "Transcription factor Foxp3 and its protein partners form a complex regulatory network." *Nat Immunol,* 13**,** 1010-9.

Sakabe, K., Wang, Z. and Hart, G. W. (2010). "Beta-N-acetylglucosamine (O-GlcNAc) is part of the histone code." *Proc Natl Acad Sci U S A,* 107**,** 19915-20.

Saleh-Gohari, N. and Helleday, T. (2004). "Conservative homologous recombination preferentially repairs DNA double-strand breaks in the S phase of the cell cycle in human cells." *Nucleic Acids Res,* 32**,** 3683-8.

San Filippo, J., Sung, P. and Klein, H. (2008). "Mechanism of eukaryotic homologous recombination." *Annu Rev Biochem,* 77**,** 229-57.

Sanjuan, R. and Marin, I. (2001). "Tracing the origin of the compensasome: evolutionary history of DEAH helicase and MYST acetyltransferase gene families." *Mol Biol Evol,* 18**,** 330-43.

Sarikas, A., Hartmann, T. and Pan, Z. Q. (2011). "The cullin protein family." *Genome Biol,* 12**,** 220.

Sartori, A. A., Lukas, C., Coates, J., Mistrik, M., Fu, S., Bartek, J., Baer, R., Lukas, J. and Jackson, S. P. (2007). "Human CtIP promotes DNA end resection." *Nature,* 450**,** 509-14.

Scharer, O. D. (2013). "Nucleotide excision repair in eukaryotes." *Cold Spring Harb Perspect Biol,* 5**,** a012609.

Schauer, G. D. and O'Donnell, M. E. (2017). "Quality control mechanisms exclude incorrect polymerases from the eukaryotic replication fork." *Proc Natl Acad Sci U S A,* 114**,** 675-680.

Scheffner, M., Nuber, U. and Huibregtse, J. M. (1995). "Protein ubiquitination involving an E1-E2-E3 enzyme ubiquitin thioester cascade." *Nature,* 373**,** 81-3.

Schiemann, A. H., Li, F., Weake, V. M., Belikoff, E. J., Klemmer, K. C., Moore, S. A. and Scott, M. J. (2010). "Sex-biased transcription enhancement by a 5' tethered Gal4-MOF histone acetyltransferase fusion protein in Drosophila." *BMC Mol Biol,* 11**,** 80.

Schmidt, C. K., Galanty, Y., Sczaniecka-Clift, M., Coates, J., Jhujh, S., Demir, M., Cornwell, M., Beli, P. and Jackson, S. P. (2015). "Systematic E2 screening reveals a UBE2D-RNF138-CtIP axis promoting DNA repair." *Nat Cell Biol,* 17**,** 1458-70.

Schones, D. E., Cui, K., Cuddapah, S., Roh, T. Y., Barski, A., Wang, Z., Wei, G. and Zhao, K. (2008). "Dynamic regulation of nucleosome positioning in the human genome." *Cell,* 132**,** 887-98.

Schotta, G., Sengupta, R., Kubicek, S., Malin, S., Kauer, M., Callen, E., Celeste, A., Pagani, M., Opravil, S., De La Rosa-Velazquez, I. A., Espejo, A., Bedford, M. T., Nussenzweig, A., Busslinger, M. and Jenuwein, T. (2008). "A chromatin-wide transition to H4K20 monomethylation impairs genome integrity and programmed DNA rearrangements in the mouse." *Genes Dev,* 22**,** 2048-61.

Schreiber, A., Stengel, F., Zhang, Z., Enchev, R. I., Kong, E. H., Morris, E. P., Robinson, C. V., da Fonseca, P. C. and Barford, D. (2011). "Structural basis for the subunit assembly of the anaphase-promoting complex." *Nature,* 470**,** 227-32.

Schunter, S., Villa, R., Flynn, V., Heidelberger, J. B., Classen, A. K., Beli, P. and Becker, P. B. (2017). "Ubiquitylation of the acetyltransferase MOF in Drosophila melanogaster." *PLoS One,* 12**,** e0177408.

Schwaiger, M., Stadler, M. B., Bell, O., Kohler, H., Oakeley, E. J. and Schubeler, D. (2009). "Chromatin state marks cell-type- and gender-specific replication of the Drosophila genome." *Genes Dev,* 23**,** 589-601.

Schwarz, L. A. and Patrick, G. N. (2012). "Ubiquitin-dependent endocytosis, trafficking and turnover of neuronal membrane proteins." *Mol Cell Neurosci,* 49**,** 387-93.

Schwertman, P., Bekker-Jensen, S. and Mailand, N. (2016). "Regulation of DNA double-strand break repair by ubiquitin and ubiquitin-like modifiers." *Nat Rev Mol Cell Biol,* 17**,** 379-94.

Shanbhag, N. M., Rafalska-Metcalf, I. U., Balane-Bolivar, C., Janicki, S. M. and Greenberg, R. A. (2010). "ATM-dependent chromatin changes silence transcription in cis to DNA double-strand breaks." *Cell,* 141**,** 970-81.

Sharma, G. G., So, S., Gupta, A., Kumar, R., Cayrou, C., Avvakumov, N., Bhadra, U., Pandita, R. K., Porteus, M. H., Chen, D. J., Cote, J. and Pandita, T. K. (2010). "MOF and histone H4 acetylation at lysine 16 are critical for DNA damage response and double-strand break repair." *Mol Cell Biol,* 30**,** 3582-95.

Sher, N., Bell, G. W., Li, S., Nordman, J., Eng, T., Eaton, M. L., Macalpine, D. M. and Orr-Weaver, T. L. (2012). "Developmental control of gene copy number by repression of replication initiation and fork progression." *Genome Res,* 22**,** 64-75.

Shiotani, B. and Zou, L. (2009). "Single-stranded DNA orchestrates an ATM-to-ATR switch at DNA breaks." *Mol Cell,* 33**,** 547-58.

Shogren-Knaak, M., Ishii, H., Sun, J. M., Pazin, M. J., Davie, J. R. and Peterson, C. L. (2006). "Histone H4-K16 acetylation controls chromatin structure and protein interactions." *Science,* 311**,** 844-847.

Shogren-Knaak, M. and Peterson, C. L. (2006). "Switching on chromatin: mechanistic role of histone H4-K16 acetylation." *Cell Cycle,* 5**,** 1361-5.

Sibanda, B. L., Chirgadze, D. Y., Ascher, D. B. and Blundell, T. L. (2017). "DNA-PKcs structure suggests an allosteric mechanism modulating DNA double-strand break repair." *Science,* 355**,** 520-524.

Singleton, B. K., Torres-Arzayus, M. I., Rottinghaus, S. T., Taccioli, G. E. and Jeggo, P. A. (1999). "The C terminus of Ku80 activates the DNA-dependent protein kinase catalytic subunit." *Mol Cell Biol,* 19**,** 3267-77.

Smit, J. J., Monteferrario, D., Noordermeer, S. M., van Dijk, W. J., van der Reijden, B. A. and Sixma, T. K. (2012). "The E3 ligase HOIP specifies linear ubiquitin chain assembly through its RING-IBR-RING domain and the unique LDD extension." *EMBO J,* 31**,** 3833-44.

Smith, E. R., Cayrou, C., Huang, R., Lane, W. S., Cote, J. and Lucchesi, J. C. (2005). "A human protein complex homologous to the Drosophila MSL complex is responsible for the majority of histone H4 acetylation at lysine 16." *Mol Cell Biol,* 25**,** 9175-88.

Smith, J., Tho, L. M., Xu, N. and Gillespie, D. A. (2010). "The ATM-Chk2 and ATR-Chk1 pathways in DNA damage signaling and cancer." *Adv Cancer Res,* 108**,** 73-112.

Sobhian, B., Shao, G., Lilli, D. R., Culhane, A. C., Moreau, L. A., Xia, B., Livingston, D. M. and Greenberg, R. A. (2007). "RAP80 targets BRCA1 to specific ubiquitin structures at DNA damage sites." *Science,* 316**,** 1198-202.

Sobol, R. W. and Wilson, S. H. (2001). "Mammalian DNA beta-polymerase in base excision repair of alkylation damage." *Prog Nucleic Acid Res Mol Biol,* 68**,** 57-74.

Sorensen, C. S., Syljuasen, R. G., Lukas, J. and Bartek, J. (2004). "ATR, Claspin and the Rad9-Rad1-Hus1 complex regulate Chk1 and Cdc25A in the absence of DNA damage." *Cell Cycle,* 3**,** 941-5.

Sparks, J. L., Chon, H., Cerritelli, S. M., Kunkel, T. A., Johansson, E., Crouch, R. J. and Burgers, P. M. (2012). "RNase H2-initiated ribonucleotide excision repair." *Mol Cell,* 47**,** 980-6.

Spierer, A., Begeot, F., Spierer, P. and Delattre, M. (2008). "SU(VAR)3-7 links heterochromatin and dosage compensation in Drosophila." *PLoS Genet,* 4**,** e1000066.

Spierer, A., Seum, C., Delattre, M. and Spierer, P. (2005). "Loss of the modifiers of variegation Su(var)3-7 or HP1 impacts male X polytene chromosome morphology and dosage compensation." *J Cell Sci,* 118**,** 5047-57.

Stadler, J. and Richly, H. (2017). "Regulation of DNA Repair Mechanisms: How the Chromatin Environment Regulates the DNA Damage Response." *Int J Mol Sci,* 18.

Stauffer, M. E. and Chazin, W. J. (2004). "Physical interaction between replication protein A and Rad51 promotes exchange on single-stranded DNA." *J Biol Chem,* 279**,** 25638-45.

Stewart, G. S., Panier, S., Townsend, K., Al-Hakim, A. K., Kolas, N. K., Miller, E. S., Nakada, S., Ylanko, J., Olivarius, S., Mendez, M., Oldreive, C., Wildenhain, J., Tagliaferro, A., Pelletier, L., Taubenheim, N., Durandy, A., Byrd, P. J., Stankovic, T., Taylor, A. M. R. and Durocher, D. (2009). "The RIDDLE Syndrome Protein Mediates a Ubiquitin-Dependent Signaling Cascade at Sites of DNA Damage." *Cell,* 136**,** 420-434.

Stewart, G. S., Wang, B., Bignell, C. R., Taylor, A. M. and Elledge, S. J. (2003). "MDC1 is a mediator of the mammalian DNA damage checkpoint." *Nature,* 421**,** 961-6.

Stieglitz, B., Morris-Davies, A. C., Koliopoulos, M. G., Christodoulou, E. and Rittinger, K. (2012). "LUBAC synthesizes linear ubiquitin chains via a thioester intermediate." *EMBO Rep,* 13**,** 840-6.

Stiff, T., Walker, S. A., Cerosaletti, K., Goodarzi, A. A., Petermann, E., Concannon, P., O'Driscoll, M. and Jeggo, P. A. (2006). "ATR-dependent phosphorylation and activation of ATM in response to UV treatment or replication fork stalling." *EMBO J,* 25**,** 5775-82.

Strahl, B. D. and Allis, C. D. (2000). "The language of covalent histone modifications." *Nature,* 403**,** 41-5.

Straub, T. and Becker, P. B. (2007). "Dosage compensation: the beginning and end of generalization." *Nat Rev Genet,* 8**,** 47-57.

Straub, T., Gilfillan, G. D., Maier, V. K. and Becker, P. B. (2005). "The Drosophila MSL complex activates the transcription of target genes." *Genes Dev,* 19**,** 2284-8.

Straub, T., Grimaud, C., Gilfillan, G. D., Mitterweger, A. and Becker, P. B. (2008). "The chromosomal high-affinity binding sites for the Drosophila dosage compensation complex." *PLoS Genet,* 4**,** e1000302.

Strober, W. (2001). "Monitoring cell growth." *Curr Protoc Immunol,* Appendix 3**,** Appendix 3A.

Strzalka, W. and Ziemienowicz, A. (2011). "Proliferating cell nuclear antigen (PCNA): a key factor in DNA replication and cell cycle regulation." *Ann Bot,* 107**,** 1127-40.

Stucki, M., Clapperton, J. A., Mohammad, D., Yaffe, M. B., Smerdon, S. J. and Jackson, S. P. (2005). "MDC1 directly binds phosphorylated histone H2AX to regulate cellular responses to DNA double-strand breaks." *Cell,* 123**,** 1213-26.

Su, J., Wang, F., Cai, Y. and Jin, J. (2016). "The Functional Analysis of Histone Acetyltransferase MOF in Tumorigenesis." *Int J Mol Sci,* 17.

Suganuma, T., Gutierrez, J. L., Li, B., Florens, L., Swanson, S. K., Washburn, M. P., Abmayr, S. M. and Workman, J. L. (2008). "ATAC is a double histone acetyltransferase complex that stimulates nucleosome sliding." *Nat Struct Mol Biol,* 15**,** 364-72.

Sugiyama, T. and Kowalczykowski, S. C. (2002). "Rad52 protein associates with replication protein A (RPA)-single-stranded DNA to accelerate Rad51-mediated displacement of RPA and presynaptic complex formation." *J Biol Chem,* 277**,** 31663-72.

Sulli, G., Di Micco, R. and d'Adda di Fagagna, F. (2012). "Crosstalk between chromatin state and DNA damage response in cellular senescence and cancer." *Nat Rev Cancer,* 12**,** 709-20.

Sun, J. and Kong, D. (2010). "DNA replication origins, ORC/DNA interaction, and assembly of pre-replication complex in eukaryotes." *Acta Biochim Biophys Sin (Shanghai),* 42**,** 433-9.

Sun, L., Fernandez, H. R., Donohue, R. C., Li, J., Cheng, J. and Birchler, J. A. (2013). "Male-specific lethal complex in Drosophila counteracts histone acetylation and does not mediate dosage compensation." *Proc Natl Acad Sci U S A,* 110**,** E808-17.

Sun, Y., Jiang, X., Chen, S., Fernandes, N. and Price, B. D. (2005). "A role for the Tip60 histone acetyltransferase in the acetylation and activation of ATM." *Proc Natl Acad Sci U S A,* 102**,** 13182-7.

Sun, Y., Jiang, X., Xu, Y., Ayrapetov, M. K., Moreau, L. A., Whetstine, J. R. and Price, B. D. (2009). "Histone H3 methylation links DNA damage detection to activation of the tumour suppressor Tip60." *Nat Cell Biol,* 11**,** 1376-82.

Sun, Y., Xu, Y., Roy, K. and Price, B. D. (2007). "DNA damage-induced acetylation of lysine 3016 of ATM activates ATM kinase activity." *Mol Cell Biol,* 27**,** 8502-9.

Sung, P., Krejci, L., Van Komen, S. and Sehorn, M. G. (2003). "Rad51 recombinase and recombination mediators." *J Biol Chem,* 278**,** 42729-32.

Sural, T. H., Peng, S., Li, B., Workman, J. L., Park, P. J. and Kuroda, M. I. (2008). "The MSL3 chromodomain directs a key targeting step for dosage compensation of the Drosophila melanogaster X chromosome." *Nat Struct Mol Biol,* 15**,** 1318-25.

Sykes, S. M., Mellert, H. S., Holbert, M. A., Li, K., Marmorstein, R., Lane, W. S. and McMahon, S. B. (2006). "Acetylation of the p53 DNA-binding domain regulates apoptosis induction." *Mol Cell,* 24**,** 841-51.

Szymczak, A. L., Workman, C. J., Wang, Y., Vignali, K. M., Dilioglou, S., Vanin, E. F. and Vignali, D. A. (2004). "Correction of multi-gene deficiency in vivo using a single 'self-cleaving' 2A peptide-based retroviral vector." *Nat Biotechnol,* 22**,** 589-94.

Taipale, M., Rea, S., Richter, K., Vilar, A., Lichter, P., Imhof, A. and Akhtar, A. (2005). "HMOF histone acetyltransferase is required for histone H4 lysine 16 acetylation in mammalian cells." *Molecular and Cellular Biology,* 25**,** 6798-6810.

Takizawa, C. G. and Morgan, D. O. (2000). "Control of mitosis by changes in the subcellular location of cyclin-B1-Cdk1 and Cdc25C." *Curr Opin Cell Biol,* 12**,** 658-65.

Tan, M., Luo, H., Lee, S., Jin, F., Yang, J. S., Montellier, E., Buchou, T., Cheng, Z., Rousseaux, S., Rajagopal, N., Lu, Z., Ye, Z., Zhu, Q., Wysocka, J., Ye, Y., Khochbin, S., Ren, B. and Zhao, Y. (2011). "Identification of 67 histone marks and histone lysine crotonylation as a new type of histone modification." *Cell,* 146**,** 1016-28.

Tang, J., Cho, N. W., Cui, G., Manion, E. M., Shanbhag, N. M., Botuyan, M. V., Mer, G. and Greenberg, R. A. (2013). "Acetylation limits 53BP1 association with damaged chromatin to promote homologous recombination." *Nat Struct Mol Biol,* 20**,** 317-25.

Tang, Y., Luo, J., Zhang, W. and Gu, W. (2006). "Tip60-dependent acetylation of p53 modulates the decision between cell-cycle arrest and apoptosis." *Mol Cell,* 24**,** 827-39.

Tasaki, T., Mulder, L. C., Iwamatsu, A., Lee, M. J., Davydov, I. V., Varshavsky, A., Muesing, M. and Kwon, Y. T. (2005). "A family of mammalian E3 ubiquitin ligases that contain the UBR box motif and recognize N-degrons." *Mol Cell Biol,* 25**,** 7120-36.

Taylor, G. C., Eskeland, R., Hekimoglu-Balkan, B., Pradeepa, M. M. and Bickmore, W. A. (2013). "H4K16 acetylation marks active genes and enhancers of embryonic stem cells, but does not alter chromatin compaction." *Genome Res,* 23**,** 2053-65.

Teo, G., Liu, G., Zhang, J., Nesvizhskii, A. I., Gingras, A. C. and Choi, H. (2014). "SAINTexpress: improvements and additional features in Significance Analysis of INTeractome software." *J Proteomics,* 100**,** 37-43.

Tessarz, P. and Kouzarides, T. (2014). "Histone core modifications regulating nucleosome structure and dynamics." *Nat Rev Mol Cell Biol,* 15**,** 703-8.

Thole, T. M., Lodrini, M., Fabian, J., Wuenschel, J., Pfeil, S., Hielscher, T., Kopp-Schneider, A., Heinicke, U., Fulda, S., Witt, O., Eggert, A., Fischer, M. and Deubzer, H. E. (2017). "Neuroblastoma cells depend on HDAC11 for mitotic cell cycle progression and survival." *Cell Death Dis,* 8**,** e2635.

Thomas, T., Dixon, M. P., Kueh, A. J. and Voss, A. K. (2008). "Mof (MYST1 or KAT8) is essential for progression of embryonic development past the blastocyst stage and required for normal chromatin architecture." *Mol Cell Biol,* 28**,** 5093-105.

Thorne, A. W., Sautiere, P., Briand, G. and Crane-Robinson, C. (1987). "The structure of ubiquitinated histone H2B." *EMBO J,* 6**,** 1005-10.

Thorslund, T., Ripplinger, A., Hoffmann, S., Wild, T., Uckelmann, M., Villumsen, B., Narita, T., Sixma, T. K., Choudhary, C., Bekker-Jensen, S. and Mailand, N. (2015). "Histone H1 couples initiation and amplification of ubiquitin signalling after DNA damage." *Nature,* 527**,** 389-93.

Thorsteinsdottir, U., Kroon, E., Jerome, L., Blasi, F. and Sauvageau, G. (2001). "Defining roles for HOX and MEIS1 genes in induction of acute myeloid leukemia." *Mol Cell Biol,* 21**,** 224-34.

Toth, J., Varga, B., Kovacs, M., Malnasi-Csizmadia, A. and Vertessy, B. G. (2007). "Kinetic mechanism of human dUTPase, an essential nucleotide pyrophosphatase enzyme." *J Biol Chem,* 282**,** 33572-82.

Trowitzsch, S., Bieniossek, C., Nie, Y., Garzoni, F. and Berger, I. (2010). "New baculovirus expression tools for recombinant protein complex production." *J Struct Biol,* 172**,** 45-54.

Trowitzsch, S., Palmberger, D., Fitzgerald, D., Takagi, Y. and Berger, I. (2012). "MultiBac complexomics." *Expert Rev Proteomics,* 9**,** 363-73.

Unoki, M., Masuda, A., Dohmae, N., Arita, K., Yoshimatsu, M., Iwai, Y., Fukui, Y., Ueda, K., Hamamoto, R., Shirakawa, M., Sasaki, H. and Nakamura, Y. (2013). "Lysyl 5-hydroxylation, a novel histone modification, by Jumonji domain containing 6 (JMJD6)." *J Biol Chem,* 288**,** 6053-62.

Urbe, S. (2005). "Ubiquitin and endocytic protein sorting." *Essays Biochem,* 41**,** 81-98.

Utley, R. T. and Cote, J. (2003). "The MYST family of histone acetyltransferases." *Curr Top Microbiol Immunol,* 274**,** 203-36.

Valton, A. L., Hassan-Zadeh, V., Lema, I., Boggetto, N., Alberti, P., Saintome, C., Riou, J. F. and Prioleau, M. N. (2014). "G4 motifs affect origin positioning and efficiency in two vertebrate replicators." *EMBO J,* 33**,** 732-46.

Vander Kooi, C. W., Ohi, M. D., Rosenberg, J. A., Oldham, M. L., Newcomer, M. E., Gould, K. L. and Chazin, W. J. (2006). "The Prp19 U-box crystal structure suggests a common dimeric architecture for a class of oligomeric E3 ubiquitin ligases." *Biochemistry,* 45**,** 121-30.

Vaquerizas, J. M., Suyama, R., Kind, J., Miura, K., Luscombe, N. M. and Akhtar, A. (2010). "Nuclear pore proteins nup153 and megator define transcriptionally active regions in the Drosophila genome." *PLoS Genet,* 6**,** e1000846.

Vashee, S., Cvetic, C., Lu, W., Simancek, P., Kelly, T. J. and Walter, J. C. (2003). "Sequence-independent DNA binding and replication initiation by the human origin recognition complex." *Genes Dev,* 17**,** 1894-908.

Ventii, K. H. and Wilkinson, K. D. (2008). "Protein partners of deubiquitinating enzymes." *Biochem J,* 414**,** 161-75.

Vignard, J., Mirey, G. and Salles, B. (2013). "Ionizing-radiation induced DNA double-strand breaks: a direct and indirect lighting up." *Radiother Oncol,* 108**,** 362-9.

Vijayachandran, L. S., Viola, C., Garzoni, F., Trowitzsch, S., Bieniossek, C., Chaillet, M., Schaffitzel, C., Busso, D., Romier, C., Poterszman, A., Richmond, T. J. and Berger, I. (2011). "Robots, pipelines, polyproteins: enabling multiprotein expression in prokaryotic and eukaryotic cells." *J Struct Biol,* 175**,** 198-208.

Villa, R., Forne, I., Muller, M., Imhof, A., Straub, T. and Becker, P. B. (2012). "MSL2 combines sensor and effector functions in homeostatic control of the Drosophila dosage compensation machinery." *Mol Cell,* 48**,** 647-54.

Vissers, J. H., Nicassio, F., van Lohuizen, M., Di Fiore, P. P. and Citterio, E. (2008). "The many faces of ubiquitinated histone H2A: insights from the DUBs." *Cell Div,* 3**,** 8.

Volle, C. and Dalal, Y. (2014). "Histone variants: the tricksters of the chromatin world." *Curr Opin Genet Dev,* 25**,** 8-14,138.

Walker, J. R., Corpina, R. A. and Goldberg, J. (2001). "Structure of the Ku heterodimer bound to DNA and its implications for double-strand break repair." *Nature,* 412**,** 607-14.

Walker, M., Black, E. J., Oehler, V., Gillespie, D. A. and Scott, M. T. (2009). "Chk1 C-terminal regulatory phosphorylation mediates checkpoint activation by de-repression of Chk1 catalytic activity." *Oncogene,* 28**,** 2314-23.

Wallace, J. A. and Orr-Weaver, T. L. (2005). "Replication of heterochromatin: insights into mechanisms of epigenetic inheritance." *Chromosoma,* 114**,** 389-402.

Wang, H., Wang, L., Erdjument-Bromage, H., Vidal, M., Tempst, P., Jones, R. S. and Zhang, Y. (2004). "Role of histone H2A ubiquitination in Polycomb silencing." *Nature,* 431**,** 873-8.

Wang, H., Zhai, L., Xu, J., Joo, H. Y., Jackson, S., Erdjument-Bromage, H., Tempst, P., Xiong, Y. and Zhang, Y. (2006). "Histone H3 and H4 ubiquitylation by the CUL4-DDB-ROC1 ubiquitin ligase facilitates cellular response to DNA damage." *Mol Cell,* 22**,** 383-94.

Wang, T., Yin, L., Cooper, E. M., Lai, M. Y., Dickey, S., Pickart, C. M., Fushman, D., Wilkinson, K. D., Cohen, R. E. and Wolberger, C. (2009). "Evidence for bidentate substrate binding as the basis for the K48 linkage specificity of otubain 1." *J Mol Biol,* 386**,** 1011-23.

Wang, X., Herr, R. A., Chua, W. J., Lybarger, L., Wiertz, E. J. and Hansen, T. H. (2007). "Ubiquitination of serine, threonine, or lysine residues on the cytoplasmic tail can induce ERAD of MHC-I by viral E3 ligase mK3." *J Cell Biol,* 177**,** 613-24.

Wang, Z., Zang, C., Rosenfeld, J. A., Schones, D. E., Barski, A., Cuddapah, S., Cui, K., Roh, T. Y., Peng, W., Zhang, M. Q. and Zhao, K. (2008). "Combinatorial patterns of histone acetylations and methylations in the human genome." *Nat Genet,* 40**,** 897-903.

Ward, I. M. and Chen, J. (2001). "Histone H2AX is phosphorylated in an ATR-dependent manner in response to replicational stress." *J Biol Chem,* 276**,** 47759-62.

Ward, I. M., Minn, K. and Chen, J. (2004). "UV-induced ataxia-telangiectasia-mutated and Rad3-related (ATR) activation requires replication stress." *J Biol Chem,* 279**,** 9677-80.

Wei, Z., Liu, C., Wu, X., Xu, N., Zhou, B., Liang, C. and Zhu, G. (2010). "Characterization and structure determination of the Cdt1 binding domain of human minichromosome maintenance (Mcm) 6." *J Biol Chem,* 285**,** 12469-73.

Wenzel, D. M., Lissounov, A., Brzovic, P. S. and Klevit, R. E. (2011a). "UBCH7 reactivity profile reveals parkin and HHARI to be RING/HECT hybrids." *Nature,* 474**,** 105-8.

Wenzel, D. M., Stoll, K. E. and Klevit, R. E. (2011b). "E2s: structurally economical and functionally replete." *Biochem J,* 433**,** 31-42.

Werner, M. and Ruthenburg, A. J. (2011). "The United States of histone ubiquitylation and methylation." *Mol Cell,* 43**,** 5-7.

West, M. H. and Bonner, W. M. (1980). "Histone 2B can be modified by the attachment of ubiquitin." *Nucleic Acids Res,* 8**,** 4671-80.

Wilkinson, K. D. (1987). "Protein ubiquitination: a regulatory post-translational modification." *Anticancer Drug Des,* 2**,** 211-29.

Williams, J. S., Lujan, S. A. and Kunkel, T. A. (2016). "Processing ribonucleotides incorporated during eukaryotic DNA replication." *Nat Rev Mol Cell Biol,* 17**,** 350-63.

Wilson, M. D., Benlekbir, S., Fradet-Turcotte, A., Sherker, A., Julien, J. P., McEwan, A., Noordermeer, S. M., Sicheri, F., Rubinstein, J. L. and Durocher, D. (2016). "The structural basis of modified nucleosome recognition by 53BP1." *Nature,* 536**,** 100-3.

Windheim, M., Peggie, M. and Cohen, P. (2008). "Two different classes of E2 ubiquitin-conjugating enzymes are required for the mono-ubiquitination of

proteins and elongation by polyubiquitin chains with a specific topology." *Biochem J,* 409**,** 723-9.

Wolf, E., Vassilev, A., Makino, Y., Sali, A., Nakatani, Y. and Burley, S. K. (1998). "Crystal structure of a GCN5-related N-acetyltransferase: Serratia marcescens aminoglycoside 3-N-acetyltransferase." *Cell,* 94**,** 439-49.

Wong, J. M., Ionescu, D. and Ingles, C. J. (2003). "Interaction between BRCA2 and replication protein A is compromised by a cancer-predisposing mutation in BRCA2." *Oncogene,* 22**,** 28-33.

Wong, M. M., Cox, L. K. and Chrivia, J. C. (2007). "The chromatin remodeling protein, SRCAP, is critical for deposition of the histone variant H2A.Z at promoters." *J Biol Chem,* 282**,** 26132-9.

Wu, J., Huen, M. S., Lu, L. Y., Ye, L., Dou, Y., Ljungman, M., Chen, J. and Yu, X. (2009). "Histone ubiquitination associates with BRCA1-dependent DNA damage response." *Mol Cell Biol,* 29**,** 849-60.

Wu, L. and Hickson, I. D. (2003). "The Bloom's syndrome helicase suppresses crossing over during homologous recombination." *Nature,* 426**,** 870-4.

Wu, L., Li, L., Zhou, B., Qin, Z. and Dou, Y. (2014a). "H2B ubiquitylation promotes RNA Pol II processivity via PAF1 and pTEFb." *Mol Cell,* 54**,** 920-31.

Wu, L., Zee, B. M., Wang, Y., Garcia, B. A. and Dou, Y. (2011). "The RING finger protein MSL2 in the MOF complex is an E3 ubiquitin ligase for H2B K34 and is involved in crosstalk with H3 K4 and K79 methylation." *Mol Cell,* 43**,** 132-44.

Wu, Z., Liu, J., Yang, H. and Xiang, H. (2014b). "DNA replication origins in archaea." *Front Microbiol,* 5**,** 179.

Xu, Z., Kohli, E., Devlin, K. I., Bold, M., Nix, J. C. and Misra, S. (2008). "Interactions between the quality control ubiquitin ligase CHIP and ubiquitin conjugating enzymes." *BMC Struct Biol,* 8**,** 26.

Yang, X. J. (2004). "The diverse superfamily of lysine acetyltransferases and their roles in leukemia and other diseases." *Nucleic Acids Res,* 32**,** 959-76.

Yano, K., Morotomi-Yano, K. and Akiyama, H. (2009). "Cernunnos/XLF: a new player in DNA double-strand break repair." *Int J Biochem Cell Biol,* 41**,** 1237-40.

Ye, Y. and Rape, M. (2009). "Building ubiquitin chains: E2 enzymes at work." *Nat Rev Mol Cell Biol,* 10**,** 755-64.

Yeeles, J. T., Deegan, T. D., Janska, A., Early, A. and Diffley, J. F. (2015). "Regulated eukaryotic DNA replication origin firing with purified proteins." *Nature,* 519**,** 431-5.

Yoon, H. G., Chan, D. W., Reynolds, A. B., Qin, J. and Wong, J. (2003). "N-CoR mediates DNA methylation-dependent repression through a methyl CpG binding protein Kaiso." *Mol Cell,* 12**,** 723-34.

You, A., Tong, J. K., Grozinger, C. M. and Schreiber, S. L. (2001). "CoREST is an integral component of the CoREST- human histone deacetylase complex." *Proc Natl Acad Sci U S A,* 98**,** 1454-8.

Yuan, H., Rossetto, D., Mellert, H., Dang, W., Srinivasan, M., Johnson, J., Hodawadekar, S., Ding, E. C., Speicher, K., Abshiru, N., Perry, R., Wu, J., Yang, C., Zheng, Y. G., Speicher, D. W., Thibault, P., Verreault, A., Johnson, F. B., Berger, S. L., Sternglanz, R., McMahon, S. B., Cote, J. and Marmorstein, R. (2012). "MYST protein acetyltransferase activity requires active site lysine autoacetylation." *EMBO J,* 31**,** 58-70.

Zee, B. M., Levin, R. S., DiMaggio, P. A. and Garcia, B. A. (2010). "Global turnover of histone post-translational modifications and variants in human cells." *Epigenetics Chromatin,* 3**,** 22.

Zegerman, P., Canas, B., Pappin, D. and Kouzarides, T. (2002). "Histone H3 lysine 4 methylation disrupts binding of nucleosome remodeling and deacetylase (NuRD) repressor complex." *J Biol Chem,* 277**,** 11621-4.

Zeman, M. K. and Cimprich, K. A. (2014). "Causes and consequences of replication stress." *Nat Cell Biol,* 16**,** 2-9.

Zentner, G. E. and Henikoff, S. (2013). "Regulation of nucleosome dynamics by histone modifications." *Nat Struct Mol Biol,* 20**,** 259-66.

Zhang, J., Bao, S., Furumai, R., Kucera, K. S., Ali, A., Dean, N. M. and Wang, X. F. (2005). "Protein phosphatase 5 is required for ATR-mediated checkpoint activation." *Mol Cell Biol,* 25**,** 9910-9.

Zhang, L., Fairall, L., Goult, B. T., Calkin, A. C., Hong, C., Millard, C. J., Tontonoz, P. and Schwabe, J. W. (2011a). "The IDOL-UBE2D complex mediates sterol-dependent degradation of the LDL receptor." *Genes Dev,* 25**,** 1262-74.

Zhang, Y., Ng, H. H., Erdjument-Bromage, H., Tempst, P., Bird, A. and Reinberg, D. (1999). "Analysis of the NuRD subunits reveals a histone deacetylase core complex and a connection with DNA methylation." *Genes Dev,* 13**,** 1924-35.

Zhang, Z., Tan, M., Xie, Z., Dai, L., Chen, Y. and Zhao, Y. (2011b). "Identification of lysine succinylation as a new post-translational modification." *Nat Chem Biol,* 7**,** 58-63.

Zheng, S., Wang, J., Feng, Y., Wang, J. and Ye, K. (2012). "Solution structure of MSL2 CXC domain reveals an unusual Zn3Cys9 cluster and similarity to pre-SET domains of histone lysine methyltransferases." *PLoS One,* 7**,** e45437.

Zheng, Y., Huang, X. and Kelleher, N. L. (2016). "Epiproteomics: quantitative analysis of histone marks and codes by mass spectrometry." *Curr Opin Chem Biol,* 33**,** 142-50.

Zheng, Y., Thomas, P. M. and Kelleher, N. L. (2013). "Measurement of acetylation turnover at distinct lysines in human histones identifies long-lived acetylation sites." *Nat Commun,* 4**,** 2203.

Zhou, C. Y., Johnson, S. L., Gamarra, N. I. and Narlikar, G. J. (2016). "Mechanisms of ATP-Dependent Chromatin Remodeling Motors." *Annu Rev Biophys,* 45**,** 153-81.

Zhou, W., Zhu, P., Wang, J., Pascual, G., Ohgi, K. A., Lozach, J., Glass, C. K. and Rosenfeld, M. G. (2008). "Histone H2A monoubiquitination represses transcription by inhibiting RNA polymerase II transcriptional elongation." *Mol Cell,* 29**,** 69-80.

Zhou, Y. G., Schmitz, K. M., Mayer, C., Yuan, X. J., Akhtar, A. and Grummt, I. (2009). "Reversible acetylation of the chromatin remodelling complex NoRC is required for non-coding RNA-dependent silencing." *Nature Cell Biology,* 11**,** 1010-U229.

Zhu, B., Zheng, Y., Pham, A. D., Mandal, S. S., Erdjument-Bromage, H., Tempst, P. and Reinberg, D. (2005). "Monoubiquitination of human histone H2B: the factors involved and their roles in HOX gene regulation." *Mol Cell,* 20**,** 601-11.

Zhu, P., Zhou, W., Wang, J., Puc, J., Ohgi, K. A., Erdjument-Bromage, H., Tempst, P., Glass, C. K. and Rosenfeld, M. G. (2007). "A histone H2A deubiquitinase

complex coordinating histone acetylation and H1 dissociation in transcriptional regulation." *Mol Cell,* 27**,** 609-21.

Zimmermann, M., Lottersberger, F., Buonomo, S. B., Sfeir, A. and de Lange, T. (2013). "53BP1 regulates DSB repair using Rif1 to control 5' end resection." *Science,* 339**,** 700-4.

Zippo, A., Serafini, R., Rocchigiani, M., Pennacchini, S., Krepelova, A. and Oliviero, S. (2009). "Histone Crosstalk between H3S10ph and H4K16ac Generates a Histone Code that Mediates Transcription Elongation." *Cell,* 138**,** 1122-1136.

Zou, L. and Elledge, S. J. (2003). "Sensing DNA damage through ATRIP recognition of RPA-ssDNA complexes." *Science,* 300**,** 1542-8.

Zou, L., Liu, D. and Elledge, S. J. (2003). "Replication protein A-mediated recruitment and activation of Rad17 complexes." *Proc Natl Acad Sci U S A,* 100**,** 13827-32.

Appendices

Appendix 1 - MSL2 and MSL1 antibody optimization

MSL2 in-house antibody

In house MSL2 mouse monoclonal antibody was generated by Dr. Simona Moravcova. MSL2 peptide sequence between 86-412 expressed in *E.coli* and sent for immunization to Dundee Cell. To identify the binding sites for MSL in vitro expression was carried out using overlapping protein fraction from the peptide sequence the antibody was raised against (Figure A 1).

Coding sequences for each fragment were amplified with an *XhoI* and *SpeI* restriction enzyme containing overhang and following digestion were inserted into pET-41a(+) plasmid. Protein expression was performed in *E.coli* cells at 25^{o}C. Protein expression was induced in one half of the samples using 2 mM IPTG. 2 h after induction cells were pelleted and lysed using Lysis buffer and protein extracts were subjected to western blot analysis (Figure A 1).

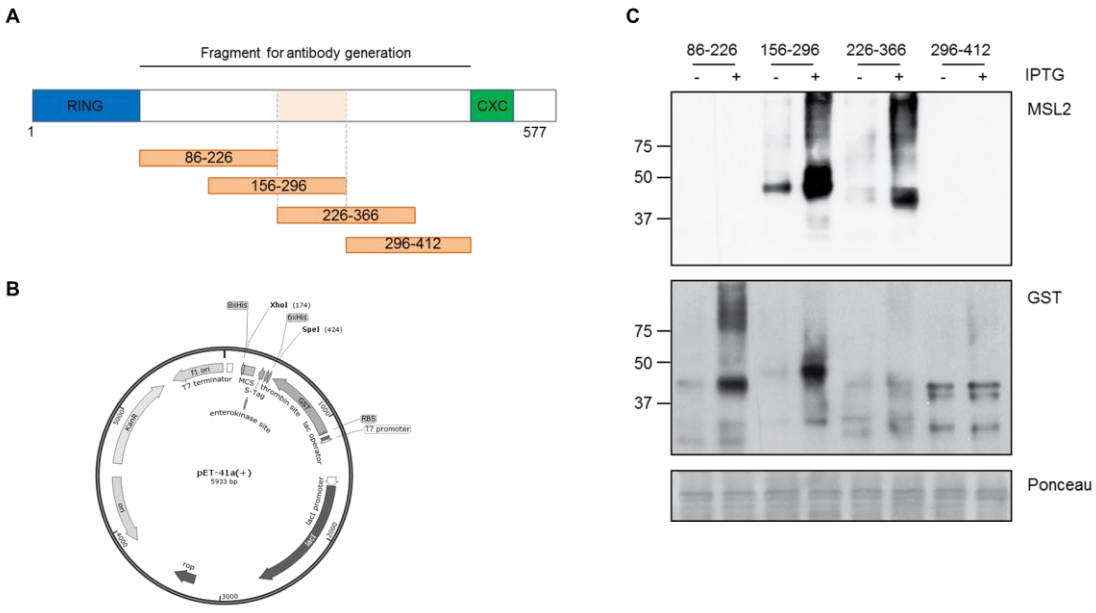

Figure A 1: MSL2 antibody binding site identification. A) Peptide sequences generated for binding site identification with overlapping regions. Fragmented line shows the identified binding region. B) Plasmid map for protein expression in *E. coli* with N-terminal GST tag. C) Western blot analysis for binding site identification. GST blot shows fragment expression with and without IPTG induction. MSL2 blot shows which fragments are recognised by the antibody.

The analysis revealed that the MSL2 antibody binding site is within the 226 and 296 peptide region. The experiment with the exception of the primer design was carried out by Alan O'Dwyer.

However, the antibody did not show reliability in western blots using human cell extracts or for immunofluorescence analysis (figure not shown). While the monoclonal antibody was able to specifically bind MSL2 using in vitro expressed peptides (Figure A 11).

From the same peptide sequence an antigen that containing aminoacids 100-460 of the human protein was later used for immunization in rabbit in collaboration with Dr. Raimundo Freire (Unidad de Investigación, Hospital Universitario de Canarias, Tenerife, Spain). The affinity purified polyclonal antibody (1:300 dilution in 2% milk with overnight incubation) was in a western blot analysis probed against RPE-1 nuclear protein extracts (Figure A 2). The obtained result showed that the affinity purified antibody in combination with cellular frationation enables the detection of endogenous MSL2 protein. As expected, there was no detectable MSL2 signal in the RPE-1 *MSL2*$^{-/-}$ cell line. In addition *MSL1*$^{-/-}$ cells showed a lower level of MSL2 expression in comparison to wild type cells which could possibly due to the disruption of the MSL complex. This will be a very useful tool for future works on MSL2, but further experiments are required to validate the antibody in different assays.

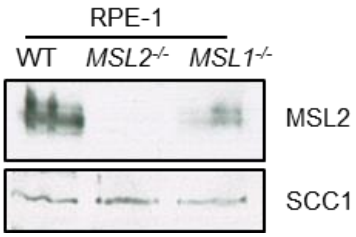

Figure A 2:Affinity purified polyclonal MSL2 antibody test. Nuclear protein extracts from RPE-1 WT *MSL2*$^{-/-}$ and *MSL1*$^{-/-}$ cells were subjected to western blot analysis using affinity purified rabbit MSL2polyclonal antibody.

MSL1 in house antibody

MSL1polyclonal rabbit antibody raised against human MSL1 showed similarly poor specificity for western blot using human protein extracts, but was found to bind with high affinity to a recombinant 6His-mMsl1 construct used as control (Figure A 3). This antibody was used only for in vitro expressed MSL1 in further experiments.

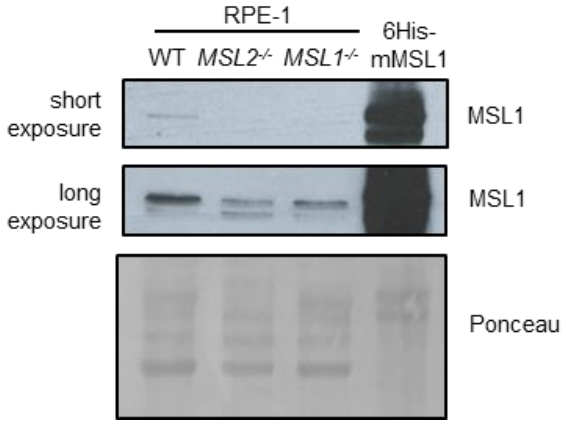

Figure A 3: *In house* polyclonal MSL1 antibody test. Whole cell RPE-1 WT *MSL2*$^{-/-}$ and *MSL1*$^{-/-}$ cells were subjected to western blot analysis using *in house* MSL1 antibody. As positive control recombinant 6His-mMsl1 construct generated using baculoviral infection and expressed in High Five insect cells was used.

Appendix 2 – Expanded IRIF foci formation images

γH2A.X IRIF foci formation

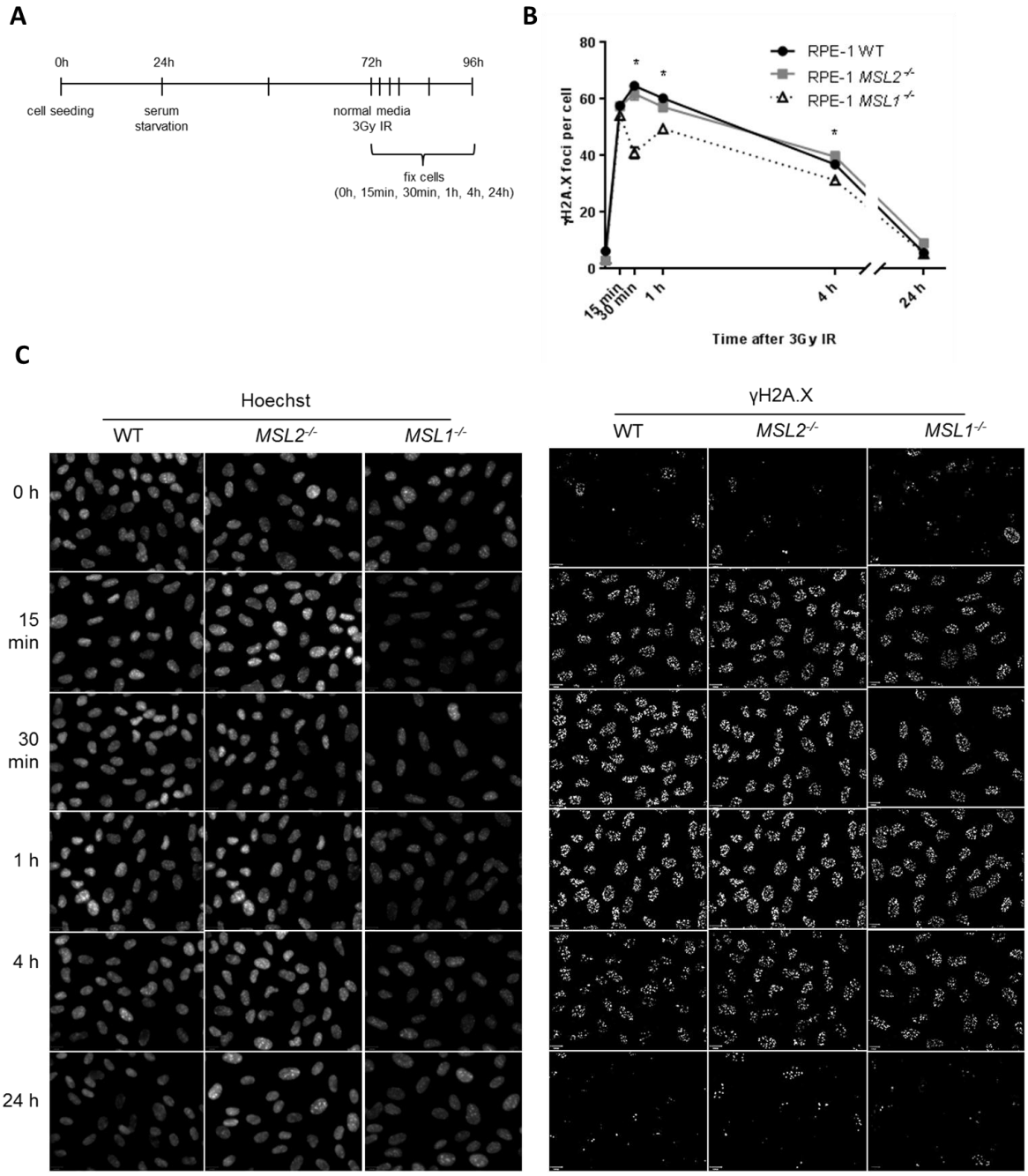

Figure A 4: γH2A.X IRIF foci formation. A) Schematic representation of the IRIF experimental setup. B) Quantification of the number of γH2A.X foci per cell after 3Gy IR (n=3). Error bars represent 95% CI. Asterix represents significant difference between measurements. Statistical analysis was performed using one-way ANOVA and Dunn's multiple comparison tests. Detailed significances are as followed: 30min: WT vs. *MSL1*$^{-/-}$ ****, *MSL2*$^{-/-}$ vs. *MSL1*$^{-/-}$ ****; 1h: WT vs. *MSL1*$^{-/-}$ ****, *MSL2*$^{-/-}$ vs. *MSL1*$^{-/-}$**; 4h: WT vs. *MSL1*$^{-/-}$ *, *MSL2*$^{-/-}$ vs. *MSL1*$^{-/-}$ **. P value: (0.0332)*, (0.0021)**, (<0.0001)****. C) γH2A.X foci formation in wild type and *MSL2*$^{-/-}$ RPE-1 cells. Scale bar indicates 12 µm.

MDC1 IRIF foci formation

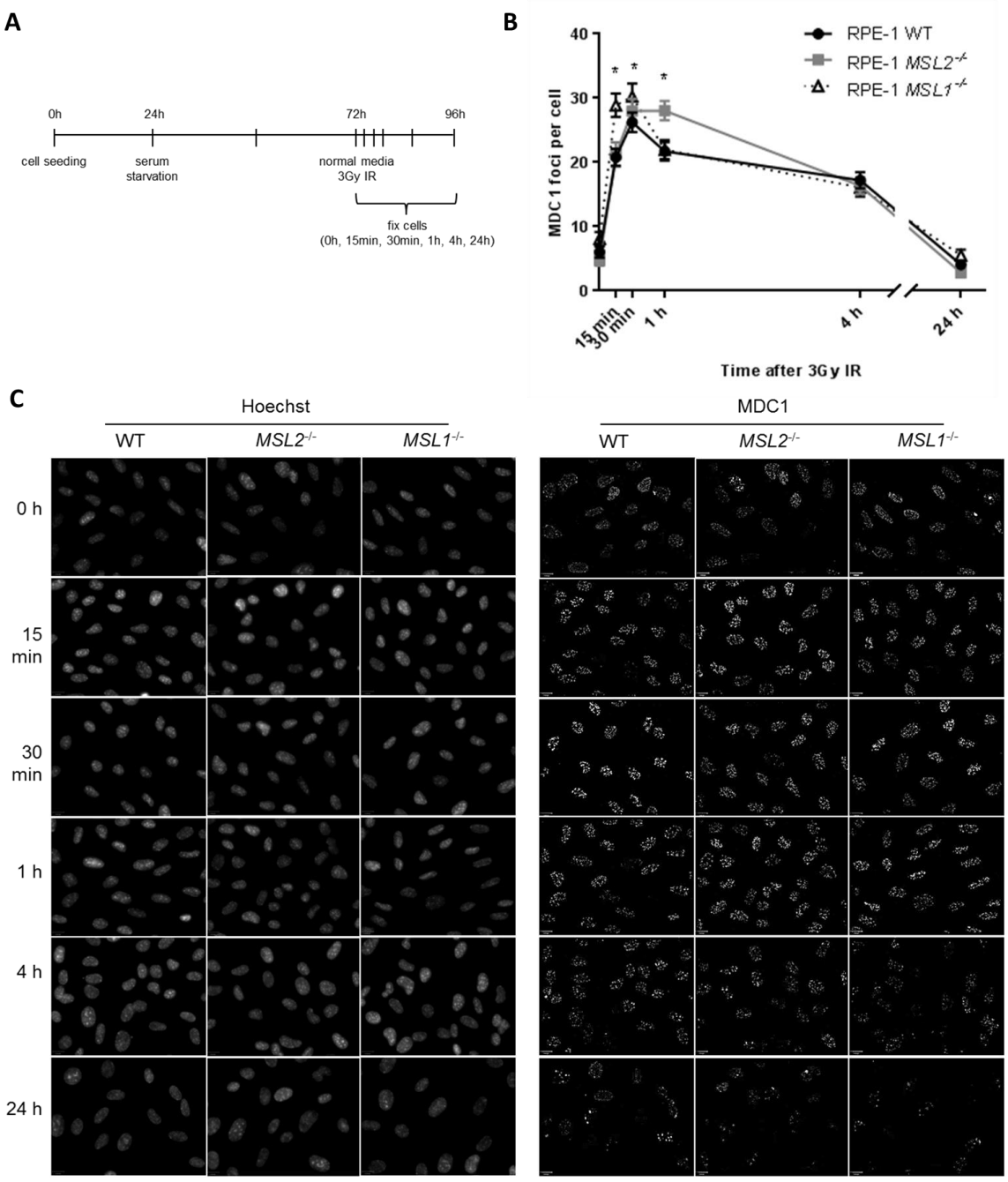

Figure A 5: MDC1 IRIF foci formation. A) Schematic representation of the IR IF experimental setup. B) MDC1 foci formation after IR (n=3). Error bars represent 95% CI. Asterix represents significant difference between measurements. Statistical analysis was performed using one-way ANOVA and Dunn's multiple comparison tests. Detailed significances are as followed: 15min: WT vs. *MSL1*$^{-/-}$ ****, *MSL2*$^{-/-}$ vs. *MSL1*$^{-/-}$ ****; 30min: WT vs. *MSL1*$^{-/-}$ **, 1h: WT vs. *MSL2*$^{-/-}$ ****, *MSL2*$^{-/-}$ vs. *MSL1*$^{-/-}$ ****. P value: (0.0021)**, (<0.0001)****. C) IRIF of MDC1 foci formation in wild type, *MSL2*$^{-/-}$ and *MSL1*$^{-/-}$ RPE-1 cells. Scale bar indicates 12 µm.

BRCA1 IRIF foci formation

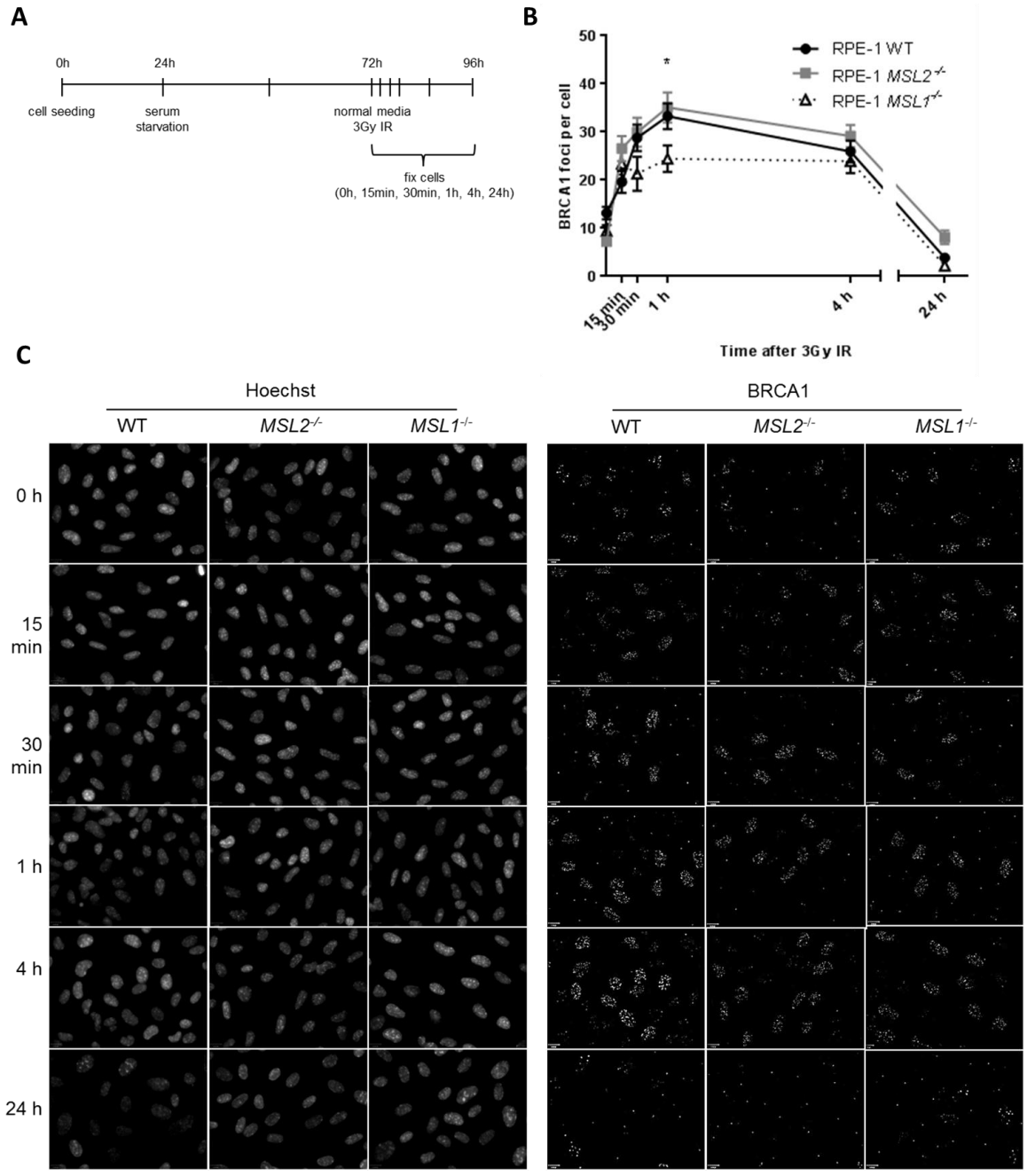

Figure A 6: BRCA1 IRIF foci formation. A) Schematic representation of the IRIF experimental setup. B) BRCA1 foci formation after IR. (n=2). Error bars represent 95% CI. Asterix represents significant difference between measurements. Statistical analysis was performed using one-way ANOVA (nonparametric) and Dunn's multiple comparison tests. Detailed significances are as followed: 1h: WT vs. *MSL1*$^{-/-}$ **, *MSL2*$^{-/-}$ vs. *MSL1*$^{-/-}$ **. P value: (0.0021)**. C) IRIF of BRCA1 foci formation in wild type, *MSL2*$^{-/-}$ and *MSL1*$^{-/-}$ RPE-1 cells. Scale bar indicates 12 µm.

53BP1 IRIF foci formation

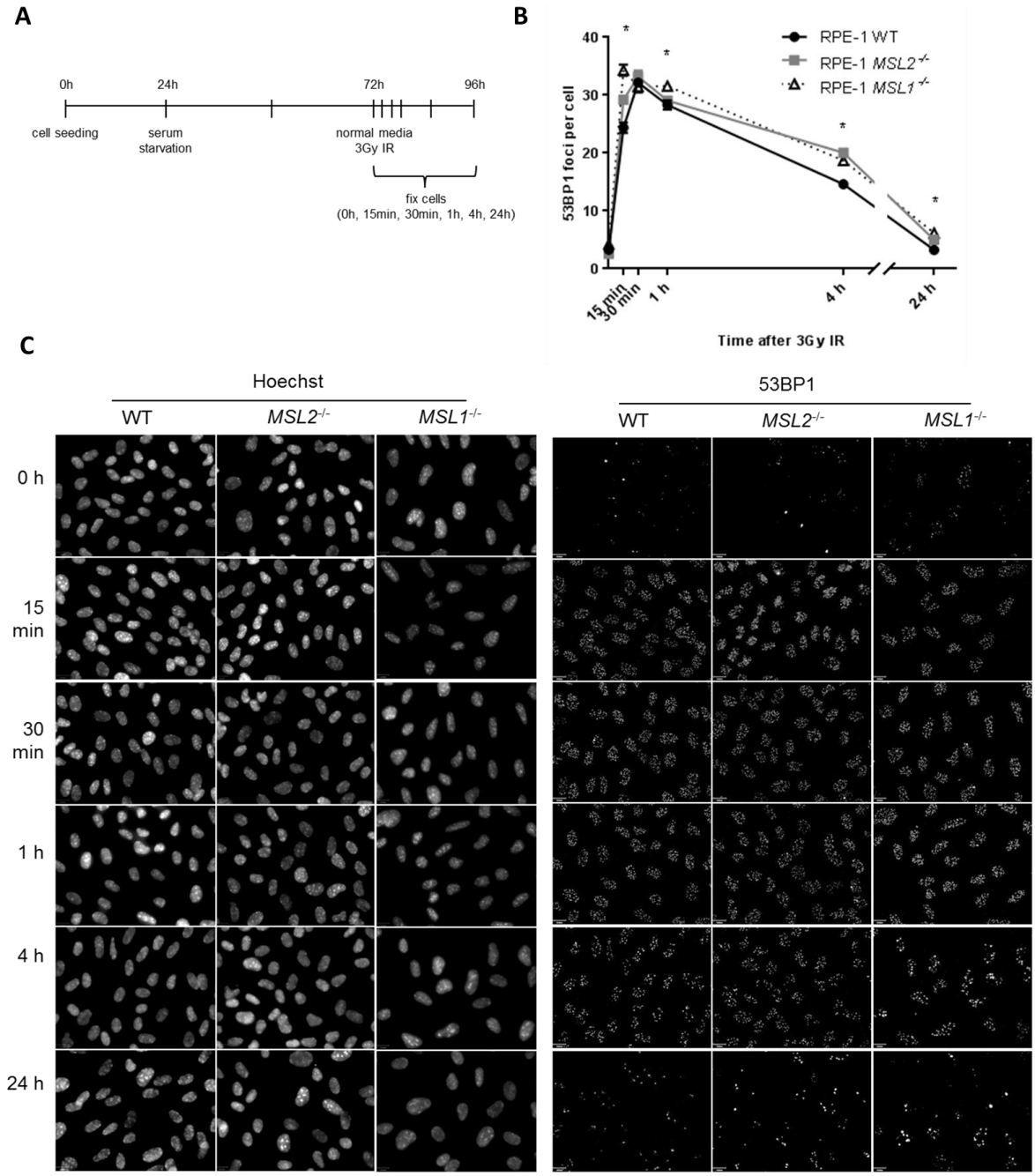

Figure A 7: 53BP1 IRIF foci formation. A) Schematic representation of the IR IF experimental setup. 53BP1 foci formation after IR (n=3). Error bars represent 95% CI. Asterix represents significant difference between measurements. Statistical analysis was performed using one-way ANOVA and Dunn's multiple comparison tests. Detailed significances are as followed: 15min: WT vs. *MSL2*$^{-/-}$ ****, WT vs. *MSL1*$^{-/-}$ ****, *MSL2*$^{-/-}$ vs. *MSL1*$^{-/-}$ ***; 1h: WT vs. *MSL1*$^{-/-}$ **, *MSL2*$^{-/-}$ vs. *MSL1*$^{-/-}$ *; 4h: WT vs. *MSL2*$^{-/-}$ ****, WT vs. *MSL1*$^{-/-}$ ****; 24h: WT vs. *MSL2*$^{-/-}$ **, WT vs. *MSL1*$^{-/-}$ ****. P value: (0,0332)*, (0.0021)**, (<0.0001)****. C) IRIF of MDC1 foci formation in wild type, *MSL2*$^{-/-}$ and *MSL1*$^{-/-}$ RPE-1 cells. Scale bar indicates 12 µm.

Appendix 3 – 53BP1 nuclear body definition

Since there is no defined formula or other markers for 53BP1 identification and definition, in this work nuclear bodies were defined by size exclusion. Nuclear body size in 24 h post irradiated cells were measured and compared with 53BP1 IRIF foci size. To capture all potential nuclear bodies in the analysis a focus was considered as a nuclear body if their area was equal or greater than 0.6 μM^2 (Figure A 8). The size of defining nuclear bodies was based on the smallest foci observed in non-damaged cells to include the maximum number of nuclear bodies for each cell. By choosing this method potential DNA damage foci could also be included in the counting which is indicated by the increased numbers after 15 min, 30 min and 1 h. These timepoints should only contain IRIF foci and the limitation of this strategy should be taken into consideration. Stricter gating methods have also been tested but excluded far too many nuclear bodies form the analysis.

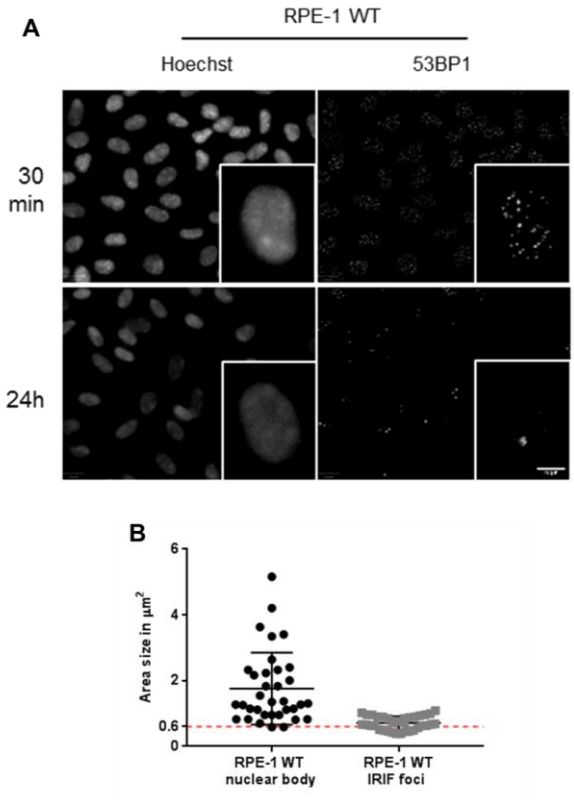

Figure A 8: RPE-1 nuclear body and IRIF foci size measurements. A) Representative image of 53BP1 foci at the indicated timepoints. B) 53BP1 foci area was measured in RPE-1 WT cells at 30 min and 24 h after IR using ImageJ programme. Nuclear bodies were defined using the second smallest area measured at the 24 h timepoint.

Appendix 4 – Endogenously tagged conditional MSL2 cell line generation

In order to generate an endogenously tagged conditional knock-in MSL2 cell line a CRISPR/Cas9 mediated approach was used.

To monitor endogenous MSL2 levels in the absence of a reliable antibody a GFP-MSL2 fusion construct was designed. The expression of GFP also facilitates Immunofluorescence analysis and live-cell imaging. This was further supplemented with the introduction of an auxin-inducible degradation system (Nishimura et al., 2009). Plant-derived TIR1 ubiquitin ligase is able to form an SCF (Skp1–Cullin–F-box) complex with SCF proteins common in eukaryotes. TIR1 determines substrate specificity by recognising a degron peptide derived from the *Arabidopsis thaliana* IAA17 protein (AID). This AID sequence can be conjugated to target proteins for TIR1-SCF mediated polyubiquitylation and subsequent proteasomal degradation (Figure A 9). For the activation and binding of TIR1 the addition of an auxin family hormone such as IAA (indole-3-acetic acid) is required. The protein depletion by this method is very fast, reportedly with a half-life of 10–20min and the process is reversible enabling a temporary conditional depletion (Holland et al., 2012, Natsume et al., 2016).

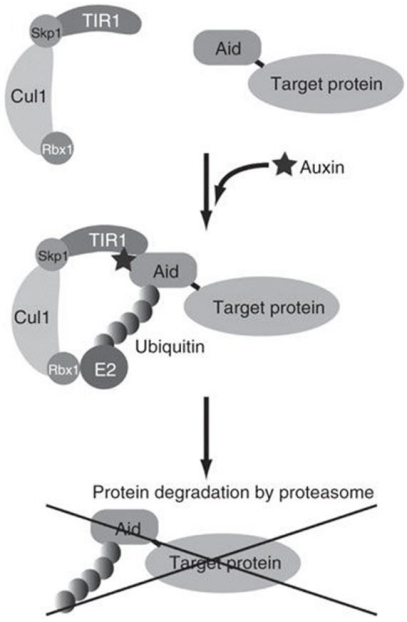

Figure A 9: Schematic illustration of the auxin-inducible protein degradation system. Auxin binding of TIR1 promotes interaction with the AID peptide and promotes polyubiquitylation mediated proteasomal degradation.

For site specific DNA double-strand break induction two guide sequences were introduced to the cells using the px335 Cas9n nickase plasmid. This construct generates 3' overhangs through cutting only one strand at a site. The guide sequences were designed to target the 3' UTR of the MSL2 protein coding region close to the C terminal end of exon 2 and within a 25 bp region from each other. For repair template construct 2.5kb long homology arms were amplified from the *MSL2* encoding exon 2 part and the 3' UTR region. In between the two homology arms the template also contained and AID-GFP construct (Figure A 10 A). The constructs were generated using PCR amplification and were assembled using fusion PCR. The final PCR product was A-tailed and inserted into pGEM-T Easy vector. To decrease the number of plasmids a modified transfection strategy was also used, where the transfected a puromycin resistance coding sequence was inserted into the px330 plasmid after the Cas9 encoding region. The puromycin resistance sequence was separated with a T2A self-cleavage peptide allowing the use of the Cas9 promoter and facilitating cleavage during translation (Szymczak et al., 2004, Kim et al., 2011). Using this single guide a double-strand break was introduced at the C terminal of exon 2 MSL2 sequence.

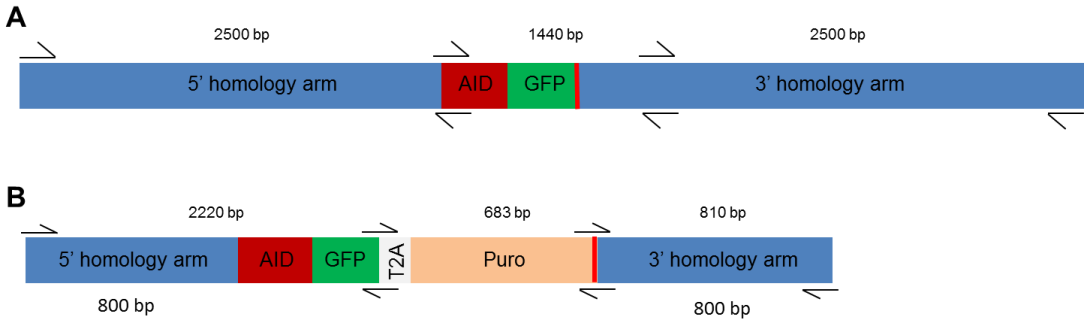

Figure A 10: Homology mediated DNA repair template generation. A) Schematic representation of the homology repair template indicating the PCR fragments generated for fusion PCR with 2500bp homology arms. B) Schematic representation of the modified homology repair template indicating the PCR fragments generated for fusion PCR with T2A-puromycin sequence and 800bp homology arms.

Alternatively a modified repair template has also been generated to contain shorter (800bp) homology arms as well as a puromycin resistance encoding sequence joined to the C-terminal AID-GFP with a T2A sequence (Figure A 10 B). The repair template was PCR amplified in three parts and assembled using sequential fusion PCR

The different CRISPR/Cas9 guide constructs and repair template sequences were transfected into RPE-1, HEK293T and U2OS cells for test expression. While PCR amplification of the repair template showed integration into the genome protein expression was not detectable either in western blot analysis or immunofluorescence assay using GFP antibody. Unfortunately time limitations did not allow further optimisation of this system, but the results obtained are promising and in the future based on this work the generation of an endogenously tagged MSL2 cell line can be executed.

Appendix 5 - In vitro manipulation of the human MSL complex

A1. Introduction

While MSL2 is a known E3 ubiquitin ligase there are very little information on its potential substrates. This project aims to establish an *in vitro* system enabling potential substrate validation identified in the modified BioID assay alongside other experiments and also the identification of MSL2 specific ubiquitylation sites of known substrates. By expressing all four members of the MSL complex the effect of MSL2 on the other subunits and the dynamics of the complex can also be studied in a simplified more controllable environment. Also, while there is evidence that MSL2 ubiquitylates the other members of the MSL complex in *Drosophila* thus maintaining its stoichiometry (Villa et al., 2012) there is no data on how MSL2 affects the acetyltransferase activity of MOF the only other enzymatically active MSL member.

In order to achieve high quality protein expression and facilitate the folding and assembly of the complex a baculoviral protein expression system was used. Proteins expressed and purified with this method will then be used to address the effect of ubiquitylation on the MSL complex by MSL2. Using an *in vitro* ubiquitylation assay, potential substrates will be further analysed. To address the question if the acetylation activity of MOF is affected by MSL2 mediated ubiquitylation two experiments will be performed. First, an *in vitro* ubiquitylation assay will be performed using MSL2 as an E3 ligase and MOF as substrate. This will be followed by an *in vitro* HAT assay using unmodified MOF and MSL2 ubiquitylated MOF where the acetyltransferase activity will be studied.

A2. Baculoviral protein expression system

For recombinant protein expression most commonly *E. coli* based methods are used, and while it is a cheap and easily accessible system providing robust protein expression it has certain limitations, such as folding of expressed proteins might be required after purification and larger plasmid constructs also show sequence instability in the cultured cells (Rosano and Ceccarelli, 2014). However, in recent years a versatile insect-derived (baculoviral) recombinant protein expression system has emerged (Airenne et al., 2013). The *Baculoviridae* family has a circular, double-

stranded DNA genome (80–180 kb) and naturally infect mainly Lepidoptera (butterflies and moth) larvae hosts (Blissard, 1996, Herniou et al., 2003) which makes them a safe delivery system to use. In addition easy manipulation and the ability to carry large (at least 38 kbp) inserts makes baculoviral expression vectors (BEVs) an advantageous choice for several applications (Airenne et al., 2013). Moreover, the insect post-translational machinery enables proper folding of the expressed protein and it also facilitates modification such as phosphorylation (Fernandez, 1999).

Since the purification and proper folding of MSL2 was challenging in previous works performed in the lab, this project will take advantage of the BEV system to provide high quality protein for further applications.

A3. *In vitro* expression of the MSL complex members

For *in vitro* protein expression, two different baculoviral system was used, the standard Bac-to-Bac and the further optimised MultiBac expression method (Luckow, 1993, Trowitzsch et al., 2010, Vijayachandran et al., 2011). As host organisms Sf9, Sf21 and High Five insect cells were used.

A3.1. Plasmid and bacmid generation for Bac-to-Bac system

For the standard Bac-to-Bac expression previously generated 6His tagged mMsl1, Flag tagged MSL3 and HA tagged MOF pFastBac constructs were used. For MSL2 expression, MSL2 encoding cDNA was inserted into pFastBac-6His plasmid using *SalI* and *XbaI* restriction sites.

For bacmid generation the different MSL protein containing pFastBac plasmids were transformed into DH10Bac *E. coli* cells. The DH10Bac cells already contain a baculoviral particle encoding bacmid and recombination between this bacmid DNA and the protein encoding plasmid sequence is propagated within the cells. The final expression bacmid generation is facilitated via site-specific (Cre-Lox) transposition (Luckow, 1993).

A3.2. Test transfection and protein expression

For viral stock generation Sf9 cells were used and to test the stability of the viruses different viral passages were collected and tested for protein expression in High Five

cells (Figure A 11). Using hypotonic lysis buffer soluble and insoluble protein fractions were separated. Single infections of the four MSL protein coding viruses showed that while MOF and MSL3 were both present in the soluble and insoluble fractions MSL1 and MSL2 seemed to be insoluble (Figure A 11 A). To test if the present of the other members of the complex helps to improve solubility, all 4 viral stocks have been co-infected and the protein expression was tested as described before. This method improved the solubility of MOF, MSL3 and MSL1which were found only in the soluble fraction. Unfortunately the solubility of MSL2 did not change and further optimisations are required for soluabilization (Figure A 11 B).

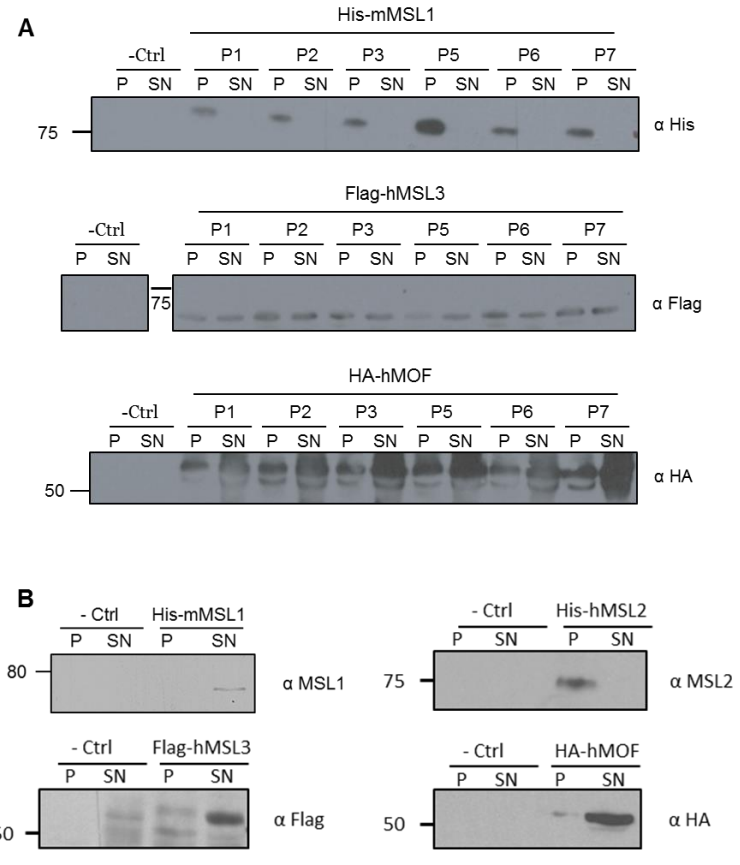

Figure A 11: Baculoviral mediated expression of the MSL complex members. A) Protein expression and solubility test of different passage of baculoviral stocks. P1-7-passage number, P and SN – pellet and supernatant fractions. B) Protein expression test and solubility of co-infected MSL1, MSL2, MSL3 and MOF encoding baculoviral stocks.

A3.3. Plasmid and bacmid generation for the Multibac system

In hope to help the solubility problems and generate higher quality proteins for downstream applications the Multibac expression system was also utilised. Besidses

the know advantage of a BEVs this setup also facilitates modular combination of heterologous genes (multigene expression) with a minimal unique restriction enzyme requirement and an engineered baculovirus genome facilitates the reduction of virus-dependent proteolytic activity (Trowitzsch et al., 2010, Trowitzsch et al., 2012).

The protein coding sequences in pFastBac plasmids were utilised to generate donor and acceptor plasmids for protein expression in the MultiBac system. For the insertion PCR amplification followed by restriction digest and ligation or direct digest from the Bacmid plasmids was performed. Each sequence was inserted into a different antibiotic resistance containing plasmid (gentamycin, kanamycin, chloramphenicol or spectinomycin). These plasmids were then fused together using *Cre* recombinase enzyme in a stepwise manner to create different combinations of the MSL complex members for expression. Each plasmid has been validated with different combination of restriction digest and sequencing. With this method the following combinations were made: mMsl1 and MOF alone, mMsl1-MSL2, mMsl1-MSL2-MOF and mMsl1-MSL2-MOF-MSL3.

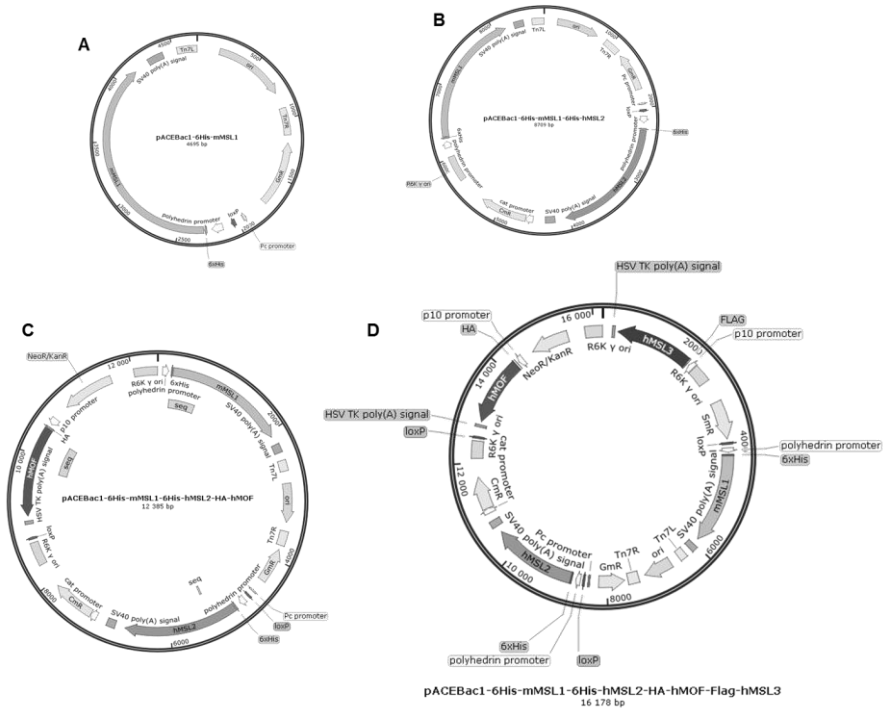

Figure A 12: Transfer vector maps of different MSL protein encoding sequences. A) pACEBac1-6His-mMsl1 plasmid map. B) pACEBac1-6His-mMsl1-6His-MSL2 plasmid map. C) pACEBac1-6His-mMsl1-6His-MSL2-HA-MOF plasmid map. D) pACEBac1-6His-mMsl1-6His-MSL2-HA-MOF-Flag-MSL3 plasmid map. Fusion construct were generated using *Cre* recombination reactions in a stepwise manner.

The Multibac system acceptor plasmids were transformed into DH10EmBacY *E. coli* cells already containing a bacmid sequence similar to the DH10Bac cells. These contain a Tn7 transposition for integrating the acceptor plasmids for the final expression bacmid generation. The bacmid backbone here also contains a YFP coding region which facilitates an early stage expression control after infection. Insect cells infected with this constructs can be pre-screened for YFP expression 7 days after infection to see if the bacmid got integrated and the proteins are able to express.

A3.4. Test transfection and protein expression

For viral stock generation and test expression Sf21 cells were transfected with four different combination of MSL proteins: MSL1 alone, MOF alone, MSL1 and MSL2 together and all four members of the MSL complex. The transfection mixture was removed from the cells after 4 h and replaced by normal media. The cells were cultured for 6 days, then harvested and the supernatant containing the first viral stock was saved as well. Exponentially growing Sf21 cells were then infected with the viral stock and cultured for 7 days. The second viral stock was saved the same was as before and the cells were also harvested.

To test if the infection was efficient and the proteins encoded in the bacmid were translated, the expression of YFP was measured. This sequence is encoded in the DH10EmBacY *E. coli* strain. For the measurements the two viral stocks were analysed alongside the cell lysates. To separate soluble and insoluble fractions cells were lysed in 500µl Lysis buffer, sonicated for 30 sec with 10 sec pulses and centrifuged for 15 min at 14000 rpm. The supernatant was saved as soluble fraction and the pellet was washed twice and resuspended in 500µl Lysis buffer. 50µl of each fractions and the viral stock was then measured in triplicates on a VarioskanFlash plate reader at 514/527 nm. Measurement showed expression of YFP protein in all samples (Figure A 13) indicating successful transfection and viral infection.

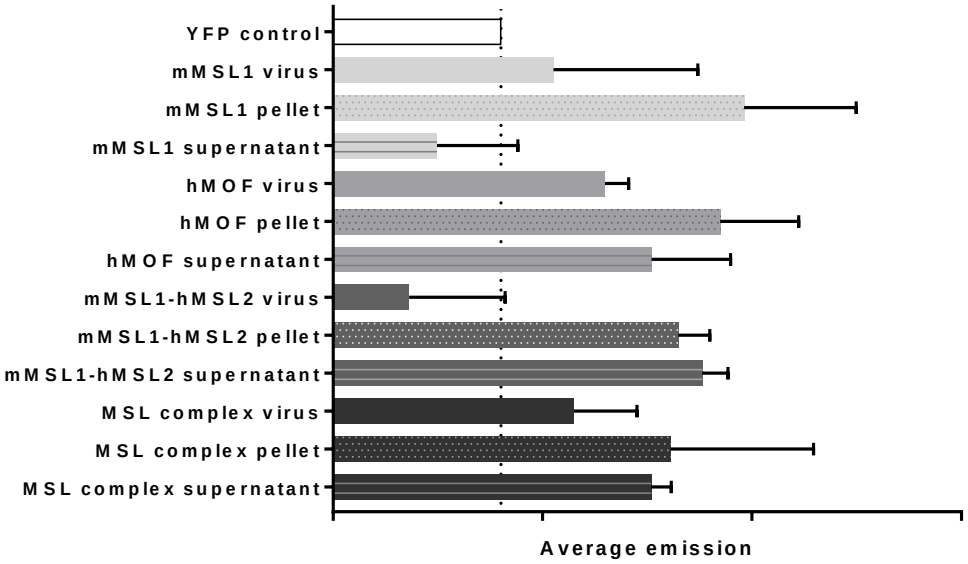

Figure A 13: YFP expression measurement for protein expression validation prior western blot analysis. YFP protein expression was measured at 514/527 nm tin the indicated baculovirus constructs o verify protein expression from the generated bacmid constructs. YFP signal was measured in the harvested viral stock as well as in the cell lysates separating soluble (supernatant) and insoluble (pellet) fractions.

Due to time limitations the protein expression and *in vitro* assay setup was terminated. However, the MultiBac system was successfully established in the lab and further experiments will benefit the generated plasmid and bacmid constructs.

Appendix 6 – Potential MSL2 interacting proteins and potential MSL2 substrates

Table A 1: Filtered MSL2 interactors (full list)

Prey	PreyGene	AvgSpec	ctrlCounts	FoldChange
A6NGQ3	OBSCN	93	0|0|0|0|0|0|0|0|0|0|1|0	930
D3DSW5	GPR124	74	0|0|0|0|0|0|0|0|0|0|0|0	740
Q5THJ4	VPS13D	65	0|0|1|0|0|0|0|0|0|0|0|0	650
C0JYZ1	DNAH11	61	0|0|0|0|0|0|0|0|0|0|0|0	610
Q5XPV6	Q5XPV6	53	0|0|0|0|0|0|0|0|0|0|0|0	530
Q9UL03	INTS6	47	0|0|0|0|0|0|0|0|0|0|0|0	470
J3KNF5	J3KNF5	44	0|0|0|0|0|0|0|0|0|0|0|0	440
B8XCX8	B8XCX8	44	0|0|0|0|0|0|0|0|0|0|0|0	440
J9R021	eIF3a	37	0|0|0|0|0|0|0|0|0|0|0|0	370
B4DN41	B4DN41	34	0|0|0|0|0|0|0|0|0|0|0|0	340
Q6N022	TENM4	32	0|0|0|0|0|0|0|0|0|0|0|0	320
B4DN49	B4DN49	31	0|0|0|0|0|0|0|0|0|0|0|0	310
F4ZW65	NF90b	31	0|0|0|0|0|0|0|0|0|0|0|0	310
Q8WWQ8	STAB2	31	0|0|0|0|0|0|0|0|0|0|0|0	310
Q4LE58	EIF4G1 variant	28	0|0|0|0|0|0|0|0|0|0|0|0	280
A0A1S5UZ39	HBA2	27	0|0|0|0|0|0|0|0|0|0|0|0	270
Q4ZHG4	FNDC1	27	0|0|0|0|0|0|0|0|0|0|0|0	270
A0A0X1KG71	NELFB	27	0|0|0|0|0|0|0|0|0|0|0|0	270
Q07283	TCHH	27	0|0|0|0|0|0|0|0|0|0|0|0	270
B4DJ44	B4DJ44	26	0|0|0|0|0|0|0|0|0|0|0|0	260
Q9C0A1	ZFHX2	25	0|0|0|0|0|0|0|0|0|0|0|0	250
A8K5V5	A8K5V5	24	0|0|0|0|0|0|0|0|0|0|0|0	240
Q9P227	ARHGAP23	24	0|0|0|0|0|0|0|0|0|0|0|0	240
B7Z388	B7Z388	24	0|0|0|0|0|0|0|0|0|0|0|0	240
A0A0C4DGG8	A0A0C4DGG8	23	0|0|0|0|0|0|0|0|0|0|0|0	230
A0A0G2JQF5	KANSL1	23	0|0|0|0|0|0|0|0|0|0|0|0	230
Q6ZRS2	SRCAP	44	0|0|0|0|0|0|0|0|1|0|0|1	220
Q5K651	SAMD9	22	0|0|0|0|0|0|0|0|0|0|0|0	220
A8K2F4	A8K2F4	22	0|0|0|0|0|0|0|0|0|0|0|0	220
Q9NVW2	RLIM	22	0|0|0|0|0|0|0|0|0|0|0|0	220
A0A024RC47	A0A024RC47	21	0|0|0|0|0|0|0|0|0|0|0|0	210
B4DHJ3	B4DHJ3	21	0|0|0|0|0|0|0|0|0|0|0|0	210
A0A1C9J732	A0A1C9J732	20	0|0|0|0|0|0|0|0|0|0|0|0	200
Q9BV37	Q9BV37	20	0|0|0|0|0|0|0|0|0|0|0|0	200
B4DMD3	B4DMD3	20	0|0|0|0|0|0|0|0|0|0|0|0	200
H7BXJ2	H7BXJ2	20	0|0|0|0|0|0|0|0|0|0|0|0	200
J3QSX3	J3QSX3	19	0|0|0|0|0|0|0|0|0|0|0|0	190
G3V4W0	G3V4W0	19	0|0|0|0|0|0|0|0|0|0|0|0	190

Prey	PreyGene	AvgSpec	ctrlCounts	FoldChange
B3KWN0	B3KWN0	19	0|0|0|0|0|0|0|0|0|0|0|0	190
Q96MG7	NDNL2	19	0|0|0|0|0|0|0|0|0|0|0|0	190
B7Z5H0	B7Z5H0	19	0|0|0|0|0|0|0|0|0|0|0|0	190
D6W648	KIAA1543	19	0|0|0|0|0|0|0|0|0|0|0|0	190
Q8TBT6	Q8TBT6	19	0|0|0|0|0|0|0|0|0|0|0|0	190
J3KNA0	J3KNA0	19	0|0|0|0|0|0|0|0|0|0|0|0	190
Q8N1C8	Q8N1C8	19	0|0|0|0|0|0|0|0|0|0|0|0	190
A4D1Z4	AP5Z1	19	0|0|0|0|0|0|0|0|0|0|0|0	190
A0A1U9X8P6	A0A1U9X8P6	18	0|0|0|0|0|0|0|0|0|0|0|0	180
A0A0A0MQX1	A0A0A0MQX1	18	0|0|0|0|0|0|0|0|0|0|0|0	180
B2RDE0	B2RDE0	18	0|0|0|0|0|0|0|0|0|0|0|0	180
O15055	PER2	17	0|0|0|0|0|0|0|0|0|0|1|0	170
S4R2X9	MBIP	17	0|0|0|0|0|0|0|0|0|0|0|0	170
A0A0U1RRH6	A0A0U1RRH6	17	0|0|0|0|0|0|0|0|0|0|0|0	170
Q59HH7	Q59HH7	17	0|0|0|0|0|0|0|0|0|0|0|0	170
F8WE04	F8WE04	16	0|0|0|0|0|0|0|0|0|0|0|0	160
Q2TSD0	Q2TSD0	16	0|0|0|0|0|0|0|0|0|0|0|0	160
Q8NCK5	Q8NCK5	16	0|0|0|0|0|0|0|0|0|0|0|0	160
B4DM14	B4DM14	16	0|0|0|0|0|0|0|0|0|0|0|0	160
Q6P9B9	INTS5	16	0|0|0|0|0|0|0|0|0|0|0|0	160
B2R5R9	B2R5R9	15	0|0|0|0|0|0|0|0|0|0|0|0	150
J3QQJ0	J3QQJ0	15	0|0|0|0|0|0|0|0|0|0|0|0	150
A8K1Y7	A8K1Y7	15	0|0|0|0|0|0|0|0|0|0|0|0	150
Q4KMQ8	Q4KMQ8	15	0|0|0|0|0|0|0|0|0|0|0|0	150
A0A0A0MSA4	A0A0A0MSA4	15	0|0|0|0|0|0|0|0|0|0|0|0	150
A0A1W2PPS1	A0A1W2PPS1	15	0|0|0|0|0|0|0|0|0|0|0|0	150
Q6ZUX2	Q6ZUX2	15	0|0|0|0|0|0|0|0|0|0|0|0	150
A0A024R6E3	A0A024R6E3	15	0|0|0|0|0|0|0|0|0|0|0|0	150
I6TRR8	I6TRR8	15	0|0|0|0|0|0|0|0|0|0|0|0	150
A0A0D9SEN2	A0A0D9SEN2	15	0|0|0|0|0|0|0|0|0|0|0|0	150
B4DDX2	B4DDX2	15	0|0|0|0|0|0|0|0|0|0|0|0	150
C3UMV3	C3UMV3	14	0|0|0|0|0|0|0|0|0|0|0|0	140
Q6FG59	Q6FG59	14	0|0|0|0|0|0|0|0|0|0|0|0	140
G3V119	G3V119	14	0|0|0|0|0|0|0|0|0|0|0|0	140
Q53HL1	Q53HL1	14	0|0|0|0|0|0|0|0|0|0|0|0	140
B7Z6D1	B7Z6D1	14	0|0|0|0|0|0|0|0|0|0|0|0	140
B7Z565	B7Z565	14	0|0|0|0|0|0|0|0|0|0|0|0	140
A0A024RA92	GLI3	14	0|0|0|0|0|0|0|0|0|0|0|0	140
B4DDG3	B4DDG3	14	0|0|0|0|0|0|0|0|0|0|0|0	140
B4DGM5	B4DGM5	14	0|0|0|0|0|0|0|0|0|0|0|0	140
B4DDC9	B4DDC9	14	0|0|0|0|0|0|0|0|0|0|0|0	140
Q9H147	DNTTIP1	14	0|0|0|0|0|0|0|0|0|0|0|0	140

Prey	PreyGene	AvgSpec	ctrlCounts	FoldChange
B2RAG9	B2RAG9	14	0|0|0|0|0|0|0|0|0|0|0|0	140
B4DQY2	B4DQY2	13	0|0|0|0|0|0|0|0|0|0|0|0	130
B3KV06	B3KV06	13	0|0|0|0|0|0|0|0|0|0|0|0	130
A8K7F6	A8K7F6	13	0|0|0|0|0|0|0|0|0|0|0|0	130
D6RID8	GTF2H2C	13	0|0|0|0|0|0|0|0|0|0|0|0	130
P06746	POLB	13	0|0|0|0|0|0|0|0|0|0|0|0	130
E9JVC4	MAEL	13	0|0|0|0|0|0|0|0|0|0|0|0	130
O95206	PCDH8	13	0|0|0|0|0|0|0|0|0|0|0|0	130
B7ZLP5	B7ZLP5	13	0|0|0|0|0|0|0|0|0|0|0|0	130
Q0VGD6	Q0VGD6	13	0|0|0|0|0|0|0|0|0|0|0|0	130
A0A087WUK2	A0A087WUK2	13	0|0|0|0|0|0|0|0|0|0|0|0	130
A0A024R6Q8	A0A024R6Q8	13	0|0|0|0|0|0|0|0|0|0|0|0	130
R4GMX3	R4GMX3	13	0|0|0|0|0|0|0|0|0|0|0|0	130
Q4LE34	Q4LE34	13	0|0|0|0|0|0|0|0|0|0|0|0	130
D9HTE9	D9HTE9	13	0|0|0|0|0|0|0|0|0|0|0|0	130
A8K3B0	A8K3B0	13	0|0|0|0|0|0|0|0|0|0|0|0	130
Q58DX5	NAALADL2	13	0|0|0|0|0|0|0|0|0|0|0|0	130
Q53FE8	Q53FE8	13	0|0|0|0|0|0|0|0|0|0|0|0	130
B3KXY3	B3KXY3	13	0|0|0|0|0|0|0|0|0|0|0|0	130
Q6FI51	Q6FI51	12	0|0|0|0|0|0|0|0|0|0|0|0	120
B4DN17	B4DN17	12	0|0|0|0|0|0|0|0|0|0|0|0	120
P0DN76	P0DN76	12	0|0|0|0|0|0|0|0|0|0|0|0	120
P0C1Z6	TFPT	12	0|0|0|0|0|0|0|0|0|0|0|0	120
J3QSV6	J3QSV6	12	0|0|0|0|0|0|0|0|0|0|0|0	120
Q9UJC3	HOOK1	12	0|0|1|0|0|0|0|0|0|0|0|0	120
F2YMM1	F2YMM1	12	0|0|0|0|0|0|0|0|0|0|0|0	120
Q8IYH5	ZZZ3	12	0|1|0|0|0|0|0|0|0|0|0|0	120
M0R1M6	M0R1M6	12	0|0|0|0|0|0|0|0|0|0|0|0	120
Q7Z426	Q7Z426	12	0|0|0|0|0|0|0|0|0|0|0|0	120
A8K1N6	A8K1N6	12	0|0|0|0|0|0|0|0|0|0|0|0	120
M4VP52	M4VP52	12	0|0|0|0|0|0|0|0|0|0|0|0	120
Q96N64	PWWP2A	11	0|0|0|0|0|0|0|0|0|0|0|0	110
A0A024R1J3	A0A024R1J3	11	0|0|0|0|0|0|0|0|0|0|0|0	110
A0A0A6YYJ8	A0A0A6YYJ8	11	0|0|0|0|0|0|0|0|0|0|0|0	110
B3KSR8	B3KSR8	11	0|0|0|0|0|0|0|0|0|0|0|0	110
M1VKI3	M1VKI3	11	0|0|0|0|0|0|0|0|0|0|0|0	110
G3V203	G3V203	11	0|0|0|0|0|0|0|0|0|0|0|0	110
A0A024QZH6	A0A024QZH6	11	0|0|0|0|0|0|0|0|0|0|0|0	110
A0A087WZ13	A0A087WZ13	11	0|0|0|0|0|0|0|0|0|0|0|0	110
A0A024QZP7	A0A024QZP7	11	0|0|0|0|0|0|0|0|0|0|0|0	110
M0R0R2	M0R0R2	11	0|0|0|0|0|0|0|0|0|0|0|0	110
G9BCY7	G9BCY7	11	0|0|0|0|0|0|0|0|0|0|0|0	110

Prey	PreyGene	AvgSpec	ctrlCounts	FoldChange
Q86Y79	PTRH1	11	0|0|0|0|0|0|0|0|0|0|0	110
F6M2K3	F6M2K3	11	0|0|0|0|0|0|0|0|0|0|0	110
A0A024R0M6	A0A024R0M6	11	0|0|0|0|0|0|0|0|0|0|0	110
A0A024QZM0	A0A024QZM0	11	0|0|0|0|0|0|0|0|0|0|0	110
M0QYH2	M0QYH2	11	0|0|0|0|0|0|0|0|0|0|0	110
Q59HH1	Q59HH1	11	0|0|0|0|0|0|0|0|0|0|0	110
A7MD06	A7MD06	10	0|0|0|0|0|0|0|0|0|0|0	100
B3KPR7	B3KPR7	10	0|0|0|0|0|0|0|0|0|0|0	100
A0A1B4Z394	A0A1B4Z394	10	0|0|0|0|0|0|0|0|0|0|0	100
Q8NDL9	AGBL5	10	0|0|0|0|0|0|0|0|0|0|0	100
Q6NWZ1	Q6NWZ1	10	0|0|0|0|0|0|0|0|0|0|0	100
B4E356	B4E356	10	0|0|0|0|0|0|0|0|0|0|0	100
Q9H7H0	METTL17	10	0|0|0|0|0|0|0|0|0|0|0	100
B2R7R5	B2R7R5	10	0|0|0|0|0|0|0|0|0|0|0	100
J3KPX7	J3KPX7	10	0|0|0|0|0|0|0|0|0|0|0	100
A0A0A0MSI2	A0A0A0MSI2	10	0|0|0|0|0|0|0|0|0|0|0	100
B4DE30	B4DE30	10	0|0|0|0|0|0|0|0|0|0|0	100
Q5RLJ0	Q5RLJ0	10	0|0|0|0|0|0|0|0|0|0|0	100
A0A087X1A5	A0A087X1A5	10	0|0|0|0|0|0|0|0|0|0|0	100
A8K2P6	A8K2P6	10	0|0|0|0|0|0|0|0|0|0|0	100
Q9UHB4	NDOR1	9	0|0|0|0|0|0|0|0|0|0|0	90
Q9UJW2	TINAG	9	0|0|0|0|0|0|0|0|0|0|0	90
F8W8T1	F8W8T1	9	0|0|0|0|0|0|0|0|0|0|0	90
Q9BVG4	PBDC1	9	0|0|0|0|0|0|0|0|0|0|0	90
A0A0A0MS90	A0A0A0MS90	9	0|0|0|0|0|0|0|0|0|0|0	90
A0A0C4DG44	A0A0C4DG44	9	0|0|0|0|0|0|0|0|0|0|0	90
B5BU83	B5BU83	9	0|0|0|0|0|0|0|0|0|0|0	90
U4PP31	U4PP31	9	0|0|0|0|0|0|0|0|0|0|0	90
B3KN59	B3KN59	9	0|0|0|0|0|0|0|0|0|0|0	90
H7C422	H7C422	9	0|0|0|0|0|0|0|0|0|0|0	90
Q8IWC5	Q8IWC5	9	0|0|0|0|0|0|0|0|0|0|0	90
Q9NWK9	ZNHIT6	8	0|0|0|0|0|0|0|0|0|0|0	80
B3KSI4	B3KSI4	8	0|0|0|0|0|0|0|0|0|0|0	80
H0Y3X6	H0Y3X6	8	0|0|0|0|0|0|0|0|0|0|0	80
Q8N8R7	ARL14EP	8	0|0|0|0|0|0|0|0|0|0|0	80
Q59GW7	Q59GW7	8	0|0|0|0|0|0|0|0|0|0|0	80
A0A0S2Z472	A0A0S2Z472	8	0|0|0|0|0|0|0|0|0|0|0	80
J3KR12	J3KR12	8	0|0|0|0|0|0|0|0|0|0|0	80
B7Z2E2	B7Z2E2	8	0|0|0|0|0|0|0|0|0|0|0	80
A8K5A5	A8K5A5	8	0|0|0|0|0|0|0|0|0|0|0	80
Q9P0A0	Q9P0A0	7	0|0|0|0|0|0|0|0|0|0|0	70
B4DWA7	B4DWA7	7	0|0|0|0|0|0|0|0|0|0|0	70

Prey	PreyGene	AvgSpec	ctrlCounts	FoldChange
A8K8J5	A8K8J5	7	0|0|0|0|0|0|0|0|0|0|0|0	70
E9PPD1	BRMS1	7	0|0|0|0|0|0|0|0|0|0|0|0	70
E9PN81	RNASEH2C	7	0|0|0|0|0|0|0|0|0|0|0|0	70
B4DT94	B4DT94	7	0|0|0|0|0|0|0|0|0|0|0|0	70
Q9H987	SYNPO2L	7	0|0|0|0|0|0|0|0|0|0|0|0	70
B4DRY7	B4DRY7	7	0|0|0|0|0|0|0|0|0|0|0|0	70
Q96P20	NLRP3	7	0|0|0|0|0|0|0|0|0|0|0|0	70
B2R6U8	B2R6U8	7	0|0|0|0|0|0|0|0|0|0|0|0	70
A0A087WWP5	A0A087WWP5	7	0|0|0|0|0|0|0|0|0|0|0|0	70
Q6P2H3	CEP85	7	0|0|0|0|0|0|0|0|0|0|0|0	70
B3KRR4	B3KRR4	7	0|0|0|0|0|0|0|0|0|0|0|0	70
B4DKE6	B4DKE6	7	0|0|0|0|0|0|0|0|0|0|0|0	70
F6RGN5	F6RGN5	7	0|0|0|0|0|0|0|0|0|0|0|0	70
Q9HAK2	EBF2	7	0|0|0|0|0|0|0|0|0|0|0|0	70
Q6ZSX8	Q6ZSX8	7	0|0|0|0|0|0|0|0|0|0|0|0	70
F6KSZ4	DHH	7	0|0|0|0|0|0|0|0|0|0|0|0	70
B3KUE6	B3KUE6	7	0|0|0|0|0|0|0|0|0|0|0|0	70
Q499Z2	Q499Z2	6	0|0|0|0|0|0|0|0|0|0|0|0	60
A4UCR9	A4UCR9	6	0|0|0|0|0|0|0|0|0|0|0|0	60
A0A1U9X8Y8	A0A1U9X8Y8	6	0|0|0|0|0|0|0|0|0|0|0|0	60
B2RCC2	B2RCC2	6	0|0|0|0|0|0|0|0|0|0|0|0	60
A0A024R254	A0A024R254	6	0|0|0|0|0|0|0|0|0|0|0|0	60
O75956	CDK2AP2	6	0|0|0|0|0|0|0|0|0|0|0|0	60
Q96CD0	FBXL8	6	0|0|0|0|0|0|0|0|0|0|0|0	60
Q96MM3	ZFP42	6	0|0|0|0|0|0|0|0|0|0|0|0	60
X6RJP6	X6RJP6	6	0|0|0|0|0|0|0|0|0|0|0|0	60
B2R9R2	B2R9R2	6	0|0|0|0|0|0|0|0|0|0|0|0	60
A8K8A4	A8K8A4	6	0|0|0|0|0|0|0|0|0|0|0|0	60
I6L9C8	I6L9C8	6	0|0|0|0|0|0|0|0|0|0|0|0	60
A0A0B4J295	A0A0B4J295	6	0|0|0|0|0|0|0|0|0|0|0|0	60
A0A087WVZ9	A0A087WVZ9	6	0|0|0|0|0|0|0|0|0|0|0|0	60
A0A1U9X8V7	A0A1U9X8V7	6	0|0|0|0|0|0|0|0|0|0|0|0	60
H0YH81	H0YH81	6	0|0|0|0|0|0|0|0|0|0|0|0	60
A0A1B0GTG9	A0A1B0GTG9	6	0|0|0|0|0|0|0|0|0|0|0|0	60
Q9Y2V3	RAX	6	0|0|0|0|0|0|0|0|0|0|0|0	60
A8K3N2	A8K3N2	6	0|0|0|0|0|0|0|0|0|0|0|0	60
L0R5A1	CSF2RB	6	0|0|0|0|0|0|0|0|0|0|0|0	60
Q969J2	ZKSCAN4	15	0|0|1|1|1|0|0|0|0|0|0|0	50
B3KN15	B3KN15	5	0|0|0|0|0|0|0|0|0|0|0|0	50
A0A024R5M3	A0A024R5M3	5	0|0|0|0|0|0|0|0|0|0|0|0	50
E7ENQ6	YJEFN3	5	0|0|0|0|0|0|0|0|0|0|0|0	50
A8K773	RPUSD3	5	0|0|0|0|0|0|0|0|0|0|0|0	50

Prey	PreyGene	AvgSpec	ctrlCounts	FoldChange
A0A087WYP2	A0A087WYP2	5	0|0|0|0|0|0|0|0|0|0|0|0	50
B2RDU4	B2RDU4	5	0|0|0|0|0|0|0|0|0|0|0|0	50
Q8TAX8	Q8TAX8	5	0|0|0|0|0|0|0|0|0|0|0|0	50
H0Y4R1	H0Y4R1	5	0|0|0|0|0|0|0|0|0|0|0|0	50
Q8TBM3	ATP6V0A2	5	0|0|0|0|0|0|0|0|0|0|0|0	50
Q10588	BST1	5	0|0|0|0|0|0|0|0|0|0|0|0	50
K7EMM8	K7EMM8	5	0|0|0|0|0|0|0|0|0|0|0|0	50
F8WET0	F8WET0	5	0|0|0|0|0|0|0|0|0|0|0|0	50
A0A024R4P4	A0A024R4P4	5	0|0|0|0|0|0|0|0|0|0|0|0	50
Q9NY99	SNTG2	5	0|0|0|0|0|0|0|0|0|0|0|0	50
B3KNP0	B3KNP0	5	0|0|0|0|0|0|0|0|0|0|0|0	50
Q53H17	Q53H17	5	0|0|0|0|0|0|0|0|0|0|0|0	50
Q7Z4Q2	HEATR3	5	0|0|0|0|0|0|0|0|0|0|0|0	50
A0A0A0MRR3	A0A0A0MRR3	5	0|0|0|0|0|0|0|0|0|0|0|0	50
Q92560	BAP1	12	0|0|0|0|0|0|0|0|2|1|0|0	40
D6R9G1	CDK7	12	0|3|0|0|0|0|0|0|0|0|0|0	40
D6RHD5	ALB	8	0|0|0|0|2|0|0|0|0|0|0|0	40
Q96A72	MAGOHB	8	0|0|0|0|0|0|0|0|1|1|0|0|0	40
H7BYN3	H7BYN3	4	0|0|0|0|0|0|0|0|0|0|0|0	40
X6R700	X6R700	4	0|0|0|0|0|0|0|0|0|0|0|0	40
Q6NVY0	Q6NVY0	4	0|0|0|0|0|0|0|0|0|0|0|0	40
G3V1T9	G3V1T9	4	0|0|0|0|0|0|0|0|0|0|0|0	40
Q6PUJ7	Q6PUJ7	4	0|0|0|0|0|0|0|0|0|0|0|0	40
Q2PEG2	Q2PEG2	4	0|0|0|0|0|0|0|0|0|0|0|0	40
E5RGZ9	ENDOV	4	0|0|0|0|0|0|0|0|0|0|0|0	40
Q9H7Z6	KAT8	4	0|0|1|0|0|0|0|0|0|0|0|0	40
A0A0S2Z5D2	A0A0S2Z5D2	4	0|0|0|0|0|0|0|0|0|0|0|0	40
M0R050	M0R050	4	0|0|0|0|0|0|0|0|0|0|0|0	40
M0R117	M0R117	4	0|0|0|0|0|0|0|0|0|0|0|0	40
H0YKC5	H0YKC5	4	0|0|0|0|0|0|0|0|0|0|0|0	40
Q53FC3	Q53FC3	4	0|0|0|0|0|0|0|0|0|0|0|0	40
U4PSC4	U4PSC4	4	0|0|0|0|0|0|0|0|0|0|0|0	40
P51810	GPR143	4	0|0|0|0|0|0|0|0|0|0|0|0	40
H0YIC4	H0YIC4	4	0|0|0|0|0|0|0|0|0|0|0|0	40
W4VSQ8	W4VSQ8	4	0|0|0|0|0|0|0|0|0|0|0|0	40
H0Y586	H0Y586	4	0|0|0|0|0|0|0|0|0|0|0|0	40
Q16577	Q16577	4	0|0|0|0|0|0|0|0|0|0|0|0	40
F8VV56	CD63	4	0|0|0|0|0|0|0|0|0|0|0|0	40
Q96H79	ZC3HAV1L	4	0|0|0|0|0|0|0|0|0|0|0|0	40
A0A024RA28	A0A024RA28	4	0|0|0|0|0|0|0|0|0|0|0|0	40
A0A0B4J213	A0A0B4J213	4	0|0|0|0|0|0|0|0|0|0|0|0	40
Q01658	DR1	7	0|0|0|0|0|0|0|0|0|0|1|1	35

Prey	PreyGene	AvgSpec	ctrlCounts	FoldChange
Q5QP19	NFS1	16	0|0|0|0|0|0|5|0|0|0|0|0	32
Q71SM9	Q71SM9	3	0|0|0|0|0|0|0|0|0|0|0|0	30
B2R4D5	B2R4D5	3	0|0|0|0|0|0|0|0|0|0|0|0	30
F8WD73	F8WD73	3	0|0|0|0|0|0|0|0|0|0|0|0	30
P62699	YPEL5	3	0|0|0|0|0|0|0|0|0|0|0|0	30
K7EMM5	K7EMM5	3	0|0|0|0|0|0|0|0|0|0|0|0	30
B3KS16	B3KS16	3	0|0|0|0|0|0|0|0|0|0|0|0	30
H3BPR2	H3BPR2	3	0|0|0|0|0|0|0|0|0|0|0|0	30
Q9UBK9	UXT	3	0|0|0|0|0|0|0|0|0|0|0|0	30
Q9H6X1	Q9H6X1	3	0|0|0|0|0|0|0|0|0|0|0|0	30
A0A087WZ21	A0A087WZ21	3	0|0|0|0|0|0|0|0|0|0|0|0	30
K7ES31	K7ES31	3	0|0|0|0|0|0|0|0|0|0|0|0	30
B2R5H5	B2R5H5	3	0|0|0|0|0|0|0|0|0|0|0|0	30
Q9H3S7	PTPN23	34	2|1|1|2|1|0|1|0|2|2|0|0|1	26.15
O75376	NCOR1	47	4|2|0|2|1|0|1|0|1|3|1|2|3	23.5
B7Z970	B7Z970	2	0|0|0|0|0|0|0|0|0|0|0|0	20
Q9NWM3	CUEDC1	2	0|0|0|0|0|0|0|0|0|0|0|0	20
B4DUI1	MB	2	0|0|0|0|0|0|0|0|0|0|0|0	20
B3KUJ9	MED20	2	0|0|0|0|0|0|0|0|0|0|0|0	20
B2R506	B2R506	2	0|0|0|0|0|0|0|0|0|0|0|0	20
H0Y829	H0Y829	2	0|0|0|0|0|0|0|0|0|0|0|0	20
A4D1G5	A4D1G5	2	0|0|0|0|0|0|0|0|0|0|0|0	20
Q5JNZ5	Q5JNZ5	2	0|0|0|0|0|0|0|0|0|0|0|0	20
C9JJU7	C21orf70	2	0|0|0|0|0|0|0|0|0|0|0|0	20
J3KTJ8	J3KTJ8	2	0|0|0|0|0|0|0|0|0|0|0|0	20
H7BZ09	H7BZ09	2	0|0|0|0|0|0|0|0|0|0|0|0	20
Q9NV56	MRGBP	2	0|0|0|0|0|0|0|0|0|0|0|0	20
F8SNU7	F8SNU7	2	0|0|0|0|0|0|0|0|0|0|0|0	20
Q6FI35	Q6FI35	2	0|0|0|0|0|0|0|0|0|0|0|0	20
G3V1D4	G3V1D4	2	0|0|0|0|0|0|0|0|0|0|0|0	20
H0YFY3	H0YFY3	2	0|0|0|0|0|0|0|0|0|0|0|0	20
E7EQ64	PRSS1	7	2|0|0|0|0|0|2|0|0|0|0|0	17.5
O15379	HDAC3	8	0|0|1|1|0|0|1|0|1|0|0|0|1	16
O95619	YEATS4	3	0|0|1|0|1|0|0|0|0|0|0|0	15
Q6P4R8	NFRKB	13	2|3|0|0|0|0|1|0|0|2|0|0|1	14.44
O94864	SUPT7L	10	0|0|2|0|0|0|1|0|1|4|0|0|1	11.11
Q8NEM7	SUPT20H	8	0|0|1|1|0|0|0|0|2|1|1|1|1	10
Q9NX00	TMEM160	3	0|0|1|0|0|1|0|0|1|0|0|0|0	10
E7EV10	MTA3	34	1|2|3|4|5|3|2|0|4|3|4|3|5	9.44
Q9GZU8	FAM192A	6	1|0|0|0|0|2|3|0|1|0|0|0|0	8.57
Q9UIL1	SCOC	3	0|0|0|0|0|0|2|0|1|1|0|0|0	7.5
P35580	MYH10	64	0|1|13|8|11|0|0|0|11|19|12|10|16	6.34

Prey	PreyGene	AvgSpec	ctrlCounts	FoldChange
Q9NRF8	CTPS2	10	2|4|0|4|2|3|2|0|0|2|1|0|2	4.55
Q9ULM3	YEATS2	18	14|8|2|5|4|0|1|0|3|9|0|0|7	3.4
Q96JH7	VCPIP1	32	6|9|18|8|5|15|26|0|7|6|6|5|6	2.99
P24941	CDK2	7	0|0|3|2|3|3|5|0|3|3|2|4|2	2.33
P52655	GTF2A1	3	4|3|1|0|0|0|0|0|1|2|1|1|1	2.14
P46108	CRK	22	14|7|13|16|7|32|22|0|11|11|5|5|9	1.55

Prey: Uniprot accession number, PreyGene: Corresponding protein coding gene name, AvgSpec: Average spectral counts representing the number of peptides detected in the analysis, ctrlCounts: Control counts representing the number of peptides detected in each control separately, Fold change: Protein enrichment fold change compared to the controls.

Table A 2: Filtered ubiquitylated MSL2 interactors (full list)

Prey	PreyGene	AvgSpec	ctrlCounts	FoldChange
Q5THJ4	VPS13D	48	0|0|1|0|0|0|0|0|0|0|0|0	480
Q8TB01	Q8TB01	39	0|0|0|0|0|0|0|0|0|0|0|0	390
Q02224	CENPE	37	0|0|0|0|0|0|0|0|0|0|0|0	370
Q9NR48	ASH1L	32	0|0|0|0|0|0|0|0|0|0|0|0	320
B7Z8Z6	B7Z8Z6	32	0|0|0|0|0|0|0|0|0|0|0|0	320
A0A0C4DH75	MPP2	31	0|0|0|0|0|0|0|0|0|0|0|0	310
A0A0G2JPP5	SCRIB	30	0|0|0|0|0|0|0|0|0|0|0|0	300
B4DQX5	B4DQX5	28	0|0|0|0|0|0|0|0|0|0|0|0	280
B2RAH5	B2RAH5	28	0|0|0|0|0|0|0|0|0|0|0|0	280
Q9H0D2	ZNF541	27	0|0|0|0|0|0|0|0|0|0|0|0	270
A0A1K0GXZ1	GLNC1	26	0|0|0|0|0|0|0|0|0|0|0|0	260
Q58EX2	SDK2	26	0|0|0|0|0|0|0|0|0|0|0|0	260
B7Z2B5	B7Z2B5	25	0|0|0|0|0|0|0|0|0|0|0|0	250
Q96RY7	IFT140	23	0|0|0|0|0|0|0|0|0|0|0|0	230
B4E2K0	B4E2K0	23	0|0|0|0|0|0|0|0|0|0|0|0	230
A8K9P0	A8K9P0	23	0|0|0|0|0|0|0|0|0|0|0|0	230
A0A024RA92	GLI3	23	0|0|0|0|0|0|0|0|0|0|0|0	230
B4DWL1	B4DWL1	23	0|0|0|0|0|0|0|0|0|0|0|0	230
A0A087WSZ2	ACTN3	22	0|0|0|0|0|0|0|0|0|0|0|0	220
A9UF07	BCR/ABL fusion	22	0|0|0|0|0|0|0|0|0|0|0|0	220
O14924	RGS12	22	0|0|0|0|0|0|0|0|0|0|0|0	220
B1ALM3	CACNA1S	21	0|0|0|0|0|0|0|0|0|0|0|0	210
E5RJH9	SQLE	21	0|0|0|0|0|0|0|0|0|0|0|0	210
B3KTJ9	B3KTJ9	21	0|0|0|0|0|0|0|0|0|0|0|0	210
S4R2X9	S4R2X9	20	0|0|0|0|0|0|0|0|0|0|0|0	200
B3KRM2	B3KRM2	20	0|0|0|0|0|0|0|0|0|0|0|0	200
B4DSH1	B4DSH1	20	0|0|0|0|0|0|0|0|0|0|0|0	200
B7Z2Z8	B7Z2Z8	19	0|0|0|0|0|0|0|0|0|0|0|0	190

Prey	PreyGene	AvgSpec	ctrlCounts	FoldChange
O00512	BCL9	18	0|0|0|0|0|0|0|0|0|0|0	180
B2RTS4	B2RTS4	18	0|0|0|0|0|0|0|0|0|0|0	180
B3KM48	B3KM48	18	0|0|0|0|0|0|0|0|0|0|0	180
B7Z852	B7Z852	18	0|0|0|0|0|0|0|0|0|0|0	180
Q08999	RBL2	18	0|0|0|0|0|0|0|0|0|0|0	180
Q86YR7	MCF2L2	18	0|0|0|0|0|0|0|0|0|0|0	180
A0A1U9XBD9	A0A1U9XBD9	18	0|0|0|0|0|0|0|0|0|0|0	180
B7Z5R5	B7Z5R5	18	0|0|0|0|0|0|0|0|0|0|0	180
A0A0D9SFG6	A0A0D9SFG6	18	0|0|0|0|0|0|0|0|0|0|0	180
Q53F48	Q53F48	17	0|0|0|0|0|0|0|0|0|0|0	170
A0A0A0MTH3	A0A0A0MTH3	17	0|0|0|0|0|0|0|0|0|0|0	170
Q8N1K5	THEMIS	17	0|0|0|0|0|0|0|0|0|0|0	170
R9QF97	R9QF97	17	0|0|0|0|0|0|0|0|0|0|0	170
J3QKS7	J3QKS7	17	0|0|0|0|0|0|0|0|0|0|0	170
B4DYC8	B4DYC8	17	0|0|0|0|0|0|0|0|0|0|0	170
B4E1W3	B4E1W3	17	0|0|0|0|0|0|0|0|0|0|0	170
A0A024R7U6	A0A024R7U6	17	0|0|0|0|0|0|0|0|0|0|0	170
P21108	P21108	16	0|0|0|0|0|0|0|0|0|0|0	160
A0A024R4A5	A0A024R4A5	16	0|0|0|0|0|0|0|0|0|0|0	160
Q9BYM8	RBCK1	16	0|0|0|0|0|0|0|0|0|0|0	160
Q96J71	ELAVL3	16	0|0|0|0|0|0|0|0|0|0|0	160
Q8TDY2	RB1CC1	16	0|0|0|0|0|0|0|0|0|0|0	160
Q59G16	Q59G16	15	0|0|0|0|0|0|0|0|0|0|0	150
F8W7U8	F8W7U8	15	0|0|0|0|0|0|0|0|0|0|0	150
A0A0D9SFL2	A0A0D9SFL2	15	0|0|0|0|0|0|0|0|0|0|0	150
B2RBA6	B2RBA6	15	0|0|0|0|0|0|0|0|0|0|0	150
A0A1U9X7J2	A0A1U9X7J2	14	0|0|0|0|0|0|0|0|0|0|0	140
A0A024R8D4	A0A024R8D4	14	0|0|0|0|0|0|0|0|0|0|0	140
Q0VAB1	Q0VAB1	14	0|0|0|0|0|0|0|0|0|0|0	140
R9S252	R9S252	14	0|0|0|0|0|0|0|0|0|0|0	140
H0YKT5	H0YKT5	14	0|0|0|0|0|0|0|0|0|0|0	140
B2R623	B2R623	14	0|0|0|0|0|0|0|0|0|0|0	140
Q53ZX9	Q53ZX9	14	0|0|0|0|0|0|0|0|0|0|0	140
A8K3A8	A8K3A8	13	0|0|0|0|0|0|0|0|0|0|0	130
B4DZR0	B4DZR0	13	0|0|0|0|0|0|0|0|0|0|0	130
B4DM22	B4DM22	13	0|0|0|0|0|0|0|0|0|0|0	130
A0A1B0GTJ7	A0A1B0GTJ7	13	0|0|0|0|0|0|0|0|0|0|0	130
Q5TCS8	AK9	12	0|0|0|0|0|0|0|0|0|0|0	120
A0A024R9J7	A0A024R9J7	12	0|0|0|0|0|0|0|0|0|0|0	120
L8B4J3	L8B4J3	12	0|0|0|0|0|0|0|0|0|0|0	120
H0YJI1	H0YJI1	12	0|0|0|0|0|0|0|0|0|0|0	120
L8E931	L8E931	12	0|0|0|0|0|0|0|0|0|0|0	120

Prey	PreyGene	AvgSpec	ctrlCounts	FoldChange
B2R5M9	B2R5M9	12	0|0|0|0|0|0|0|0|0|0|0	120
B4DDX2	B4DDX2	12	0|0|0|0|0|0|0|0|0|0|0	120
B2RBR9	B2RBR9	12	0|0|0|0|0|0|0|0|0|0|0	120
Q8WYN0	ATG4A	12	0|0|0|0|0|0|0|0|0|0|0	120
H7BZ94	H7BZ94	12	0|0|0|0|0|0|0|0|0|0|0	120
Q8NBJ5	COLGALT1	12	0|0|0|0|0|0|0|0|0|0|0	120
Q9Y6N6	LAMC3	12	0|0|0|0|0|0|0|0|0|0|0	120
B3KR37	B3KR37	12	0|0|0|0|0|0|0|0|0|0|0	120
Q05DK5	Q05DK5	12	0|0|0|0|0|0|0|0|0|0|0	120
A0A0G2JL47	A0A0G2JL47	12	0|0|0|0|0|0|0|0|0|0|0	120
A4D1Z4	KIAA0415	12	0|0|0|0|0|0|0|0|0|0|0	120
B3KRP3	B3KRP3	11	0|0|0|0|0|0|0|0|0|0|0	110
B4DGF8	B4DGF8	11	0|0|0|0|0|0|0|0|0|0|0	110
B3KM36	B3KM36	11	0|0|0|0|0|0|0|0|0|0|0	110
B4DLG0	B4DLG0	11	0|0|0|0|0|0|0|0|0|0|0	110
B6E4X6	B6E4X6	11	0|0|0|0|0|0|0|0|0|0|0	110
O95741	CPNE6	11	1|0|0|0|0|0|0|0|0|0|0	110
B2R787	B2R787	11	0|0|0|0|0|0|0|0|0|0|0	110
H0YGW7	H0YGW7	11	0|0|0|0|0|0|0|0|0|0|0	110
B4DPW9	B4DPW9	11	0|0|0|0|0|0|0|0|0|0|0	110
O94805	ACTL6B	11	0|0|0|0|0|0|0|0|0|0|0	110
J3KMZ8	J3KMZ8	11	0|0|0|0|0|0|0|0|0|0|0	110
G3V4C1	G3V4C1	11	0|0|0|0|0|0|0|0|0|0|0	110
B4DDM5	B4DDM5	11	0|0|0|0|0|0|0|0|0|0|0	110
A0A0A0MSI0	A0A0A0MSI0	11	0|0|0|0|0|0|0|0|0|0|0	110
A0A1X7SBZ2	A0A1X7SBZ2	11	0|0|0|0|0|0|0|0|0|0|0	110
B4DRT3	B4DRT3	10	0|0|0|0|0|0|0|0|0|0|0	100
Q96F44	TRIM11	10	0|0|0|0|0|0|0|0|0|0|0	100
F4ZW66	F4ZW66	10	0|0|0|0|0|0|0|0|0|0|0	100
A0A0C4DGN6	A0A0C4DGN6	10	0|0|0|0|0|0|0|0|0|0|0	100
Q8NFP4	MDGA1	10	0|0|0|0|0|0|0|0|0|0|0	100
Q2TSD0	Q2TSD0	10	0|0|0|0|0|0|0|0|0|0|0	100
X6RAB3	X6RAB3	10	0|0|0|0|0|0|0|0|0|0|0	100
Q9BVG8	KIFC3	10	0|0|0|0|0|0|0|0|0|0|0	100
Q658P7	Q658P7	10	0|0|0|0|0|0|0|0|0|0|0	100
Q53F90	Q53F90	10	0|0|0|0|0|0|0|0|0|0|0	100
A0A0C4DG21	A0A0C4DG21	10	0|0|0|0|0|0|0|0|0|0|0	100
B4DEF9	B4DEF9	10	0|0|0|0|0|0|0|0|0|0|0	100
A8K2H4	A8K2H4	10	0|0|0|0|0|0|0|0|0|0|0	100
F8W0J6	F8W0J6	10	0|0|0|0|0|0|0|0|0|0|0	100
U3KQC1	U3KQC1	10	0|0|0|0|0|0|0|0|0|0|0	100
C9J7L5	ACSS2	10	0|0|0|0|0|0|0|0|0|0|0	100

Prey	PreyGene	AvgSpec	ctrlCounts	FoldChange
A8MW19	TSPEAR	10	0|0|0|0|0|0|0|0|0|0|0	100
Q6ZS99	Q6ZS99	10	0|0|0|0|0|0|0|0|0|0|0	100
B4DYA7	B4DYA7	10	0|0|0|0|0|0|0|0|0|0|0	100
A8K9D2	A8K9D2	9	0|0|0|0|0|0|0|0|0|0|0	90
H0Y6Y8	H0Y6Y8	9	0|0|0|0|0|0|0|0|0|0|0	90
G5E9V5	G5E9V5	9	0|0|0|0|0|0|0|0|0|0|0	90
A0A1U9X8Y2	A0A1U9X8Y2	9	0|0|0|0|0|0|0|0|0|0|0	90
B3KP90	B3KP90	9	0|0|0|0|0|0|0|0|0|0|0	90
H3BPS8	H3BPS8	9	0|0|0|0|0|0|0|0|0|0|0	90
F4ZW63	F4ZW63	9	0|0|0|0|0|0|0|0|0|0|0	90
B4DJW1	B4DJW1	9	0|0|0|0|0|0|0|0|0|0|0	90
B4DV73	B4DV73	9	0|0|0|0|0|0|0|0|0|0|0	90
P29376	LTK	9	0|0|0|0|0|0|0|0|0|0|0	90
B4DW25	B4DW25	9	0|0|0|0|0|0|0|0|0|0|0	90
Q86YV9	HPS6	9	0|0|0|0|0|0|0|0|0|0|0	90
B3KWX7	B3KWX7	9	0|0|0|0|0|0|0|0|0|0|0	90
A0A024QZB7	A0A024QZB7	9	0|0|0|0|0|0|0|0|0|0|0	90
A0A024QZE9	A0A024QZE9	9	0|0|0|0|0|0|0|0|0|0|0	90
A0A1W2PR68	A0A1W2PR68	9	0|0|0|0|0|0|0|0|0|0|0	90
C9JJV1	TSSC4	9	0|0|0|0|0|0|0|0|0|0|0	90
B4DPM4	B4DPM4	9	0|0|0|0|0|0|0|0|0|0|0	90
P14616	INSRR	9	0|0|0|0|0|0|0|0|0|0|0	90
B4DII5	B4DII5	9	0|0|0|0|0|0|0|0|0|0|0	90
O75628	REM1	9	0|0|0|0|0|0|0|0|0|0|0	90
A0A0D9SEU5	A0A0D9SEU5	9	0|0|0|0|0|0|0|0|0|0|0	90
I3L1Q2	I3L1Q2	9	0|0|0|0|0|0|0|0|0|0|0	90
K7EIJ0	K7EIJ0	9	0|0|0|0|0|0|0|0|0|0|0	90
B7Z437	B7Z437	8	0|0|0|0|0|0|0|0|0|0|0	80
B3KVY2	B3KVY2	8	0|0|0|0|0|0|0|0|0|0|0	80
Q59FZ4	Q59FZ4	8	0|0|0|0|0|0|0|0|0|0|0	80
G5EA36	G5EA36	8	0|0|0|0|0|0|0|0|0|0|0	80
B3KM81	B3KM81	8	0|0|0|0|0|0|0|0|0|0|0	80
B4DQI7	B4DQI7	8	0|0|0|0|0|0|0|0|0|0|0	80
A8K2R3	A8K2R3	8	0|0|0|0|0|0|0|0|0|0|0	80
B2RDD7	B2RDD7	8	0|0|0|0|0|0|0|0|0|0|0	80
Q9NUP1	BLOC1S4	8	0|0|0|0|0|0|0|0|0|0|0	80
P08514	ITGA2B	8	0|0|0|0|0|0|0|0|0|0|0	80
A0A0C4DGS1	A0A0C4DGS1	8	0|0|0|0|0|0|0|0|0|0|0	80
Q86Y79	PTRH1	8	0|0|0|0|0|0|0|0|0|0|0	80
A0A087WZZ9	A0A087WZZ9	8	0|0|0|0|0|0|0|0|0|0|0	80
A0A0R4J2F3	A0A0R4J2F3	8	0|0|0|0|0|0|0|0|0|0|0	80
Q9H1B7	IRF2BPL	8	0|0|0|0|0|0|0|0|0|0|0	80

Prey	PreyGene	AvgSpec	ctrlCounts	FoldChange
Q68EM7	ARHGAP17	14	0|0|0|0|0|1|0|0|1|0|0|0	70
Q53F09	Q53F09	7	0|0|0|0|0|0|0|0|0|0|0|0	70
P37023	ACVRL1	7	0|0|0|0|0|0|0|0|0|0|0|0	70
J3KRP0	J3KRP0	7	0|0|0|0|0|0|0|0|0|0|0|0	70
B4E0C7	B4E0C7	7	0|0|0|0|0|0|0|0|0|0|0|0	70
A0A088AWN2	A0A088AWN2	7	0|0|0|0|0|0|0|0|0|0|0|0	70
Q8IXR5	FAM178B	7	0|0|0|0|0|0|0|0|0|0|0|0	70
B3KN49	B3KN49	7	0|0|0|0|0|0|0|0|0|0|0|0	70
Q8TDH9	BLOC1S5	7	0|0|0|0|0|0|0|0|0|0|0|0	70
B7Z6D1	B7Z6D1	7	0|0|0|0|0|0|0|0|0|0|0|0	70
Q8IZ69	TRMT2A	7	0|0|0|0|0|0|0|0|0|0|0|0	70
A8K492	A8K492	7	0|0|0|0|0|0|0|0|0|0|0|0	70
H3BM58	H3BM58	7	0|0|0|0|0|0|0|0|0|0|0|0	70
F8VXI9	F8VXI9	7	0|0|0|0|0|0|0|0|0|0|0|0	70
Q9NVH6	TMLHE	7	0|0|0|0|0|0|0|0|0|0|0|0	70
Q6QNY0	BLOC1S3	7	0|0|0|0|0|0|0|0|0|0|0|0	70
Q9Y296	TRAPPC4	7	0|0|0|0|0|0|0|0|0|0|0|0	70
B7Z5N5	B7Z5N5	7	0|0|0|0|0|0|0|0|0|0|0|0	70
Q9Y5G6	PCDHGA7	7	0|0|0|0|0|0|0|0|0|0|0|0	70
B3KUR4	B3KUR4	7	0|0|0|0|0|0|0|0|0|0|0|0	70
Q9BW61	DDA1	7	0|0|0|0|0|0|0|0|0|0|0|0	70
B3KQF5	B3KQF5	7	0|0|0|0|0|0|0|0|0|0|0|0	70
O60826	CCDC22	13	0|0|0|0|0|0|0|2|0|0|0|0	65
B7Z8K4	B7Z8K4	6	0|0|0|0|0|0|0|0|0|0|0|0	60
E9PRT1	KCTD21	6	0|0|0|0|0|0|0|0|0|0|0|0	60
Q567R0	Q567R0	6	0|0|0|0|0|0|0|0|0|0|0|0	60
J3KN66	J3KN66	6	0|0|0|0|0|0|0|0|0|0|0|0	60
Q6IAW3	Q6IAW3	6	0|0|0|0|0|0|0|0|0|0|0|0	60
E9PRK7	C11orf46	6	0|0|0|0|0|0|0|0|0|0|0|0	60
O15116	LSM1	6	0|0|0|0|0|0|0|0|0|0|0|0	60
Q53HC2	Q53HC2	6	0|0|0|0|0|0|0|0|0|0|0|0	60
B7Z4H7	B7Z4H7	6	0|0|0|0|0|0|0|0|0|0|0|0	60
B7Z6W5	B7Z6W5	6	0|0|0|0|0|0|0|0|0|0|0|0	60
B2R782	B2R782	6	0|0|0|0|0|0|0|0|0|0|0|0	60
A0A1B0GVH3	A0A1B0GVH3	6	0|0|0|0|0|0|0|0|0|0|0|0	60
Q9UBY5	LPAR3	6	0|0|0|0|0|0|0|0|0|0|0|0	60
Q6FI91	Q6FI91	6	0|0|0|0|0|0|0|0|0|0|0|0	60
Q96GI7	FAM89A	6	0|0|0|0|0|0|0|0|0|0|0|0	60
B2R7I1	B2R7I1	6	0|0|0|0|0|0|0|0|0|0|0|0	60
Q9NPD8	UBE2T	6	1|0|0|0|0|0|0|0|0|0|0|0	60
H3BSS5	H3BSS5	6	0|0|0|0|0|0|0|0|0|0|0|0	60
A0A1B0GV23	A0A1B0GV23	6	0|0|0|0|0|0|0|0|0|0|0|0	60

Prey	PreyGene	AvgSpec	ctrlCounts	FoldChange
A0A024RDL9	A0A024RDL9	6	0|0|0|0|0|0|0|0|0|0|0	60
Q53GA1	Q53GA1	6	0|0|0|0|0|0|0|0|0|0|0	60
A0A1B2JLU7	A0A1B2JLU7	6	0|0|0|0|0|0|0|0|0|0|0	60
B4DT51	B4DT51	6	0|0|0|0|0|0|0|0|0|0|0	60
A0A0C4DFT3	A0A0C4DFT3	6	0|0|0|0|0|0|0|0|0|0|0	60
A0A0S2Z5K3	A0A0S2Z5K3	6	0|0|0|0|0|0|0|0|0|0|0	60
Q59GP6	Q59GP6	6	0|0|0|0|0|0|0|0|0|0|0	60
F8VV56	F8VV56	6	0|0|0|0|0|0|0|0|0|0|0	60
B4E3E6	B4E3E6	6	0|0|0|0|0|0|0|0|0|0|0	60
B2RA50	B2RA50	6	0|0|0|0|0|0|0|0|0|0|0	60
B2RAU5	B2RAU5	6	0|0|0|0|0|0|0|0|0|0|0	60
Q1AHP8	Q1AHP8	6	0|0|0|0|0|0|0|0|0|0|0	60
J3KNZ9	J3KNZ9	6	0|0|0|0|0|0|0|0|0|0|0	60
A0A024R442	A0A024R442	6	0|0|0|0|0|0|0|0|0|0|0	60
Q5JPH6	EARS2	10	0|0|0|0|0|0|2|0|0|0|0	50
A8K2I7	A8K2I7	5	0|0|0|0|0|0|0|0|0|0|0	50
Q8N8V2	GBP7	5	0|0|0|0|0|0|0|0|0|0|0	50
Q6I9T1	Q6I9T1	5	0|0|0|0|0|0|0|0|0|0|0	50
F5H5V4	PSMD9	5	0|0|0|0|0|0|0|0|0|0|0	50
B3KTL6	B3KTL6	5	0|0|0|0|0|0|0|0|0|0|0	50
M0QXY9	M0QXY9	5	0|0|0|0|0|0|0|0|0|0|0	50
B2RD96	B2RD96	5	0|0|0|0|0|0|0|0|0|0|0	50
B3KN28	B3KN28	5	0|0|0|0|0|0|0|0|0|0|0	50
A0A0A0MRK6	A0A0A0MRK6	5	0|0|0|0|0|0|0|0|0|0|0	50
B0QY54	CBY1	5	0|0|0|0|0|0|0|0|0|0|0	50
B2RDH6	B2RDH6	5	0|0|0|0|0|0|0|0|0|0|0	50
C9JG97	AAMP	5	0|0|0|0|0|0|0|0|0|0|0	50
H3BVE0	H3BVE0	5	0|0|0|0|0|0|0|0|0|0|0	50
K7EKQ2	K7EKQ2	5	0|0|0|0|0|0|0|0|0|0|0	50
B3KSQ7	B3KSQ7	5	0|0|0|0|0|0|0|0|0|0|0	50
Q8N8D1	PDCD7	5	0|0|0|0|0|0|0|0|0|0|0	50
B4DJH7	B4DJH7	5	0|0|0|0|0|0|0|0|0|0|0	50
K7EN32	K7EN32	5	0|0|0|0|0|0|0|0|0|0|0	50
A0A0C4DFV9	A0A0C4DFV9	5	0|0|0|0|0|0|0|0|0|0|0	50
Q9NZI6	TFCP2L1	5	0|0|0|0|0|0|0|0|0|0|0	50
Q9H871	RMND5A	5	0|0|0|0|0|0|0|0|0|0|0	50
A0A0U1RRC2	A0A0U1RRC2	5	0|0|0|0|0|0|0|0|0|0|0	50
R4SCC4	R4SCC4	5	0|0|0|0|0|0|0|0|0|0|0	50
O60926	O60926	5	0|0|0|0|0|0|0|0|0|0|0	50
K7EP45	K7EP45	5	0|0|0|0|0|0|0|0|0|0|0	50
Q9Y375	NDUFAF1	5	0|0|0|0|0|0|0|0|0|0|0	50
H0Y9M9	H0Y9M9	5	0|0|0|0|0|0|0|0|0|0|0	50

Prey	PreyGene	AvgSpec	ctrlCounts	FoldChange
Q96ER9	CCDC51	5	0|0|0|0|0|0|0|0|0|0|0	50
H3BV69	H3BV69	5	0|0|0|0|0|0|0|0|0|0|0	50
Q8N8M0	NAT16	5	0|0|0|0|0|0|0|0|0|0|0	50
A0A0R4J2E5	A0A0R4J2E5	5	0|0|0|0|0|0|0|0|0|0|0	50
B4DWK8	B4DWK8	5	0|0|0|0|0|0|0|0|0|0|0	50
A8MWD9	A8MWD9	5	0|0|0|0|0|0|0|0|0|0|0	50
Q15599	SLC9A3R2	5	0|0|0|0|0|0|0|0|0|0|0	50
B7Z4A1	B7Z4A1	5	0|0|0|0|0|0|0|0|0|0|0	50
Q8IXE5	Q8IXE5	5	0|0|0|0|0|0|0|0|0|0|0	50
H3BPN4	H3BPN4	5	0|0|0|0|0|0|0|0|0|0|0	50
A0A087X0F0	A0A087X0F0	5	0|0|0|0|0|0|0|0|0|0|0	50
B3KUE6	B3KUE6	5	0|0|0|0|0|0|0|0|0|0|0	50
B4DLF8	B4DLF8	5	0|0|0|0|0|0|0|0|0|0|0	50
P42574	CASP3	5	0|0|0|0|0|0|0|0|0|0|0	50
A8K8T1	A8K8T1	5	0|0|0|0|0|0|0|0|0|0|0	50
Q4LE70	APC	48	5|1|1|0|2|0|0|0|2|0|0|1	40
A8K1F4	A8K1F4	4	0|0|0|0|0|0|0|0|0|0|0	40
Q5T2Q4	Q5T2Q4	4	0|0|0|0|0|0|0|0|0|0|0	40
Q5TDH0	DDI2	4	0|0|0|0|0|0|0|0|0|0|0	40
Q9P000	COMMD9	4	0|0|0|0|0|0|0|0|0|0|0	40
B4DXG0	B4DXG0	4	0|0|0|0|0|0|0|0|0|0|0	40
Q9Y664	KPTN	4	0|0|0|0|0|0|0|0|0|0|0	40
A0A0S2Z580	A0A0S2Z580	4	0|0|0|0|0|0|0|0|0|0|0	40
H7C2Y5	H7C2Y5	4	0|0|0|0|0|0|0|0|0|0|0	40
H0YLA4	H0YLA4	4	0|0|0|0|0|0|0|0|0|0|0	40
K7EIZ3	K7EIZ3	4	0|0|0|0|0|0|0|0|0|0|0	40
Q9UI09	NDUFA12	4	0|0|0|0|0|0|0|0|0|0|0	40
P56282	POLE2	4	0|0|0|0|0|0|0|0|0|0|0	40
F8W057	F8W057	4	0|0|0|0|0|0|0|0|0|0|0	40
A0A0G2JLD8	A0A0G2JLD8	4	0|0|0|0|0|0|0|0|0|0|0	40
A0A0A0N0L3	A0A0A0N0L3	4	0|0|0|0|0|0|0|0|0|0|0	40
Q59FJ0	Q59FJ0	4	0|0|0|0|0|0|0|0|0|0|0	40
H0YEB6	H0YEB6	4	0|0|0|0|0|0|0|0|0|0|0	40
B3KNB4	B3KNB4	4	0|0|0|0|0|0|0|0|0|0|0	40
A0A024RD01	A0A024RD01	4	0|0|0|0|0|0|0|0|0|0|0	40
Q53G17	Q53G17	4	0|0|0|0|0|0|0|0|0|0|0	40
Q96BR5	SELRC1	4	0|0|0|0|0|0|0|0|0|0|0	40
Q8NEZ2	VPS37A	4	0|0|0|0|0|0|0|0|0|0|0	40
Q6GVN4	Q6GVN4	4	0|0|0|0|0|0|0|0|0|0|0	40
L0R5A1	L0R5A1	4	0|0|0|0|0|0|0|0|0|0|0	40
M0R389	M0R389	3	0|0|0|0|0|0|0|0|0|0|0	30
H0Y4E5	H0Y4E5	3	0|0|0|0|0|0|0|0|0|0|0	30

Prey	PreyGene	AvgSpec	ctrlCounts	FoldChange
A0A087WZ38	A0A087WZ38	3	0|0|0|0|0|0|0|0|0|0|0	30
Q68E00	Q68E00	3	0|0|0|0|0|0|0|0|0|0|0	30
F8VSA1	F8VSA1	3	0|0|0|0|0|0|0|0|0|0|0	30
Q8N0Z8	PUSL1	3	0|0|0|0|0|0|0|0|0|0|0	30
K7EIY6	K7EIY6	3	0|0|0|0|0|0|0|0|0|0|0	30
A0A0A0MSF9	A0A0A0MSF9	3	0|0|0|0|0|0|0|0|0|0|0	30
B4DW81	B4DW81	3	0|0|0|0|0|0|0|0|0|0|0	30
Q59GU5	Q59GU5	3	0|0|0|0|0|0|0|0|0|0|0	30
H3BRG4	H3BRG4	3	0|0|0|0|0|0|0|0|0|0|0	30
H3BNU9	H3BNU9	3	0|0|0|0|0|0|0|0|0|0|0	30
Q9GZQ3	COMMD5	3	0|0|0|0|0|0|0|0|0|0|0	30
B2RC50	B2RC50	3	0|0|0|0|0|0|0|0|0|0|0	30
A0A0B4J1R7	A0A0B4J1R7	3	0|0|0|0|0|0|0|0|0|0|0	30
B7ZLB7	C5orf44	3	0|0|0|0|0|0|0|0|0|0|0	30
Q13850	Q13850	3	0|0|0|0|0|0|0|0|0|0|0	30
K7EPJ1	K7EPJ1	3	0|0|0|0|0|0|0|0|0|0|0	30
A0A0B4J223	A0A0B4J223	3	0|0|0|0|0|0|0|0|0|0|0	30
Q9Y2Y1	POLR3K	3	0|0|0|0|0|0|0|0|0|0|0	30
Q9Y5B8	NME7	3	0|0|0|0|0|1|0|0|0|0|0	30
J3KPS0	J3KPS0	3	0|0|0|0|0|0|0|0|0|0|0	30
D6RA92	ANAPC10	3	0|0|0|0|0|0|0|0|0|0|0	30
Q9H081	MIS12	3	0|0|0|0|0|0|0|0|0|0|0	30
P42773	CDKN2C	3	0|0|0|0|0|0|0|0|0|0|0	30
Q5TA31	RNF187	3	0|0|0|0|0|0|0|0|0|0|0	30
A0A087WXC5	A0A087WXC5	3	0|0|0|0|0|0|0|0|0|0|0	30
Q59EH3	Q59EH3	3	0|0|0|0|0|0|0|0|0|0|0	30
Q2NLC9	Q2NLC9	3	0|0|0|0|0|0|0|0|0|0|0	30
Q8N4T8	CBR4	3	0|0|0|0|0|0|0|0|0|0|0	30
I0EZ61	I0EZ61	3	0|0|0|0|0|0|0|0|0|0|0	30
Q4VXZ8	DECR2	3	0|0|0|0|0|0|0|0|0|0|0	30
Q9NPL8	TIMMDC1	3	0|0|0|0|0|0|0|0|0|0|0	30
Q96H79	ZC3HAV1L	3	0|0|0|0|0|0|0|0|0|0|0	30
A0A087WYU2	A0A087WYU2	3	0|0|0|0|0|0|0|0|0|0|0	30
A0A024QZV0	A0A024QZV0	3	0|0|0|0|0|0|0|0|0|0|0	30
Q13433	SLC39A6	3	0|0|0|0|0|0|0|0|0|0|0	30
Q9Y4G6	TLN2	32	1|0|3|2|1|2|0|0|1|1|0|2|1	22.86
D6RAD4	CDK7	6	0|3|0|0|0|0|0|0|0|0|0	20
Q86U42	PABPN1	4	0|0|0|0|0|0|0|0|2|0|0|0	20
U5XKY1	U5XKY1	2	0|0|0|0|0|0|0|0|0|0|0	20
F5H6B6	TRPT1	2	0|0|0|0|0|0|0|0|0|0|0	20
H7C5E5	H7C5E5	2	0|0|0|0|0|0|0|0|0|0|0	20
Q9BTT4	MED10	2	0|0|0|0|0|0|0|0|0|0|0	20

Prey	PreyGene	AvgSpec	ctrlCounts	FoldChange
H9KV45	H9KV45	2	0|0|0|0|0|0|0|0|0|0|0	20
B3KUJ0	B3KUJ0	2	0|0|0|0|0|0|0|0|0|0|0	20
F8VXU5	F8VXU5	2	0|0|0|0|0|0|0|0|0|0|0	20
Q92567	FAM168A	2	0|0|0|0|0|0|0|0|0|0|0	20
G3V2Q3	G3V2Q3	2	0|0|0|0|0|0|0|0|0|0|0	20
E9PIN9	ACER3	2	0|0|0|0|0|0|0|0|0|0|0	20
B7Z9F3	B7Z9F3	2	0|0|0|0|0|0|0|0|0|0|0	20
F8WF69	F8WF69	2	0|0|0|0|0|0|0|0|0|0|0	20
D6RCT8	DTNBP1	2	0|0|0|0|0|0|0|0|0|0|0	20
A8MYR4	GTF2A2	2	0|0|0|0|1|0|0|0|0|0|0	20
I3L2J1	I3L2J1	2	0|0|0|0|0|0|0|0|0|0|0	20
H3BRW3	H3BRW3	2	0|0|0|0|0|0|0|0|0|0|0	20
Q6PJD5	SHARPIN	2	0|0|0|0|0|0|0|0|0|0|0	20
A0A087WY54	A0A087WY54	2	0|0|0|0|0|0|0|0|0|0|0	20
K7ESJ4	K7ESJ4	2	0|0|0|0|0|0|0|0|0|0|0	20
A3FMQ3	A3FMQ3	2	0|0|0|0|0|0|0|0|0|0|0	20
B4DHP4	B4DHP4	2	0|0|0|0|0|0|0|0|0|0|0	20
Q4TT61	SNRNP25	2	0|0|0|0|0|0|0|0|0|0|0	20
Q5U0A0	Q5U0A0	2	0|0|0|0|0|0|0|0|0|0|0	20
Q5QP19	NFS1	8	0|0|0|0|0|0|5|0|0|0|0	16
P51948	MNAT1	7	1|1|0|0|0|1|2|0|0|0|0|0	14
O75113	N4BP1	9	0|0|2|0|0|3|2|0|0|0|1|0|1	10
F5H0F9	ANAPC5	7	0|0|7|1|2|0|1|0|3|2|0|1|0	4,12
E7EQY4	MTA3	14	1|2|3|4|5|3|2|0|4|3|4|3|5	3,89
Q96PK6	RBM14-RBM4;RBM14	14	0|0|5|6|8|3|0|2|0|5|0|0|9	3,68
Q9Y305	ACOT9	5	0|0|0|1|0|0|1|15|0|0|0|0|0	2,94
Q15811	ITSN1	20	0|0|12|5|9|5|6|0|5|8|6|6|8	2,86
P52655	GTF2A1	4	4|3|1|0|0|0|0|0|1|2|1|1|1	2,86
Q8N0X7	SPG20	7	0|3|7|0|0|3|3|0|3|2|3|1|1	2,69

Prey: Uniprot accession number, PreyGene: Corresponding protein coding gene name, AvgSpec: Average spectral counts representing the number of peptides detected in the analysis, ctrlCounts: Control counts representing the number of peptides detected in each control separately, Fold change: Protein enrichment fold change compared to the controls.

Appendix 7 – Posters and presentations

Posters:

Meller A., Lai Z., Moravcova S., Lane K., Rea S. (2017): Investigation of the role of MSL2 and MSL1 in the DNA damage response, IFOM meeting, National University of Ireland, Galway, Ireland

Meller A., Lai Z., Moravcova S., Lane K., Rea S. (2016): Investigation of hMSL2 ubiquitylation and its role in the DNA damage response, SAB meeting, National University of Ireland, Galway, Ireland

Meller A., Lai Z., Moravcova S., Rea S. (2015): Investigation of hMSL2 ubiquitylation and its role in the DNA damage response, YLS Galway, National University of Ireland, Galway

Lane K., **Meller A**., Eykelenboom J., Andrejewski L., Rea S. (2015): Gene editing of the MSL complex for functional characterization, Gene-editing, Transgenics and Stem Cells (ISCA Dublin 2015), Trinity Biomedical Science Institute, Dublin, Ireland

Presentations:

Meller A., Lai Z., Moravcova S., Rea S. (2015): Investigation of hMSL2 ubiquitylation and its role in the DNA damage response, COST Practical course on ubiquitin and ubiquitin-like proteins, Goethe University School of Medicine, Frankfurt, Germany

Meller A., Lai Z., Moravcova S., Rea S. (2014): TouGal meeting, Centre for Integrative Biology, Toulouse, France